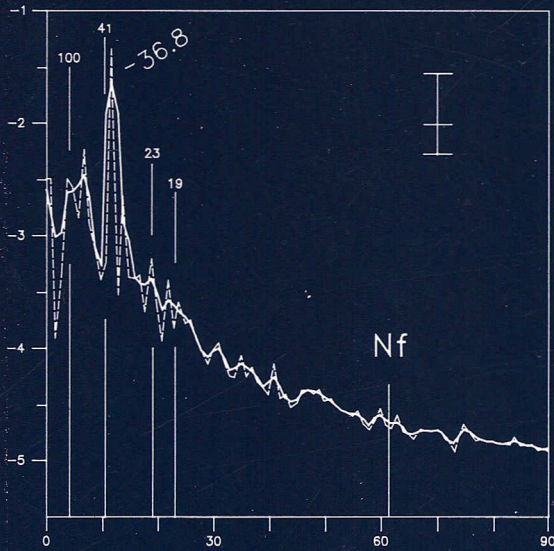


GEOLOGICA ULTRAIECTINA

Mededelingen van de
Faculteit Aardwetenschappen der
Universiteit Utrecht

No. 93

ASTRONOMICAL FORCING AND GEOCHRONOLOGICAL APPLICATION OF SEDIMENTARY CYCLES IN THE MEDITERRANEAN PLIOCENE-PLEISTOCENE



FREDERIK J. HILGEN

GEOLOGICA ULTRAIECTINA

Mededelingen van de
Faculteit Aardwetenschappen der
Universiteit Utrecht

No. 93

ASTRONOMICAL FORCING AND GEOCHRONOLOGICAL
APPLICATION OF SEDIMENTARY CYCLES IN THE
MEDITERRANEAN PLIOCENE-PLEISTOCENE

24 - 011

CIP-GEGEVENS KONINKLIJKE BIBLIOTHEEK, DEN HAAG

Hilgen, Frederik Johan

Astronomical forcing and geochronological application of sedimentary cycles in the Mediterranean Pliocene-Pleistocene / Frederik Johan Hilgen. - [Utrecht: Faculteit Aardwetenschappen der Rijksuniversiteit Utrecht]. - (Geologica Ultraiectina, ISSN 0072-1026; no. 93) Proefschrift Rijksuniversiteit Utrecht. - Met lit. opg. - Met samenvattig in het Nederlands.
ISBN 90-71577-47-3
Trefw.: paleontologie.

ASTRONOMICAL FORCING AND GEOCHRONOLOGICAL APPLICATION OF
SEDIMENTARY CYCLES IN THE MEDITERRANEAN PLIOCENE - PLEISTOCENE

ASTRONOMISCHE FORCERING EN GEOCHRONOLOGISCHE TOEPASSING VAN
SEDIMENTAIRE CYCLI IN HET MEDITERRANE PLIOCEEN - PLEISTOCEEN

(met een samenvatting in het Nederlands)

Proefschrift

ter verkrijging van de graad van doctor aan
de Rijksuniversiteit te Utrecht, op gezag van
de Rector Magnificus, Prof. Dr. J.A. van Ginkel,
ingevolge het besluit van het College van Dekanen
in het openbaar ter verdedigen op dinsdag
26 november 1991 des namiddags te 12.45 uur

door

Frederik Johan Hilgen
geboren op 21 november 1957 te Almelo

PROMOTORES: PROF. DR. C.W. DROOGER
PROF. DR. J.D.A. ZIJDERVELD

Dit proefschrift werd mede mogelijk gemaakt met financiële steun van de Stichting Aardwetenschappelijk Onderzoek (AWON) met een subsidie van de Nederlandse Organisatie voor Wetenschappelijk Onderzoek (NWO).

..... a process of gradual indoctrination would become part of the cult, as beginners would move through a series of stages in which they would be taught the necessary astronomical concepts and their religious implications

From: D. Ulansey, 1989. The origins of the Mithraic mysteries (Cosmology and Salvation in the Ancient World, Oxford, Univ. Press (p.84).

to Marian and Sander (for his first birthday)
to the memory of my mother

Contents

Summary	ix
Samenvatting	xiii
Chapter 1. Introduction.	1
Chapter 2. Sedimentary cycles and high-resolution chronostratigraphic correlations in the Mediterranean Pliocene.	9
Chapter 3. Closing the gap in the Plio-Pleistocene boundary stratotype sequence at Crotona.	29
Chapter 4. The age of the Miocene-Pliocene boundary in the Capo Rossello area (Sicily).	39
Chapter 5. The Rossello composite: A Mediterranean and global reference section for the Early to early Late Pliocene.	49
Chapter 6. Integrated magnetostratigraphy and biostratigraphy of the upper Pliocene - lower Pleistocene from the Monte Singa and Crotona areas in Calabria (Italy).	65
Chapter 7. Periodicities of CaCO ₃ cycles in the Pliocene of Sicily: Discrepancies with the quasi-periods of the Earth's orbital cycles?	83
Chapter 8. Astronomical calibration of Gauss to Matuyama sapropels in the Mediterranean and implication for the Geomagnetic Polarity Time Scale.	91
Chapter 9. Extension of the astronomically calibrated (polarity) time scale to the Miocene/Pliocene boundary.	111
Chapter 10. The new astronomically calibrated time scale for the late Pliocene confirmed.	131

Chapters 2, 3, 4, 5, 6, 7, 8 and 9 have already been published and are included in this thesis with the permission of the publishers. Chapters 2 and 3 are reproduced with the permission of Gebrüder Borntraeger, chapters 4, 5, 6, 8 and 9 are reproduced with the permission of Elsevier Science Publishers and chapter 7 with the permission of Blackwell Scientific Publications.

References:

- Ch. 2: Hilgen, F.J., 1987. Sedimentary cycles and high-resolution chronostratigraphic correlations in the Mediterranean Pliocene. *Newsletters on Stratigraphy*, 17, 109-127.
- Ch. 3: Hilgen, F.J., 1990. Closing the gap in the Plio-Pleistocene boundary stratotype sequence at Crotona (southern Italy). *Newsletters on Stratigraphy*, 22, 43-51.
- Ch. 4: Hilgen, F.J., and C.G. Langereis, 1988. The age of the Miocene-Pliocene boundary in the Capo Rossello area (Sicily). *Earth and Planetary Science Letters*, 91, 214-222.
- Ch. 5: Langereis, C.G., and F.J. Hilgen, 1991. The Rossello composite: A Mediterranean and global reference section for the Early to early Late Pliocene. *Earth and Planetary Science Letters*, 104, 211-225.
- Ch. 6: Zijderveld, J.D.A., F.J. Hilgen, C.G. Langereis, P.J.J.M. Verhallen and W.J. Zachariasse, 1991. Integrated magnetostratigraphy and biostratigraphy of the upper Pliocene - lower Pleistocene from the Monte Singa and Crotona areas in Calabria, Italy. *Earth and Planetary Science Letters*, 107, 697-714.
- Ch. 7: Hilgen, F.J., and C.G. Langereis, 1989. Periodicities of CaCO₃ cycles in the Pliocene of Sicily: Discrepancies with the quasi-periods of the Earth's orbital cycles? *Terra Nova*, 1, 409-415.
- Ch. 8: Hilgen, F.J., 1991. Astronomical calibration of Gauss to Matuyama sapropels in the Mediterranean and implication for the Geomagnetic Polarity Time Scale. *Earth and Planetary Science Letters*, 104, 226-244.
- Ch. 9: Hilgen, F.J., 1991. Extension of the astronomically calibrated (polarity) time scale to the Miocene/Pliocene boundary. *Earth and Planetary Science Letters*, 107, 349-368.

SUMMARY

A new, astronomically calibrated time scale is presented for the Mediterranean Pliocene based on the correlation of sedimentary cycles to astronomical curves which describe the quasi-periodic variations in the Earth's orbit during the last 5.5 Ma. These sedimentary cycles are found in a continuous deep-sea marl sequence emerged above present sea-level due to tectonic uplift. For this sequence, an integrated high-resolution magnetostratigraphy, (planktonic foraminiferal) biostratigraphy and lithostratigraphy is established which underlies the new time scale. This time scale differs substantially from more conventional time scales which rely entirely on K/Ar radiometric dating.

The total Pliocene sequence is composed of various, partly overlapping subsections and embraces sediments of both the lower Pliocene Trubi Formation and the upper Pliocene to lower Pleistocene Narbone Formation. The Trubi consists of (continuously) rhythmically bedded - grey and white - marls and the Narbone of a (discontinuous) rhythmic alternation of homogeneous blue/grey marls and brownish coloured, laminated beds, loosely termed sapropels. The land-based sections are all but one located in southern Italy, namely on Sicily (Capo Rossello, Punta di Maiata, P. Grande, P. Piccola, Eraclea Minoa, Capo Bianco and Monte San Nicola) and in adjacent Calabria (southern Calabria: Singa; northern Calabria: Vrica and Semaforo). The parallel section of Francocastello is located on Crete (Greece). Connections between partial and parallel sections are based on high-resolution lithostratigraphic correlations which possess chronostratigraphic significance and which are confirmed by magnetostratigraphic and biostratigraphic correlations.

The magnetostratigraphic investigations are based on stepwise thermal demagnetization of the natural remanent magnetization of a large number of stratigraphically closely spaced, oriented samples. This method generally yielded good to excellent results which allowed the identification of (a) primary component(s) necessary for a reliable determination of the direction or at least the polarity of the Earth's magnetic field at about the time of deposition. Analytical results were often better for the Trubi part of the sequence due to the presence of a stable, high temperature (magnetite) component of primary origin. In addition, the conspicuous post-Pliocene clockwise of Sicily, on which most of our Trubi sections are located, allowed to make an easy distinction between primary and secondary components. In the Narbone marls this high temperature component is generally absent and therefore the primary remanence of these

marls becomes more easily overprinted by remagnetization due to weathering. In spite of the consequent local difficulties a distinct and consistent polarity sequence could also be established for the Narbone Formation. The calibration of the polarity patterns to the Geomagnetic Polarity Time Scale showed unambiguously that the combined polarity sequence obtained for the Mediterranean Pliocene ranges from slightly below the Thvera subchron of the Gilbert to well above the Olduvai subchron of the Matuyama Chron.

The biostratigraphic investigations are based mainly on a qualitative analysis of the planktonic foraminiferal content. This procedure yielded a large number of successive and often easily recognizable biohorizons defined by first and last occurrences. Semi-quantitative analysis allowed to distinguish between first and last *common* occurrences and *truly* first and last occurrences in a number of cases. A quantitative approach was applied as well to locate the exact position of the first significant increase of sinistrally coiled neogloboquadrinids. In terms of existing biozonations for the Mediterranean Pliocene, the composite sequence ranges from the *Sphaeroidinellopsis* Acme zone into the *N. pachyderma* Zone. The first zone marks the basal Pliocene in the Mediterranean, the last one belongs already to the Pleistocene.

The lithostratigraphic investigations were focussed primarily on the detailed logging of rhythmic variations in lithology, i.e. the alternation of CaCO₃-rich and CaCO₃-poor marlbeds in the Trubi and of homogeneous and laminated marls in the Narbone Formation. This inventory led to the identification and subsequent informal numbering and coding of all sedimentary rhythmites in our composite sequence. In addition, the relationship between the two types of rhythmic bedding was established in the Punta Piccola section. This section contains the (gradual) transition from the Trubi marls to the marls/clays of the Narbone Formation.

The resulting integrated magnetostratigraphy, biostratigraphy and lithostratigraphy provided a solid base for the final goal of our research, the construction of an astronomically calibrated time scale for the Mediterranean Pliocene. This time scale was established by calibrating the sedimentary cycles to the new astronomical curves for the quasi-periodic variations in the Earth's orbit. Phase relations between sedimentary and astronomical cycles were determined by correlating late Pleistocene sapropels to the astronomical record. This correlation revealed that individual sapropels correspond to minimum peak values of the precession index and that small- and large-scale sapropel clusters correspond to 100 and 400 ka eccentricity maxima, respectively. These phase relations were subsequently employed to correlate the late Pliocene to early Pleistocene sapropel patterns to precession and eccentricity. The almost complete lack of the

influence of the obliquity cycle is explained by the fact that these sedimentary cycles reflect changes in (circum)Mediterranean and monsoonal climate and the relatively low latitudinal position of the Mediterranean. The astronomical calibration of sedimentary cycles could be extended down to the Miocene/Pliocene boundary by using the detailed record of CaCO₃ cycles in the Trubi and their relationships to the sapropel cycles. Based on this astronomical calibration, a Mediterranean Precession Related Cycle code was introduced according to which sedimentary cycles are coded after the correlative precession peak numbered from the Recent. More importantly, all sedimentary cycles could be dated with an accuracy of 1 ky if we assume the new astronomical solution to be accurate in the time domain and consider a time lag of 3-4 ky between orbital forcing, and climate response resulting in sapropel formation.

In combination with the magnetostratigraphic and biostratigraphic data, very accurate ages could further be assigned to both geomagnetic reversal boundaries and planktonic foraminiferal biohorizons; they provided the framework for the new time scale for the Mediterranean Pliocene. Astronomically calibrated ages of polarity transitions were thus obtained for the Olduvai (1.79 - 1.95 Ma), Reunion (2.14 - 2.15), Gauss/Matuyama (2.59/2.62), Kaena (3.04 - 3.11), Mammoth (3.22 - 3.33), Gilbert/Gauss (3.58), Cochiti (4.18 - 4.29), Nunivak (4.48 - 4.62), Sidufjall (4.80 - 4.89) and Thvera (4.98 - 5.23). These ages differ considerably from the conventional ages which, for this time interval, rely entirely on K/Ar radiometric dating. The discrepancy of 3 up to 10 % can be attributed most plausibly to the loss of radiogenic argon which results in radiometric ages that are too young. The new ages for the Pliocene/Pleistocene and Miocene/Pliocene boundaries arrived at 1.81 and 5.32 Ma, as compared with their conventional ages of 1.68 and 4.86 Ma, respectively.

Finally, we tested the validity of the new time scale by extracting precession and obliquity related frequency components from late Pliocene to early Pleistocene climatic proxy records in the Mediterranean and compared them with the respective orbital time series. The new time scale is confirmed by the good to excellent coherence between the filtered 21 ky components and precession and the consistent relationship between the 41 ky components and obliquity. Only a slight discrepancy of 2 ky is found if we compare late Pliocene phase relations between orbital forcing and climate response with those obtained for the late Pliocene. This discrepancy can be explained by a change in these phase relations, by a small error in the astronomical solution or by a combination of these factors.

SAMENVATTING

Een nieuwe, astronomisch gecalibreerde tijdschaal wordt gepresenteerd voor het Mediterrane Pliocen. Deze tijdschaal is gebaseerd op de correlatie van sedimentaire cycli naar astronomische curves die de quasi-periodieke variaties in de baan van de aarde om de zon beschrijven. De sedimentaire cycli maken deel uit van een continue Pliocene diepze opeenvolging die ten gevolge van latere opheffing op het land ontsloten is. Voor deze opeenvolging zijn een gedetailleerde magnetostratigrafie, (planktonische foraminiferen) biostratigrafie en lithostratigrafie opgesteld, die de basis vormen van de nieuwe tijdschaal. Deze tijdschaal blijkt in aanzienlijke mate te verschillen van de bestaande tijdschalen, die voornamelijk gebaseerd zijn op K/Ar radiometrische dateringen.

De bestudeerde diepze opeenvolging is opgebouwd uit meerdere secties en omvat de sedimenten van de onder Pliocene Trubi Formatie en de boven Pliocene tot onder Pleistocene Narbone Formatie. De Trubi Fm. bestaat uit een doorlopend ritmisch - grijs en wit - gebankte mergel en de Narbone Fm. uit een (onderbroken) ritmische afwisseling van homogene grijze mergels en bruin gekleurde, vaak gelamineerde lagen, sapropelen genaamd. De gebruikte land secties bevinden zich op één na in Zuid Italië, en wel op Sicilië (Capo Rossello, Punta di Maiata, P. Grande, P. Piccola, Eraclea Minoa, C. Bianco, Ribera en Monte San Nicola) en in Calabrië (Singa, Vrica en Semaforo). De parallel sectie van Francocastello is op Creta (Griekenland) gelegen. De onderlinge samenhang tussen de verschillende deel en parallel secties is gebaseerd op zeer gedetailleerde lithostratigrafische correlaties. Deze correlaties, die verondersteld worden tijdslijnen te representeren, worden bevestigd door de magnetostratigrafische en biostratigrafische correlaties.

Het magnetostratigrafisch onderzoek is gebaseerd op een stapsgewijze thermische demagnetisatie van de natuurlijke remanente magnetisatie van een groot aantal op korte stratigrafische afstand genomen georiënteerde gesteentemonsters. In verreweg de meeste gevallen was het mogelijk de primaire magnetische gesteente component(en) in de mergel te onderscheiden, hetgeen van groot belang is voor een betrouwbare bepaling van de richting of in elk geval de polariteit van het aardmagneetveld ten tijde van de afzetting. De resultaten voor de Trubi waren vaak beter dan voor de Narbone Formatie. Dit is een gevolg van het voorkomen van een stabiele primaire, hoge temperatuur component in de Trubi mergels; deze (extra) component ontbreekt meestal in de Narbone. Voorts kunnen in de Siciliaanse secties van de Trubi de primaire en secundaire componenten duidelijk onderscheiden worden omdat Sicilië na het Pliocen een duidelijke kloksgwijze draaiing heeft ondergaan, waardoor de primaire component deze rotatie vertoont en de secundaire

niet. Door het ontbreken van de stabiele hoge temperatuur component is het in de Narbone mergels vaak moeilijker een scheiding aan te brengen tussen de primaire component en de secundaire component die het gevolg is van remagnetisatie door verwering. Desalniettemin bleek ook voor de Narbone Formatie een duidelijke en consequente polariteit zoning op te stellen. De calibratie van het patroon in de lengtes van de opeenvolgende polariteits zones met de "Geomagnetic Polarity Time Scale" toont duidelijk aan dat de gecombineerde, Trubi en Narbone polariteit zoning het interval omvat van kort voor de Thvera (subchron) in de Gilbert (Chron) tot na de Olduvai in de Matuyama.

Het biostratigrafisch onderzoek is voornamelijk gebaseerd op een kwalitatieve analyse van planktonische foraminiferen fauna's. De gevolgde procedure leverde een groot aantal opeenvolgende en vaak eenvoudig te bepalen biohorizonten op die bepaald worden door de eerste en laatste voorkomens van bepaalde soorten planktonische foraminiferen. Semi-quantitatieve analyses maakten het daarnaast mogelijk om in een aantal gevallen onderscheid te maken tussen eerste en laatste *algemene* voorkomens en *werkelijke* eerste en laatste voorkomens. Een quantitative benadering werd toegepast om de exacte positie van de eerste significante toename in links gewonden neogloboquadrina's te bepalen. In termen van bestaande biozoneringen voor het Mediterrane Pliocen loopt de onderzochte opeenvolging van de *Sphaeroidinellopsis* Acme zone tot in de *N. pachyderma* Zone. De eerst genoemde zone markeert het basale Pliocen in de Middellandse Zee, de laatste behoort al tot het Pleistoceen.

Het lithostratigrafisch onderzoek heeft zich vooral bezig gehouden met de registratie van ritmische variaties in het gesteente, dwz. de afwisseling van kalkarme en kalkrijke mergels in de Trubi en van homogene en gelamineerde mergels in de Narbone Fm. Het resulteerde in de identificatie en informele nummering en codering van alle sedimentaire ritmieken in de sedimentaire opeenvolging. In de Punta Piccola sectie, die de grens tussen de Trubi en de Narbone bevat, kon de relatie tussen de twee soorten sedimentaire ritmieken worden vastgesteld.

De verkregen, geïntegreerde magnetostratigrafie, biostratigrafie en lithostratigrafie vormde een solide basis voor het uiteindelijke doel van ons onderzoek, het opstellen van een astronomisch gecalibreerde tijdschaal voor het Mediterrane Pliocen. Deze tijdschaal werd opgesteld door de sedimentaire ritmieken in de Pliocene opeenvolging te correleren naar de meest recente astronomische curves voor de quasi-periodieke veranderingen in de aardbaan voor de laatste 5.5 miljoen jaar. Eerst werden de fase relaties bepaald tussen de sedimentaire en de astronomische cycli door de meest recente sapropelen (van laat Pleistocene ouderdom) te correleren naar de astronomische curves. Deze correlatie toont dat individuele sapropelen samenvallen met minima van de precessie index en dat kleine

en grotere groepen van sapropelen samenvallen met 100.000 en 400.000 jaars maxima in excentriciteit. Deze fase relaties werden vervolgens gebruikt om de laat Pliocene tot vroeg Pleistocene sapropelen met de precessie en excentriciteit curves te verbinden. De astronomische calibratie van sedimentaire cycli werd vervolgens uitgebreid tot aan de Mioceen/Pliocene grens met behulp van de CaCO₃ cycli van de Trubi Formatie. Uitgaande van de correlatie met precessie is een MPRC ('Mediterranean Precession Related Cycle') codering voor de kleinschalige sedimentaire cycli in het Mediterrane Pliocene en Pleistoceen opgesteld. Volgens deze codering wordt een cyclus het nummer van de correlatieve precessie piek gegeven. Veel belangrijker is dat de ouderdom van alle sedimentaire cycli nu met een nauwkeurigheid van ongeveer 1000 jaar vastgesteld kan worden, indien we aannemen dat de nieuwe astronomische oplossing nauwkeurig is in het tijdsbereik en rekening houden met het optreden van een vertraging van zo'n 3 tot 4.000 jaar tussen de astronomische beïnvloeding, en de verandering in het klimaat resulterend in de afzetting van een sapropel. De ouderdommen van de geregistreerde polariteitsomkeringen van het aardmagneetveld en de planktonische foraminiferen biohorizonten konden vervolgens met behulp van lineaire interpolatie bepaald worden; deze dateringen vormen het kader van de nieuwe tijdschaal voor het Mediterrane Pliocene.

De aldus verkregen ouderdommen voor de polariteitsomkeringen van het aardmagneetveld (Olduvai (1.79-1.95 miljoen jaar), Reunion (2.14-2.15), Gauss/Matuyama (2.59/2.62), Kaena (3.04-3.11), Mammoth (3.22-3.33), Gilbert/Gauss (3.58), Cochiti (4.18-4.29), Nunivak (4.48-4.62), Sidufjall (4.80-4.89) en Thvera (4.98-5.23)) blijken systematisch te verschillen van de conventionele, radiometrische (K/Ar) ouderdommen. Het verschil, dat varieert tussen 3 en 10 %, kan verklaard worden als een gevolg van het verlies van radiogeen argon, wat in te jonge radiometrische ouderdommen resulteert. De nieuwe ouderdommen voor de Pliocene/Pleistoceen en de Mioceen/Pliocene grens komen uit op respectievelijk 1.81 en 5.32 miljoen jaar terwijl zij volgens de conventionele tijdschaal slechts 1.68 en 4.86 miljoen jaar oud zijn.

Tenslotte hebben we de nieuwe tijdschaal getest door astronomisch bepaalde frequentie componenten in laat Pliocene tot vroeg Pleistocene klimatologische "proxy" curves voor het Middellandse Zee gebied te filteren en te vergelijken met de respectievelijke curves van de betreffende astronomische parameters. De nieuwe tijdschaal werd overtuigend bevestigd door de goede tot uitstekende coherentie tussen de gefilterde 21.000 jaar componenten en precessie en de consequente relatie tussen de gefilterde 41.000 jaar componenten en obliquity. De vergelijking van laat Pleistocene fase relaties tussen astronomische cycli en de daarmee samenhangende klimaatsveranderingen met die voor het laat Pliocene leverde slechts een geringe discrepantie op van 2.000 jaar. Deze discrepantie kan verklaard worden door een verandering in de fase relaties, door een kleine fout in de astronomische oplossing of door een combinatie van deze factoren.

Chapter 1

INTRODUCTION

1.1 Purpose and framework of the investigation

The astronomical theory of climate and the ice ages

The Earth's orbit around the sun is influenced by gravitational interactions with the other planets and with the moon. The resulting orbital perturbations give rise to variations in eccentricity, obliquity and precession with main periods of 400 and 100, 41, and 23 and 19 ky, respectively (Berger, 1978). Eccentricity is a measure of the degree of elongation of the orbit and varies between nearly zero (circular orbit) and 0.06 (slightly elliptical orbit). Obliquity describes the angle between the Earth's axis of rotation and the orbital plane and varies between 22 and 25°. Axial precession describes the slow movement of the rotational axis around a circular path with one revolution completed every 26 ky. Due to the opposite movement of the eccentric orbit itself, the precession of the equinoxes, also called climatic precession, completes one full cycle about every 21 ky. These variations in the Earth's orbit are climatically important because they affect both the seasonal as well as the latitudinal distribution of the solar insolation.

The astronomical theory of climatic oscillations is at present widely accepted. This theory, according to which climatic changes are linked to the variations in the Earth's orbit, was first expressed by Adhémar (1842) who suggested that the occurrence of the ice ages might be astronomically controlled. This ice age theory was elaborated by Croll (1864) and, later on, especially by Milankovitch (1941). As early as 1895, Gilbert employed the more general astronomical theory of climate to estimate the amount of time represented by rhythmically bedded sequences of the Cretaceous (see also Fischer, 1980). He used the periodicity of the precession cycle for the explanation of these sedimentary cycles.

Milankovitch's ideas concerning the astronomical origin of the Pleistocene ice ages initially met with wide approval. Scepticism soon prevailed, however, mainly because the first ¹⁴C-datings of distinct glacial or interglacial intervals were not consistent with Milankovitch's predictions (this inconsistency actually resulted from the fact that Milankovitch underestimated the contribution of precession to the occurrence of the ice ages; see Imbrie and Imbrie, 1979). This deadlock was overcome with the introduction of stable isotope analysis of (foraminiferal) carbonate in combination with the study of deep-sea records recovered by piston cores. The piston cores provided the long and continuous

deep-sea sequences necessary to acquire a detailed record of glacial history through time. The principles of stable isotope analysis, introduced by Urey (1947), were first applied systematically to deep-sea records by Emiliani (1955). Although interpreted initially as an estimate for seawater temperature (variations), $\delta^{18}\text{O}$ proved a highly sensitive recorder of changes in ice volume (Shackleton and Opdyke, 1973). The resulting $\delta^{18}\text{O}$ record could therefore be used to test the validity of the astronomical theory of the ice ages.

An additional factor which contributed to the revival of the astronomical theory to explain the ice ages was the development of the Global Polarity Time Scale. This time scale was essentially based on the radiometric dating of past reversals of the Earth's magnetic field (see Mankinen and Dalrymple, 1979) and it allowed deep-sea sequences to be accurately dated by means of magnetostratigraphic calibration to the GPTS. A last important aspect to be mentioned here was the continuous improvement of the astronomical solution for the variations in the Earth's orbit. In 1978, this resulted in astronomical records which were supposed to be reliable for at least the last 1.5 Ma (Berger, 1978.). At the same time, the astronomical theory of the ice ages was convincingly demonstrated (Hays et al., 1976; Imbrie et al., 1984). Climatic proxy records, mainly that of ice volume ($\delta^{18}\text{O}$), had been correlated to the astronomical record to evaluate (and confirm!) this theory and to establish a high-resolution time scale for the late Pleistocene. At present, this astronomically-calibrated time scale is well established and widely used for the last 700,000 years. Such a time scale is in principle more accurate and has a higher resolution than more conventional time scales which had been mainly based on radiometric dating of lavas of known polarity. It is furthermore a prerequisite to a better understanding of the complex interactions in the ocean-climate system because it allows us to determine consistent phase relations between the orbital variations and different components in the ocean-climate system (McIntyre et al., 1989; Imbrie et al., 1989).

Extension of the late Pleistocene type of research to the Pliocene - early Pleistocene

It is self-evident that this type of research soon became extended to the early Pleistocene and Pliocene, i.e. the time interval marked by rapidly expanding northern (and southern) hemisphere ice sheets and the onset of high-amplitudinal glacial cycles (Shackleton et al., 1984; Ruddiman et al., 1986a) that governed global climate up to the present day. Such an extension was strongly hampered in the beginning by problems encountered in recovering older, undisturbed and continuous deep-sea sequences which, except for areas with extremely low sediment accumulation rates, were beyond the reach of ordinary piston cores. Sedimentary sequences from such areas are less suitable for detailed studies, however, because the resolution of deep-sea records is generally inversely proportional to the sedimentation rate. This major problem concerning the recovery of uninterrupted, high-resolution deep-sea records was ultimately solved by the application of advanced piston

coring of multiple holes. These parallel sites are necessary to avoid stratigraphic problems encountered at core breaks (Ruddiman et al., 1986b).

Similar, good sequences of Pliocene-Pleistocene age are also found on-land, in areas that underwent a strong uplift which eventually resulted in the subaerial exposure of relatively young deep-sea sediments. One of these areas, undoubtedly, is the Mediterranean. The Mediterranean has the additional advantage that its latitudinal position in combination with its semi-enclosed, land-locked configuration make its sediments particularly sensitive to record astronomically induced oscillations in climate. Sedimentary cycles of late Pleistocene age, termed sapropels (brownish coloured, organic-rich and often laminated beds), were recovered in numerous piston cores from the eastern Mediterranean (Ryan, 1972; Cita et al., 1978). These sapropels have been related to enhanced fluvial run-off, which pronouncedly affected the Mediterranean water budget and led to a diminished vertical water exchange, an- or dysoxic bottom water conditions and the deposition of a sapropel. The enhanced run-off has been connected with an increased discharge of the river Nile and European rivers due to a periodical intensification of, among others, the monsoonal system which in turn results from orbitally forced variations in low latitude summer insolation (Rossignol-Strick, 1983; Rohling and Hilgen, 1991). Periodical variations in run-off, however, do not necessarily result in sapropels because their formation depends on other factors such as basin configuration as well. Fluctuations in run-off may also lead to rhythmic variations in CaCO₃ % in the sediment due to the enhanced supply of river-borne terrigenous material at times of increased precipitation and, hence, enhanced continental run-off. This model has been put forward to explain grey coloured, CaCO₃-poor beds in the marl rhythmites of the lower Pliocene Trubi marl Formation (de Visser et al., 1989). Evidently, these rhythmites are connected with the same processes which underlie the formation of sapropels.

Such sedimentary (sapropel, CaCO₃) cycles have been found exposed on-land and in deep-sea cores throughout the Mediterranean Neogene; they are particularly common in marine sequences of Pliocene to Pleistocene age. Although it had been repeatedly suggested that these sedimentary rhythmites are connected with the Earth's orbital cycles, the inferred astronomical forcing and its potential geochronological application have never been studied systematically for the pre-Pleistocene sequences.

Reconstruction of long and uninterrupted sequences of rhythmically bedded sediments

Several factors seem to have contributed to this obvious lack of interest. The first one concerns (once more) the availability of sufficiently long and continuous sequences of rhythmically bedded sediments. Although rhythmically bedded sediments are widely exposed in the Mediterranean, especially in southern Italy, no such long sequences without breaks were yet reconstructed. Imperfections in the stratigraphic record marked in

particular the composite sequences obtained from the two key-areas for the study of the Mediterranean Pliocene - early Pleistocene: Capo Rossello (southern Sicily) for the early Pliocene and Crotona (northern Calabria) for the late Pliocene to early Pleistocene.

At an initial stage of our research, field-stratigraphic surveys were therefore carried out to overcome these stratigraphic flaws. In the area of Capo Rossello, we constructed an alternative composite section (Ch. 2). This new section is totally different from the original Capo Rossello composite of Cita and Gartner (1973; their section has been designated as neostratotype for the lowermost Pliocene stage, the Zanclean, and was formally proposed as the Miocene/Pliocene boundary stratotype), which appeared to contain a hiatus in its upper part. The new composite on the contrary contains a complete and undisturbed succession of rhythmically bedded marls of the Trubi and the lowermost part of the overlying Narbone Formation in which brownish coloured, often laminated sediments (sapropels) first occur.

The other key-area is found in the direct vicinity of Crotona in northern Calabria where a thick succession of marly clays with numerous sapropelitic interbeds of the Narbone Formation is exposed. In this area, the Pliocene/Pleistocene boundary stratotype section of Vrica and the lower-down section of Semaforo (or Stuni) are located. These two sections were supposed to be separated by a non-exposed interval with a stratigraphic thickness of less than 50 m. In order to cover this missing interval, we resorted to adjacent southern Calabria where, in the slopes of the Monte Singa, a continuous succession of the Narbone Formation could be logged (see Ch. 2). This Singa section had the additional and important advantage that, in contrast to the Vrica/Semaforo sections, it contains a stratigraphic overlap with our new Rossello composite section. For an investigation of discrepancies observed between the stratigraphic records of Monte Singa and Vrica/Semaforo, a detailed field stratigraphic survey was carried out in the Crotona area. This study unambiguously revealed that the Vrica and Semaforo sections are not separated by a non-exposed interval, but that they actually contain a considerable stratigraphic overlap (Ch. 3).

Summarizing, the new Rossello section in combination with the Singa and Vrica sections provide for a continuous composite sequence of open marine, rhythmically bedded sediments in the Mediterranean all through the Pliocene and into the early Pleistocene.

Magnetostratigraphy and the construction of a time-stratigraphic frame

Another important factor that obstructed a detailed investigation into the inferred astronomical forcing of the rhythmic bedding in the Mediterranean Pliocene and Pleistocene concerned the time-stratigraphic framework. Until recently, time-stratigraphic scales for the Mediterranean Pliocene-Pleistocene based on direct magnetostratigraphic control were completely lacking and, as a consequence, were based primarily on long-distance biostratigraphic correlations to well-dated extra-Mediterranean sequences and events (Berggren, 1973; Berggren and Van Couvering, 1974). Early attempts to establish

magnetostratigraphic records proved inconclusive (Nakagawa et al., 1975) or yielded ambiguous results (see Kennett and Watkins, 1974). Despite these rather discouraging prospects, all our sections proved suitable for the gathering of magnetostratigraphic data (Ch. 3-6). Most surprisingly, all sections in the marls of the Trubi Formation yielded good to excellent results with the exception of the thoroughly weathered lower part of the Capo Rossello composite of Cita and Gartner. Unfortunately, it was precisely this section which had been studied paleomagnetically several times before, due to the fact that it corresponds to the Miocene-Pliocene boundary stratotype.

Summarizing again, high-resolution magnetostratigraphic records have now been established for the Rossello composite section (Ch. 4, 5) as well as for the Singa and Vrica sections (Ch. 5). Combined, these records cover the complete Pliocene and lower Pleistocene and range from the lower reversed Thvera subchron of the Gilbert to well above the Olduvai subchron of the Matuyama. The resulting continuous, magnetostratigraphically controlled, composite sequence of rhythmically bedded, open marine sediments served as a starting point for our investigation into the astronomical forcing and geochronometrical application of the sedimentary cycles in the Mediterranean Pliocene-Pleistocene.

Astronomical forcing of the rhythmites and the construction of an astronomically-calibrated (polarity) time scale for the Pliocene to early Pleistocene

In order to find supportive evidence for the inferred astronomical forcing of the rhythmic bedding of the marls of the Trubi Formation (i.e. Ch. 2), we sampled the Rossello composite section in detail for CaCO₃ analyses. We applied spectral analysis on the resulting CaCO₃ record. The straightforward correlation of the high-resolution magnetostratigraphy to the Geomagnetic Polarity Time Scale (GPTS) provided us with the age calibration points necessary to generate our CaCO₃ time series (Ch. 7). Strongly significant peaks in the CaCO₃ spectrum were found in the frequency bands of the Earth's orbital cycles, indicating that CaCO₃ variations in the Trubi are indeed connected with the astronomical cycles of precession and eccentricity and, to a lesser extent, with that of obliquity. Despite this good correspondence, the spectral peaks showed a consistent shift to slightly higher frequencies than those of the orbital cycles. This shift could only be explained by an error in the conventional GPTS we used to (magnetostratigraphically) age-calibrate our CaCO₃ record. We established an alternative GPTS for the major part of the Gilbert and Gauss Chrons by applying an average periodicity of 21.7 ky of the precession cycle to the periodicity of small-scale, precession related CaCO₃ cycles in the Trubi. The Gilbert/Gauss Chron boundary dated radiometrically at 3.40 Ma was used as fixed age calibration point. This time scale, however, still depends essentially on the accuracy of the (radiometric) age of 3.40 Ma for the Gilbert/Gauss boundary. We therefore decided to make the construction of a *totally independent*, astronomically calibrated (polarity) time

scale the ultimate goal of our research.

This new, astronomically-calibrated time scale was established in two successive steps. In the first we dealt with the correlation of the rhythmically bedded sapropel sequences of late Pliocene and early Pleistocene age to the astronomical record (Ch. 8). We first established the phase relations between the sapropels and orbital cycles by tying the youngest sapropels of late Pleistocene age to the astronomical record. These phase relations were subsequently employed to calibrate the older sapropels of the late Pliocene - early Pleistocene. Because the oldest sapropels in our composite sequence start to be intercalated as late as the late Pliocene, we had to employ the CaCO₃ cycles of the Trubi Formation to extend the resulting astronomically-calibrated time scale backwards to the Miocene-Pliocene boundary (Ch. 9). In the second step of constructing the new time scale, we had to determine the sequential relationship between the CaCO₃ cycles and the sapropel cycles. Once found, this relationship subsequently allowed us to correlate the CaCO₃ cycles straightforward to the astronomical records, while using the fixed astronomical calibration points provided by the oldest sapropels in the top part of our CaCO₃ record, in addition. Accepting the accuracy of the astronomical solution, this calibration of the sedimentary cycles permits us to date all sapropels and CaCO₃ cycles with an accuracy of 1 ky. It must be noted that the use of the new astronomical solution of Berger and Loutre (1988) is of crucial importance. In contrast to the old solution, the new one is considered accurate for the last 5.0 Ma in the time domain. Since high-resolution magnetostratigraphic records are presently available for all our sections, this further implies that geomagnetic reversal boundaries can be dated with in principle the same accuracy. The new astronomically calibrated GPTS deviates considerably from the conventional time scales which, for this interval of time, rely heavily on K/Ar radiometric dating (Ch. 8, 9).

For the construction of the new astronomically calibrated GPTS for the last 5.5 Ma, we correlated the sedimentary cycles in the Mediterranean Pliocene-Pleistocene primarily to the astronomical precession and eccentricity records (Ch. 8, 9). This procedure was followed because both the sapropel and CaCO₃ cycles reflect changes in regional, low latitude climate which were dominantly controlled by precession and eccentricity in the form of 20, 100 and 400 ky cycles. However, from approximately 2.8 Ma onwards, the influence of the obliquity cycle is also clearly reflected in the planktonic foraminiferal faunal and stable isotope records from the late Pliocene and early Pleistocene (Lourens et al., *subm.*). These (obliquity forced) faunal and isotope cycles reflect glacial-interglacial alternations, which at that time were controlled dominantly by obliquity, and have, in combination with the precession and eccentricity related patterns, been used to test both the validity of the new time scale and the accuracy of the astronomical solution from 2.7 to 1.7 Ma (Ch. 10).

1.2 Acknowledgements

I am indebted to Prof. C.W. Drooger for his confidence and his efforts to secure financial support at the turning point of this investigation. I am grateful to Prof. J.E. Meulenkamp for introducing me into the geology of the Mediterranean Neogene. He let me have my way when I drastically changed the subject of my thesis. I am also grateful to Prof. J.D.A. Zijdeveld for the good cooperation and for generously tolerating the presence of a cyclostratigrapher at the Paleomagnetic Laboratorium "Fort Hoofddijk", and to Jan Willem Zachariasse and Bert van der Zwaan for their continuous support. As determined or reputed autocyclist, Bert compelled me to prove the contrary. Special thanks are due to Cor Langereis for the harmonic and productive cooperation, which I hope will continue in the future. He also is a master in users' friendly computer programming. Jan-Willem Biekart, Jan-Pieter van Dijk, Ben Driever, Larus Gudjonsson, Frans Jorissen, Lucas Lourens, Eelco Rohling, Paul Sjoerdsma, Peter Verhallen, Jan de Visser and Emiel Wijffelman are thanked for fruitful discussions on the most divergent topics.

I thank Gerrit van 't Veld and Geert Ittman for sample preparation and carbonate analysis. They put me to great expenses because of the black-pastry. Tom van Hinte and Wil den Hartog skillfully prepared most of the figures and photographs. Tom further introduced me into the magic world of autocad. Piet Jan Verplak carried out most of the paleomagnetic analyses.

The numerous fieldtrips, usually in the company of the Fort, were very pleasant indeed and not only because of the sun, wine and food. The hospitality of the Grossi family of Hotel Cerviani at the foot of the Vrica section and the Ragusa family of "Ristorante Gabbiano" at Eraclea Minoa deserves special attention.

I thank Andre Berger and Marie-France Loutre for the pleasant cooperation and stays at Louvain-la-Neuve. They always provided me kindly with their newest astronomical solution although I will never forget my despair after the receipt of Ber_89. Jean-Luc Melice patiently helped me with the statistical analyses carried out at Louvain-la-Neuve.

I am much indebted to A. Berger, W.A. Berggren, P. de Boer, M.F. Loutre, J. Oerlemans and N. Shackleton for scientific discussions. Individual chapters benefitted greatly from critical reviews of J. Channell, M.B. Cita, J. Imbrie, C. Laj, C. Kissel, W. Lowrie, I. Premoli-Silva, W.F. Ruddiman, D. Smith and several anonymous referees.

Many thanks are due to my parents for their support and to my father for his assistance and company in the field during several sample campaigns. I thank Bolle for the relaxing outings. He once even caught an almost dead and, therefore, non-edible rabbit close to the institute. Marian gave me a patient hearing of all geological (non)sense and was always willing to have another look at again and again the same (kind of) figures. Sander finally restored my ability to relativize. I hereby congratulate him with his first birthday.

References

- Adhémar, J.A., *Révolutions de la mer*, privately published, 1842.
- Berger, A., Long term variations of daily insolation and Quaternary climatic changes, *J. Atmos. Sci.*, 35, 2362-2367, 1978.
- Berger and Loutre, Insolation values for the climate of the last 10 million years, *Quat. Sci. Reviews*, 10, 1991 (in press).
- Berggren, W.A., The Pliocene time scale: calibration of planktonic foraminiferal and calcareous nannoplankton zones, *Nature*, 243, 391-397, 1973.
- Berggren, W.A. and J.A. Van Couvering, The late Neogene: biostratigraphy, geochronology and paleoclimatology of the last 15 million years in marine and continental sequences, *Palaeogeogr., Palaeoclimat., Palaeoecol.*, 16, 1-216, 1974.
- Cita, M.B. and S. Gartner, Studi sul Pliocene e sugli strati del passaggio dal Miocene al Pliocene, IV. The Zanclean stratotype. Foraminiferal and nannofossil biostratigraphy, *Riv. Ital. Pal. Stratigr.*, 79, 503-558, 1973.
- Croll, On the physical cause of the change of climate during geological epochs, *Phil. Mag.*, 28, 121-137, 1864.
- Emiliani, C., Pleistocene temperatures, *J. Geol.*, 63, 538-578, 1955.
- Fischer, A.G., Gilbert-bedding rhythms and geochronology, In: *The scientific ideas of G.K. Gilbert*, E.L. Yochelson (ed.), *Spec. Pap. geol. Soc. Am.*, 183, 93-104, 1980.
- Gibert, G.K., Sedimentary measurement of geologic time, *J. Geol.*, 3, 121-127, 1895.
- Hays, J.D., J. Imbrie and N.J. Shackleton, Variations in the Earth's orbit: Pacemaker of the Ice Ages, *Science*, 194, 1121-1132, 1976.
- Imbrie, J., J.D. Hays, D.G. Martinson, A. McIntyre, A.C. Mix, J.J. Morley, N.G. Pisias, W.L. Prell and N.J. Shackleton, The orbital theory of Pleistocene climate: Support from a revised chronology of the marine $\delta^{18}O$ record, In: *Milankovitch and Climate*, A.L. Berger et al. (eds.), *NATO ASI Ser. C*, 126, 269-305, 1984.
- Imbrie, J., A. McIntyre and A. Mix, Oceanic response to orbital forcing in the late Quaternary: observational and experimental strategies, In: *Climate and Geo-Sciences*, A.L. Berger et al. (eds.), *NATO ASI Ser. C*, 1989.
- Imbrie, J. and K. Palmer Imbrie, *Ice ages - Solving the mystery*, Harvard Univ. Press, 1-224, 1979.
- Kennett, J.P. and N.D. Watkins, Late Miocene - Early Pliocene paleomagnetic stratigraphy, paleoclimatology and biostratigraphy in New Zealand, *Bull. Geol. Soc. Am.*, 85, 1385-1398, 1974.
- Lourens, L.J., F.J. Hilgen and W.J. Zachariasse, Late Pliocene - early Pleistocene, astronomically forced surface water productivity and temperature variations in the Mediterranean (subm. to *Mar. Micropal.*).
- Mankinen, E.A. and G.B. Dalrymple, Revised geomagnetic polarity time scale for the interval 0-5 m.y. B.P., *J. Geophys. Res.*, 84, 615-626, 1979.
- McIntyre, A., W.F. Ruddiman, K. Karlin and A.C. Mix, Surface water response of the equatorial Atlantic to orbital forcing, *Paleoceanography*, 4, 19-55, 1989.
- Milankovitch, M., *kanon der Erdbestrahlung und seine Anwendung auf das Eiszeitenproblem*, *Royal Serb. Acad., Spec. Publ.*, 133, 1-633, 1941.
- Nakagawa, H., N. Niitsuma, K. Kimura and T. Sakai, Magnetic stratigraphy of Late Cenozoic stages in Italy and their correlatives in Japan, In: *Late Neogene epoch boundaries*, *Micropaleontol., Spec. Publ.*, 1, 64-70, 1975.
- Rohling, E. and F.J. Hilgen, The eastern Mediterranean climate at times of sapropel formation: a review, *Geol. & Mijnb.*, 70, 253-264, 1991.
- Rosignol-Strick, M., African monsoons, an immediate climatic response to orbital insolation, *Nature*, 303, 46-49, 1983.
- Ruddiman, W.F., D. Cameron and B.M. Clement, Sediment disturbance and correlation of offset holes drilled with the hydraulic piston corer: Leg 94, *Init. Repts. DSDP*, 94, 615-634, 1986a.
- Ruddiman, W.F., A. McIntyre and M. Raymo, Paleoenvironmental results from North Atlantic sites 607 and 609, *Init. Repts. DSDP*, 94, 855-878, 1986b.
- Ryan, W.B.F., Stratigraphy of Late Quaternary sediments in the eastern Mediterranean, In: *The Mediterranean Sea: A natural sedimentation laboratory*, D.J. Stanley (ed.), Dowden, Hutchinson and Ross, Stroudsburg, Pa., 146-169, 1972.
- Shackleton, N.J. and N.D. Opdyke, Oxygen isotope and paleomagnetic stratigraphy of equatorial Pacific core V28-238: Oxygen isotope temperatures and ice volume on a 105 and 106 year scale, *Quat. Res.*, 3, 39-55, 1973.
- Shackleton, N.J., J. Backman, H. Zimmerman, D.V. Kent, M.A. Hall, D.G. Roberts, D. Schnitker, J.G. Baldauf, A. Desprairies, R. Homrighausen, P. Huddleston, J.B. Keene, A.J. Kaltenback, K.A.O. Krumsiek, A.C. Morton, J.W. Murray and J. Westberg-Smith, Oxygen isotope calibration of the onset of ice-rafting and history of glaciation in the North Atlantic region, *Nature*, 307, 620-623, 1984.
- de Visser, J.P., J.H.J. Ebbing, L. Gudjonsson, F.J. Hilgen, F.J. Jorissen, P.J.J.M. Verhallen and D. Zevenboom, The origin of the rhythmic bedding in the Pliocene Trubi Formation of Sicily, southern Italy, *Palaeogeogr., Palaeoclim., Palaeoecol.*, 69, 45-66, 1989.
- Urey, The Thermodynamic properties of isotopic substances, *J. Chem. Soc.*, 562-581, 1947.

Chapter 2

Sedimentary rhythms and high-resolution chronostratigraphic correlations in the Mediterranean Pliocene

by FREDERIK J. HILGEN*

with 8 figures

Abstract. In the Mediterranean Pliocene, rhythmic lithological variations in the Trubi and Narbone Formations (Pliocene – Lower Pleistocene) of Sicily and Calabria can be used to obtain detailed (“bed-to-bed”) chronostratigraphic correlations with a potential resolution of 20,000 years or less.

The superimposed sedimentary rhythms can be attributed mainly to the differential dilution of carbonates by terrigenous clastics, the process being caused by periodical fluctuations in precipitation and runoff. Our calculations suggest that the rhythms are connected with the astronomical cycles of precession (21 Ka) and eccentricity (100 and 400 Ka).

Interpolation of the rhythmites permits a calibration of the total Mediterranean Pliocene to the numerical time-scale.

Zusammenfassung. Rhythmische Schichtung in den Trubi- und Narbone-Formationen von Sizilien und Kalabrien (Pliozän – Unter-Pleistozän) ermöglicht im Prinzip chronostratigraphische Korrelationen mit einem potentiellen Auflösungsvermögen von 20.000 Jahren oder sogar weniger.

Die vorliegenden sedimentären Rhythmen sind in erster Linie auf die variierende Verdünnung der Karbonat-Komponente durch terrigenes Material zurückzuführen. Das wiederum wurde durch periodische Fluktuationen von Niederschlag und oberirdischem Abfluß verursacht. Unsere Kalkulationen deuten auf einen Zusammenhang mit den astronomischen Zyklen der Präzession (21 Ka) und Exzentrizität (100 und 400 Ka).

Die Interpolation der Rhythmite erlaubt eine absolute Kalibrierung des gesamten mediterranen Pliozäns.

Introduction

At present detailed biostratigraphic correlations can be made on the basis of existing biozonations in the Mediterranean Pliocene using planktonic foraminifera (CITA 1975a, SPAAK 1983) and calcareous nannofossils (RAFFI & RIO 1979). It is suggested that the regional zonal units in question bear chronostratigraphic significance. A further refinement can be obtained by utilizing rhythmic sedimentation patterns characterized by sapropelitic or diatomaceous intercalations as shown by RYAN (1972) and THUNELL et al. (1977) for the Pleistocene of the Eastern Mediterranean and by JONKERS (1984) for the Pliocene of Crete.

* Author's address: FREDERIK J. HILGEN, Department of Stratigraphy/Micropaleontology, State University of Utrecht, Budapestlaan 4, 3508 TA Utrecht, The Netherlands.

The occurrence of rhythmic bedded sediments in the Mediterranean Pliocene is widespread in marginal (MEULENKAMP et al. 1979, JONKERS 1984) as well as in deep-sea basins (KIDD et al. 1978). In the present paper we study the application of high-resolution chronostratigraphic correlations using the rhythmic sediment patterns in the Pliocene Trubi and Monte Narbone Formations of Sicily and Calabria. The rhythmicity is characterized by fluctuations in the carbonate content of marls in the Trubi or, in case of the Monte Narbone Formation, by alternations of homogeneous marly clays and sapropelitic sediments.

Geological setting and sections

For our study we selected several sections which jointly cover the Pliocene in the appropriate, rhythmic bedded lithofacies. These sections are situated on the external side of the Calabro – Sicilian Arc, i. e. in the Caltanissetta Basin of Sicily and the Crotona – Spartivento Basin of Calabria (Fig. 1).

Three formations can generally be distinguished in the Pliocene to Lower Pleistocene of the Caltanissetta Basin. Rhythmic bedded marls of the Trubi Formation which usually conformably overlie Upper Messinian deposits constitute the lowermost Pliocene unit in this area. The next higher unit consists of marly clays, locally with sapropelitic interbeds, of the Narbone Formation, which underlie sandstones of the Agrigento Formation. The formations can be correlated to their lithostratigraphic equivalents in South Calabria.

The Caltanissetta Basin is well known for its Pliocene outcrops, especially along the south coast and the line Enna – Centuripe (DI GRANDE et al. 1976) on central Sicily. For our study the coastal sections are more suitable since in that area, in contrast to central Sicily, the deposition of rhythmic bedded sediments was continuous into the Late Pliocene. This is mainly due to the time-transgressive nature of the Trubi – Narbone – Agrigento depositional system in which the facies-transitions become younger towards the south.

For this reason we selected the south coast of Sicily as location for a standard section. Due to the absence of sapropelitic interbeds in the upper part of the Narbone Formation in this area, we chose the South Calabrian Singa section as an additional standard. Furthermore ZIJDERVELD et al. (1986) provided us with a reliable magnetostratigraphy for the lower part of this section.

Standard sections

The Rossello-Eraclea Minoa composite section of Sicily

Excellent Pliocene sections along the south coast of Sicily are exposed in the classical Rossello area and at Eraclea Minoa (Fig. 1). Several Pliocene composite sections based on exposures in the Rossello area have been introduced in the literature during the last fifteen years (CITA & GARTNER 1973, BROLSMA 1978, SPAAK 1983, RIO et al. 1984). These sections, however, proved to be only partly suitable for our study.

The Capo Rossello section as described in detail by CITA & GARTNER (1973) is known to contain a hiatus between the Trubi and Narbone Formations (RIO et al. 1984). The Capo Rossello composite section of SPAAK (1983) on the contrary contains several “slump” levels in

Sedimentary rhythms

the Punta di Maiata section. RIO et al. (1984) incorporated the Punta Piccola section of BROLSMA (1978) and SPAAK (1983) in the Capo Rossello composite section of CITA & GARTNER (1973). However, according to RIO et al. (1984) the existence of a small gap in the top part of the Trubi still cannot be ruled out. This gap can be avoided by using the Punta Grande section (Fig. 1B).

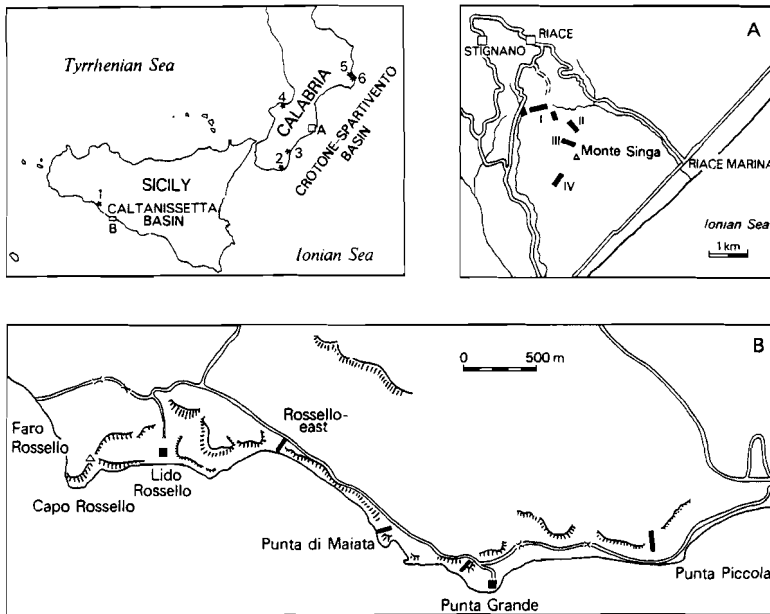


Fig. 1. Locations of the Sicilian - Calabrian sections: 1. Eraclea Minoa; 2. Spropolo; 3. Careri; 4. Paradisani; 5. Vrica; 6. Semaforo section; 1A: Singa area, and 1B: Rossello area.

In the classical Rossello area we selected the sections Rossello-east, Punta di Maiata, Punta Grande and Punta Piccola (for locations see Fig. 1B) which jointly cover a complete and relatively undisturbed succession. The Rossello-east section is identical to sample interval A and C of CITA & GARTNER (1973) and corresponds partly to exposure 3 of BROLSMA (1978) since the latter continues into the diatomite-bearing sequence that lies above. In this respect our Rossello-east section exactly matches the lithostratigraphic intervals A-C of GUERRERA et al. (1984). Our Punta di Maiata section consists of the lower part (i. e. preceding the "slump" levels) of the Punta di Maiata section of SPAAK (1983). The Punta Piccola section corresponds to the Punta Piccola section of BROLSMA (1978) and SPAAK (1983) but was extended further

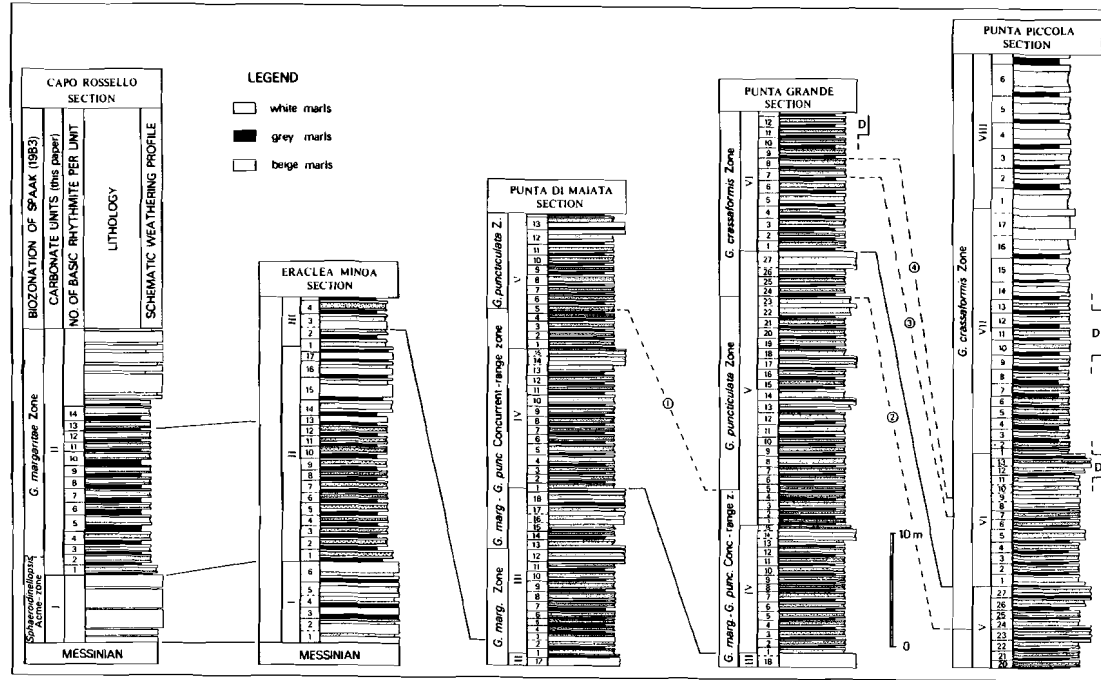


Fig. 2. The Rossello composite section showing lithology, biostratigraphy and subdivision in carbonate units and basic rhythmities. Beige marls are shown schematically with respect to the white marls except in the prominent carbonate levels. Sapropelitic interbeds are not shown separately with respect to the grey marls in the Punta Piccola section. Solid lines represent lithostratigraphic correlations. Dashed lines represent biostratigraphic correlations: 1. LOD of *G. margaritae*; 2. LOD of *G. punctulata*; 3. Re-appearance datum of *G. crassaformis*, and 4. FOD of *G. bononiensis*. D: dextral intervals of *G. crassaformis*. Biostratigraphy is based on SPAAK (1983) and unpublished data. The boundary between carbonate unit VI and VII corresponds to the Trubi - Narbone transition.

Sedimentary rhythms

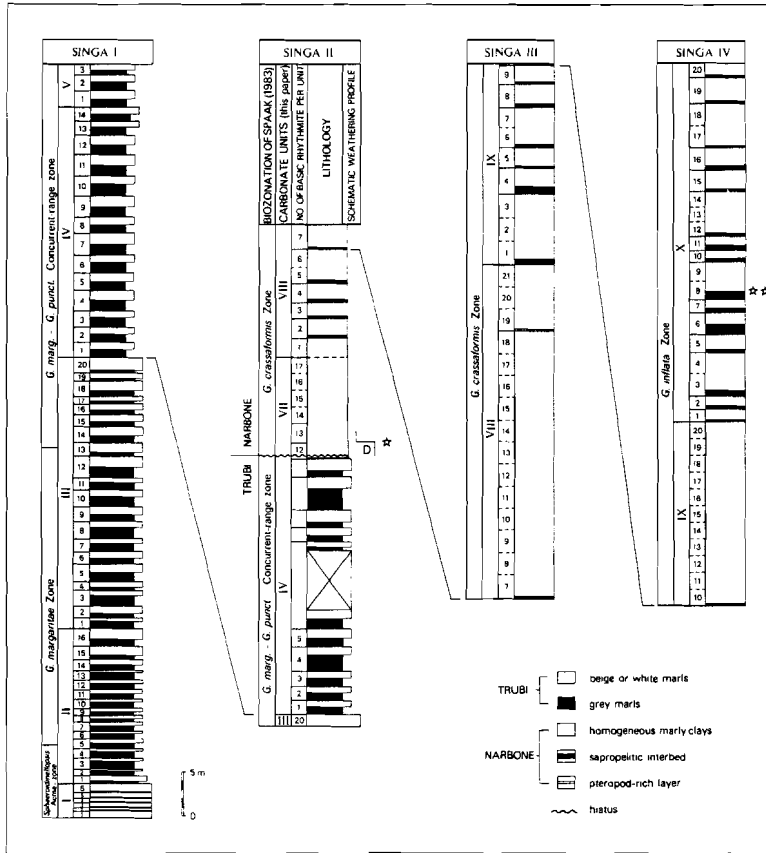


Fig. 3. The Singa composite section showing lithology, biostratigraphy and subdivision in carbonate units and basic rhythmites. Solid lines represent lithostratigraphic correlations. D: dextral *G. crassaformis*. The asterisk marks the top of the second dextral interval of *G. crassaformis* of SPAAK (1983) used for correlation to the Rossello – Eraclea Minoa composite section. The double asterisk marks the Plio-Pleistocene boundary based on the detailed correlation to the Vrica section (VERHALLEN, in press).

downwards as in RIO et al. (1984). For this study we further included the Eraclea Minoa section, located some 20 km to the west, as a suitable alternative for the Rossello-east section.

The resulting Rossello – Eraclea Minoa composite section, including both the Rossello-east and Eraclea Minoa sections, is shown in detail in Fig. 2. The Punta Piccola section contains the transition from the Trubi to the Narbone Formation which biostratigraphically falls within the *G. crassaformis* Zone of SPAAK (1983). The top of our composite section still belongs to this planktonic foraminiferal zone (Fig. 2).

The Singa section of South Calabria

The Singa composite section and biostratigraphic data are shown in detail in Fig. 3. The locations of the subsections I–IV are indicated in Fig. 1A.

The succession can be divided into two major lithostratigraphic units which show a strong resemblance to the Sicilian Trubi and Narbone Formations. Biostratigraphic data (Fig. 3) indicate that these two units are separated by a major hiatus which corresponds to part of the *G. margaritae* – *G. puncticulata* Concurrent-range zone, the entire *G. puncticulata* Zone and part of the *G. crassaformis* Zone of SPAAK (1983). Above the hiatus the sedimentary record is continuous into the Pleistocene.

The sediment patterns

Basic rhythmite: In South Calabria the internal structure of the sedimentary rhythms is less complex than in the Trubi Formation of the Caltanissetta Basin of Sicily (Fig. 4). The Calabrian equivalent of the Sicilian Trubi consists of a rhythmic alternation of beige or white, indurated, carbonate-rich marls and grey, softer, carbonate-poor marls.

BASIC RHYTHMITE	LITHOLOGY	SICILIAN TRUBI			BASIC RHYTHMITE	LITHOLOGY	CALABRIAN TRUBI	
		a = grey	b, d = white	c = beige marls			A = grey	B = beige or white marls
3	c	[Pattern: dotted]			3	B	[Pattern: dotted]	
	b	[Pattern: white]				A	[Pattern: white]	
	a	[Pattern: grey]				[Pattern: grey]		
2	d	[Pattern: white]			2	B	[Pattern: dotted]	
	c	[Pattern: dotted]				A	[Pattern: white]	
	b	[Pattern: white]				[Pattern: white]		
	a	[Pattern: grey]				[Pattern: grey]		
1	d	[Pattern: white]			1	B	[Pattern: dotted]	
	c	[Pattern: dotted]				A	[Pattern: white]	
	a	[Pattern: grey]				[Pattern: grey]		

Fig. 4. Internal build-up of typical basic rhythmite in the Trubi of Sicily and South Calabria.

Sedimentary rhythms

The Sicilian Trubi usually shows a further differentiation owing to differences in colour and the degree of induration in the indurated marl beds. Beige marls are intercalated between white, more indurated and carbonate-rich beds. Occasionally this feature can vaguely be recognized in the marl doublets of the Calabrian Trubi. Consequently a marl doublet in South Calabria matches a quadruplet in the Sicilian Trubi (Fig. 4).

Irrespective of the laminated diatomaceous sediments at Rossello, as described in detail by BROLSMA & BROEKMAN (1978) and GUERRERA et al. (1984), these doublets or quadruplets provide the basic sedimentary rhythm in the Trubi successions and are further referred to as basic rhythmmites. The top of such a basic rhythmite is placed arbitrarily at the base of the softer, grey marl. The rhythmmites can also be recognized in the Punta Piccola section, the sapropelitic interbeds of the Narbone Formation being intercalated in the grey marls (a in Fig. 4; see also Fig. 5).

Carbonate units: In addition to these basic rhythmmites several well-pronounced, thicker and more indurated marl levels can be identified in the successions.

In Sicily such prominent levels do not result from an increase in bed-thickness only, since they are internally composed of the same basic rhythmmites. Preliminary results of carbonate analyses suggest that these levels are characterized by an overall increase of the carbonate content in the beige, and especially in the grey marls relative to the white marls. Consequently both softer types of marls (a and c in Fig. 4) start to resemble the white marls (b and d) in the quadruplets and the individual beds of the basic rhythmmites become difficult to distinguish.

In the Sicilian standard section the prominent levels occur singly or in composite groups at relatively regularly spaced intervals in the succession (see Figs. 2, 5). Up to three normal marl quadruplets can be intercalated between successive prominent levels of such a composite group (see Fig. 2). Their presence permits a subdivision into larger-scale units, the boundaries of which have been placed at the top of such a single or composite group of prominent levels. These units are further termed carbonate units as they reflect large-scale fluctuations in the carbonate content.

Within these carbonate units the individual quadruplets have been counted and numbered (Figs. 2, 5). However, carbonate unit boundaries do not necessarily coincide with the top of a quadruplet. Such quadruplets straddling a unit-boundary are incorporated in the carbonate unit to which the more indurated lithologies (b-d, Fig. 4) belong.

Calabria: In the Singa area the visual impression of the Trubi is dominated by the recurrence of prominent, thick and indurated marl beds in the succession. These prominent beds coincide with a stepwise decrease in the degree of induration of the marls, as indicated schematically in Fig. 3. The presence of these beds allows for a subdivision into carbonate units analogous to the Sicilian record (Fig. 3).

Above the hiatus in the Singa section, the succession contains numerous sapropelitic intercalations like the Narbone Formation in the Punta Piccola section of Sicily. These interbeds occur in three major groups separated by homogeneous marly clay intervals (see Fig. 3).

As a consequence of the hiatus, direct counting and numbering of basic rhythmmites and carbonate units from the base of the Pliocene can only be realized for the Trubi Formation in

the Singa section. However, the numbering can be continued above the hiatus in the upper, Narbone part of the section due to the detailed biostratigraphic correlation between the Singa and the Rossello – Eraclea Minoa standard sections (Figs. 2, 3; top second dextral interval of *G. crassaformis* in Zone 6 of SPAAK 1983). Although this correlation solves the problem of the hiatus, we are, nevertheless, faced with two major problems in the Narbone Formation of the Singa section: 1) how to recognize the basic rhythmites, and 2) how to recognize the carbonate units.

1) Above the hiatus the bedding is distinct only for the sapropelitic interbeds. The base of a sapropel can hereby be assumed to correspond to the base of a basic rhythmite since in the Punta Piccola section the sapropelitic interbeds of the Narbone Formation are clearly intercalated in the grey marls (a in Fig. 4) of the basic rhythmites (see also Fig. 5). However, the presence of relatively thick, homogeneous marly clay intervals both within and between the major groups of sapropelitic interbeds seems to exclude further counting of the basic rhythmites in this part of the Pliocene record.

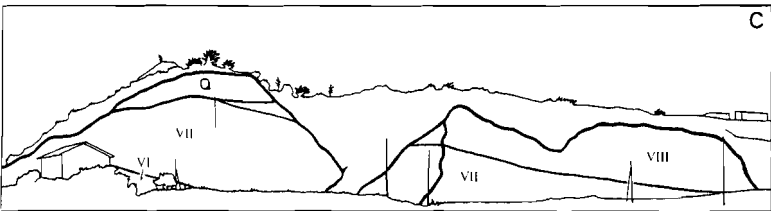
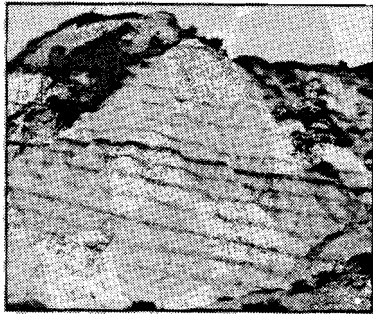
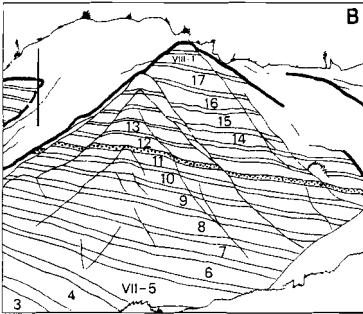
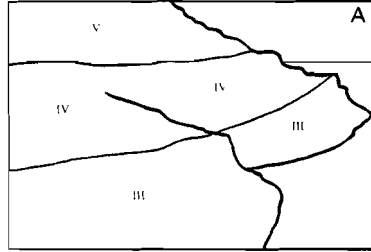
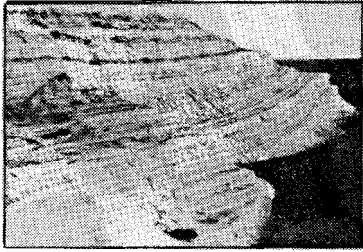
In order to tackle this complication we obtained the mean thickness of basic rhythmites by calculating the average distance between regularly spaced sapropelitic interbeds thus excluding intervals in which the inter-sapropel distance is significantly larger. Interpolation and extrapolation of this average thickness to the excluded homogeneous intervals (both within and between the major groups of sapropelitic interbeds) provides us with an estimate of the total number of basic rhythmites. Hereby we assume that the sapropelitic interbeds, i. e. the lithologic expression of the basic rhythmites in the Narbone Formation, are not developed in these homogeneous intervals, the assumption being confirmed by our observations in the Punta Piccola section in which both the basic rhythmites and the sapropelitic interbeds are visible.

2) The (i. e. in contrast to the Narbone Formation in the Punta Piccola section) obvious lack of the prominent carbonate levels previously used to delimit carbonate units seems to prevent a meaningful numbering of successive carbonate units in the Narbone Formation of the Singa section.

However, the basic rhythmites in the prominent carbonate levels in the upper part of the Punta Piccola section clearly lack sapropelitic interbeds, the latter being generally well developed in between (Fig. 5). On the basis of this observation we assume that these prominent levels correspond or are at least partly equivalent to the thick, homogeneous marly clay intervals intercalated between the major groups of sapropelitic interbeds in the upper part of the Singa section. Boundaries of carbonate units have been placed at the base of the first sapropelitic interbed of a major group, as suggested by the transition from unit VII to VIII in the Punta Piccola section (see Fig. 5).

Fig. 5. Figures showing the position of the carbonate units in the Punta di Maiata section (A) and of the carbonate units and the basic rhythmites in the Punta Piccola section (B,C). Note the position of the sapropelitic interbeds with respect to the basic rhythmites and the prominent carbonate levels in the Punta Piccola section. The dotted bed corresponds to sapropel G of BROLSMA (1978). Q: Quaternary terrace deposits. Photo's B and C after BROLSMA (1978).

Sedimentary rhythms



If we assume the procedures outlined above to be correct we can continue delimiting and numbering the carbonate units and the basic rhythmities (per carbonate unit) in the upper part of the Singa section, as indicated in Fig. 3. We calculated the number of basic rhythmities separately for the Narbone Formation in Singa II, III and IV in order to reduce the influence of changes in sedimentation rates.

Correlations: Nature, accuracy and potential

High-resolution lithostratigraphic correlations in the Trubi and Narbone Formations of Sicily and Calabria

Trubi Formation: The succession of the Trubi in the Singa section and the corresponding biostratigraphic interval of the Rossello – Eraclea Minoa composite section are depicted in Fig. 6, which demonstrates that there is a close correspondence in the number and pattern of the basic rhythmities.

The significantly thicker than average rhythmities nos. 6 and 20–22 can be recognized in both sections. The thicker than average rhythmite no. 42 in the Singa section can be correlated to no. 41 in the Sicilian record. This difference may be due to the problems encountered in logging the most prominent marl level in the Punta di Maiata section.

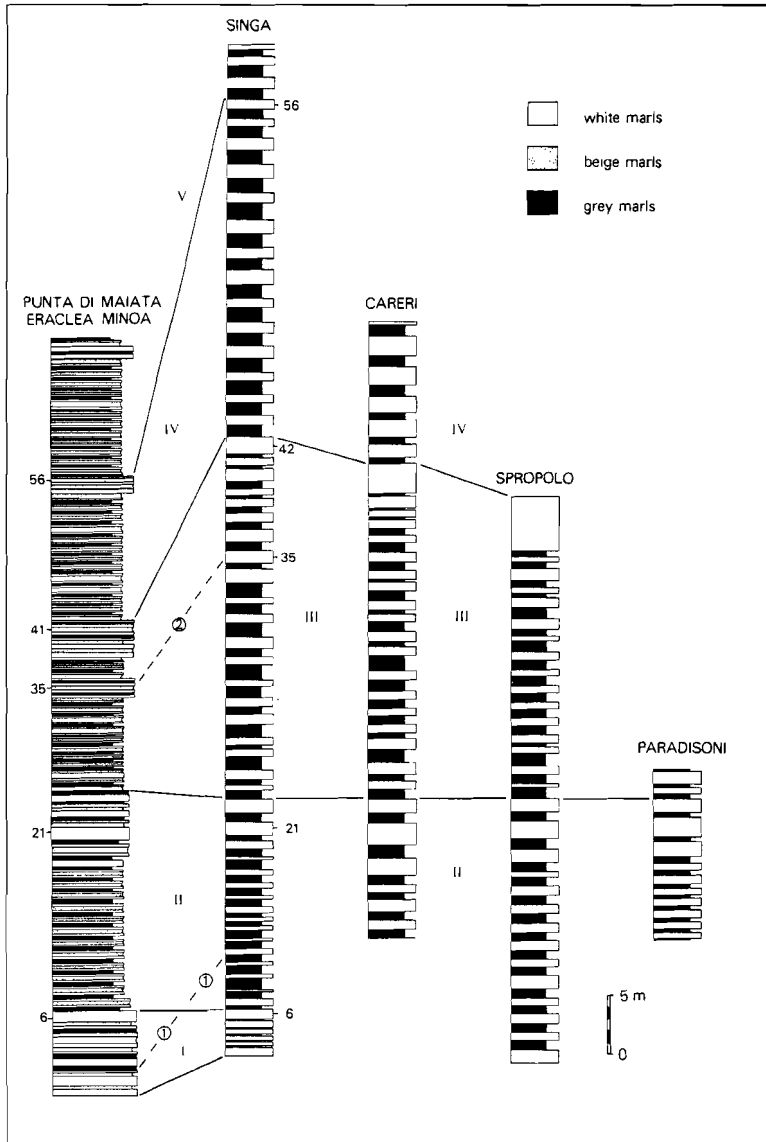
However, small discrepancies in the number of basic rhythmities per carbonate unit can be observed between the standard sections. This can be explained by the arbitrariness of the criterion used to delimit carbonate units in relation to differences in the appearance of the Sicilian and Calabrian Trubi. The carbonate units I–IV, nevertheless, contain the same total number of basic rhythmities in both standard sections.

A number of additional Calabrian sections (for locations see Fig. 1) have been included in the lithostratigraphic correlation scheme (Fig. 6) in order to illustrate the correlation potential of our subdivision.

Narbone Formation: In the Narbone Formation high-resolution lithostratigraphic correlations are necessarily based upon the characteristic pattern of the sapropelitic interbeds. We assume this procedure to be correct since VERHALLEN (in press) demonstrated that the sapropelitic interbeds in the Singa section perfectly match the pattern in the Vrica – Semaforo composite section (North Calabria; for location see Fig. 1). The major groups of sapropelitic interbeds can also be recognized in the Sicilian Monte San Nicola section of SPAAK (1983).

Fig. 6. Correlation scheme for the Trubi Formation showing Singa I and (part of) the Rossello – Eraclea Minoa composite section as well as some additional South Calabrian sections. Solid lines represent lithostratigraphic correlations of the carbonate units indicated by roman numerals. Total nos. of relevant basic rhythmities in the standard sections are indicated by normal figures. Dashed lines represent biostratigraphic correlations: 1. FOD of *G. margaritae*, and 2. FOD of *G. puncticulata*.

Sedimentary rhythms



Time-stratigraphic significance

Planktonic foraminiferal datum planes are considered to represent an accurate approximation of isochronous horizons in the Mediterranean Pliocene. Therefore the time-stratigraphic significance of the lithostratigraphic correlations outlined above is strongly supported by the position of the FOD (first occurrence datum) of *G. puncticulata*. The flood-entry of this species, which marks one of the most reliable Pliocene Mediterranean datum planes, is recorded in the indurated marl bed of basic rhythmite no. 35 in both standard sections (Fig. 6). Planktonic foraminiferal datum planes further perfectly match the detailed lithostratigraphic correlations between the Singa and the Vrica – Semaforo composite section based on the characteristic pattern of sapropelitic interbeds as proposed by VERHALLEN (in press).

The FOD of *G. margaritae* is the only exception (Fig. 6). However we assume that sporadic specimens of this species may be encountered from the base of the Pliocene onwards since SPROVIERI (1978) pinpointed *G. margaritae* directly above the base in the Miocene – Pliocene boundary stratotype section (CITA 1975b) at Rossello. The FOD of *G. margaritae* thus precedes the *Sphaeroidinellopsis* acme in this section.

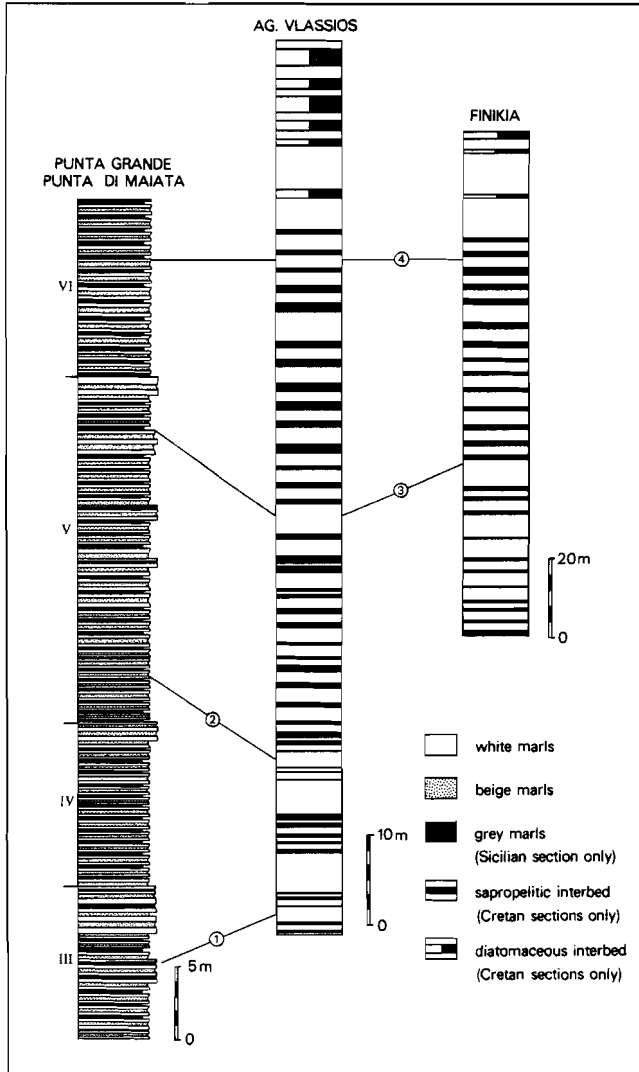
Mean durations of the rhythms and accuracy of the correlations

ZIJDERVELD et al. (1986) presented a detailed magnetostratigraphic record for the lower, Trubi part of the Singa section. On the basis of the calibration to the geomagnetic timescale, they calculated a mean duration of 20.5 Ka for the deposition of a basic rhythmite.

For the total Pliocene the estimated number of basic rhythmites comes to 161 as evidenced in the composite column of the Sicilian and Calabrian standard sections (Figs. 2, 3). As the Pliocene boundaries have been reliably dated at 4.84 (ZIJDERVELD et al. 1986) and 1.64 Ma. (AGUIRRE & PASINI 1985), this amounts to a mean duration of 19.9 Ka, the value being close to that obtained for parts of the Singa section (ZIJDERVELD et al. 1986). Evidently the rhythmic bedding is determined by a cyclic sedimentation process. Hence chronostratigraphic correlations with a resolution of some 20,000 years and interpolated fractions thereof can be obtained for the Trubi and Narbone Formations of Sicily and Calabria.

For the Pliocene this furthermore leads to a mean duration of 370 Ka for a carbonate unit if we exclude the supposedly incomplete carbonate units I and X $((3,200,000 - 12 \times 20,000) / 8$, eight being the number of carbonate units, twelve the number of basic rhythmites of the carbonate units I and X in the Pliocene). Carbonate unit I is abruptly preceded by the Arenazzolo unit in the Rossello – Eraclea Minoa composite section and by conglomeratic sandstones in the Singa section, which are both considered to be of Late Messinian age; the Plio – Pleistocene boundary is located within carbonate unit X (Fig. 3).

Fig. 7. Scheme showing biostratigraphic correlations between part of the Sicilian standard section and a number of Cretan sections: 1. FOD of *G. puncticulata*; 2. LOD of *G. margaritae*; 3. LOD of *G. puncticulata*, and 4. FOD of *G. bononiensis*. Roman numerals indicate the carbonate units in the Sicilian standard. Cretan sections after JONKERS (1984).



The pattern of sapropelitic interbeds in the Singa section reveals the existence of a third rhythm, this one being of intermediate duration. Especially the sapropelitic interbeds in the middle and upper sapropel group can be easily arranged into smaller concentrations of 1 to 4 sapropels. Such concentrations usually comprise 4 to 6 basic rhythmites between the first sapropelitic interbeds of successive subgroups. This amounts to a duration of 80–120 Ka for the deposition of this intermediate rhythm. Such an arrangement of basic rhythmites is also recognizable in the Punta Grande and Punta Piccola sections (Fig. 2) and in the weathering profile of Punta di Maiata (Fig. 5). Obviously this rhythm accounts for the occurrence of the prominent marl levels in composite groups.

Mediterranean correlations

JONKERS (1984) gave a detailed account of rhythmic bedded sediments from the Pliocene of Crete. In Fig. 7 we correlated the corresponding biostratigraphic interval of the Rossello – Eraclea Minoa composite section to the more suitable sections of JONKERS.

The number of basic rhythmites in the Sicilian standard matches exactly the number of sapropelitic interbeds in the Cretan sections for the interval between the LOD of *G. puncticulata* (its position in all sections confirmed by the first influx of *G. crassaformis* slightly below) and the FOD of *G. bononensis*. Discrepancies we found for the biostratigraphic intervals below the LOD of *G. puncticulata*. The discrepancy is small for the interval between the LOD's of *G. margaritae* and *G. puncticulata*, but increases strongly downwards. For these intervals the number of basic rhythmites in Sicily exceeds the number of sapropelitic interbeds in the Cretan sections. Apparently the basic rhythmites are not recorded in the succession when sapropelitic interbeds are missing conformable the situation in the Narbone Formation of the Singa section. This may explain why periodicities calculated solely from the number of sapropels (MEULENKAMP et al. 1979) give exceedingly high values of the order of 30,000–40,000 years.

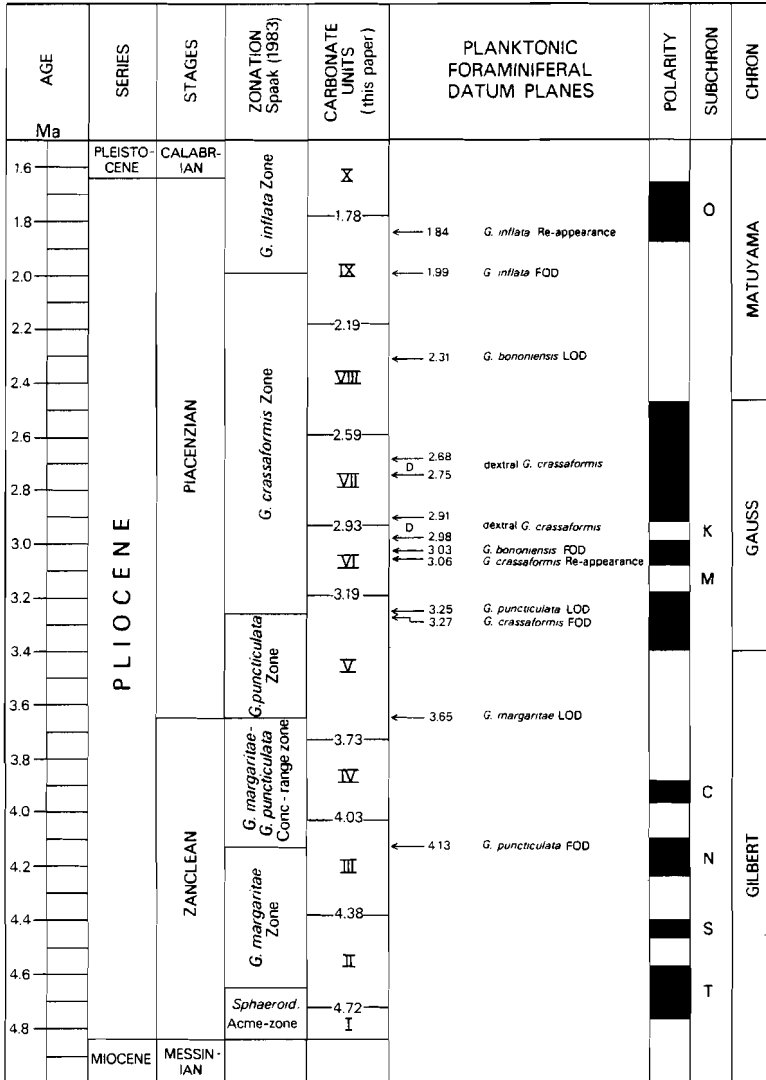
The biostratigraphic correlations further show that the prominent Sicilian marl levels delimiting our carbonate units can be correlated with the anomalously thick homogeneous levels reported by JONKERS (1984) in his Cretan sections (Fig. 7).

Pliocene time-scale

Direct calibration of the Mediterranean Pliocene record to the numerical time-scale has not been possible until recently due to the scarcity or unreliability of paleomagnetic and radiometric data. As a consequence previous attempts to realize a Mediterranean Pliocene time-frame-work were based mainly upon biostratigraphic correlations to the calibrated extra-Mediterranean record and should therefore be used with caution.

Fig. 8. Pliocene time-scale for the Mediterranean based on the interpolation of basic rhythmites showing numerical ages for selected planktonic foraminiferal datum planes and standard carbonate units. Standard carbonate units I–VII are defined in the Rossello – Eraclea Minoa composite section and standard carbonate units VIII–X in the Singa section. The geomagnetic time-scale is that of BERGGREN et al. (in press).

Sedimentary rhythms



Recent paleomagnetic and radiometric studies (OBRADOVITZ et al. 1982, TAUXE et al. 1982, ZIJDERVELD et al. 1986) now permit reliable dating of the Pliocene boundaries. However, these studies are limited to the lower and uppermost parts of the Mediterranean Pliocene. Interpolation of basic rhythmites allows the total Pliocene record to be calibrated to the numerical time-scale using as calibration points the numerical ages of 4.84 (ZIJDERVELD et al. 1986) and 1.64 (AQUIRRE & PASINI 1985) Ma for the boundaries. The resulting scheme for the Mediterranean Pliocene is shown in Fig. 8. Numerical ages for selected datum-planes and for standard carbonate units have been included in this figure. For the subdivision in standard carbonate units we selected the Rossello – Eraclea Minoa composite section for the carbonate units I–VII and the Singa section for the units VIII–X.

Origin of the rhythmic variations

As should be clear from the preceding sections the characteristic rhythms in the Trubi and Narbone Formations must be the result of similar sedimentary processes. In fact we consider the sapropelitic interbeds to represent a different sedimentary expression of the carbonate-poor beds (a, A in Fig. 4) in the basic rhythmites of the Trubi Formation.

Primary rhythmic or cyclic variations in the carbonate content in hemipelagic successions, which are considered to cause the characteristic sedimentary patterns of the Trubi Formation, can generally be attributed to fluctuations in either carbonate dissolution, carbonate production or dilution by terrigenous clastics (EINSELE 1982, ARTHUR et al. 1984). Dissolution as the primary factor can be excluded since the frequency patterns of planktonic foraminifera show no indications in this direction and the dissolution-susceptible taxa are generally well preserved in the carbonate-poor beds (based on the data of SPAAK 1983). Primary production is very unlikely to have played a decisive role either. The frequency patterns of the planktonic foraminifera point to even more fertile conditions in the upper water layers during the deposition of laminated beds (SPAAK 1983) which are intercalated in the carbonate-poor marls of the Punta Piccola section.

Various arguments indicate that the sedimentary successions of the Trubi and Narbone do indeed represent records of differences in the amount of admixture of terrigenous clastics. JONKERS (1984) attributed a higher pelite content in sapropels to a greater input of terrigenous clastic material. He further mentioned the occurrence of turbiditic sand-layers in thick sapropelitic interbeds in a proximal setting. Such intercalations evidently suggest a local source for the terrigenous clastics.

Several authors (SPAAK 1983, JONKERS 1984, GUDJONSSON & VAN DER ZWAAN 1985) attributed the formation of Pliocene laminites to periodical increases in continental run-off. According to these authors increased run-off promotes the development of a low salinity surface layer and a density stratification of the water column. This process eventually results in an oxygen depletion of the bottom waters. The deposition of sapropelitic sediments starts when the threshold value of 0.5 ml O₂/l is reached (DEMAISON & MOORE 1980).

Stronger run-off also accounts for the increased influx of terrigenous clastics during the deposition of the laminites. In fact we consider this mechanism to be responsible for the deposition of the more clayey interbeds (a, A in Fig. 4) in the basic rhythmites of the Trubi as

Sedimentary rhythms

well. At present this assumption is strongly confirmed by the stable isotope data from the lower part of the Singa section (GUDJONSSON, in press). The difference in sedimentary expression of the basic rhythmities in the Trubi and Narbone Formations may simply be related to variations in the intensity of the processes outlined above. However, other important controlling factors as basin configuration (MEULENKAMP et al. 1979) and sedimentation rate (DEMAISON & MOORE 1980) can be held responsible as well.

Fluctuations in run-off can be climatically translated into relatively humid spells alternating with dry climatic conditions. An elaborate precipitation model has been developed by ROSSIGNOL-STRICK (1983, 1985) in connection with Middle and Upper Pleistocene sapropels in the Eastern Mediterranean. She attributed their formation to a periodical increase of the discharge of the river Nile under influence of variations in the monsoonal precipitation activity in its catchment area. However this model does not account for the supposedly local origin of the terrigenous clastics in the Pliocene. Furthermore GUDJONSSON & VAN DER ZWAAN (1985) showed that there was a similarity between the stable isotope composition of the Pliocene run-off waters and present-day mid-latitude river discharge. These data are, at least for the Pliocene, difficult to reconcile with the river Nile as the main fresh water source. In fact this may imply that during this period of time the monsoonal activity extended periodically far to the north.

According to the model of ROSSIGNOL-STRICK, the monsoonal precipitation activity is determined by the solar insolation in the tropical latitudes. Long-term variations in the insolation are controlled by astronomical cycles (which describe the variation in the Earth's orbit), in the low latitudes especially by the cycles of precession and eccentricity (BERGER 1978).

The periodicity of the precession cycle of 21,000 years (BERGER 1984) corresponds well with the mean duration we calculated for the deposition of the basic rhythmities. The eccentricity cycle of about 400,000 years would match the average duration of our carbonate units. The intermediate rhythm recognized in the arrangement of sapropelitic interbeds may reflect the 100,000 years eccentricity cycle.

We assume that all these astronomical cycles have a distinct influence on the amount of precipitation and run-off and that their interference pattern can be expected to be reflected in the sediment. Such an interference pattern may also account for irregularities as a consequence of opposite effects. It explains the varying number of basic rhythmities in our carbonate units as well as the rare occurrence of sapropels in the Eastern Mediterranean during Pleistocene glacial periods (see also ROSSIGNOL-STRICK 1983, 1985).

We suggest that the "precipitation" cycles represent a regional climatic process which can be correlated to time-equivalent global changes. This is perfectly understandable in view of the suggested relationship between the inferred rhythmic sedimentary/regional climatic processes and the astronomical cycles as the controlling mechanism. In this respect the Pliocene fluctuations correspond to the Pleistocene cyclic climatic processes, although the intensity seems to be far less due to supposed differences in feed-back mechanisms. The "precipitation" cycles in fact correspond to the old Pleistocene concept of pluvials and interpluvials.

Finally high-resolution chronostratigraphic correlations are an indispensable tool if we are to better understand the detail of these processes.

Acknowledgements. Thanks are due to J. E. MEULENKAMP and J. P. DE VISSER for their assistance in the field. C. W. DROOGER, L. GUDJONSSON, J. E. MEULENKAMP, J. W. ZACHARIASSE and G. J. VAN DER ZWAAN critically read earlier versions of the manuscript. Their suggestions are gratefully acknowledged. The illustrations were made by W. DEN HARTOG, T. VAN HINTE and P. HOONHOUT. Linguistic corrections were made by S. M. McNAB.

References

- AQUIRRE, E. & G. PASINI (1985): The Pliocene – Pleistocene boundary. – *Episodes* 8: 116–120.
- ARTHUR, M. A., W. E. DEAN, D. BOTTJER & P. A. SCHOLLE (1984): Rhythmic bedding in Mesozoic–Cenozoic pelagic carbonate sequences: the primary and diagenetic origin of Milankovitch-like cycles. – In: A. BERGER, J. IMBRIE, J. HAYS, G. KUKLA & B. SALTZMAN (eds.): *Milankovitch and Climate*. – NATO ASI Ser. C. 126 (1): 191–222.
- BERGER, A. L. (1978): Long-term variations of caloric insolation resulting from the earth's orbital elements. – *Quat. Res.* 9: 139–167.
- BERGER, A. (1984): Accuracy and frequency stability of the earth's orbital elements during the Quaternary. – In: A. BERGER, J. IMBRIE, J. HAYS, G. KUKLA & B. SALTZMAN: *Milankovitch and Climate*. – D. Riedel Publ. Comp., NATO ASI Ser. C. 126 (1): 3–39.
- BERGGREN, W. A., D. V. KENT, J. J. FLYNN & J. A. VAN COUVERING (in press): Cenozoic geochronology. – To be published in: W. J. SNELLING (ed.): *Geochronology and the geologic time scale*. – Geol. Soc., Spec. Pap., London.
- BROLSMA, M. J. (1978): Quantitative foraminiferal analysis and environmental interpretation of the Pliocene and topmost Miocene on the south coast of Sicily. – *Utrecht Micropal. Bull.* 18: 1–159.
- BROLSMA, M. J. & J. A. BROEKMAN (1978): The section and the samples. – In: W. J. ZACHARIASSE, W. R. RIEDEL et al.: *Micropaleontological counting methods and techniques – an exercise on an eight metres section of the Lower Pliocene of Capo Rossello, Sicily*. – *Utrecht Micropal. Bull.* 17: 11–18.
- CITA, M. B. (1975a): Planktonic foraminiferal biozonation of the Mediterranean Pliocene deep sea record. A revision. – *Riv. It. Paleont.* 81: 527–544.
- (1975b): The Miocene – Pliocene boundary: history and definition. – In: T. SAITO & L. H. BURCKLE (eds.): *Late Neogene Epoch Boundaries*. – *Micropal., Spec. Publ.* 1: 1–30.
- CITA, M. B. & S. GARTNER (1973): Studi sul Pliocene e sugli strati di passaggio dal Miocene al Pliocene, IV. – The stratotype Zanclean foraminiferal and nannofossil biostratigraphy. – *Riv. Ital. Paleontol. Stratigr.* 79: 503–558.
- DEMAISON, G. J. & G. T. MOORE (1980): Anoxic environments and oil source bed genesis. – *Org. Geochem.* 2: 9–31.
- DI GRANDE, A., M. GRASSO, F. LENTINI & G. SCAMARDA (1976): Facies e stratigrafia dei depositi Pliocenici tra Leonforte e Centuripe (Sicilia centro-orientale). – *Boll. Soc. Geol. It.* 95: 1319–1345.
- EINSELE, G. (1982): Limestone – marl cycles (periodites): Diagnosis, significance, causes – a review. – In: G. EINSELE & A. SEILACHER (eds.): *Cyclic and event stratification*. – Springer-Verlag, Berlin, Heidelberg, New York: 8–53.
- GUERRERA, F., R. COCCIONI, D. CORRADINI & R. BERTOLI (1984): Caratteristiche lito-sedimentologiche e micropaleontologiche (Foraminiferi, Dinoflagellati, pollini e spore) di successioni "tripolacee" plioceniche del Bacino di Caltanissetta. – *Boll. Soc. Geol. It.* 103: 629–660.
- GUDJONSSON, L. & G. J. VAN DER ZWAAN (1985): Anoxic events in the Pliocene Mediterranean: stable isotope evidence of run-off. – *Proc. Kon. Ned. Akad. Wet., ser. B* 88 (1): 69–82.
- GUDJONSSON, L. (in press): Local and global effects on the Early Pliocene Mediterranean stable isotope records. – *Mar. Micropal.*
- JONKERS, H. A. (1984): Pliocene benthonic foraminifera from homogeneous and laminated marls on Crete. – *Utrecht Micropal. Bull.* 31: 1–180.
- KIDD, R. B., M. B. CITA & W. B. F. RYAN (1978): Stratigraphy of eastern Mediterranean sapropel sequences recovered during DSDP Leg 42A and their paleoenvironmental significance. – In: K. J. HSÜ, L. MONTADERT et al. (eds.): *Init. Repts. DSDP* 42 (1): 421–443.
- MEULENKAMP, J. E., B. W. M. DRIEVER, H. A. JONKERS, P. SPAAK, W. J. ZACHARIASSE & G. J. VAN DER ZWAAN (1979): Late Miocene – Pliocene climatic fluctuations and marine "cyclic" sedimentation patterns. – *Ann. Geol. Pays Hellen., Tome hors ser. II:* 831–842.

Sedimentary rhythms

- OBRADOVITZ, J. D., C. W. NAESER, G. A. IZETT, G. PASINI & G. BIGAZZI (1982): Age constraints on the proposed Plio-Pleistocene boundary stratotype at Vrica, Italy. – *Nature* 298: 55–59.
- RAFFI, I. & D. RIO (1979): Calcareous nannofossil biostratigraphy of DSDP Site 132 – Leg 13 (Tyrrhenian Sea – Western Mediterranean). – *Riv. Ital. Paleontol. Stratigr.* 85: 127–172.
- RIO, D., R. SPROVIERI & I. RAFFI (1984): Calcareous plankton biostratigraphy and biochronology of the Pliocene – Lower Pleistocene succession of the Capo Rossello area, Sicily. – *Mar. Micropal.* 9: 135–180.
- ROSSIGNOL-STRIX, M. (1983): African monsoons, an immediate climate response to orbital insolation. – *Nature* 304: 46–49.
- (1985): Mediterranean Quaternary sapropels, an immediate response of the African monsoon to variation of insolation. – *Palaeogeogr., Palaeoclim., Palaeoecol.* 49: 237–263.
- RYAN, W. B. F. (1972): Stratigraphy of late Quaternary sediments in the eastern Mediterranean. – In: D. J. STANLEY (ed.): *The Mediterranean Sea: a natural sedimentation laboratory*. – Dowden, Hutchinson and Ross, Stroudsburg: 149–169.
- SPAAR, P. (1983): Accuracy in correlation and ecological aspects of the Mediterranean Pliocene. – *Utrecht Micropal. Bull.* 28: 1–160.
- SPROVIERI, R. (1978): I foraminiferi bentonici della sezione plio-pleistocenica di Capo Rossello (Agrigento, Sicilia). – *Boll. Soc. Paleont. It.* 17: 68–97.
- TAUXE, L., N. D. OPDYKE, G. PASINI & C. ELMI (1982): Age of the Plio – Pleistocene boundary in the Vrica section, southern Italy. – *Nature* 304: 125–129.
- THUNELL, R. C., D. G. WILLIAMS & J. P. KENNETT (1977): Late Quaternary paleoclimatology, stratigraphy and sapropel history in eastern Mediterranean deep-sea sediments. – *Mar. Micropal.* 2: 371–388.
- VERHALLEN, P. J. J. M. (in press): Early development of *Bulimina marginata* in relation to paleoenvironmental changes in the Mediterranean. – *Proc. Kon. Ned. Akad. Wet., ser. B* 90.
- ZIJDERVELD, J. D. A., J. W. ZACHARIASSE, P. J. J. M. VERHALLEN & F. J. HILGEN (1986): The age of the Miocene-Pliocene boundary. – *Newsl. Stratigr.* 16: 169–181.

Chapter 3

Closing the gap in the Plio-Pleistocene boundary stratotype sequence of Crotona (southern Italy)

by FREDERIK J. HILGEN

with 4 figures

Abstract. Results of a detailed fieldstratigraphic study carried out in the area south of Crotona (southern Italy) evidently demonstrate that the segments of the Crotona sequence exposed in the Plio-Pleistocene boundary stratotype section of Vrica and the lower section of Semaforo (= Stuni) are not separated by a non-exposed interval, as hitherto assumed, but that they include a considerable overlap.

Zusammenfassung. Diese Arbeit bringt neue Erkenntnisse über das Gebiet des Plio-/Pleistozän-Stratotyps südlich von Crotona in Süd-Italien. Es erwies sich, daß die Profil-Teilstücke von Vrica und Semaforo (= Stuni) der Crotona-Folge nicht – wie bisher angenommen – durch einen nicht aufgeschlossenen Bereich getrennt werden, sondern daß sie sich beträchtlich überlappen.

Introduction

The Upper Pliocene – Lower Pleistocene sequence of Crotona (southern Italy) was originally introduced with the aim to establish the Pliocene-Pleistocene boundary stratotype in its upper part as exposed in section Vrica (PASINI et al. 1975; SELLI et al. 1977). In this section, the Pliocene-Pleistocene boundary was formally defined at the base of the homogeneous claystones which conformably overlie the sapropelitic marker bed with the codation e (AGUIRRE & PASINI 1985). The study of the complete and continuous sequence of Crotona, however, is still hampered by the presence of a non-exposed interval between those parts of the sequence exposed in the Vrica section and in the lower section of Semaforo (= Stuni) (TAUXE et al. 1983; BACKMAN et al. 1983; SPAAK 1983; VERHALLEN 1987; COMBOURIEU-NEBOUT 1987; GHIDALIA 1988). Geometric constructions showed that less than 50 m of sediment is missing between the two sections (TAUXE et al. 1983).

Japanese workers obviously avoided this non-exposed interval by incorporating an interjacent section instead of Semaforo, but they failed to provide conclusive evidence as to the stratigraphic connection between this section and section Vrica (NAKAGAWA et al. 1980; NAKAGAWA 1981). Moreover, comparison of all stratigraphic data available (NAKAGAWA 1981;

* Authors address: FREDERIK J. HILGEN, Department of Geology, Institute of Earth Sciences, Budapestlaan 4, 3584 CD Utrecht, The Netherlands.

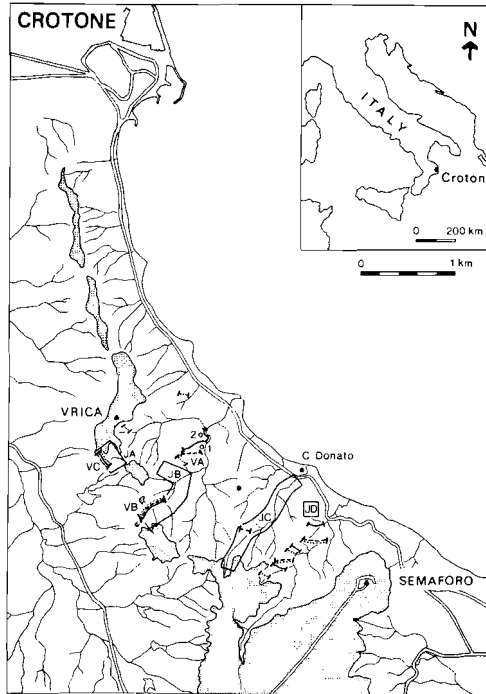


Fig. 1. Location of sections and sample trajectories in the area of badlands south of Crotona. Full line shows the trajectory followed by PASINI et al. (1975), SELLI et al. (1977) and TAUXE et al. (1983), dashed line that by SPAAK (1983) and VERHALLEN (1987) and dotted line that by COMBOURIEU-NEBOUT (1987). VA, VB and VC represent the various subsections of Vrica coded A, B and C after PASINI et al. (1975). Further indicated are the gully complexes JA, JB, JC and JD studied by NAKAGAWA et al. (1980) and NAKAGAWA (1981). The locations of the handdrilled holes at the base of Vrica A are shown as o1 and o2. The dotted area marks the marine (Milazzian) terrace at an altitude of 150 m and the asterisk the position of the watertanks.

TAUXE et al. 1983; VERHALLEN 1987; COMBOURIEU-NEBOUT 1987) shows that this section (referred to as Semaforo Donato in the present paper) is largely equivalent to section Semaforo. This continuing uncertainty regarding the stratigraphic succession imposes strong limitations on current and future chronostratigraphic and geochronometric as well as paleoenvironmental and paleoclimatic interpretations of the Crotona sequence. To put these limitations to an end and to obtain a complete record of this sequence, a detailed fieldstratigraphic survey was carried out in the area (Fig. 1).

The lithology and the sections: A review

The Crotona sequence is more than 500 m thick and composed of marine bathyal sediments, which for the greater part consist of grey to blueish coloured, marly to silty clays. These clays regularly alternate with brownish coloured, sapropelitic layers and, more occasionally, with terrigenous sand and volcanic ash beds. In the area of badlands south of Crotona, the Crotona sequence is dipping 5–15° to the west to westsouthwest. Segments of the sequence are generally well-exposed in northern flanks of roughly NE-SW directed river valleys which, westwardly, rise to the marine (Milazzian) terraces reached at an altitude of 150 m (Fig. 1). The various sections in this area are all located in these northern valley flanks (Fig. 1). The detailed lithological logs of these sections according to the literature have been summarized in Figure 2.

The lower section Semaforo (= Stuni), located north of the former lighthouse, contains more than 200 m of sediments. Some 9 to 10 sapropelitic layers are present of which the lowermost but one is underlain by a pronounced and locally 40 cm thick, white coloured ash bed (Fig. 2). In addition, one less prominent ashbed has been found. This ashbed underlies the middle sapropelitic layer of a distinct cluster of three of these layers recognizable in the top part of the section (Fig. 2).

The interjacent section studied by NAKAGAWA *et al.* (1980), NAKAGAWA (1981) and COMBOURIEU-NEBOUT (1987) is largely equivalent to section Semaforo. In the present paper this section is referred to as Semaforo Donato. At its base, the pronounced ashbed of section Semaforo is exposed, while, in its upper part, two less prominent ashbeds are found (COMBOURIEU-NEBOUT, 1987). The latter two underlie sapropelitic layers which are correlatable to the lower and middle sapropel of the cluster of three in the top part of section Semaforo (Fig. 2).

The upper section Vrica contains more than 250 m of sediment and is composed of three, partly overlapping, subsections termed A, B and C after PASINI *et al.* (1975; see for location Fig. 1; note that partly different trajectories were followed by the Dutch and Japanese working on this section). Altogether, 15–19 sapropelitic layers have been distinguished, most of which are arranged in distinct clusters of 3–4 interbeds (Fig. 2). In addition, several terrigenous sandbeds and a single ashbed are present in the middle part of the section (= Vrica B). For this study, however, only the lower subsection (= Vrica A) is relevant. In the upper part of this section, two distinct clusters of 2 (or 3) and 4 sapropelitic intercalations can be recognized. These sapropel clusters overlie a long interval of homogeneous clays in which only one single, vaguely laminated sapropelitic layer is found (Fig. 2). The exceptionally thick homogeneous interval, which underlies this vague laminitic in the lithologic log of PASINI *et al.* (1975) and SELLI *et al.* (1977) is badly exposed and does not form part of the regular section. Moreover, field observations showed that the extreme thickness of this interval is partly an artefact since the sample trajectory mainly follows strike.

Closing the gap between the Vrica and Semaforo sections

First of all, the weathered surface and overgrowth of the rather poorly exposed basal part of section Vrica A was removed. This disclosed the presence of 1) an additional, rather well developed sapropelitic layer, 7.30 m on top of the already known, vaguely laminated interbed (see Fig. 2), and 2) an ashbed 1.00 m stratigraphically below this same vague laminitic. Section

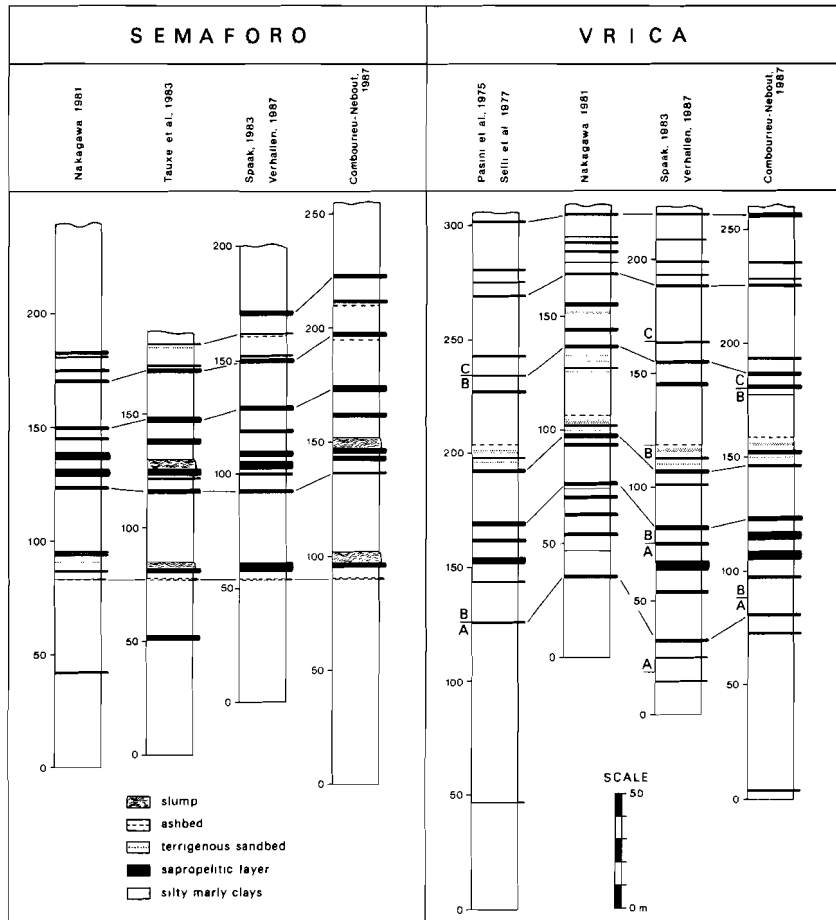


Fig. 2. Lithology of sections Semaforo and Vrica according to the literature. Parts of the sequence logged in the standard subsections of Vrica have been indicated by A, B and C next to the lithological columns. Note that the lithological column of section Semaforo in COMBOUREU-NEBOUT (1987) includes in its uppermost part the top of section Semaforo Donato. The Semaforo section of NAKAGAWA (1981) represents section Semaforo Donato for the greater part.

Closing the gap in the Plio-Pleistocene boundary stratotype sequence of Crotona

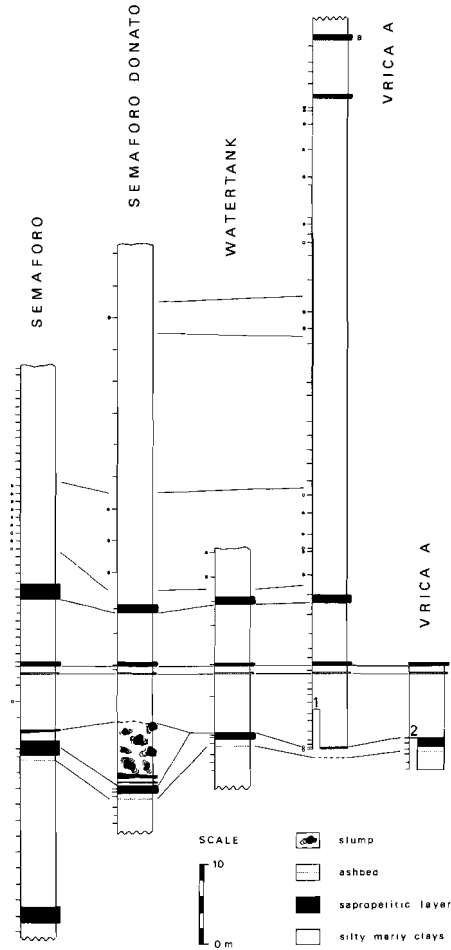


Fig. 3. Lithology of the relevant parts of sections Semaforo, Semaforo Donato and Vrica. Section watertank is located interjacently between Vrica and Semaforo Donato, 100 to 250m north of the water-tanks indicated in Figure 1. Biostratigraphic data show the presence/absence of *Globorotalia inflata* (○ = rare; ● = common) and *G. truncatulinoides* (*). The a denotes the sapropel according to the codation of SELLI et al. (1977). 1 and 2 mark the first and second handdrilled hole at the base of Vrica A.

Vrica A was further extended downwards with the use of a simple handdrill. In the first hole drilled at the base of the section, distinctly laminated sediments of sapropelitic character were reached at a vertical depth of 4.75 m. The base of this new laminite was not reached. A second hole was therefore drilled 200 m to the north (Fig. 1). At this site, drilling could start at a slightly lower stratigraphic level, i.e. directly on top of the laminite found at the bottom of the first hole. Distinct laminations remained present downhole to a depth of 0.90 m. A thin, rather coarsely grained ashbed was reached next at 1.60 m. Consequently, the resultant succession in lithology of the basal part of the Vrica A section now closely matches that of the top part of section Semaforo, despite the fact that some of the individual layers differ considerably in thickness over this short distance of only 2 km.

To definitively settle whether these parts of the Vrica and Semaforo sections are correlatable or not, the surface trace of the distinct ashbed underlying the vague sapropelitic layer at the base of Vrica A was followed in the direction of Semaforo (for this purpose an ashbed was selected because it can more easily be traced through rather badly exposed terrains than a sapropelitic layer). Halfway, a complete succession of the three sapropelitic layers and associated ashbeds of the basal part of section Vrica A could be logged (Fig. 3; section watertank). The ashbed was further traced to section Semaforo Donato and section Semaforo where it proved to connect perfectly with the uppermost ashbed in these sections (Figs. 3, 4).

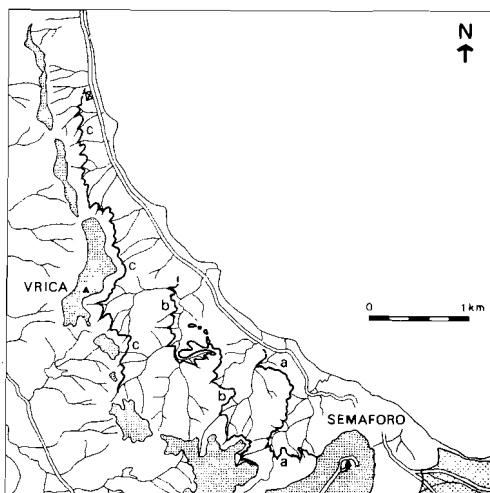


Fig. 4. Surface trace of the three principle ashbeds of the Crotona sequence south of Crotona. A: the pronounced Pliocene ashbed exposed in the middle part of section Semaforo Donato and at the base of section Semaforo Donato; B: the double ashlayer traced from the base of section Vrica to the top of section Semaforo; and C: the Pleistocene ashbed (l according to the codation of PASINI et al. (1975) and SELLI et al. (1977) exposed in the middle part of section Vrica B.

Moreover, the following characteristics of this particular ashbed could be recognized in all sections: The bed actually represents a double ash layer, the individual beds of which are separated by a 5–10 cm thick interval of homogeneous clays. With the exception of section Semaforo, the upper, less prominent of these ashbeds is always mingled with clay particles indicating that it is redeposited. The stronger internal coherence of this upper ash in section Semaforo, however, suggests that it is not a product of redeposition of the lower ash but represents another ash level.

On the other hand, the detailed lithological logs of the various sections reveal some remarkable differences as well (Fig. 3). In section Semaforo Donato, a conspicuous, 8 m thick slump level is found. The main body of this slump consists of disconnected and often rotated blocks of sapropelitic sediment floating in a matrix of clay (Fig. 3). Its base could accurately be pinpointed directly on top of the lowermost laminites of the distinct cluster of three. Very remarkably, no clear indications for the presence of this slump level were found both at Vrica A and in the section located interjacently between Semaforo Donato and Vrica A (Fig. 3). In section Semaforo, this slump level is present, but less conspicuous and less thick. The base of the slump is further not located on top but in the middle of the correlative sapropelitic layer (Fig. 3). The disproportionate thickness of this sapropelitic layer in section Semaforo (almost twice as thick as in the other sections) can thus be explained by a repetition of this laminites. It is easily imaginable that such a slide of a sapropelitic layer eventually developed into a slump as found in section Semaforo Donato. Slump levels in section Semaforo are found predominantly on top of sapropelitic layers suggesting that a causal connection exists between the occurrence of these slumps and the formation of the sapropels. Whether this is related to differences in lithology only is at present not well understood.

Biostratigraphic correlations

The lithostratigraphic correlations between the Vrica and Semaforo sections are totally confirmed by biostratigraphic analysis of planktonic foraminifers (Fig. 3). In all sections, the distinct cluster of three sapropelitic layers is succeeded by a level marked by a major influx of *Globorotalia inflata*. This influx overlies an interval in which *G. inflata* is rare and discontinuously present. The base of this poorly defined interval represents the actual first occurrence of this species in the Mediterranean. At present, it is pinpointed in the lower sapropel of the distinct cluster of three (Fig. 3).

The *G. inflata* influx is in turn succeeded by a long absence interval of this species. From its level of re-appearance in Vrica A (Fig. 3), the species is more or less continuously present up to the top of the Vrica section (see SPAAK 1983). According to the data presented in NAKAGAWA et al. (1980) and COMBOURIEU-NEBOUT (1987), this biohorizon is also reached in the top part of section Semaforo Donato, but this could not be substantiated in our sample set. Finally, this re-appearance of *G. inflata* follows shortly upon another important biohorizon, i.e. the first occurrence c.q. influx of *Globorotalia truncatulinoides* (Fig. 3; see also RIO et al. 1984). This biohorizon is recorded both in section Vrica A and in section Semaforo Donato. The newly established stratigraphic connection between these sections (Fig. 3) indicates that the two separate occurrences of this species reported by COMBOURIEU-NEBOUT (1987) actually represent one and the same event.

Regional correlations

The characteristic succession of sapropelitic layers and planktonic foraminiferal events now recognized in the overlap of sections Vrica and Semaforo is very similar to the one found in section Singa in adjacent southern Calabria (VERHALLEN 1987; HILGEN 1987) and in section Monte San Nicola on Sicily (unpublished data), although in the latter section less sapropelitic layers have developed in this particular interval.

Conclusions

The top part of the Semaforo section corresponds with the basal part of section Vrica. Hence, these sections are not separated by a non-exposed interval, as hitherto assumed, but they actually contain a considerable overlap. This overlap of the Vrica section with the sections of Semaforo measures some 40 m in case of section Semaforo and some 60 m if section Semaforo Donato is considered (see Fig. 3). The continuity of the surface trace of the "double" ashbed (Fig. 4) furthermore indicates that no (tectonic) complications are to be found between these sections. This implies that the "geometric calculations" on which the missing interval was originally based (TAUXE et al. 1983) are incorrect (for clarity, TAUXE et al. did not include the extended top part of the Semaforo section in their study (see Fig. 3), but even without this extension the overlap still measures 15 m at a minimum). This is not surprisingly in view of the inconsistency found in both the strike and dip of the bedding plane in this area (see e.g. NAKAGAWA et al. 1980). It shows that such indirect methods are inaccurate to determine stratigraphic connections between sections and, if possible, should be avoided. In case of the Crotone sequence, this miscalculation eventually led to the revelation of fictitious sapropels (the vague sapropelitic layer at the base of Vrica A in TAUXE et al. (1983) and COMBOURIEU-NEBOUT (1987)) and repetitive faunal events (the additional *G. inflata* and *G. truncatulinoides* influxes reported by COMBOURIEU-NEBOUT 1987).

Our data seem to confirm earlier findings by NAKAGAWA et al. (1980). However, they also failed to present conclusive evidence as to the stratigraphic connection of the Semaforo sections with section Vrica and it can not be excluded that their composite column includes a small overlap as well. Such an overlap may, in addition to secondary magnetization (TAUXE et al. 1983), even be partly responsible for the complex polarity sequence NAKAGAWA (1981) found for the Olduvai.

The data presented in the present paper, however, for the first time show how all sections in this area are stratigraphically connected and how a complete record of the Crotone sequence can be obtained. Finally, the characteristic succession of sapropelitic layers and planktonic foraminiferal events provide a powerful tool to establish very detailed correlations on at least a regional scale.

Acknowledgements. J.E. MEULENKAMP and W.J. ZACHARIASSE read an earlier version of the manuscript. We thank G.J. VAN 'T VELD and G. ITTMAN for preparing the micropaleontological samples, A.J. HILGEN and C. PICCOLO for their assistance and company in the field and the family CERVIANI for their hospitality and the pleasant stay in their hotel at the foot of the Vrica section.

References

- AGUIRRE, E. & G. PASINI (1985): The Pliocene-Pleistocene boundary. – *Episodes*, **8**: 116–120.
- BACKMAN, J., N.J. SHACKLETON & L. TAUXE (1983): Quantitative nannofossil correlation to open ocean deep-sea section from Plio-Pleistocene boundary at Vrica, Italy. – *Nature*, **304**: 156–158.
- COMBOURIEU-NEBOUT, N. (1987): Les premiers cycles glaciaire-interglaciaire en région méditerranéenne d'après l'analyse palynologique de la série plio-pleistocène de Crotona (Italie méridionale). – Thésis, Univ. Sci. Tech. Languedoc, Montpellier: 1–161.
- GHIDALIA, M.-J. (1988): Les Gephyrocapsaceae (Coccolithophoridées) des coupes de Stuni et de Vrica, Italie, stratotype de la limite Plio-Pleistocène. Étude systématique et intérêt stratigraphique. – *Cahiers de Micropaléontologie*, **3**, 1: 5–49.
- HILGEN, F. J. (1987): Sedimentary rhythms and high-resolution chronostratigraphic correlations in the Mediterranean Pliocene. – *Newsl. Stratigr.*, **17**: 109–127.
- NAKAGAWA, H., N. NIITSUMA, T. TAKAYAMA, S. TOKUNAGA, H. KITAZATO & I. KOIZUMI (1980): Preliminary results of magneto- and biostratigraphy of the Vrica section (Calabria, southern Italy). – *Proc. 2nd Symp. on Neogene/Quaternary boundary (U.S.S.R., 1977)*: 145–156.
- NAKAGAWA, H. (1981): Neogene/Quaternary boundary and correlation of Vrica section. – *Proc. Neogene/Quaternary boundary field conference (India, 1979)*: 107–111.
- PASINI, G., R. SELLI, R. TAMPIERI, M.L. COLALONGA, S. D'ONOFRIO, A.M. BORSETTI & F. CATI (1975): – The Vrica section. In: SELLI, R. (ed.): *The Neogene-Quaternary boundary. II Symp. Bologna-Crotona. Excursion Guide-book*: 62–72.
- RIO, D., R. SPROVIERI, E. DI STEFANO & I. RAFFI (1984): *Globorotalia truncatulinoides* (D'ORBIGNY) in the Mediterranean Upper Pliocene geologic record. – *Micropaleontology*, **30**: 121–137.
- SELLI, R., C.A. ACCORSI, M. BANDINI MAZZANTI, D. BERTOLANI MARCHETTI, G. BIGAZZI, F.P. BONADONNA, A.M. BORSETTI, F. CATI, M.-L. COLALONGA, S. D'ONOFRIO, W. LANDINI, E. MENSINI, R. MEZZETTI, G. PASINI, C. SAVELLI & R. TAMPIERI (1977): The Vrica section (Calabria, Italy). A potential Neogene/Quaternary boundary stratotype. – *Giorn. Geol.*, **42**: 181–201.
- SPAAR, P. (1983): Accuracy in correlation and ecological aspects of the planktonic foraminiferal zonation of the Mediterranean Pliocene. – *Utrecht Micropal. Bull.*, **28**: 1–160.
- TAUXE, L., N.D. OPDYKE, G. PASINI & C. ELMI (1983): Age of the Plio-Pleistocene boundary in the Vrica section, southern Italy. – *Nature*, **304**: 125–129.
- VERHALLEN, P. J. J. M. (1987): Early development of *Bulimina marginata* in relation to paleoenvironmental changes in the Mediterranean. – *Proc. Kon. Ned. Akad. Wetensch.*, **B**, **90**: 161–180.

Chapter 4

The age of the Miocene–Pliocene boundary in the Capo Rossello area (Sicily)

F.J. Hilgen¹ and C.G. Langereis²

¹ *Institute of Earth Sciences, University of Utrecht, Budapestlaan 4, 3584 CD Utrecht (The Netherlands)*

² *Paleomagnetic Laboratory, Fort Hoofddijk, Budapestlaan 17, 3584 CD Utrecht (The Netherlands)*

Detailed correlations of magnetostratigraphy, biostratigraphy and lithostratigraphy reveal that the basal Pliocene is equally complete in the Eraclea Minoa and Capo Rossello sections (Sicily) and the Singa section (Calabria), and that, in accordance with the model of the Pliocene flooding event in the Mediterranean, the deposition of the pelagic marls of the Trubi Formation started synchronously on Sicily and in adjacent Calabria. In addition, the data obtained from the Trubi in the Eraclea Minoa section allows the age of the Miocene–Pliocene boundary to be adjusted slightly from 4.83–4.84 [1] to 4.86 Ma because downward extrapolation of both sedimentation rate and average duration of small-scale sedimentary cycles in the Trubi yields this age for the boundary in this section. Linearly interpolated ages for the top of the *Sphaeroidinellopsis* acme and the first substantial increase in *Globorotalia margaritae* (the FOD of this species is non-existent in the Mediterranean Pliocene) at Eraclea Minoa arrive at 4.74 and 4.63 Ma respectively.

Because of the detailed magnetostratigraphy and the very accurate dating of the Miocene–Pliocene boundary, it is preferable to select the Eraclea Minoa section as the boundary stratotype rather than the Capo Rossello section.

Finally, this age of 4.86 Ma for the Miocene–Pliocene boundary suggests that the beginning of the Pliocene is connected with the termination of a series of latest Miocene glaciations and that the re-establishment of open marine conditions in the Mediterranean might be of glacio-eustatic origin.

1. Introduction

The Miocene–Pliocene (M-P) boundary was formally proposed by Cita [2] to be defined at the base of the pelagic marls of the Trubi Formation at Capo Rossello (Sicily). In the boundary stratotype, the Trubi marls abruptly overlie non-marine, silico-clastic sediments of the Upper Messinian Arenazzolo unit. This major break in sedimentary facies reflects the permanent restoration of the Atlantic–Mediterranean connection and the instantaneous return to open marine conditions in the Mediterranean after the Messinian “salinity crisis” [2,3].

Since the basal Pliocene at Capo Rossello [1,4] and in DSDP Site 132 [5] proved to be paleomagnetically unsuitable to establish a reliable magnetostratigraphy, Zijdeveld et al. [1] resorted to adjacent southern Calabria and provided the first accurate age estimates for the M-P boundary on the basis of a detailed magneto-

stratigraphy of the basal part of the Trubi in the Singa and Roccella sections. In Calabria, the boundary was anchored slightly below the base of the Thvera subchron and has linearly extrapolated ages of 4.83 and 4.84 Ma. Outside the Mediterranean, the M-P boundary could be equated with the base of planktonic foraminiferal zone N19 and with carbonate spike GI 14 in the equatorial Pacific [1].

The base of Pliocene pelagic depositional sequences, however, is often diachronous in the Mediterranean [6,7]. This has been related to bottom currents [8], which resulted in periods of non-deposition or even submarine erosion, or to tectonically controlled processes of redeposition [7]. This is especially relevant considering the inferred incompleteness of the basal part of the Trubi Formation at Capo Rossello [7,9,10]. For this reason we decided to investigate in detail whether the basal Pliocene in the Rossello stratotype section is equally complete as in the Calabrian

Singa section used by Zijdeveld et al. [1]. Since magnetic properties in the Rossello stratotype proved unsuitable for establishing a reliable magnetostratigraphy, conclusive evidence was gathered from the nearby Eraclea Minoa section.

2. Miocene–Pliocene boundary sections

The Eraclea Minoa and Rossello sections are situated in a series of cliffs along the south coast of Sicily (Fig. 1) in which the marls of the Trubi are excellently exposed. At both localities, the M-P boundary is characterized by a sharp break between non-marine, finegrained silico-clastic sediments of the Upper Messinian Arenazzolo unit and full-marine Trubi marls of the Lower Zanclean [11]. The lower part of the Trubi at Eraclea Minoa, however, is less weathered and tectonically less disturbed than at Capo Rossello. The Eraclea Minoa section has been sampled at the far end of the camping-site where the steep cliffs are accessible to the top (Fig. 1).

The Singa section in Calabria is that of Zijdeveld et al. [1] (Fig. 1). Here, the M-P boundary is materialized by a sharp change-over from Upper Messinian non-marine, coarse grained sediments to full-marine marls of the Lower Pliocene Trubi.

3. Lithostratigraphy and biostratigraphy

3.1. Lithostratigraphy

The most obvious lithological feature of the Trubi are the small-scale sedimentary cycles which are described in detail by Hilgen [12]. In Calabria, these small-scale cycles are usually bipartite and consist of an indurated, whitish-coloured, CaCO_3 -rich and a grey-coloured, CaCO_3 -poor marl-bed. On Sicily these small-scale cycles are generally quadripartite due to the intercalation of an additional, beige-coloured, CaCO_3 -poor marl-bed in the white marls. The small-scale cycles were found to have an average duration of approximately 20 ka and have been interpreted in terms of climatic variations that are induced by the orbital cycle of precession [1,12,15].

High-resolution bed-to-bed correlations in the Trubi of Sicily and Calabria can be obtained on the basis of distinct variations in thickness of the small-scale cycles [12]. The disproportionately thick cycles 6 and 20–22, for example, are excellent marker-beds which have been used to correlate the Calabrian Singa section to the Eraclea Minoa section on Sicily ([12] Fig. 2). The first six cycles of the Trubi are recognizable both in the

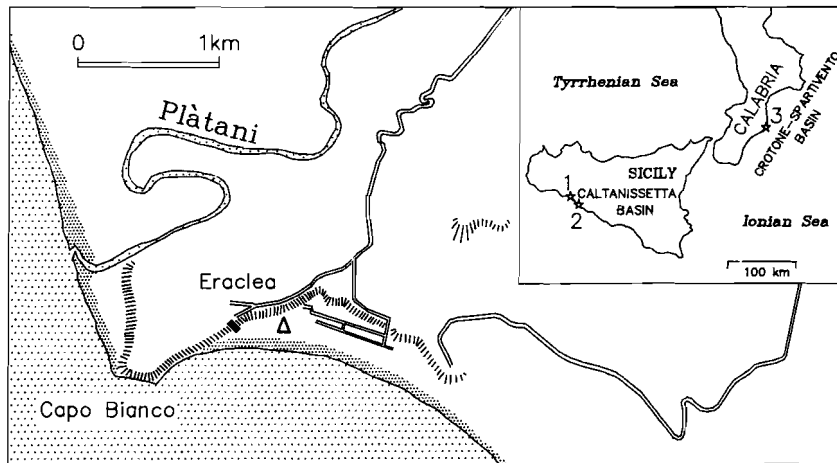


Fig. 1. Location map of the Eraclea Minoa (1 + detailed map), Capo Rossello (2) and Monte Singa (3) sections. Triangle denotes the Eraclea Minoa camping-site.

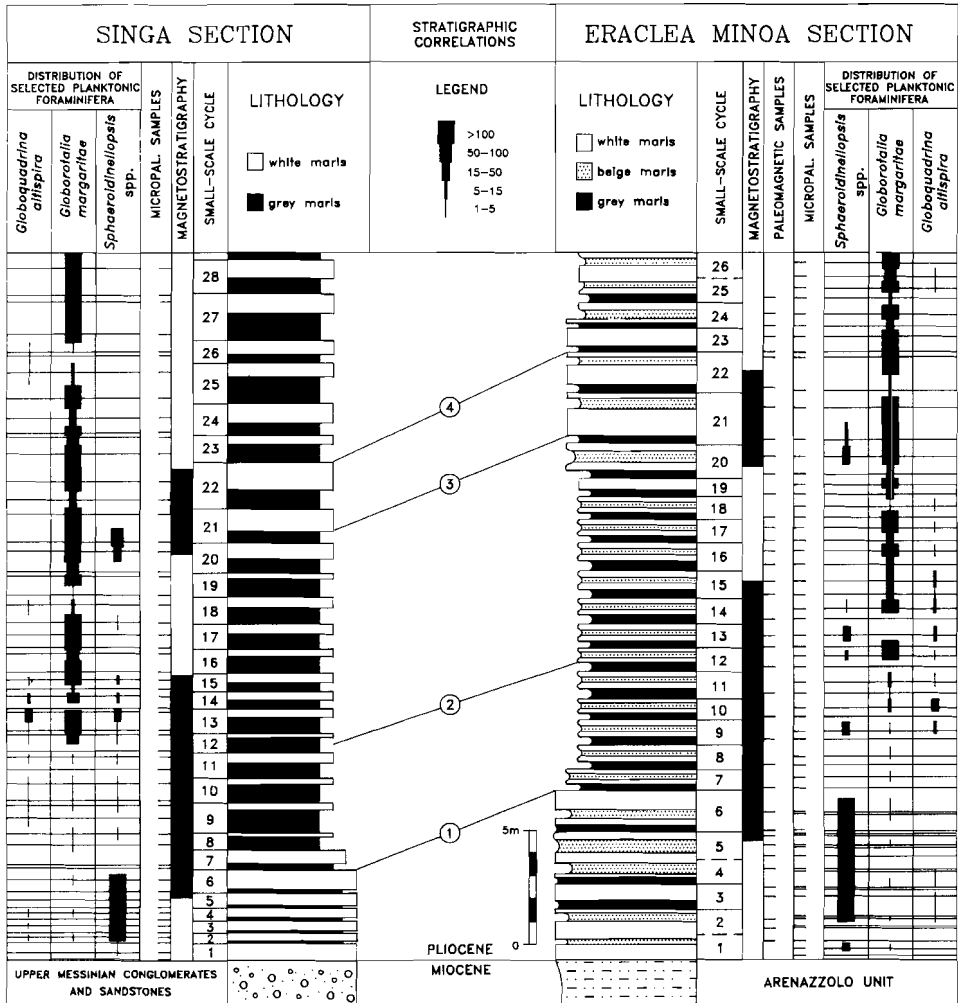


Fig. 2. Magnetostratigraphy, biostratigraphy and lithostratigraphy of the Eraclea Minoa and Singa sections. The magnetostratigraphy and lithostratigraphy of the Singa section is based on Zijdeveld et al. [1], the magnetostratigraphy of Eraclea on the data presented in Fig. 5. The two normal polarity zones in the Singa section represent the Thvera and Sidufjall subchrons [1]. The subdivision in small-scale sedimentary cycles is after Hilgen [12]. Cycles 6, 21 are disproportionately thick and are considered to be a composite of 2 cycles. Semi-quantitative faunal data are based on surveying one picking tray of 10,000–15,000 specimens. Numbered stratigraphic correlations refer to (1) top small-scale cycle 6, (2) first substantial increase of *G. margaritae*; (3) cycle 21, and (4) top cycle 22. The top of the *Sphaeroidinellopsis* acme corresponds with top cycle 6.

Singa and Eraclea Minoa section (Fig. 2), but are difficult to distinguish at Capo Rossello (Fig. 3). Nevertheless, the disproportionately thick cycle 6

as well as the well-developed beige marl-beds of cycles 2, 4 and 6 are easily recognized and used to correlate the Eraclea Minoa and Capo Rossello

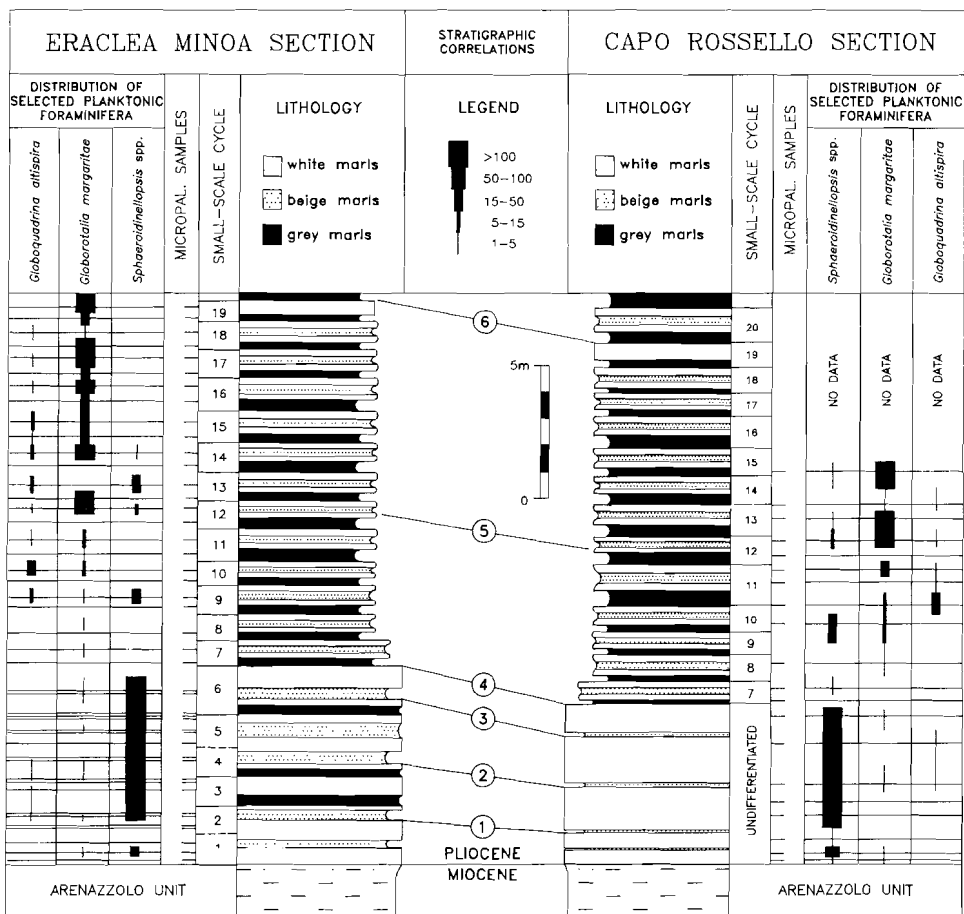


Fig. 3. Biostratigraphy and lithostratigraphy of the basal Trubi at Eraclea Minoa and Capo Rossello. Numbered stratigraphic correlations refer to (1) base beige marls of cycle 2, (2) base beige marls of cycle 4, (3) base beige marls of cycle 6, (4) top cycle 6, (5) first substantial increase of *G. margaritae*, and (6) top cycle 19. The top of the *Sphaeroidinellopsis* acme corresponds with top cycle 6.

sections (Fig. 3). Supportive evidence for this correlation is provided by the absence of the beige marl-bed within cycle 19 in both the Sicilian sections.

3.2. Biostratigraphy

Biostratigraphic correlations between all three M-P boundary sections are possible by using semi-quantitative data on the distribution of the

planktonic foraminifers *Sphaeroidinellopsis* spp., *Globobuccina margaritae* and *Globobuccina altispira* (Figs. 2, 3). The interval with relatively abundant specimens of *Sphaeroidinellopsis* in the basal part of the Trubi is recognizable in all sections and corresponds with the Mediterranean *Sphaeroidinellopsis* Acme-zone [16-18]. The top of this Acme-zone provides a useful biohorizon located between small-scale cycle 6 and 7, whereas

the base falls within cycle 2 (Figs. 2, 3). From the base of the Trubi up to cycle 12, *G. margaritae* is rare and discontinuously present. In small-scale cycle 12, *G. margaritae* substantially increases for the first time in all sections providing another useful Early Pliocene biohorizon in the Mediterranean.

4. Magnetostratigraphy

Magnetic properties in the Rossello stratotype section unfortunately proved to be unsuitable for

establishing a magnetostratigraphy [1,4]. The magnetostratigraphy of the Singa section has been dealt with in detail by Zijdeveld et al. [1]. In this paper we present the paleomagnetic data for the Eraclea Minoa section.

The Eraclea Minoa section has been sampled at 38 levels with an average sampling interval of ca. 75 cm (Fig. 2). At each level we took two cores of 25 mm diameter with an electric drill and a generator as power supply. At most levels it was possible to remove the weathered surface and to drill into fresh (blue-coloured) sediment. Inter-level

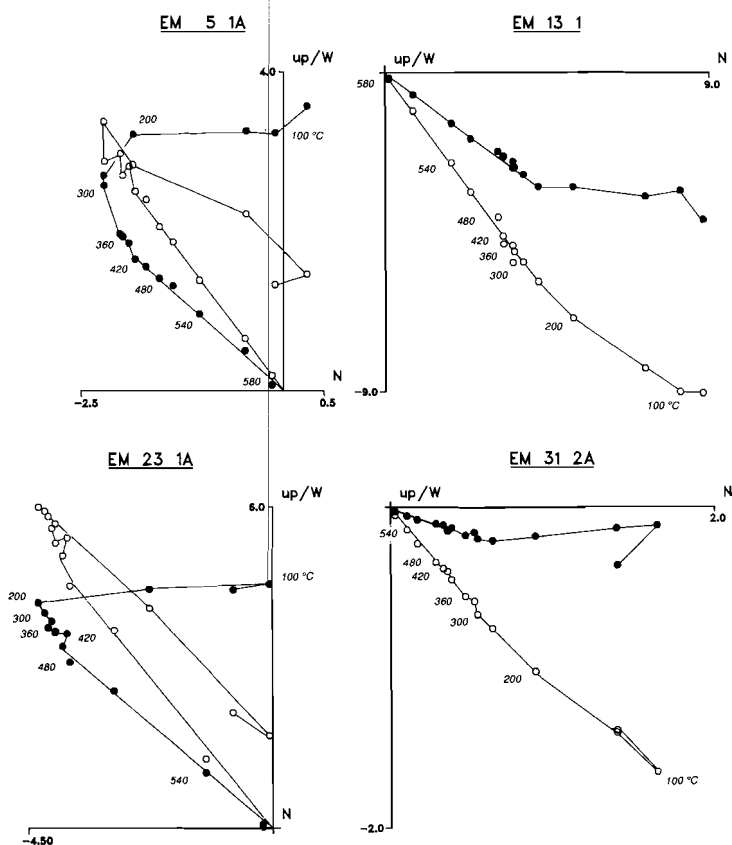


Fig. 4. Representative stepwise thermal demagnetization diagrams [24] of some selected specimens in the Eraclea Minoa section. Small temperature increments are used: 50 °C increments between 100 and 300 °C, 30 °C increments between 300 and 540 °C, and 20 °C increments between 540 and 580 °C. Solid (open) circles denote projection on the horizontal (vertical) plane; units along the axes are in mA/m.

ERACLEA MINOA

ChRM - directions

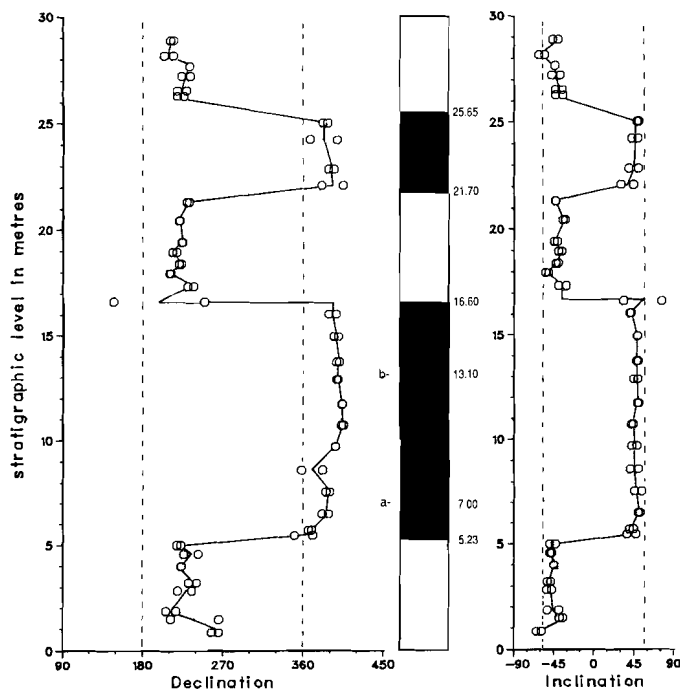


Fig. 5. Declination and inclination of ChRM in the Eraclea Minoa section. Black (white) denotes normal (reversed) polarity. Dashed lines indicate declination and inclination (57.5°) of the geocentric axial dipole field for the present latitude of the locality. Solid lines connect average declination and inclination per sampling level. Positions of polarity reversals and biostratigraphic datum planes (a = top of *Sphaeroidinellopsis* acme, b = first massive increase of *G. margaritae*) are indicated and are based on interpolation between sampling levels, except at the 16.60 m level where intermediate directions are found with a southerly and westerly declination and a positive inclination.

distances were calculated according to Langereis [19].

The natural remanent magnetization (NRM) was measured on a 2G Enterprises cryogenic magnetometer. Total NRM intensities of the Eraclea Minoa section are typically between 1.0 and 20.0 mA/m. Initial measurements revealed mainly normal polarities due to secondary overprint.

Generally two specimens per sampling level were demagnetized progressively by using stepwise thermal demagnetization over small temperature increments. The thermal demagnetizations pro-

duce excellent results. A small viscous and randomly directed component is generally removed at 100°C . Another component showing a (normal polarity) present day direction is almost or entirely removed between 100 and $200\text{--}250^\circ\text{C}$ and is supposed to be of recent origin (Fig. 4). A characteristic remanent magnetization (ChRM) component consists generally of two phases: a low-temperature (LT) phase removed between 250 and 420°C and a high-temperature (HT) phase removed between 420 and 580°C . In normal polarity specimens the LT and the HT phase have

no apparent different directions, but in reversed polarity specimens there is a clear directional difference (Fig. 4). Whether this difference is an artefact (e.g. spectral overlap of different components) or real is still being studied. The HT phase of the ChRM resides most probably in magnetite because of the maximum blocking temperature of 560–580 °C, which suggests that it is of primary origin. The direction of this (HT phase) ChRM component is used for magnetostratigraphic purposes, also because the HT phase clearly shows opposite directions for the two polarities (Fig. 4).

Inclinations of the ChRM (with an average of 46°) are consistently shallower than the inclinations of the geocentric axial dipole field for the locality (57.5°). This might indicate the presence of an inclination error due to sediment compaction and may be taken as additional evidence for the primary origin of the ChRM [20]. Normal and reversed polarity (HT phase) ChRM components in the Eraclea Minoa section are consistently grouped in three reversed and two normal polarity zones (Fig. 5).

Comparison of the results with those for the Singa section [1] (see also Fig. 2) shows that the two normal polarity zones in the Eraclea Minoa

section represent the Thvera and Sidufjall subchrons of the Gilbert Chron. The average sedimentation rate per polarity zone is fairly constant (5.7, 5.1 and 5.6 cm/ka from Thvera to Sidufjall), as well as the average duration of the small-scale cycles (18.2, 21.4 and 19.1 ka, respectively, with an overall average of 19.1 ka). Linear downward extrapolation of the Thvera sedimentation rate yields an age of 4.86 ± 0.005 Ma for the M-P boundary (Fig. 6a).

5. Discussion and conclusions

The polarity reversals occur in the small-scale cycles 5, 15, 20 and 22, in both the Eraclea Minoa and Singa sections (Fig. 2), indicating that the basal Pliocene is equally complete in the Singa, Eraclea Minoa and Capo Rossello sections since the number of pre-Thvera cycles is identical (Figs. 2, 3). This conclusion is in line with the beginning of the *Sphaeroidinellopsis* acme slightly above the base of the Trubi in all sections. Consequently, the deposition of the Trubi started at the same time both on Sicily and in Calabria. The linearly extrapolated age of 4.86 Ma for the M-P boundary in the Eraclea Minoa section (Fig. 6A, option I)

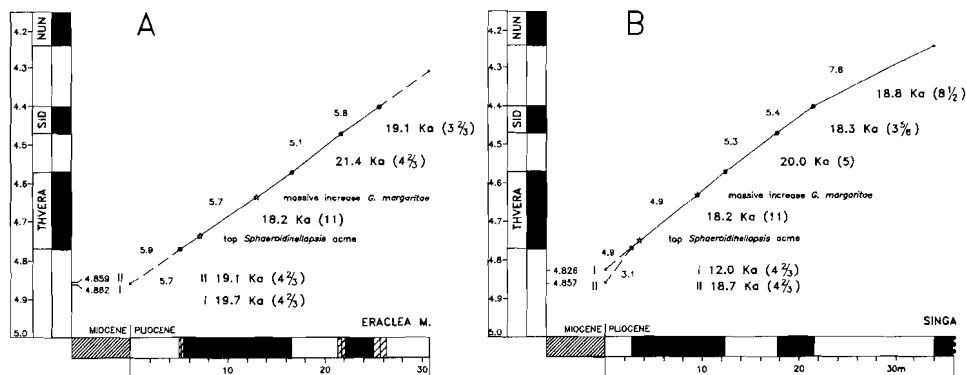


Fig. 6. Sediment accumulation curves of (A) Eraclea Minoa and (B) Singa section. Sedimentation rate, number of small-scale cycles and their average periodicity are given for each polarity interval. Note that the disproportionately thick small-scale cycles 6, 21 and 22 are considered composite cycles which contain an additional small-scale cycle. Various options to calculate the age of the M-P boundary are shown by roman numerals: (I) downward extrapolation of the Thvera sedimentation rate, and (II) downward extrapolation of the average periodicity of 19.1 and 18.7 ka for the small-scale cycles between the base of the Thvera and the top of the Sidufjall subchron in the Singa and Eraclea Minoa sections, respectively. The polarity time-scale used (shown in left columns) is that of Berggren et al. [25].

nevertheless differs slightly from the 4.83 ± 0.01 Ma age estimate for the boundary in the Singa section [1].

In the Singa section, the small-scale cycles in the pre-Thvera part are reduced in thickness compared to the cycles in the Thvera to Sidufjall polarity zones (Fig. 2). Downward extrapolation of the Thvera sedimentation rate, therefore, yields an age of 4.83 Ma for the M-P boundary and an average periodicity of 12.0 ka for the pre-Thvera cycles (Fig. 6B, option I). A periodicity of 12.0 ka, however, deviates strongly from the average periodicity of 18.7 ka for the small-scale cycles between the base of the Thvera and the top of the Sidufjall subchron in this section.

In the Eraclea Minoa section, on the other hand, small-scale cycles are equally thick throughout (Fig. 2). Downward extrapolation of the Thvera sedimentation rate yields an age of 4.86 Ma for the boundary and an average periodicity of 19.7 ka for the pre-Thvera cycles (Fig. 6, option I). A periodicity of 19.7 ka is in good agreement with the average periodicity of 19.1 ka for the small-scale cycles between the base of the Thvera and the top of the Sidufjall subchron in this section.

Downward extrapolation of the average periodicities of 18.7 and 19.1 ka for the small-scale cycles between the base of the Thvera and the top of the Sidufjall subchrons in the Eraclea Minoa and Singa sections (the small discrepancy in periodicity results from differences in sample density) yields an age of 4.86 Ma for the M-P boundary in both sections (Fig. 6A, B, option II). We therefore conclude that the age of 4.86 Ma for the M-P boundary is more accurate than the age of 4.83 Ma. The latter age probably results from a reduced sedimentation rate in the pre-Thvera part of the Singa section (Fig. 6). Indeed, field observations indicate that condensed pre-Thvera sequences are typical for the Trubi in Calabria.

Biostratigraphically, the top of the *Sphaeroidinellopsis* acme and the first substantial increase of *G. margaritae* provide the most reliable and accurate planktonic foraminiferal datum planes in the lowermost Pliocene. Both biohorizons are located within the Thvera subchron and have linearly interpolated ages of 4.74 and 4.63 Ma in the Eraclea Minoa and of 4.75 and 4.63 Ma in the Singa section. This increase of *G. margaritae* has

earlier been taken as the migrational appearance of this species in the Mediterranean [1]. However, *G. margaritae* already sparsely occurs directly above the base of the Pliocene (Figs. 2, 3), which confirms earlier findings of Cita [17]. Consequently, the presence of *G. margaritae* at the base of the Trubi does not necessarily imply that the basal part of the Trubi is missing at Capo Rossello as has been suggested by Sprovieri [7,9] and Rio et al. [10]. On the contrary, the completeness of the Trubi in the boundary stratotype of Capo Rossello—as previously suggested by Cita and Gartner [11] and Cita [2]—is now definitively proved both biostratigraphically and lithostratigraphically. The high-quality magnetostratigraphy in the Eraclea Minoa section, however, makes the Eraclea Minoa section definitely more suitable as Miocene–Pliocene boundary stratotype than Capo Rossello (see [2]).

Finally, this age of 4.86 Ma for the M-P boundary supports recent views which link the Pliocene flooding of the Mediterranean to the end of a series of latest Miocene glaciations and the beginning of a long period of relatively warm climatic conditions at approximately 4.8 Ma [21–23]. The Pliocene flooding of the Mediterranean, therefore, could be of glacioeustatic origin. If so, the present age of 4.86 Ma for the M-P boundary provides a very accurate age estimate for this deglaciation event.

Acknowledgements

P.J. Verplak assisted in the field, A. van Velzen did most of the laboratory treatment. G.J. van 't Veld and G. Ittman prepared the micropaleontological samples. C.W. Drooger, L. Gudjonsson, W.J. Zachariasse and J.D.A. Zijdeveld critically read earlier versions of the manuscript. T. van Hinte skillfully made the illustrations, S.M. McNab the linguistic improvements. This study was partly funded by the Netherlands Organization of Scientific research (NWO).

References

- 1 J.D.A. Zijdeveld, W.J. Zachariasse, P.J.J.M. Verhallen and F.J. Hilgen, The age of the Miocene–Pliocene boundary, *Newsl. Stratigr.* 16, 169–181, 1986.
- 2 M.B. Cita, The Miocene/Pliocene boundary: history and

- definition, in: Late Neogene Epoch Boundaries, T. Saito and L.H. Burckle, eds., pp. 1–30, *Micropaleontology*, Spec. Publ. 1, 1975.
- 3 K.J. Hsü, M.B. Cita and W.B.F. Ryan, The origin of the Mediterranean evaporites, in: W.B.F. Ryan, K.J. Hsü et al., *Init. Rep. DSDP 13*, pp. 1203–1231, U.S. Government Printing Office, Washington, D.C., 1973.
 - 4 M.B. Cita and J.A. McKenzie, The terminal Miocene event, in: *Mesozoic and Cenozoic Oceans*, K.J. Hsü, ed., *Am. Geophys. Union, Geodynam. Ser. 15*, 123–140, 1986.
 - 5 J.P. Kennett and N.D. Watkins, Late Miocene–Early Pliocene paleomagnetic stratigraphy, paleoclimatology and biostratigraphy in New Zealand, *Geol. Soc. Am. Bull.* 85, 1385–1398, 1974.
 - 6 M.B. Cita, The Pliocene record in Deep-sea Mediterranean sediments, 1. Biostratigraphy and chronostratigraphy, in: W.B.F. Ryan, K.J. Hsü et al., *Init. Rep. DSDP 13*, pp. 1343–1379, U.S. Government Printing Office, Washington, D.C., 1973.
 - 7 R. Sprovieri, Remarks on the Early Pliocene Trubi Formation in Sicily, *Mem. Soc. Geol. Ital.* 16, 159–163, 1976.
 - 8 M.B. Cita and W.B.F. Ryan, Time-scale and general synthesis, in: W.B.F. Ryan, K.J. Hsü et al., *Init. Rep. DSDP 13*, pp. 1405–1415, U.S. Government Printing Office, Washington, D.C., 1973.
 - 9 R. Sprovieri, I foraminiferi bentonici della plio-pleistocenica di Capo Rossello (Agrigento, Sicilia), *Boll. Soc. Paleontol. Ital.* 17, 68–97, 1978.
 - 10 D. Rio, R. Sprovieri and I. Raffi, Calcareous plankton biostratigraphy and biochronology of the Pliocene–Lower Pleistocene succession of the Capo Rossello area, Sicily, *Mar. Micropaleontol.* 9, 135–180, 1984.
 - 11 M.B. Cita and S. Gartner, Studi sul Pliocene e sugli strati del passaggio dal Miocene al Pliocene, IV. The stratotype Zanclean. Foraminiferal and nannofossil biostratigraphy, *Riv. Ital. Paleontol. Stratigr.* 79, 503–558, 1973.
 - 12 F.J. Hilgen, Sedimentary rhythms and high-resolution chronostratigraphic correlations in the Mediterranean Pliocene, *Newsl. Stratigr.* 17, 109–127, 1987.
 - 13 F.J. Hilgen, Sedimentary cycles and an astronomically controlled, oscillatory system of climatic change during the Late Cenozoic in the Mediterranean, *Paleobiol. Continentale*, Montpellier, in press.
 - 14 L. Gudjonsson, Local and global effects on the Early Pliocene Mediterranean stable isotope records, *Mar. Micropaleontol.* 12, 241–253, 1987.
 - 15 J.P. de Visser, J.H.J. Ebbing, L. Gudjonsson, F.J. Hilgen, F.J. Jorissen, P.J.J.M. Verhallen and D. Zevenboom, The origin of rhythmic bedding in the Pliocene Trubi Formation of Sicily, southern Italy, *Palaeogeogr., Palaeoclimatol., Palaeoecol.*, in press.
 - 16 G. Bizon, Contribution à la connaissance des Foraminifères planctoniques d'Épire et des îles Ioniennes (Grèce occidentale), depuis la Paléogène supérieur jusqu'au Pliocène, Thèse, Publ. Inst. Fr. Pét. 1, Technip, Paris, 1967.
 - 17 M.B. Cita, Planktonic foraminiferal biozonation of the Mediterranean Pliocene deep sea record. A revision, *Riv. Ital. Paleontol. Stratigr.* 81, 527–544, 1975.
 - 18 P. Spaak, Accuracy in correlation and ecological aspects of the planktonic foraminiferal zonation of the Mediterranean Pliocene, *Utrecht Micropalaeontol. Bull.* 28, 160 pp., 1983.
 - 19 C.G. Langereis, An attempt to correlate two adjacent Tortonian marine clay sections in western Crete using magnetostratigraphic methods, *Utrecht Micropalaeontol. Bull.* 21, 194–214, 1979.
 - 20 C. Laj, M. Jamet, D. Sorel and J.P. Valente, First results from Mio-Pliocene series of the Hellenic sedimentary Arc, *Tectonophysics* 86, 45–67, 1982.
 - 21 D.A. Hodell and J.P. Kennett, Late Miocene–Early Pliocene stratigraphy and paleoceanography of the South Atlantic and southwest Pacific oceans: a synthesis, *Paleoceanography* 1, 285–311, 1986.
 - 22 D.A. Hodell, K.M. Elmstrom and J.P. Kennett, Latest Miocene benthic $\delta^{18}\text{O}$ changes, global ice volume, sea level and the “Messinian salinity crisis”, *Nature* 320, 411–414, 1986.
 - 23 L.D. Keigwin, Towards a high-resolution chronology for latest Miocene paleoceanographic events, *Paleoceanography* 2, 639–660, 1987.
 - 24 J.D.A. Zijdeveld, A.C. demagnetization of rocks: analysis of results, in: *Methods in Palaeomagnetism*, D.W. Collinson et al., eds., pp. 254–286, Elsevier, Amsterdam, 1967.
 - 25 W.A. Berggren, D.V. Kent, J.J. Flynn and J.A. Van Couvering, Cenozoic geochronology, *Geol. Soc. Am. Bull.* 96, 1407–1418, 1985.

Chapter 5

The Rossello composite: a Mediterranean and global reference section for the Early to early Late Pliocene

C.G. Langereis ^a and F.J. Hilgen ^b

^a Paleomagnetic Laboratory, Fort Hoofddijk, Budapestlaan 17, 3584 CD Utrecht, The Netherlands

^b Department of Geology, Institute of Earth Sciences, Budapestlaan 4, 3584 CD Utrecht, The Netherlands

ABSTRACT

A high-resolution magnetostratigraphy (planktonic foraminiferal) biostratigraphy and cyclostratigraphy is presented for the Pliocene Trubi marls in the Punta di Maiata section on Sicily. The integrated stratigraphy of the Rossello composite section of Hilgen ([1], Newslett. Stratigr., 17, 1987) is thereby completed. This composite section provides an unprecedented high-quality reference section for the Early to early Late Pliocene, containing a continuous sequence ranging from below the Thvera Subchron into the Matuyama Chron (4.86–2.45 Ma).

The Punta di Maiata section extends from the Sidufjall Subchron of the Gilbert into the Gauss Chron (4.50–3.30 Ma). Linear interpolation between paleomagnetic datum planes in this section yields first-order age estimates of 3.72 (± 0.01) and 3.59 (± 0.01) Ma for the last common occurrence (LCO) and the actual last occurrence (LO) of *Globorotalia margaritae*.

In addition, this age of 3.59 Ma provides an accurate age for the Zanclean–Piacenzian (Z/P) boundary, provided the LO of *G. margaritae* is maintained as a criterion to define this boundary in the Mediterranean. Irrespective, however, of the criterion used, the Punta di Maiata and Punta Piccola subsections of the Rossello composite are at present the most suitable sections to be designated as stratotypes for the Z/P boundary. The global significance of the Rossello composite is further strongly enhanced by the establishment of an astronomically calibrated geomagnetic polarity time scale based on the correlation of the Trubi sedimentary cycles with the astronomical record.

1. Introduction

The Italian peninsula has played a prominent role in establishing a standard chronostratigraphic frame for the Pliocene because all stages of global significance have been defined there (see [2]). Age calibration of chronostratigraphic boundaries in Italian stratotype sections to the global time scale have long relied mainly on long-distance biostratigraphic correlations to extra-Mediterranean sequences [3]. Only quite recently have paleomagnetic studies provided reliable magnetostratigraphies for a number of Italian land sections, including the Pliocene–Pleistocene boundary stratotype section [4,5] and several Miocene–Pliocene boundary sections [6–8]. Magnetostratigraphic records have further been presented for the early Late Pliocene on Sicily [9,10] and for a number of deep-sea cores which together cover the complete Plio–Pleistocene in the Tyrrhenian Sea [11].

In this paper, we present new paleomagnetic

data from the Punta di Maiata section on Sicily to complete the integrated stratigraphy of the Rossello composite section (that of [1]) and, at the same time, to provide an accurate, first-order age estimate of the last occurrence (LO) of *Globorotalia margaritae* in the Mediterranean. This planktonic foraminiferal datum plane is at present commonly used to delimit the base of the Piacenzian stage in the Mediterranean [3,12,13]. Due to serious stratigraphic problems encountered in the stratotype section of the Piacenzian (see [14]), it became necessary to obtain an accurate age estimate for this important biohorizon in a continuous sequence exposed elsewhere in the Mediterranean, preferably in the stratotype section of the preceding stage, the Zanclean.

2. Sections

Punta di Maiata is a small, but prominent cape in a series of cliffs along the south coast of Sicily

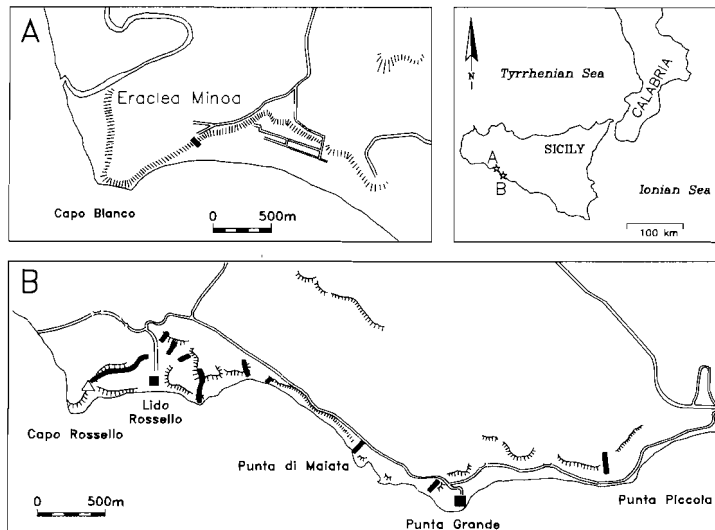


Fig. 1. Location of the Eraclea Minoa, Punta di Maiata, Punta Grande and Punta Piccola subsections of the Rossello composite section of Hilgen [1]. The location of the Miocene/Pliocene boundary annex Zanclean stratotype section of Capo Rossello [15,16] is also indicated.

(Fig. 1). It is located 1 km east of Capo Rossello where the succession of Trubi marls in the Capo Rossello section defines the neostatotype of the Zanclean [15]. In addition, Cita [16] formally proposed the Miocene–Pliocene boundary to be defined at the base of the Trubi in the same section, while there was also a proposal for a Rossellian superstage with the stratotype at Lido Rossello [17].

The Punta di Maiata section forms part of the Rossello composite section of Hilgen [1]. The rhythmically bedded marls of the Pliocene Trubi Formation are excellently exposed and the section contains a complete and relatively undisturbed succession of the Trubi. Problems such as stratigraphic hiatuses [3,15] and unnoticed slump levels [18] are thus avoided. The Rossello composite section is composed of the Eraclea Minoa section (lower part), Punta di Maiata (middle part) and the Punta Grande and Punta Piccola sections (upper part). The various subsections were correlated using characteristic thickness and colour patterns

in the cyclic bedding of the Trubi [1]. The magnetostratigraphy, biostratigraphy and cyclostratigraphy of Eraclea Minoa—comprising the Thvera and Sidufjall Subchrons of the Gilbert Chron [7]—and of Punta Grande/Piccola—containing the entire Gauss Chron [9,10]—have already been reported on elsewhere.

Sampling of the Punta di Maiata section started on the beach directly west of the cape, and, after passing a minor but distinct fault, was soon continued on the regular, western side of Punta di Maiata up to the top of the cliffs where the marls of the Trubi are discordantly overlain by Pleistocene terrace deposits (Fig. 2). Three intervals of disturbed Trubi marls in the upper part of the section have been interpreted as sedimentary slumps (Figs. 2 and 3). Sampling was nevertheless continued to reach the Gilbert–Gauss (G/G) boundary in this section and hence to provide a magnetostratigraphic correlation to the Punta Piccola section. In addition, we extended the sampling at Punta Grande slightly upwards to include

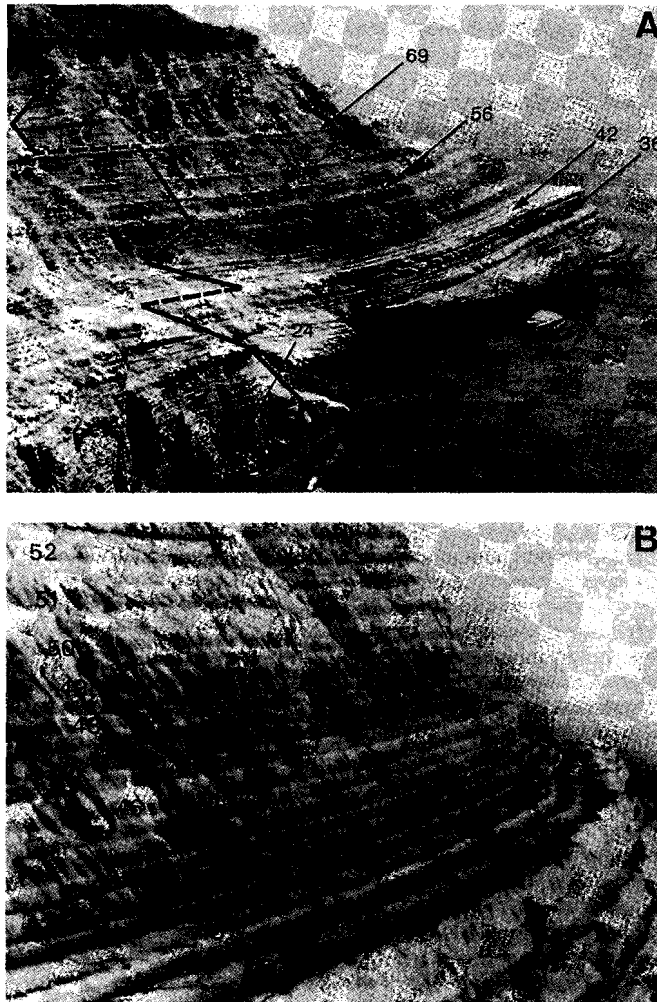
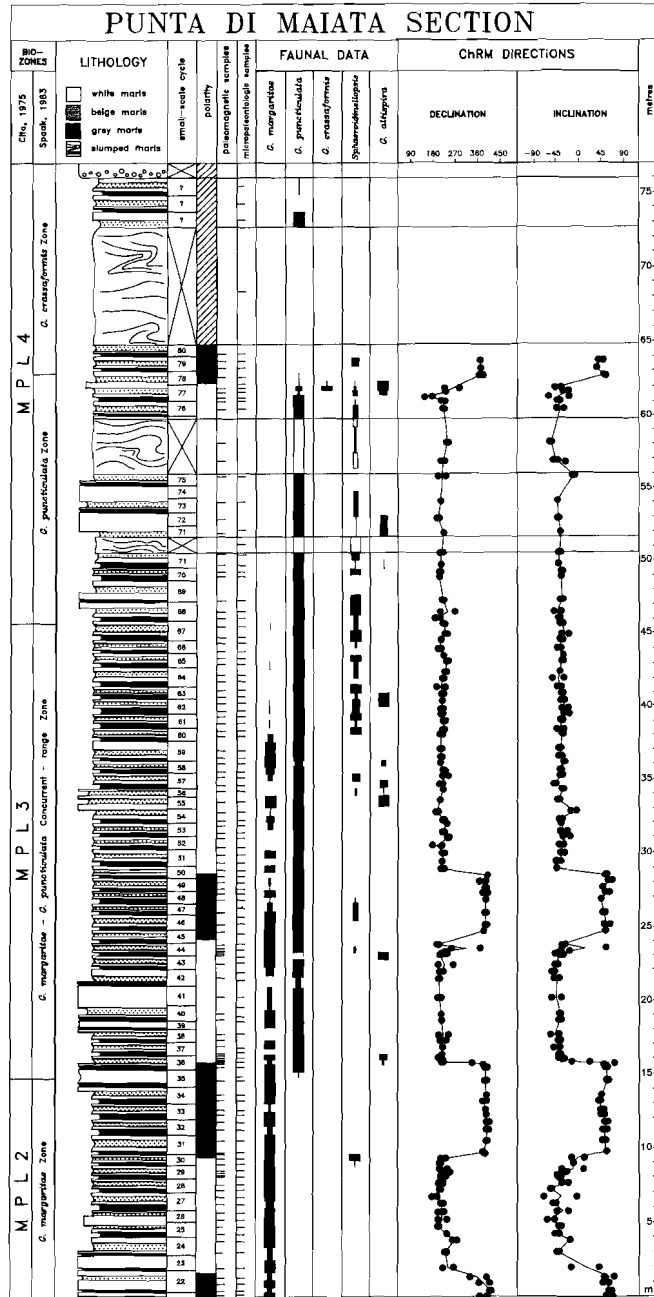


Fig. 2. (A) Western flank of Punta di Maiata. Solid line denotes sampling route. Several characteristic small-scale cycles are indicated. (B) The sedimentary cycles 42 to 52 in the middle part of the section.

the G/G boundary in this section as well. The sampling at Eraclea Minoa was extended to enlarge the overlap with the Punta di Maiata section.

Sampling was carried out following routine Utrecht procedures, i.e. using an electric water-

cooled drill and a generator as power supply. Generally, two cores of 2.5 cm diameter were taken per sampling level, yielding two or three standard specimens (22 mm) each. Care was taken to remove the weathered surface, but in the Punta



Maiata section this proved to be difficult: fresh (blue) sediment could not be sampled at several intervals.

3. Results

3.1. Punta di Maiata

At Punta di Maiata, the marls of the Trubi display the pronounced rhythmic bedding which is characteristic of this formation on Sicily. Small-scale sedimentary cycles—with an average thickness of approximately 1 m—are quadripartite and show a distinct grey–white–beige–white colour alternation in which the grey and beige marls represent the less indurated, CaCO₃-poor beds. Larger scale sedimentary cycles can be distinguished by the cyclical recurrence of relatively thick and/or indurated marly intervals in the succession (Figs. 2 and 3; see also [1]). A detailed report on how these CaCO₃ cycles in the Trubi are related to the astronomical cycles of the Earth's orbit has already been published: it was shown that the small-scale cycles are related to the precession cycle and thus represent an average duration of 21.7 ka [19].

In the Rossello composite section, the small-scale sedimentary cycles have been numbered from the base of the Trubi upwards [19]. The succession in the Punta di Maiata section up to the first slump level encompasses the small-scale cycles 22 to 71. Numbering of the sedimentary cycles could even be continued up to the third and last slump level based on the recognition of the characteristic pattern of these cycles in time-equivalent sections (Punta Grande, Punta Piccola, Lido Rossello and Capo Bianco; data in part unpublished).

The biostratigraphy of the Punta di Maiata section is based on the semi-quantitative distribution of selected planktonic foraminiferal species (Fig. 3). The following succession of events can be recognized:

(1) The first occurrence (FO) of *Globorotalia puncticulata* in small-scale cycle 35.

(2) The last common occurrence (LCO) of *Globorotalia margaritae* in small-scale cycle 60.

(3) The actual last occurrence (LO) of *G. margaritae* in small-scale cycle 67.

(4) The FO of *Globorotalia crassaformis* in the top part of small-scale cycle 77.

(5) The temporary disappearance of *G. puncticulata* in cycle 79. After its almost continuous presence in relatively large numbers from the FO of this species onward, *G. puncticulata* vanishes temporarily from the record shortly after the first occurrence (influx) of *G. crassaformis* (first absence interval of Spaak [18]).

Paleomagnetic samples were taken at 116 levels with an average spacing of 55 cm, corresponding to a resolution of approximately 10 ka. Grey and beige marls were preferentially sampled because they appeared to be less thoroughly weathered than the white marls in the small-scale sedimentary cycles. Per sampling level, two marl specimens were demagnetized by progressive thermal demagnetization using small (50 and 30°C) temperature steps, up to a maximum of 600°C.

The total natural remanent magnetization (NRM) shows low intensities of 0.1–0.5 mA/m in the lower part of the section (level 0–10 m), somewhat higher intensities of 1.5–2.0 mA/m in a subsequent interval (10–20 m) and moderately high intensities of 4.0–6.0 mA/m in most of the remaining part (20–60 m) with the exception of the uppermost part (60–65 m) where values are approximately 0.2 mA/m.

There are almost no weathered surfaces close to the shoreline. Demagnetization characteristics, however, are essentially different from those of the Trubi marls in the same interval elsewhere. The Trubi marls usually show a characteristic remanent magnetization (ChRM) consisting of both a low temperature (LT) component, possibly resid-

Fig. 3. Magnetostratigraphy, planktonic foraminiferal biostratigraphy and cyclostratigraphy of the Punta di Maiata subsection of the Rossello composite. Note the three slump levels intercalated in the upper part of the section. Numbering of small-scale sedimentary cycles pertains to the total number of cycles of the Trubi in the Rossello composite as numbered from the base of the Trubi upward [19]. Semi-quantitative faunal analysis is based on surveying one picking tray containing between 10,000 and 15,000 specimens. Declination and inclination are derived from the high-temperature (HT) component of the ChRM, except in the lower part where only the LT component is present (see also Fig. 4).

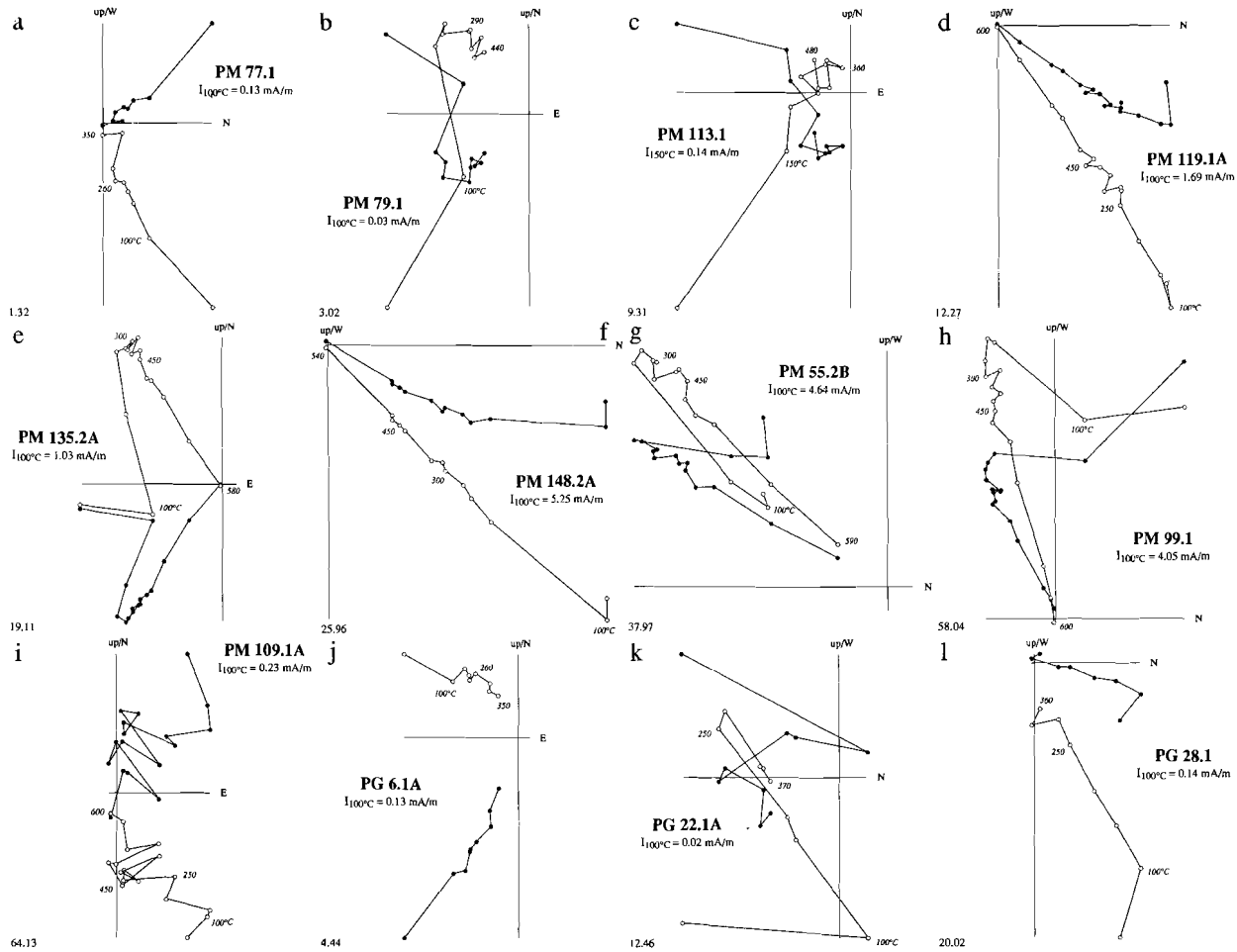


Fig. 4. Stepwise thermal demagnetization diagrams [40] of representative specimens from Punta di Maiata. Dots denote projection on the horizontal plane; circles denote projection on the vertical plane; values are temperatures ($^\circ\text{C}$).

ing in pyrrhotite, as well as a high temperature (HT) component carried by single-domain magnetite [7,9,10,20]. In the lower part of the Punta Maiata section, however, the HT component is entirely or mostly absent, and only the LT component is removed, at temperatures of 350°C or somewhat higher (Fig. 4a and b). Demagnetization at higher temperatures either produces randomly directed (viscous) magnetization, or a cluster around the vector endpoints at 330–360°C (Fig. 4c). Despite the low intensities, the polarity—if not the direction—of the ChRM is easily determined.

Approximately from the 10 m level upwards, demagnetization diagrams show the familiar components usually seen in the Trubi (Fig. 4d–g): a small viscous and laboratory-induced component removed at 100°C, a relatively small present-day field secondary component removed at 200–250°C, and a characteristic (LT and HT) remanence usually removed at 580–600°C, or occasionally at a somewhat lower temperature (540°C, Fig. 4f). The discrimination between ChRM and secondary component is facilitated by the fact that the characteristic remanence shows a consistent clockwise rotation of approximately 35°.

Samples from the second slump level (56–60 m)—deliberately taken from vertically folded layers—not only show exactly the same (viscous, secondary, LT and HT) components, but also the same (reversed) polarity as those from below and above the slump, although the ChRM direction does show a rotation of 65° rather than 35°, and a steeper inclination than usual (Fig. 4h). This indicates that either (synsedimentary) “resetting” of the remanence occurred due to the probably high water content involved in slumping, or that there is a time-lag in recording the geomagnetic field. In either case it probably concerns a post-depositional remanence (see [21]); the mechanism by which geomagnetic field changes are recorded is one of the subjects of detailed polarity reversal studies [41].

The resulting polarity sequence is composed of four normal and three reversed polarity intervals. The successive reversal boundaries occur in the top part of cycle 22, the middle part of 30, the upper part of 35, the lower part of 45, the middle part of 50 and the lower part of 78 (Fig. 3).

3.2. *Eraclea Minoa*

The *Eraclea Minoa* section has been extended with respect to the earlier sampling [7] in order to provide a more substantial overlap with Punta di Maiata. This extension encompasses cycles 26 to 33 (Fig. 5). Biostratigraphically, the FO of *G. puncticulata* was not reached and the extension thus belongs entirely to the *G. margaritae* Zone [18] or MPL 2 [22]. Thermal demagnetization shows the same characteristic remanence as observed in the previous study, where the polarity sequence revealed the presence of the Thvera and Sidufjall Subchrons. The next polarity reversal, the lower Nunivak, occurs in the middle of sedimentary cycle 30 (Fig. 5).

3.3. *Punta Grande*

The Punta Grande section has been extended upward with respect to the earlier sampling [9] to reach the Gilbert–Gauss (G/G) boundary. The weathering profile of the Trubi in this section is different and in addition the lithology does not show the same distinct grey–white–beige–white colour cycles: grey and beige layers are not easily distinguished, although the white, indurated layers are easily recognized. Nevertheless, lithological correlation with the other subsections of the Rossello composite is quite straightforward [1] and confirmed by the biostratigraphic data. In the gullies, the weathering surface is at most a few centimetres, and fresh, dark blue marl samples could be taken at all levels.

Despite the fresh, unweathered samples, NRM intensities are very low (0.05–0.30 mA/m). Thermal demagnetization shows that the magnetic properties of the (entire) Punta Grande section are very similar to the lowermost part of the Punta di Maiata section: only a LT characteristic component is removed at ca. 350°C (Fig. 4j–l); demagnetization at higher temperatures introduces only random viscous magnetizations. Time-equivalent intervals at Punta di Maiata and at Punta Piccola, in contrast, show the more familiar (LT and HT) and high-intensity components.

The different rock magnetic properties of both the lowermost part of Punta di Maiata (cycles 21–30) and the entire Punta Grande section (cycles 65–81) compared to the same cycles elsewhere may be due to local variations in the magnetic

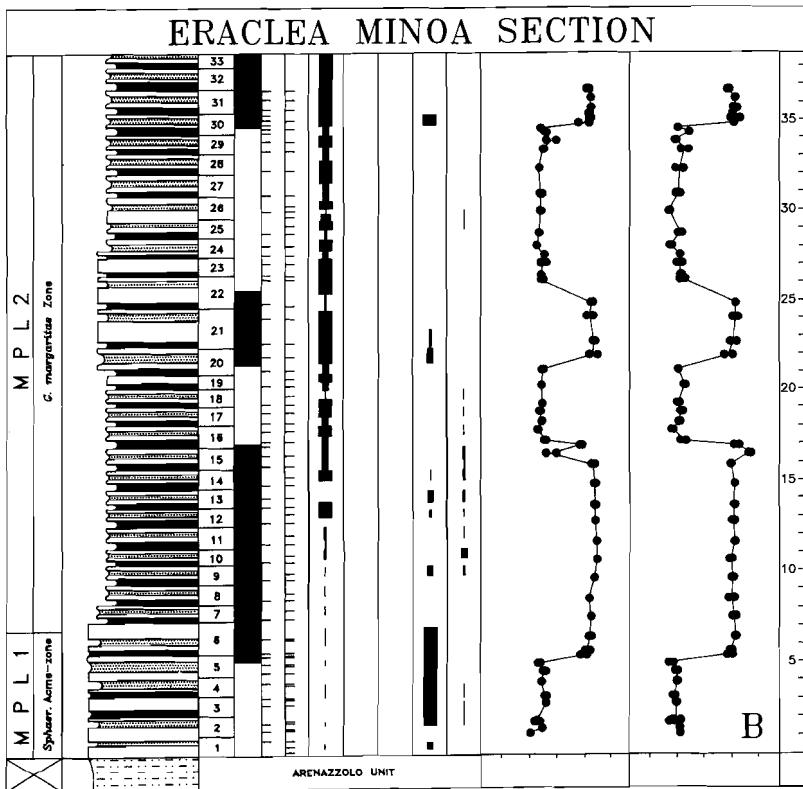
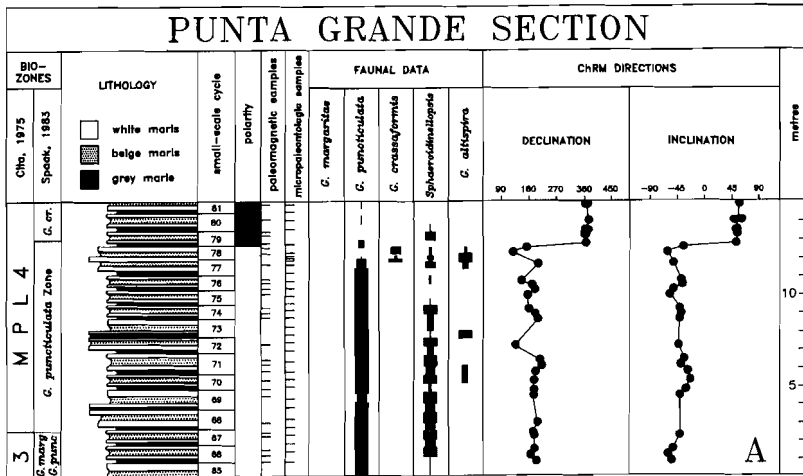


TABLE 1

Ranges and ages of datum levels in the Rossello composite section. Ages of datum planes are presented according to (1) the conventional time scale of Berggren et al. [23] and (2) the astronomical time scale of Hilgen [34]. Ages for bioevents have been calculated by linear interpolation or extrapolation between paleomagnetic reversal boundaries. The age of 2.55 Ma* is taken from Zachariasse et al. [10].

Magnetostratigraphic datum planes		Range	Age 1	Age 2
Gauss/Matuyama		129.94 - 132.79	2.47	2.59 - 2.62
Upper Kaena		103.92 - 104.61	2.92	3.02
Lower Kaena		100.76 - 101.70	2.99	3.09
Upper Mammoth		96.93 - 97.02	3.08	3.21
Lower Mammoth		91.83 - 92.87	3.18	3.33
Gilbert/Gauss		80.37 - 81.10	3.40	3.59
Upper Cochiti		53.39 - 53.84	3.88	4.23
Lower Cochiti		48.74 - 49.65	3.97	4.35
Upper Nunivak		40.72 - 40.80	4.10	4.53
Lower Nunivak		34.25 - 34.54	4.24	4.65
Upper Sidufjall		25.01 - 26.28	4.40	4.85
Lower Sidufjall		21.31 - 22.08	4.47	4.93
Upper Thvera		17.07 - 17.35	4.57	5.03
Lower Thvera		5.00 - 5.45	4.77	5.27
Biostratigraphic datum planes		Range	Age 1	Age 2
<i>N. atlantica</i>	FO	123.34 - 124.04	2.55*	2.67 - 2.70
<i>G. crassaformis</i>	D/S coiling change	109.26 - 110.38	2.78 ± 0.06	2.91 ± 0.01
<i>G. crassaformis</i>	S/D coiling change	106.03 - 106.58	2.84 - 2.89	2.98 ± 0.01
<i>G. crassaformis</i>	D/S coiling change	98.73 - 99.03	3.04 ± 0.01	3.15 - 3.16
<i>G. altispira</i>	LO	98.59 - 98.73	3.04 - 3.05	3.16
<i>S. seminulina</i>	LO	97.33 - 97.52	3.07	3.19 - 3.20
<i>G. crassaformis</i>	S/D coiling change	94.63 - 94.90	3.13 ± 0.01	3.26 - 3.27
<i>G. puncticulata</i>	reappearance	92.86 - 93.31	3.15 - 3.18	3.31 - 3.32
<i>G. crassaformis</i>	reappearance	91.33 - 91.58	3.20 ± 0.01	3.35
<i>G. puncticulata</i>	disappearance	81.62 - 81.79	3.38 ± 0.01	3.57
<i>G. crassaformis</i>	FO	80.36 - 80.63	3.40 ± 0.01	3.59 - 3.60
<i>G. margaritae</i>	LO	70.41 - 71.39	3.56 - 3.59	3.82 ± 0.01
<i>G. margaritae</i>	LCO	62.91 - 63.24	3.71 ± 0.01	4.00 - 4.01
<i>G. puncticulata</i>	FO	39.54 - 39.84	4.12 - 4.13	4.55
<i>G. margaritae</i>	FCO	12.88 - 13.30	4.64 ± 0.01	5.11 - 5.12
<i>Sphaeroidinellopsis</i>	top acme	6.48 - 7.54	4.74 ± 0.01	5.23 ± 0.01
<i>Sphaeroidinellopsis</i>	bottom acme	1.50 - 1.84	4.83 ± 0.01	5.33 - 5.34

carriers or to (presently unknown) secondary processes such as early and/or late diagenesis. The paleomagnetic data of the extended section shows that the G/G reversal boundary can be placed in the basal part of cycle 79 (Fig. 5).

4. The Rossello composite completed

The integrated magnetostratigraphy, biostratigraphy and cyclostratigraphy of the Rossello composite section of Hilgen [1] has been completed

with the present study of the Punta di Maiata subsection (Fig. 6). The positions of the reversal boundaries are presented in Table 1. The resultant polarity sequence shows that the Rossello composite extends from below the Thvera Subchron into the Matuyama Chron (Fig. 5).

The results further reveal that the polarity sequence of the Punta di Maiata section ranges from below the upper Sidufjall into the Gauss Chron. The two complete intervals of normal polarity thus represent the Nunivak and Cochiti Sub-

Fig. 5. Magnetostratigraphy, planktonic foraminiferal biostratigraphy and cyclostratigraphy of the extended subsections of Eraclea Minoa and Punta Grande. ChRM directions are based on the HT component at Eraclea Minoa and on the LT component at Punta Grande. See further explanation in Fig. 3.

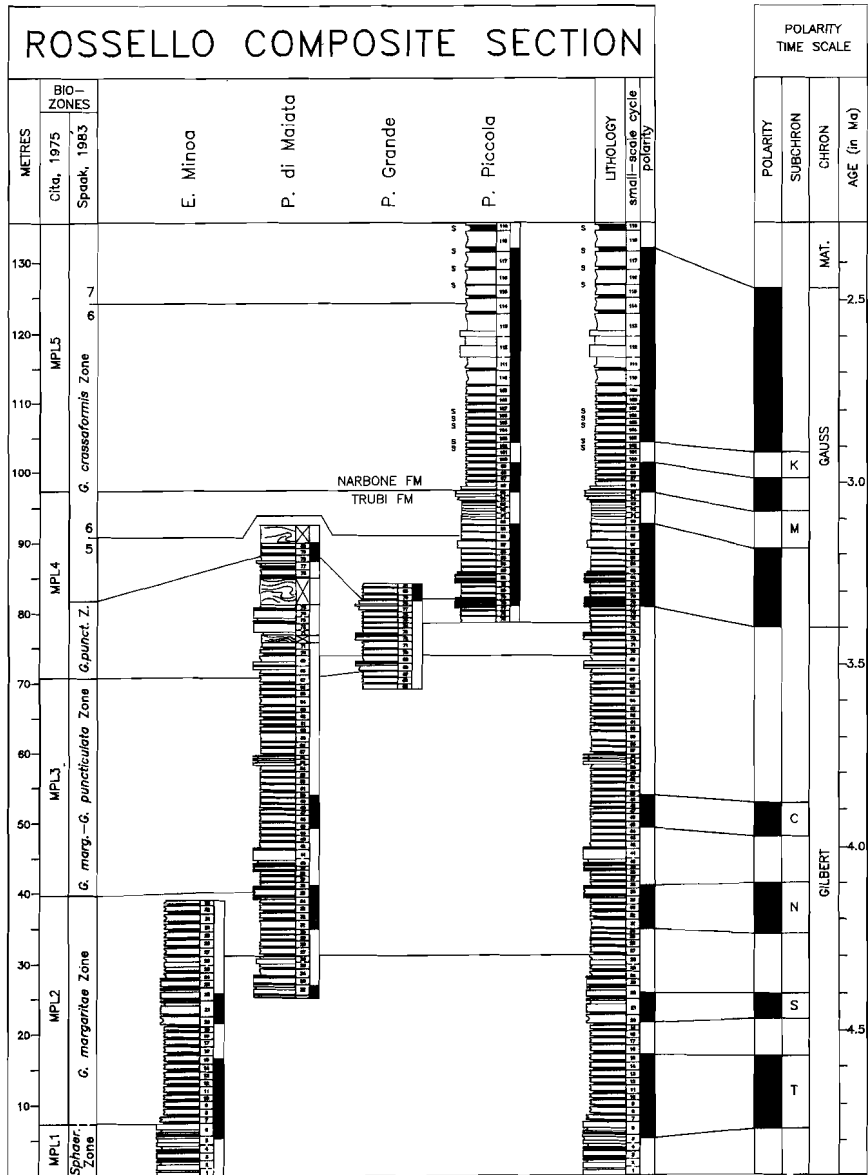


Fig. 6. Integrated stratigraphy of the Rossello composite section showing calibration of the total polarity sequence to the geomagnetic polarity time scale of Berggren et al. [23]. Horizontal lines indicate which part of which subsection has been used for the construction of the composite section. Grey levels marked with *s* in the Punta Piccola section contain brown, laminated ("spropelic") sediments.

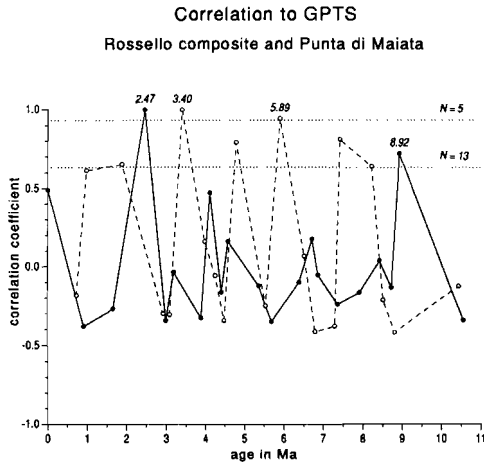


Fig. 7. Correlation coefficients between the lengths of polarity zones in the Punta di Maiata section and the Rossello composite and the durations of each succession of five and thirteen polarity zones from the polarity time scale of Berggren et al. [23] between the Recent and 11 Ma. Dashed line is based on Punta di Maiata (with the exclusion of the slumped intervals), solid line on the Rossello composite section. Values are ages of the youngest reversal in the sedimentary successions which have correlations exceeding the 99% significance level (dotted lines).

chrons. In addition, we have calculated the correlation coefficients between the stratigraphic thicknesses of the polarity zones and the durations of every possible sequence of five polarity zones from the Geomagnetic Polarity Time Scale [23]. This correlation method [24] shows that the highest correlation coefficient corresponds to an age of 3.40 Ma for the youngest reversal boundary in the Punta di Maiata section (Fig. 7) and confirms that this reversal boundary indeed represents the G/G boundary. The same method applied to all thirteen polarity zones in the Rossello composite shows an almost one to one correlation with the polarity time scale if the youngest reversal boundary represents the Gauss/Matuyama boundary with an age of 2.47 (Fig. 7).

The cyclostratigraphic (and biostratigraphic) correlations between the various subsections on which the Rossello composite section was originally based [1] are essentially confirmed by the

new paleomagnetic data from Punta di Maiata, Eraclea Minoa and Punta Grande. There is one exception: the exact position of the Gilbert/Gauss reversal boundary at Punta Grande is located in cycle 79, whereas this boundary has been found in cycle 78 at both Punta di Maiata and Punta Piccola (Figs. 3 and 5). This discrepancy could be due to an error in the logging and numbering of the sedimentary cycles, but the (high-resolution) biostratigraphy and the cyclostratigraphy have been thoroughly rechecked and the results exclude this possibility. The low intensities of the Punta Grande section, which are even lower during a polarity reversal, the low intensities in the topmost part of Punta di Maiata and/or the larger sampling spacing together with increased weathering in Punta Piccola during this interval may be responsible for this slight discrepancy. Current research on detailed polarity reversal records in the Trubi, however, is likely to resolve this problem.

5. Ages of bioevents in the Punta di Maiata section

The correlation of the polarity sequence of the Punta di Maiata section to the Geomagnetic Polarity Time Scale [23] enables us to calculate the ages of bioevents by linear interpolation between paleomagnetic datum levels.

The FO of *G. puncticulata* arrives at 4.12–4.13 Ma. This age perfectly agrees with earlier obtained ages of 4.13 and 4.15 Ma in Trubi sections from adjacent southern Calabria [6,8] and confirms once more that this bioevent represents a useful chronohorizon in the Mediterranean.

As far as the last occurrence of *G. margaritae* is concerned, a distinction can be made between the last common occurrence (LCO) of this species and its actual last occurrence (LO, see Fig. 3). Age constraints for both biohorizons, however, are less straightforward because they occur in a polarity interval which contains two (of the three) slump levels (Fig. 3). Linear interpolation would give ages that are slightly too old because these slumps are located higher in the succession than these biohorizons. A more correct age estimate is obtained if these slumps are excluded from the stratigraphic record. Linear interpolation, in that case, yields ages of 3.72 (± 0.01) and 3.59 (± 0.01) Ma for these datum planes. Approximately the same

ages—3.71 (± 0.01) and 3.56–3.59 Ma, respectively—are obtained if we use the Rossello composite section in which the interval containing the slumps has been avoided (Fig. 6). This age of 3.56–3.59 Ma for the LO of *G. margaritae* corresponds well to previous, indirect age estimates for this biohorizon in the Mediterranean (3.60 Ma, [3]), but it does not agree with the direct age estimate of 3.50 Ma obtained from Site 652 in the Tyrrhenian Sea (ODP Leg 107, [14]). Our current age shows that the LO of *G. margaritae* in the Mediterranean slightly predates its extinction in the open ocean (3.40 Ma, [25,3]).

Finally, the ages of 3.41 (± 0.01) and 3.39 (± 0.01) Ma found for the FO of *G. crassaformis* and the temporary disappearance level of *G. puncticulata* at Punta di Maiata confirm earlier results from the Punta Piccola section (3.40 and 3.38 Ma, [9]). The exact position and inferred age of all planktonic foraminiferal biohorizons in the Rossello composite have been summarized in Table 1.

6. The Zanclean/Piacenzian boundary

The age of 3.56–3.59 Ma for the LO of *G. margaritae* also provides an accurate, first-order age estimate for the Zanclean–Piacenzian (Z/P) stage boundary. In recent years there has been almost unanimous consensus in the literature in the use of Barbieri's [26] redefinition of the Piacenzian and to consider the LO of *G. margaritae* as delimiting the Zanclean and Piacenzian stages because this biohorizon coincides with the base of the Piacenzian in its stratotype section [3,12,13]. Since the type Zanclean extended well above the LO of *G. margaritae*, Mazzei et al. [13] redefined its top at the disappearance level of this species, thereby following the recommendations in the International Stratigraphic Guide [27] according to which the top of a stage is defined by the bottom of the next one.

Very recently, however, detailed biostratigraphic studies revealed that a hiatus is present at the base of the type Piacenzian and, as a consequence, that this base does not coincide with the true last occurrence of *G. margaritae* but actually post-dates it (see [14]). This stratigraphic complication evidently demands a revaluation of the Z/P boundary definition.

If the generally accepted, but not formally defined, physical boundary, i.e. the base of the type Piacenzian, is maintained, all sediments spanning the break are automatically assigned to the older Zanclean stage (see [28], p. 111). This approach is rather unfortunate because it hampers easy recognition of the boundary in sections other than the Piacenzian stratotype. The only alternative is to redefine the base of the Piacenzian, in which case the LO of *G. margaritae* may be maintained as a criterion for this boundary. This option implies that the basal part of the Piacenzian is missing in its stratotype and that the boundary should be redefined at the level of the LO of *G. margaritae* in a continuous, well-dated succession. From a biostratigraphical point of view, however, objections can be raised against the use of this biohorizon. The intermittent and rare manifestation of *G. margaritae* above its last level of common occurrence (see Fig. 3) undeniably reduces the accuracy of this bioevent for time-stratigraphic correlations, even within the Mediterranean. Moreover, this biohorizon is demonstrably diachronous from high to low latitudes in the open ocean [29]. Although the LO of *G. margaritae* from the Mediterranean roughly coincides with its final extinction around the G/G boundary [25,30], it actually seems to slightly pre-date it, as previously suggested by Rio et al. [3]. This relatively small age discrepancy—of the order of 150–200 ka—may well be explained by the observed latitudinal diachroneity of this biohorizon.

Rio et al. [14], following the discovery of the hiatus in the Piacenzian stratotype, suggested redefinition of the Z/P boundary close to the G/G boundary to facilitate worldwide recognition. In this case, the FO of *G. crassaformis* is the most suitable planktonic foraminiferal biohorizon for defining this boundary in the Mediterranean. This horizon is accurately dated at 3.40 Ma both at Punta Piccola [9] and Punta di Maiata, and, although it only represents a first, temporary influx of this species in the Mediterranean, it has been recognized in a large number of sections both on Sicily and Crete (see also [18]). Its entry with respect to the adjacent Atlantic Ocean, however, is clearly delayed [9], which greatly reduces its use in long-distance correlations. The only alternative planktonic foraminiferal event in the G/G boundary interval is the LO of *G. puncticulata* (s.s.

Spaak, 1983 [18]) dated at 3.38 Ma. However, according to present taxonomic views, *G. puncticulata* is only temporarily absent from the Mediterranean until its re-appearance at 3.16 Ma in the form of assemblages which are dominated by its eco-morphotype *G. bononiensis*. The final disappearance of *G. puncticulata* from the Mediterranean is much later (2.31 Ma, [10]) and is coincident with the extinction of this species in the open ocean [10,31].

By far the most practical solution, therefore, is to define the Z/P boundary at the level which corresponds with the G/G reversal boundary. Whatever level will finally be proposed to delimit the Zanclean and Piacenzian stages, it is clear that this boundary can best be "stratotypified" in the Rossello composite section. This section contains an excellent and continuous faunal and polarity record across the critical time interval. In addition, the presence of astronomically controlled sedimentary cycles can further be employed to provide highly accurate age constraints for this boundary, as will be dealt with in the next section.

7. The Rossello composite: a Mediterranean and global reference section for the Early to early Late Pliocene

Irrespective of its potential suitability as neostatotype for the Z/P boundary, the Rossello composite section is of global importance because of its significant role in establishing an astronomically calibrated (polarity) time scale.

Hilgen and Langereis [19] provided an alternative polarity time scale for the major part of the Gilbert and Gauss Chrons by using the average (21.7 ka [32]) quasi-period of the precession cycle as the periodicity for the sedimentary cycles in the Rossello composite section. The G/G boundary, dated radiometrically at 3.40 Ma [33], was used as an age reference point.

More recently Hilgen [34] (in this issue in fact) presented an astronomically calibrated (polarity) time scale for the late Gauss to Matuyama by correlating cyclic patterns of sapropels in the Mediterranean to the astronomical records based on the new solutions of Berger and Loutre [35]. This time scale has only one reversal boundary,

the upper Kaena, in common with the time scale of Hilgen and Langereis [19]. The new astronomically calibrated time scale can be extended back to the Miocene/Pliocene boundary by adding the age difference of 180 ka observed for this reversal boundary to the ages provided by Hilgen and Langereis [19] for the older polarity reversals. The resultant ages for the reversal boundaries as well as those for the planktonic foraminiferal biohorizons in the Rossello composite are presented in Table 1. These ages must be considered preliminary pending a more exact calibration of the sedimentary cycles in the Trubi to the astronomical record. The employment of the Rossello composite section in constructing the definite version of this time scale is further enhanced by the detailed research carried out on the reversal boundaries in this section (and in other sections of the Trubi—[36] and unpublished data). Although because of their preliminary nature the results of this research have not been incorporated in the present study, it is envisaged that eventually the position of all reversal boundaries in the Trubi will be accurately known with a resolution of at most a few thousand years.

We conclude that the Rossello composite section provides an unprecedented, high-quality reference section for the Early to early Late Pliocene. This reference section does not show the drawbacks of the one based on Site 653 from ODP Leg 107 in the Tyrrhenian Sea, which was drilled with the main purpose of recovering a continuous succession of deep marine sediments that would serve as a "deep-sea type section" for both stratigraphic and paleoenvironmental studies [37]. Unfortunately, Site 653 did not yield a reliable magnetostratigraphy due to unsuitable magnetic properties [38]. Consequently, the chronostratigraphy of Site 653 is mainly based on biostratigraphic correlations to (a very limited number of) magnetostratigraphically controlled sections elsewhere in the Mediterranean [14]. Distinct cyclic bedding has apparently not been observed in the major part of the Pliocene at this site. Moreover, no serious attempts have been made so far to cross-correlate Sites 653A and B. This will be necessary to overcome problematic core recovery at core breaks [see 39] and to obtain a real, continuous succession

8. Conclusions

The integrated magnetostratigraphy (planktonic foraminiferal) biostratigraphy and cyclostratigraphy of the Rossello composite section of Hilgen [1] has been completed with the present study of the Punta di Maiata subsection. This Rossello composite section contains a complete succession of open, deep-marine sediments, which extends from below the Thvera Subchron into the Matuyama Chron. It provides an unprecedented, high-quality standard reference section for the Early to early Late Pliocene.

Semi-quantitative biostratigraphic data from the Punta di Maiata section allow a distinction to be made between the last common occurrence and the actual last occurrence of *G. margaritae*. Linear interpolation between reversal boundaries yield accurate age estimates of 3.72 and 3.59 Ma for these biohorizons.

The Punta di Maiata section (in the case the LOD of *G. margaritae* being maintained as the boundary criterion) and the Punta Piccola section (in the case of a horizon chosen close to or at the Gilbert–Gauss reversal boundary) are at present the most suitable sections for formally designating the Zanclean–Piacenzian stage boundary.

The global significance of the Rossello composite is greatly enhanced by the fact that a major part of the astronomically calibrated (polarity) time scale for the last 5.5 Ma is based on this section.

To further improve the importance of the Rossello composite, additional studies, for example on stable isotopes and calcareous nannofossils, should be carried out. Sampling or resampling of this section will be greatly facilitated by the characteristic succession of the sedimentary cycles in the Trubi.

Acknowledgements

Piet-Jan Verplak did most of the paleomagnetic laboratory measurements, and he and Ton van Hoof have provided considerable support during the field trips. Tom van Hinte skillfully did drawings, and G.J. van 't Veld and G. Ittman prepared the micropaleontological samples. J.D.A. Zijderveld and W.J. Zachariasse critically read the

manuscript. We thank M.B. Cita, J.E.T. Channell and W. Lowrie for their reviews.

The hospitality and the good wine and food provided by the Ragusa family of the "Ristorante Il Gabbiano" at Eraclea Minoa made our numerous sampling trips in the area distinctly more pleasant.

References

- 1 F.J. Hilgen, Sedimentary rhythms and high-resolution chronostratigraphic correlations in the Mediterranean Pliocene, *Newslett. Stratigr.* 17, 109–127, 1987.
- 2 G.C. Carloni, P. Marks, R.F. Rutsch and R. Selli (eds.), *Stratotypes of Mediterranean Neogene Stages*, *G. Geol.* 37, 1971.
- 3 D. Rio, R. Sprovieri and I. Raffi, Calcareous plankton biostratigraphy and biochronology of the Pliocene–Lower Pleistocene succession of the Capo Rossello area, Sicily, *Mar. Micropaleontol.* 9, 135–180, 1984.
- 4 L. Tauxe, N.D. Opdyke, G. Pasini and C. Elmi, Age of the Plio-Pleistocene boundary in the Vrica section, southern Italy, *Nature* 304, 125–129, 1983.
- 5 J.D.A. Zijderveld, F.J. Hilgen, C.G. Langereis, P.J.J.M. Verhallen and W.J. Zachariasse, Integrated magnetostratigraphy and biostratigraphy of the upper Pliocene–lower Pleistocene from the Monte Singa and Crotona areas Calabria (Italy), *Earth Planet. Sci. Lett.*, submitted, 1991.
- 6 J.D.A. Zijderveld, W.J. Zachariasse, P.J.J.M. Verhallen and F.J. Hilgen, The age of the Miocene–Pliocene boundary, *Newslett. Stratigr.* 16, 169–181, 1986.
- 7 F.J. Hilgen and C.G. Langereis, The age of the Miocene–Pliocene boundary in the Capo Rossello area (Sicily), *Earth Planet. Sci. Lett.* 91, 214–222, 1988.
- 8 J.E.T. Channell, D. Rio and R.C. Thunell, Miocene/Pliocene boundary magnetostratigraphy at Capo Spartivento, Calabria, Italy, *Geology* 16, 1096–1099, 1988.
- 9 W.J. Zachariasse, J.D.A. Zijderveld, C.G. Langereis, F.J. Hilgen and P.J.J.M. Verhallen, Early Late Pliocene biochronology and surface water temperature variations in the Mediterranean, *Mar. Micropaleontol.* 14, 339–355, 1989.
- 10 W.J. Zachariasse, L. Gudjonsson, F.J. Hilgen, C.G. Langereis, L.J. Lourens, P.J.J.M. Verhallen and J.D.A. Zijderveld, Late Gauss to early Matuyama invasions of *Neogloboquadrina atlantica* in the Mediterranean and associated record of climatic change, *Paleoceanography* 5, 239–252, 1990.
- 11 J.E.T. Channell, M. Torii and T. Hawthorne, magnetostratigraphy of sediments recovered at Sites 650, 651, 652 and 654 (Leg 107, Tyrrhenian Sea), *Proc. ODP, Sci. Results* 107, 335–346, 1990.
- 12 W.A. Berggren and J.A. van Couvering, The Late Neogene, *Palaeogeogr., Palaeoclimatol., Palaeoecol.* 16, 1–215, 1974.
- 13 R. Mazzei, I. Raffi, D. Rio, N. Hamilton and M.B. Cita, Calibration of Late Neogene calcareous plankton datum planes with the paleomagnetic record of Site 397 and correlation with Moroccan and Mediterranean sections, *Init. Rep. DSDP* 47, 375–389, 1979.

- 14 D. Rio, R. Sprovieri and J. Channell, Pliocene-early Pleistocene chronostratigraphy and the Tyrrhenean deep-sea record from Site 653. *Proc. ODP, Sci. Results* 107, 705-714, 1990.
- 15 M.B. Cita and S. Gartner, Studi sul Pliocene e sugli strati di passaggio dal Miocene al Pliocene IV. The stratotype Zanclean. Foraminiferal and nannofossil biostratigraphy. *Riv. Ital. Paleontol. Stratigr.* 79, 503-558, 1973.
- 16 M.B. Cita, The Miocene/Pliocene boundary. History and definition, in: *Late Neogene Epoch Boundaries*, T. Saito and L.H. Burckle, eds., *Micropaleontol. Press, Spec. Publ.* 1, 1-30, 1975.
- 17 M.B. Cita and A. Decima, Rossellian: proposal of a super-stage for the marine Pliocene. *Proc. VI CMNS Congr. Bratislava*, pp. 217-227, 1975.
- 18 P. Spaak, Accuracy in correlation and ecological aspects of the planktonic foraminiferal zonation of the Mediterranean Pliocene, *Utrecht Micropaleontol. Bull.* 28, 1-160, 1983.
- 19 F.J. Hilgen and C.G. Langereis, Periodicities of CaCO₃ cycles in the Mediterranean Pliocene: Discrepancies with the quasi-periods of the Earth's orbital cycles?, *Terra Nova* 1, 409-415, 1989.
- 20 A.J. van Velzen and J.D.A. Zijderveld, Rock magnetism of the early Pliocene Trubi Formation at Eraclea Minoa (Sicily), *Geophys. Res. Lett.* 17, 791-794, 1990.
- 21 K.L. Verosub, Depositional and postdepositional processes in the magnetization of sediments, *Rev. Geophys. Space Phys.* 15, 129-142, 1977.
- 22 M.B. Cita, Planktonic foraminiferal biozonation of the Mediterranean deep sea record. A revision, *Riv. Ital. Paleontol. Stratigr.* 81, 527-544, 1975.
- 23 W.A. Berggren, D.V. Kent, J.J. Flynn and J.A. van Couvering, Cenozoic geochronology, *Geol. Soc. Am. Bull.* 96, 1407-1418, 1985.
- 24 C.G. Langereis, W.J. Zachariasse and J.D.A. Zijderveld, Late Miocene magnetostratigraphy in the Mediterranean, *Mar. Micropaleontol.* 8, 261-281, 1984.
- 25 J.D. Hays, T. Saito, N.D. Opdyke and L.H. Burckle, Pliocene-Pleistocene sediments of the equatorial Pacific. Their paleomagnetic, biostratigraphic and climatic record, *Geol. Soc. Am. Bull.* 80, 1481-1514, 1969.
- 26 F. Barbieri, The foraminifera in the Pliocene section Vernasca-Castell'Arquato including the "Piacenzian stratotype" (Piacenza Province), *Mem. Soc. Ital. Sci. Nat.* 15, 145-163, 1967.
- 27 H.D. Hedberg, *International Stratigraphic Guide. A Guide to Stratigraphic Classification, Terminology and Procedure*, Wiley, New York, 189 pp., 1976.
- 28 M.D. Miall, *Principles of Sedimentary Basin Analysis*, Springer, New York, 490 pp.
- 29 J.G. Baldauf, E. Thomas, B. Clerrert, T. Takayama, P.P.E. Weaver, J. Backman, G. Jenkins, P.J. Mudie and M.J. Westberg-Smith, Magnetostratigraphic and biostratigraphic synthesis, Deep Sea Drilling Project Leg 94, *Init. Rep. DSDP 94*, 1159-1205, 1986.
- 30 P.P.E. Weaver, J. Backman, J.G. Baldauf, J. Bloemendal, H. Manivit, K.G. Miller, E.M. Prokras, M.E. Raymo, L. Tauxe, J.-P. Valet, A. Chepstow-Lusty and G. Olafsson, Biostratigraphic synthesis: Leg 108, eastern equatorial Atlantic, *Proc. ODP, Sci. Results* 108, 455-462, 1989.
- 31 M.E. Raymo, W.F. Ruddiman, J. Backman, B.M. Clement and D.G. Martinson, Late Pliocene variation in northern hemisphere ice sheets and North Atlantic deep water circulation, *Paleoceanography* 4, 413-446, 1989.
- 32 A.L. Berger, Accuracy and frequency stability of the Earth's orbital elements during the Quaternary, in: *Milankovitch and Climate*, NATO ASI Ser. C, 126, A.L. Berger et al., eds., Riedel, Dordrecht, pp. 3-39, 1984.
- 33 E.A. Mankinen and G.B. Dalrymple, Revised geomagnetic polarity time scale for the interval 0-5 m.y. B.P., *J. Geophys. Res.*, 84, 615-626, 1979.
- 34 F.J. Hilgen, Astronomical calibration of Gauss to Matuyama sapropels in the Mediterranean and implication for the Geomagnetic Polarity Time Scale, *Earth Planet. Sci. Lett.* 104, 226-244, this issue, 1991.
- 35 A. Berger and M.F. Loutre, New insolation values for the climate of the last 10 Myr, *Inst. Astron. Geophys. G. Lemaitre, Univ. Cathol. Louvain, Init. Rep.*, 1988.
- 36 J.H. Linssen, Preliminary results of a study of four successive sedimentary geomagnetic reversal records from the Mediterranean (Upper Thvera, Lower and Upper Sidufjall, and Lower Nunivak), *Phys. Earth Planet. Inter.* 52, 207-231, 1988.
- 37 Shipboard Scientific Party, Site 653, *Proc. ODP, Init. Rep.* 107, 599-745, 1987.
- 38 J.E.T. Channell and T. Hawthorne, Progressive dissolution of titanomagnetites at ODP Site 653 (Tyrrhenian Sea), *Earth Planet. Sci. Lett.* 96, 469-480, 1990.
- 39 W.F. Ruddiman, D. Cameron and B.M. Clement, Sediment disturbance and correlation of offset holes drilled with the hydraulic piston corer: Leg 94, *Init. Rep. DSDP 94*, 615-634, 1986.
- 40 J.D.A. Zijderveld, A.C. demagnetization of rocks: analysis of results, in: *Methods in Paleomagnetism*, D.W. Collinson et al., eds., Elsevier, Amsterdam, pp. 254-286, 1967.
- 41 A.A.M. van Hoof and C.G. Langereis, Reversal records in marine marls and delayed acquisition of remanent magnetization, *Nature*, in press, 1991.

Chapter 6

Integrated magnetostratigraphy and biostratigraphy of the upper Pliocene–lower Pleistocene from the Monte Singa and Crotona areas in Calabria, Italy

J.D.A. Zijderveld ^a, F.J. Hilgen ^a, C.G. Langereis ^a, P.J.J.M. Verhallen ^b
and W.J. Zachariasse ^b

^a Paleomagnetic Laboratory, Fort Hoofddijk, Budapestlaan 17, 3584 CD Utrecht, The Netherlands

^b Institute of Earth Sciences, Budapestlaan 4, 3584 CD Utrecht, The Netherlands

ABSTRACT

The results of a detailed magnetostratigraphic and biostratigraphic study of late Pliocene to early Pleistocene marine marl sequences from the Monte Singa and Crotona areas in Calabria, Italy are presented.

The magnetostratigraphy from the Monte Singa sequence ranges from below the Gauss/Matuyama boundary up to and including the lower Olduvai boundary. Normal polarities at a level corresponding to isotope stage 81 most probably represent the Réunion subchron. From the lower Olduvai boundary upward, a reliable magnetostratigraphy could not be established due to increased weathering of the marls, resulting in mainly secondary magnetizations.

The magnetostratigraphy from the composite sequence of the Crotona area belongs to a large part of the Matuyama Chron and includes the Olduvai subchron. The position of the lower and upper boundaries of the Olduvai subzone could be established more precisely than from earlier results. Moreover, the upper boundary of the Olduvai subzone poses an ambiguity: a relatively long normal polarity interval representing the main Olduvai subchron and corresponding to a duration of 115 ka is followed by a short (30 ka) reversed subchron and the short (15 ka) normal *Vrica* subchron. Another option, and more in accordance with the duration of the Olduvai subchron in literature, would be to consider the complete N–R–N polarity succession with a total duration of 160 ka as representing the Olduvai subchron, implying that this Olduvai subchron has a short reversed interval in its upper part.

Linear interpolation and extrapolation yield ages for the most important late Pliocene–early Pleistocene biostratigraphic datum levels. An age of 1.69 Ma is found for the Pliocene–Pleistocene boundary, using the conventional polarity time scale dated with radiometric results. However Hilgen [1], in correlating the sapropel groups and patterns to the precession curve of the Earth's orbit, obtained significantly different ages for the polarity transitions of the present study. According to this astronomically calibrated polarity time scale, the age of the Pliocene–Pleistocene boundary is 1.81 Ma.

1. Introduction

A long tradition in Pliocene stratigraphy has led to the definition of many stages and boundaries for this epoch in the Mediterranean. Most of the marine sedimentary sequences involved are located on the Italian peninsula. Good paleomagnetic control has long been lacking, however, and only recently have an increasing number of magnetostratigraphic studies been published on Pliocene land sections in the Mediterranean. The Miocene–Pliocene (M/P) boundary has been studied by various authors [2–4] and now has an age, according to the conventional radiometric

time scale, of 4.86 Ma, slightly below the Thvera subchron. The early Pliocene and early late Pliocene have been the subject of detailed magnetostratigraphic and biostratigraphic research by Langereis and Hilgen [5] and Zachariasse et al. [6,7].

The present study gives a new and detailed magnetostratigraphy and biostratigraphy for the Mediterranean upper Pliocene and lower Pleistocene from southern Italy. Paleomagnetic results for this time interval in Mediterranean land-based sections have been provided earlier by Tauxe et al. [8], who studied the Pliocene–Pleistocene boundary section of *Vrica* and the lower Se-

maforo section in the Crotona area of northern Calabria. They concluded that the normal polarity interval in the middle of the Vrica section represents the Olduvai subchron. In addition, normal polarities were found in the top part of the section. However, the resolution obtained by Tauxe et al. [8] was not sufficient to define the lower and upper boundaries of the Olduvai subchron with adequate accuracy [1]. Moreover, originally the Semaforo–Vrica sequence was thought to be discontinuous. Therefore, we resorted to Monte Singa in adjacent southern Calabria (Fig. 1), where a continuous sequence of open-marine marls and clays — containing sapropelitic layers — is exposed in the upper Singa section. Due to poor paleomagnetic properties in the upper part of this Singa section, however, we had to revert to the Vrica section (Fig. 1), although in the present study sampling was carried out in appreciably more detail than previously [8]. Moreover, it could be shown that the alleged gap between the Semaforo and Vrica sections in fact does not exist [9].

With the present study, a major part of our research of the integrated magnetostratigraphy and biostratigraphy of the Mediterranean Pliocene recorded in land-based sections has been completed. The magnetostratigraphy, in combination with the orbitally forced sedimentary cycles, has resulted in a new and astronomically dated polarity time scale [1.5,10–12].

2. Sections and sampling

2.1. Monte Singa area

Monte Singa comprises 225 m of well-exposed marine marls and clays which cover a considerable part of the Pliocene, including the Miocene–Pliocene (M/P) boundary and the Pliocene–Pleistocene (P/P) boundary. In the middle of the Pliocene, however, a substantial part is missing: a hiatus of approximately 1 Ma corresponds to the interval of the uppermost part of the Gilbert Chron and a major part of the Gauss Chron [2,7]. The sequence below the hiatus (lower Singa) includes the M/P boundary and

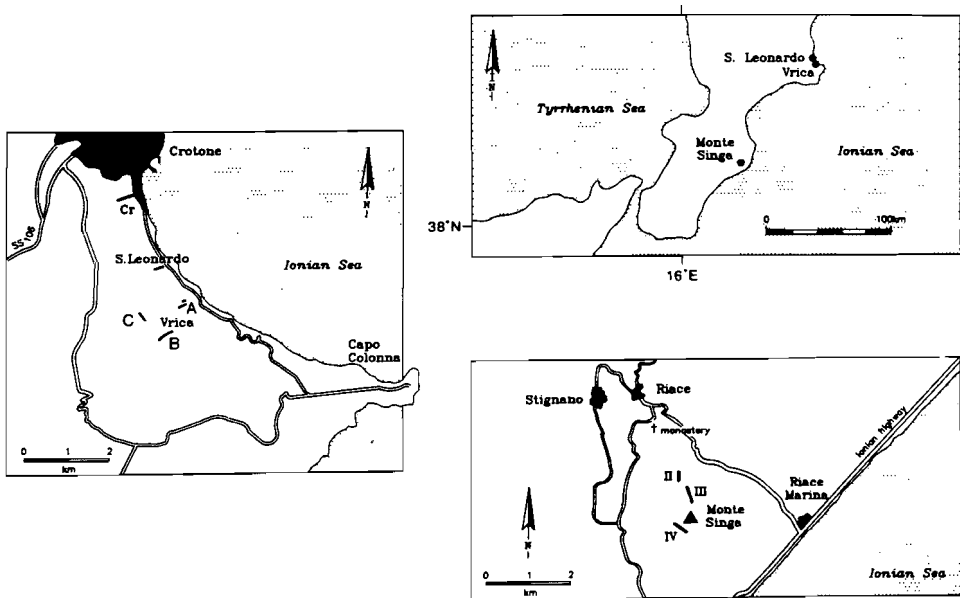


Fig. 1. Location of the studied sections.

has been the subject of a study by Zijdeveld et al. [2]. The sequence above the hiatus (upper Singa) is the subject of the present study. This upper Singa section is composed of three subsections (Singa II, III and IV) which are spread over the northeastern flanks of Monte Singa. The tilt of the strata is 5° and 15°SSE for subsections Singa II and III respectively, and 5°E for subsection Singa IV. Subsections Singa II and IV end upwards at topographical highs and consequently their upper parts are strongly weathered.

The correlation between the subsections is based on frequently occurring sapropelitic layers. Although the composition of all these sapropelitic layers may not be in complete agreement with the more restricted redefinition for sapropels by Kidd et al. [13], we prefer to use the name "sapropel" in the original meaning of Olausson [14]. The sapropels are not distributed evenly throughout the stratigraphic record, but occur in distinct clusters (Fig. 2). Three large-scale clusters have been informally coded as the A, B and C groups [15]. These large-scale clusters contain several small-scale clusters, each of which comprise two to four individual sapropels. The individual sapropels have been labeled according to their position in a cluster (A1–5, B1–7, C1–14; see fig. 2). The resulting complex pattern has been interpreted as interference patterns related to the Earth's orbital cycles [1,10].

2.2. Crotona area

The Vrica section was formally designated as the Pliocene–Pleistocene (P/P) boundary stratotype [16] and has been intensely studied [8,9,17–20]. The section consists of three subsections, Vrica A, Vrica B and Vrica C, as originally designated by Selli et al. [18], and not to be confused with our sapropel labeling. This composite sequence shows a sapropel pattern similar to that found in the Singa section (Fig. 2). Most of these sapropels, as well as several other lithological marker levels, have informally been labeled as *a* to *i* by Selli et al. [18]. The P/P boundary has been defined at the top of sapropel *e* [16]. The sapropels in the Vrica section can be unambiguously correlated to the B and C cluster from the Singa section (Fig. 2; [9,15]). This correlation implies that the P/P boundary in the upper Singa section must be placed at the top of sapropel C6.

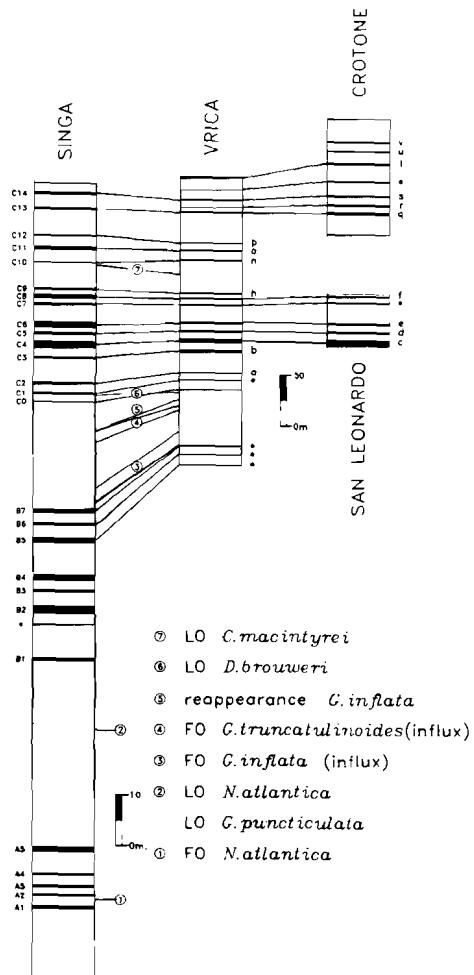


Fig. 2. Litho- and biostratigraphical correlations between the studied sections. The sapropels of the Singa and the Crotona area sections can be correlated one to one.

In the Vrica section the sequence from sapropel *c* up to *f*, containing the upper boundary of the Olduvia subzone, occupies a visibly weathered interval. Therefore, in order to obtain better results and a higher resolution, this important interval was resampled in the San Leonardo section

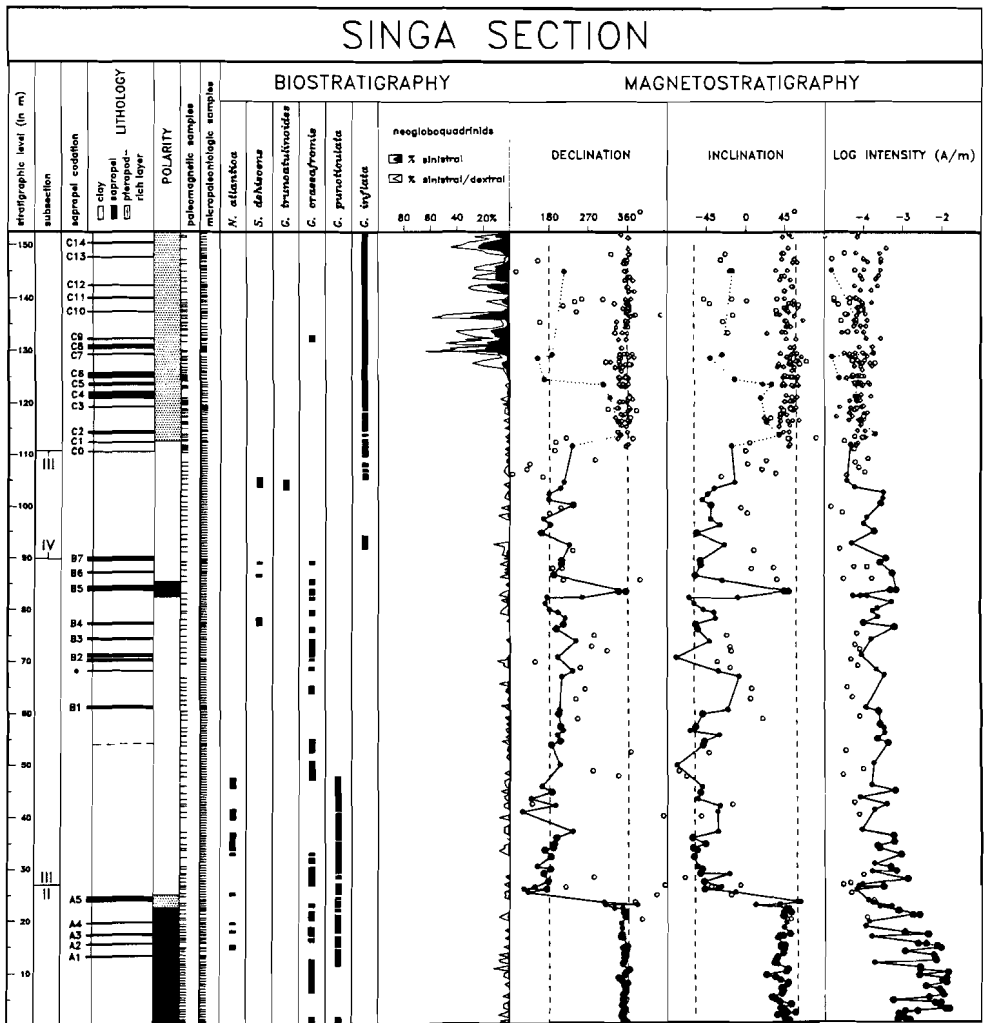


Fig. 3. Lithostratigraphy, biostratigraphy and magnetostratigraphy of the upper part of the Singa composite section. Regarding the characteristic remanent magnetization (ChRM) and remanence intensity of the upper Singa section, the analysis of the demagnetization diagrams involved the use of three reliability classes. The first class (larger dots) represents reliable characteristic remanent magnetizations (ChRM) of fresh marl samples, with almost no secondary component and a linear decrease towards the origin at temperatures higher than 200–250°C. The second class (smaller dots) are less reliable ChRMs, with a relatively large secondary overprint resulting in the directions being less well determined, but the polarities are still reliable. The third class (circles) shows a large dominating secondary overprint and it is not always certain whether a direction is truly normal or whether only, or mostly, the overprint is seen; unreliable specimens are often from parts where no fresh unweathered sediment could be obtained. The plotted intensities are those taken (where possible) at 200 or 250°C, i.e. after removal of the secondary present-day field magnetization. Diamonds denote magnetizations which have been interpreted as secondary only, corresponding intensities are those taken at 100°C. Generally, lower intensities agree well with lower class magnetizations.

(Figs. 1 and 2). For the present study the Vrica section is extended upwards by the Crotone section. This section could be tied to the Vrica section using sapropels *q*, *r* and *s* (Fig. 2). In the Crotone section the coding of Selli et al. [18] is supplemented with two extra sapropels, *u* and *v*. Fresh samples could be obtained from below *q* up to *u*, whereas between sapropels *u* and *v* this was impossible because of the extent of the

weathering. With the exception of the Vrica C subsection and the upper part of the Crotone section where tilt = $5\frac{1}{2}^{\circ}$ W, the tilt of the strata in the Vrica and Crotone area is uniformly $8\frac{1}{2}^{\circ}$ W.

2.3. Sampling

Sampling was carried out by drilling at least two cores per stratigraphic level (site), using an electric drill and a portable generator. Strati-

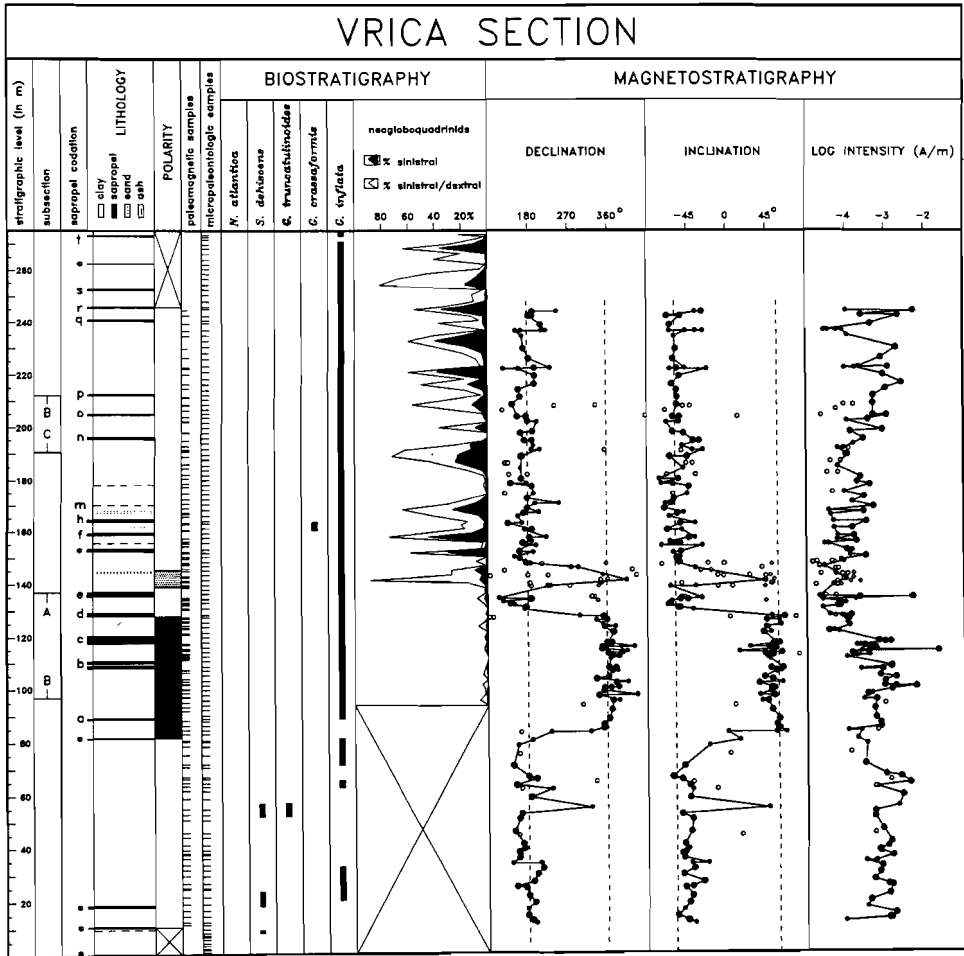


Fig. 4. Lithostratigraphy, biostratigraphy and magnetostratigraphy of the Vrica composite section. See caption to Fig. 3 for further explanation.

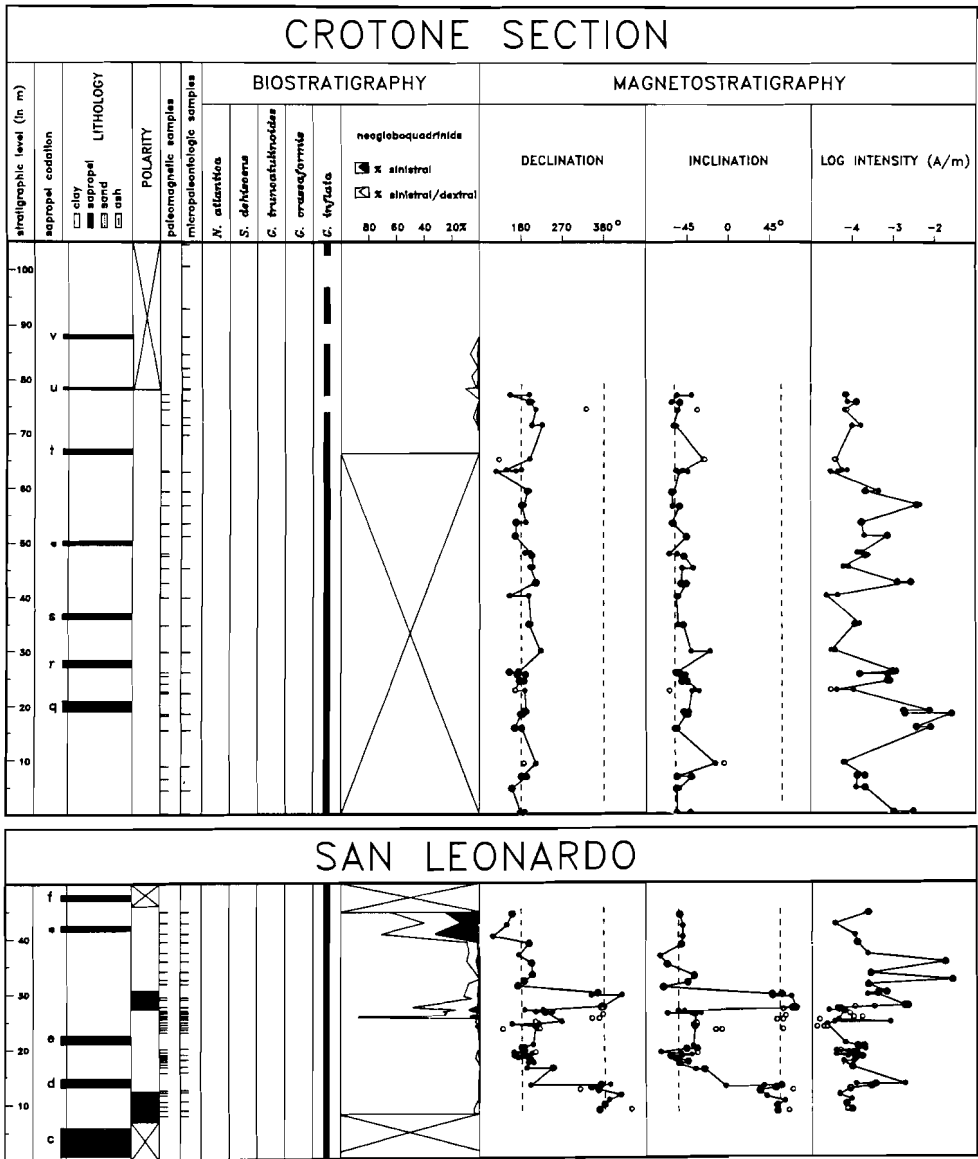


Fig. 5. Lithostratigraphy, biostratigraphy and magnetostratigraphy of the Crotone and San Leonardo sections. See caption to Fig. 3 for further explanation.

graphic positions were accurately determined using distance, azimuth and angle between levels, and orientation of the bedding plane. Considerable efforts were made to remove the weathered surface and to drill in fresh, blue-coloured sediment. If the sediment proved to be too weathered, we refrained from taking samples (e.g., between sapropels *r* and *s* in subsection Vrica C). In several cases we have resampled parts of the sampling track if another gully appeared more suitable (i.e., fresher sediment). The freshness, colour and general appearance of each level and the core details were carefully registered. This sampling procedure has enabled us to assess the validity of the paleomagnetic results in a most reliable manner.

The upper Singa section was sampled during several field trips. More than 190 paleomagnetic sites have been recorded over the total stratigraphic interval of 155 m of marine marls (Fig. 3). In the Vrica section, 155 sites were sampled over a stratigraphic interval of 235 m up to sapropel *r* (Fig. 4). In the Crotona section, 30 paleomagnetic sampling sites were sampled over the 80 m fresh interval up to sapropel *u* (Fig. 5), whereas in the San Leonardo section 41 sites were taken over the paleomagnetically sampled 36 m interval (Fig. 5).

3. Biostratigraphy

The Singa/Vrica composite sequence ranges from the *G. crassaformis* Zone (Interval 6 of Spaak [21] and MPL 5 of Cita [22]) into the Pleistocene. The stratigraphic positions of selected calcareous nannofossil events in the Singa section have been taken from Driever ([23] and unpublished data).

The planktonic foraminiferal zonation is based primarily on the absence or presence of the marker species *Globorotalia crassaformis*, *Globorotalia truncatulinoides*, *Sphaeroidinella dehiscentes*, *Neogobosquadrina atlantica* and the *Globorotalia inflata* group in fractions coarser than 125 μm (Figs. 3, 4 and 5). The *G. inflata* group includes *G. puncticulata* in the lower part of the upper Singa section, and *G. inflata* in the upper part of the upper Singa section and in the Vrica, San Leonardo and Crotona sections.

In the upper Singa section, the first occurrence (FO) of *N. atlantica* is observed between sapro-

pel A1 and A2 (Fig. 3). Subsequent occurrences of this species among the A cluster are found between A3 and A4 and between A4 and A5. Three more influxes occur in the thick homogeneous interval between the A and B sapropel clusters. These successive occurrences of *N. atlantica* have been correlated to glacial isotope stages 108, 106, 104, 100, 98 and 96 in DSDP Site 607 [7]. An even older influx of this species has recently been found slightly below the A1 in the Punta Piccola section on Sicily and correlates with stage 110 [24]. The last occurrence (LO) of *N. atlantica* in the Mediterranean is marked by the influx of this species at isotopic stage 96 and is synchronous with the final extinction of the species in the North Atlantic [7,25].

G. crassaformis is regularly but discontinuously present from the base of the upper Singa section up to sapropel B7 (Fig. 3). A last short-term influx is recorded around sapropel C9 (or *h*) in both the Singa and Vrica section. This influx, however, does not represent the actual last occurrence of this species in the Mediterranean, because younger occurrences have been also observed, for instance at ODP Site 653 in the Tyrrhenian Sea (Leg 107 [26]).

Rare and discontinuous occurrences of *S. dehiscentes* are restricted to a short stratigraphic interval which extends from sapropel B4 to well below C0 (Fig. 3). The last occurrence (LO) of this species closely coincides with the FO of *G. truncatulinoides*. This FO corresponds to a first and brief influx followed by a long period of absence. This brief influx of *G. truncatulinoides* was previously reported from time-equivalent sections elsewhere in the Mediterranean [27] and marks a very distinct bio-event. The reappearance level is not reached in our sections.

G. puncticulata is almost continuously present from the base of the upper Singa section to its disappearance level between the A and B sapropel clusters. This level coincides exactly with the LO of *N. atlantica*. The LO of *G. puncticulata* is followed by a prolonged absence interval of the *G. inflata* group (i.e., second absence interval of Spaak [21]), while *G. inflata* enters the record above sapropel B7. This first occurrence of *G. inflata* represents a brief influx, whereafter this species vanishes from the record until a level situated below C0. From this level upwards, *G.*

inflata is almost continuously present up to the top of our sections.

The percentage of sinistrally coiled neogloboquadrinids of the total of the neogloboquadrinids (excluding *N. atlantica*) as well as of the total of planktonic foraminifers has been determined. A first significant increase in left-coiling neogloboquadrinids is consistently observed slightly above the top of sapropel C6/e (Figs. 3, 4 and 5), i.e. the level which marks the P/P boundary. Percentages of sinistrally coiled neogloboquadrinids display a highly fluctuating pattern from the P/P boundary up to the top of the Vrica section.

4. Magnetostratigraphic results of the sections

Two specimens per sampling level have been progressively demagnetized, in general thermally and using small temperature increments (of 50 and 30°C). Only a small number of samples has been treated with alternating magnetic fields. We divided the demagnetization results into three reliability classes (see caption to Fig. 3), each of which was given a different symbol in the magnetostratigraphic plots (Figs. 3, 4 and 5).

The magnetic characteristics appeared to vary with stratigraphic and topographic position. Despite efforts to obtain samples that were as fresh as possible, the influence of alterations due to weathering was not always absent. These alterations cause some ambiguities at several intervals and for clarity the results of the upper Singa and Crotona sections will be treated separately. In general, the characteristic NRM components assessing the normal and reversed polarity zones reveal opposite directions with inclinations systematically lower than the present local geomagnetic direction. These paleomagnetic directions will be the subject of separate studies.

4.1. Upper Singa section

Starting immediately above the hiatus in the middle of subsection Singa II, the initial intensity of the NRM is usually well above 2 mA/m, and often up to 25 mA/m. There is no or only a small secondary remanence, which is removed at 150–200°C (Fig. 6a). The characteristic remanent magnetization (ChRM) is composite, i.e. thermal demagnetization up to 300–350°C first removes a

low-temperature (LT) component, up to 480–500°C there is almost no decay, and subsequently a high-temperature (HT) component is removed at temperatures up to 600–610°C (Fig. 6a). The LT component may reside in an iron-sulphide (pyrrhotite, greigite), whereas the HT component most likely resides in magnetite, which may be slightly cation-deficient considering that blocking temperatures are often higher than 578°C [28,29]. This NRM composition is identical to that of the early Pliocene Trubi of the lower Singa section [2,28]. A primary origin of the characteristic components has been inferred earlier [2]; a most compelling argument is the positive correlation to the geomagnetic polarity time scale (GPTS) of the polarity pattern based on these characteristic remanences in the lower Singa section.

The paleomagnetic results of the stratigraphic interval immediately above the hiatus reveal a normal polarity. The excellent magnetic properties are continuously present up to sapropel A2. Above this level, the NRM intensity gradually decreases and occasionally some more weathered sites are intercalated. Nevertheless, reliable observations of a two-component ChRM yielding normal polarity continue up to at least level 22.0 m (Fig. 3). The next few metres enclose sapropel A5 and show low magnetic intensities and intermediate paleomagnetic directions which can be associated with a transition from normal to reversed polarities. The sampling levels between 25.0 m and the top of the Singa II subsection at 27.0 m convincingly reveal reversed polarity ChRM directions (Fig. 3).

Subsection Singa III continues the magnetostratigraphic record at 3 m above sapropel A5 (i.e. at level 27.5 m in Fig. 3). Approximately at the polarity transition, the NRM changed to a composition that seems typical for the upper Pliocene and lower Pleistocene marine marls of Calabria. The initial intensity is moderate (between 0.2 and 0.5 mA/m and occasionally up to 2.0 mA/m) and the NRM consists only of the LT component, which is removed entirely at temperatures near 350°C (Fig. 6b). Usually, secondary components are relatively small and removed at 100–200°C. A subsequent linear decrease towards the origin, up to 350°C, represents the removal of a well-defined ChRM component which seems to reside exclusively in pyrrhotite or

greigite. The primary nature of this component is supported by the reversed polarity throughout the Singa III subsection. This consistent picture is only seldomly interrupted by sites with mainly

secondary or unreliable magnetizations. Only a single site at level 83.2 m (Fig. 3) reveals normal polarity, which is represented by the characteristic low blocking temperature (350°C) component.

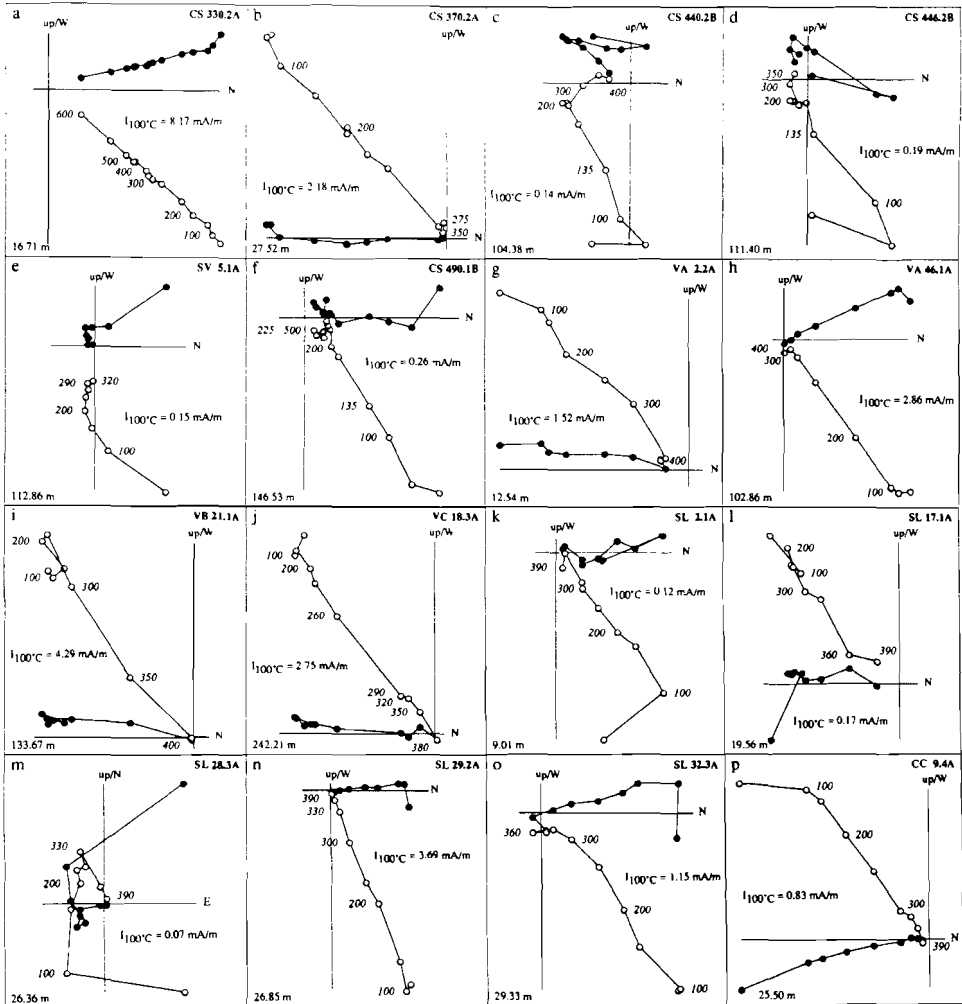


Fig. 6. Some typical examples of progressive thermal demagnetizations of the Pliocene/Pleistocene marine marls. Circles represent positions in orthogonal projection of the resultant NRM vector on the vertical N-S (or E-W) plane; dots represent those on the horizontal plane. Numbers in italics along the projection on the vertical plane are temperatures (°C). The NRM intensity after heating to 100°C is given. The number in the bottom left-hand corner of each diagram represents the level of the specimen in its section. In the top right-hand corner the specimen code is found: *CS* and *SV* pertain to the upper Singa section, *VA*, *VB* and *VC* to the Vrica sections, *SL* to the San Leonardo section, and *CC* to the Crotona section.

It will be shown that this normal polarity site led to the discovery of the Réunion subzone in the Singa section.

Subsection Singa IV continues the magnetostratigraphic record at 1 m above sapropel B7 (i.e. at level 91.3 m). The magnetic properties and composition of the NRM in the lowermost 11 m are identical to those described for the preceding Singa III subsection: the polarity stays reliably reversed throughout. The next 11 m (level 102.1 m up to level 113.5 m) display the influence of increased weathering in the top part of Monte Singa (Fig. 6c, d and e). Weathering is probably promoted by the large number of closely spaced sapropels from the C group in this interval. Although the presence of a primary LT component with reversed polarity remains perceptible, a relatively large secondary component increasingly dominates the NRM. In the examples shown, the directions of the primary component cannot be reliably determined, although they are seen to be certainly (Fig. 6c and d), or likely (Fig. 6e), of reversed polarity.

From sapropel C1 upwards it was not possible to collect fresh blue marl samples, and indeed, the paleomagnetic results appear to be inconsistent and unreliable. Normal polarities dominate, even at intervals where a reversed polarity can be expected (on the basis of biostratigraphic and sapropel correlations to the sequences in the Crotona area). The NRM has low intensities and often marl specimens reveal only a secondary remanence, a component which is removed at 200°C and which has a direction close to the present local field. Further heating results merely in a cluster of vector end points (Fig. 6f), showing that the characteristic LT component has been removed from these weathered marls.

The important stratigraphic interval containing the C group sapropels straddling the Pliocene–Pleistocene boundary in the Singa area yields insufficient coherent paleomagnetic observations for a reliable polarity zonation owing to the poor state of the section. Therefore, the magnetostratigraphic results for this stratigraphic interval could be obtained from the Crotona area only.

4.2. Sections of the Crotona area

The extensive marl sequences in the area south of the town of Crotona contain the three sections

used in the present study. The Vrica composite section is the principal one, and the San Leonardo section is parallel to a problematic interval in the central Vrica section. The Crotona section permits extension towards younger Pleistocene marls.

4.2.1. Vrica section

The Vrica composite section (Fig. 4) can be divided into three parts on the basis of its magnetic properties. The lower half of the section up to sapropel C4/c is characterized by relatively high initial NRM intensities (usually 0.5–3.0 mA/m) and an NRM composition which is virtually identical to that of subsection Singa III. Progressive thermal demagnetization generally shows a viscous laboratory component removed at 100°C, a small secondary component removed at 200°C, and finally, between 200 and 350°C, the removal of the characteristic component (Fig. 6g). The primary origin of this characteristic component is indicated by the consistently reversed polarity for the lower 80 m of the section. A single exception is the normal polarity of one site around the 55 m level (Fig. 4). The stratigraphic position of this normal polarity site — between sapropels B7 and C0 — is different from the position of the single normal polarity site in the Singa III subsection (just below B5), and consequently relates to another normal polarity subzone. From sapropel C1 upwards to at least sapropel C4/c, the characteristic component shows normal polarity (Fig. 6h), indicating a polarity transition at sapropel C1.

Immediately above sapropel C4/c the initial NRM intensity decreases drastically by one order of magnitude. This intensity decrease marks the beginning of an interval with very low intensities (0.1–0.2 mA/m) and consequently leads to demagnetization results which are difficult to interpret. It was often difficult to sample fresh marls, both in the top part of subsection Vrica A, but also in subsection Vrica B in the interval from sapropel C4/c (level 120.6 m) up to half-way between sapropels C6/e and C7 (at level 147.5 m). Indeed, the paleomagnetic results are largely dominated by secondary remanences. Still, the fresh samples between sapropel C4/c and sapropel C5/d indicate a reliable normal polarity. For the interval between sapropel C5/d and sapropel C6/e, all fresh samples clearly point to a reversed polarity (Fig. 6i). Thus the normal polarity zone

extends from sapropel C1 to sapropel C5/d (Fig. 4).

Low intensities continue above sapropel C6/e and the dominance of secondary remanences obstructs reliable magnetostratigraphic observations. There are indications of a continuation of the reversed polarity above sapropel C6/e up to level 140 m, as well as indications of normal polarities from level 140 m to 149 m (Fig. 4). However, this low-intensity interval of the Vrica section is evidently less suitable for reliable magnetostratigraphic study. Therefore, this part of Vrica has been resampled in further detail in the more promising San Leonardo section.

From about half-way between sapropels C6/e and C7 (level 149 m) up to the top of subsection Vrica B the initial NRM intensity gradually increases again and the magnetostratigraphic results are more reliable, all revealing reversed polarity (Fig. 4).

Subsection Vrica C continues to show the predominance of reliable reversed NRM types, like those observed in the upper part of subsection Vrica B. There is an evident relationship between the initial intensity and the type of NRM obtained (Fig. 4). The majority of the sites show initial intensities above 0.5 mA/m related to the most reliable reversed type: a small laboratory component, remarkably little secondary remanence, and total removal of the reversed primary component below 400°C. Sites with initial NRM intensities between 0.2 and 0.5 mA/m show a small reversed primary component and a dominant secondary overprint removed at high temperatures as well. Reversed polarities are found up to *r* (Fig. 6j and Fig. 4), although Tauxe et al. [8] found normal polarities from below C13/q up to C14/s. For the present study no reliable samples between *r* and C14/s could be taken, because in this interval the sediment was too strongly weathered and not a single site with fresh marl could be found.

4.2.2. San Leonardo section

The San Leonardo section was sampled as a less weathered substitute for the low-intensity interval in the middle of the Vrica section. Sampling stretches from 5 m below sapropel C5/d and up to just below sapropel C8/f.

In spite of the better prospects, the initial NRM intensities were low (usually between 0.1 and 0.5 mA/m), although occasionally some higher intensities were measured. Thermal demagnetization diagrams (Fig. 6k) show the presence of a normal polarity characteristic remanence up to sapropel C5/d. The entire interval between sapropels C5/d and C6/e reveals a characteristic component with a reversed polarity, in spite of the sometimes very low intensities (Fig. 6l). The reversed polarity zone between sapropel C5/d and C6/e in the Vrica section is thus reliably confirmed. The N-R polarity transition is situated near the bottom of sapropel C5/d on the basis of, both in the San Leonardo section and in the Vrica section, a site just below sapropel C5/d revealing a single specimen indicating the presence of a reversed polarity component.

The subsequent stratigraphic interval of 4 m above sapropel C6/e yields extremely low NRM intensities (below 0.08–0.16 mA/m). Despite these very low intensities, thermal demagnetization reveals, in addition to a large secondary overprint, the presence of a very small, but nevertheless clearly defined, reversed component (Fig. 6m). The reversed polarity zone, which starts near the bottom of sapropel C5/d, thus continues upward to about 4 m above sapropel C6/e (i.e., level 26.5 m in Fig. 5).

The next 4 m (level 26.5 m to 30.5 m (Fig. 5)) shows higher NRM intensities (0.3–3.7 mA/m) and normal directions throughout the entire progressive thermal demagnetization up to total removal of the NRM below 400°C (Fig. 6n and o, Fig. 5), indicating that this stratigraphic interval might represent a true normal polarity zone. From level 30.5 m upward (Fig. 5) NRM intensities vary greatly, but only reversed components are found for the entire upper part of this section.

Thus, the magnetostratigraphic results of the San Leonardo section essentially confirm the results of the central part of the Vrica section. The lower normal polarity zone which starts at sapropel C1 in the Vrica section continues up to just below sapropel C5/d. The interval between sapropel C5/d and C6/e represents a reversed polarity zone, which continues up to 4 m above sapropel C6/e, while the interval between level 26.5 m and 30.5 m represents a normal polarity subzone. The upper part of the San Leonardo

section above level 30.5 m reveals reversed polarities only.

4.2.3. *Crotone section*

The interval above sapropel *r* has been sampled in a section located in the southern outskirts of the town of Crotone (Fig. 1). This Crotone section stretches from some 20 m below sapropel C13/*q* up to sapropel *u*, and thus has an ample overlap with the top part of the Vrica section which Tauxe et al. [8] designated as their normal polarity zone N3. The magnetostratigraphic results from the Crotone section, however, based on fresh and blue-coloured marls, reveal a reversed polarity throughout (Fig. 6p). All sites up to level 61.0 m (Fig. 5) show relatively high NRM intensities and reversed magnetizations, with a small secondary remanence.

5. Magnetostratigraphy of the Plio-Pleistocene

The upper Singa section starts with an interval with stable normal polarity directions. A normal to reversed polarity transition is found at the level of sapropel A5. From this level up to sapropel C1 only reversed polarities are found, with the exception of a single site just below sapropel B5 which reveals a stable normal polarity. From C1 upward no reliable polarity zonation can be established. Predominantly normal polarities occur, most of which are clearly of secondary origin due to the intense weathering.

In the Crotone area, reversed polarities occur from sapropel B6 to C1 as well, with a single site (level 55 m) showing normal polarity. A normal polarity interval is found between C1 and C5/*d* and is followed by a reversed interval. There is evidence of a short (4 m) normal polarity zone above sapropel C6/*e*. From above the short normal polarity zone up to sapropel *r* in the composite Vrica section (Fig. 4) and up to sapropel *u* in the Crotone section (Fig. 5) only reversed polarities occur.

The small number of complete polarity zones renders a statistical correlation to the geomagnetic polarity time scale by means of the pattern of the successive polarity zones unfeasible. Nevertheless, the Plio-Pleistocene age and the prevailing reversed polarities places the stratigraphic interval undoubtedly in the Matuyama Chron (Fig.

7). The long reversed polarity zones both below and above the relatively short interval with normal polarities identifies this central normal zone as representing the Olduvai subchron. The lowermost normal polarity zone in the upper Singa section has been correlated previously to the youngest part of the Gauss chron [7].

Seeing as the lower boundary of the Olduvai subzone is located at the level of sapropel C1, the stratigraphic interval in the upper Singa section between sapropels A5 (Gauss/Matuyama) and C1 corresponds to the lowest Matuyama reversed subchron. The normal polarity site just below B5 may therefore represent the Réunion subchron. The single normal polarity site below the lower Olduvai boundary in the Vrica section certainly does not represent the same subchron because it is located distinctly higher (between B7 and C0) in the succession. A detailed investigation of the intervals in question is currently being carried out.

There are some essential differences between the present record and that published by Tauxe et al. [8] for the same stratigraphic interval (Fig. 7). The lower Olduvai polarity transition is more precisely pinpointed, mainly because of the much higher sampling density, and it is located at the level of sapropel C1, some 9 m below sapropel C2/*a*, whereas Tauxe et al. [8] located this boundary 25 m below sapropel *a*. More interestingly, Tauxe et al. have interpreted their two sites between sapropels *b* and *c* to be of reversed polarity (their zone R3), whereas the present study reveals only normal polarity results at twelve sites divided over this stratigraphic interval. The normal polarity of their site 18 (i.e., their zone N2) between sapropels *c* and *d* is confirmed by our results, and in both studies a polarity transition from normal to reversed is placed at sapropel *d*. The interval between sapropel *d* and a level half-way between sapropels *e* and *f* is interpreted by Tauxe et al. to belong to their reversed zone R4, although they do not present any data. The present study, however, reveals an additional interval of normal polarity, 4 m above sapropel *e*. Finally, the normal polarity zone N3 of Tauxe et al. from below sapropel *q* up to *s* is not confirmed. The present study reveals only reversed polarities, both in the Vrica section (up to sapropel *r*) and in the Crotone section (from below

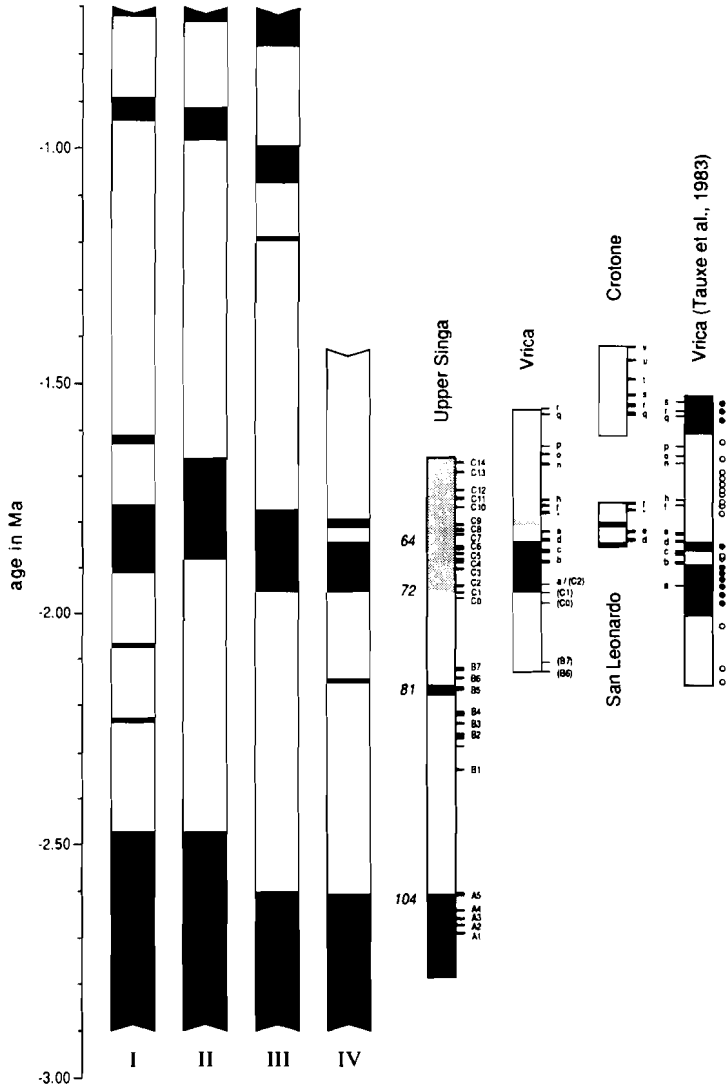


Fig. 7. Correlation of the magnetic polarity zones observed in the Calabrian Late Pliocene/Early Pleistocene sections to the geomagnetic polarity time scale. The four polarity time scales to the left: I = McDougall [30] and II = Berggren et al. [31] are dated radiometrically, and III = Shackleton et al. [32] and IV = Hilgen [1] are dated by means of astronomical calibrations. For the construction of scale IV the paleomagnetic data of the present study were used. The polarity zonation observed in the upper Singa, Vrica, San Leonardo and Crotona sections is seen to the right. The polarity zonation of the Vrica section as reported by Tauxe et al. [8] is shown on the far right. Numbers in italics to the left of the upper Singa column represent isotopic stages observed in the upper Singa section by Lourens et al. [24]. Positions and numbering of the sapropels given for each of the sections. The correlation between the sections is based on the sapropels (cf. Fig. 2). Circles along the right-hand side of the Vrica section of Tauxe et al. (1983) represent the number and position of the reversed polarity specimens given in [8]; the dots represent the number and position of the normal polarity specimens.

sapropel *q* up to *u*). The normal polarities clearly represent secondary magnetizations as a result of increased weathering in the top of the section.

An incorrect identification of the sapropels as a possible explanation for the discrepancies between our results and those of Tauxe et al. [8] can be excluded because of the very distinct and characteristic pattern in thickness and clustering of the sapropels as well as of other lithological marker beds in the Vrica sections.

6. Discussion

The Gauss/Matuyama polarity transition in the upper Singa section precedes the multiple *Discoaster* (*D. pentaradiatus*, *D. surculus*) extinction event and, in terms of planktonic foraminifera, the LO of *G. punctulata* and *N. atlantica*, and it succeeds the LO of *D. tamalis*, similar to the results obtained during ODP Leg 94. Moreover, isotopic stage 104 of Raymo et al. [25] is almost coeval with this polarity transition [7,24].

The normal polarity site just below sapropel B5 and probably corresponding to the Réunion subchron occurs in isotopic stage 81 [24]. At ODP Site 609, normal polarities were found in the same isotopic stage, and have also been interpreted in terms of the Réunion subchron [25]. An additional biostratigraphic argument supporting the proposal that we are dealing with one and the same subchron is the FO of *G. inflata*, which is recorded slightly higher in the succession, i.e., in isotopic stage 79, both in the upper Singa section and at ODP Site 609 [25].

The lower boundary of the Olduvai subzone at C1 is located in isotopic stage 72, both in the upper Singa section [24] and at ODP Site 609 [25], and coincides closely with the LO of *D. brouweri* (Fig. 2). At Site 609, the lower Olduvai polarity transition was initially placed at a lower level — in isotopic stage 73 — but a subsequent and more detailed study has revealed that this initial position was based on a single site of normal polarity well below the actual lower Olduvai boundary [25]. In the upper Singa and Vrica sections, at the level of isotopic stage 73 no normal polarities have thus far been observed. At Vrica a single normal polarity site is found to

coincide with the FO of *G. truncatulinoides*. In the Singa section, however, this influx appears to correspond to isotopic stage 75.

The position of the upper boundary of the Olduvai subzone at Vrica is very important because of the formal definition of the Pliocene–Pleistocene boundary on top of sapropel *e* in this section. The present study reveals two options for the position of the upper boundary of the Olduvai subzone. This boundary can be placed either at the level of sapropel C5/*d*, implying that an extra normal subchron — the *Vrica subchron* — is present above sapropel C6/*e* (option I), or it can be placed at the top of the extra normal polarity interval just mentioned (option II). The latter option implies that a reversed polarity interval is present in the top part of the Olduvai subchron. The further implications of the two options are as follows:

At ODP Sites 607 and 609, and at Site 552, the top of the Olduvai subzone is recorded invariably in isotopic stage 64. An argument in favour of option II is that correlation of isotopic stages between the ODP sites and the Calabrian sections shows that stage 64 is situated at the top of the extra normal polarity interval. This correlation is supported by the first common occurrence (FCO) of left-coiling neogloboquadrinids slightly below the upper Olduvai polarity transition in the northern Atlantic, as well as slightly below the top of the extra normal polarity interval in the Vrica and San Leonardo sections (Figs. 4 and 5).

The inferred duration of the Olduvai subzone provides another argument in favour of option II. The duration of the Olduvai subzone in the Vrica section can be determined accurately for both options by using the astronomical ages of the sedimentary (sapropel) cycles [1], and provides estimates of 115 ka for option I and 160 ka for option II. The duration of 115 ka is considerably less than reported for the Olduvai subchron in the literature. Linear interpolation between the Gauss/Matuyama and the Matuyama/Brunhes boundary in deep-sea cores yields an average duration of 150 ka (1.91–1.76 Ma; [30,33]), whereas analysis of near-bottom marine magnetic anomalies yields a duration of 220 ka (1.88–1.66 Ma; [31,34,35]). The second value is closely approached by the duration of 200 ka (1.87–1.67 Ma) in the polarity time scale of Mankinen and

Dalrymple [36], who apparently placed the boundaries at the oldest and youngest K/Ar ages of absolutely dated normal polarity observations. A duration of 160 ka for the Olduvai subchron agrees well with other astronomically based estimates of 170 ka (1.82–1.65 Ma; [25]) and 180 ka (1.95–1.77 Ma; [32]).

Summarizing, it can be concluded that the top of the extra normal polarity interval above sapropel *e* most probably represents the upper Olduvai polarity transition as generally found elsewhere.

This conclusion implies that a reversed interval is present in the upper part of the Olduvai subchron. Such a reversed interval has not been observed in cores from ODP Leg 94, nor in many other deep-sea cores, but it was found earlier in core V20-109 by Ninkovitch et al. [37,38]. Furthermore, several Indian Ocean deep-sea cores have revealed the presence of a single site with reversed polarity just below the upper boundary of the Olduvai subzone [39]. Nevertheless, Mankinen and Dalrymple [36] conclude that the lack of sufficient confirmation in other cores prevents the unambiguous recognition of reversed polarities below the upper boundary of the Olduvai subzone (or a short normal polarity event following the Olduvai subchron). The lack of sufficient confirmation, however, might rather be due to a lack of sufficiently detailed sampling. More recently, Heller et al. [40] found a short reversed polarity interval in the top part of the Olduvai subzone in loess deposits of the Chinese Loess Plateau.

The presence of a reversed interval in the upper part of the Olduvai subzone also raises a problem in terminology. The classical Olduvai interval has been denoted as a subchron and the reversed interval would place a subchron within a subchron. The alternative would be to redefine the extent of the Olduvai subchron and to distinguish a sequence of a relatively long normal subchron (the Olduvai according to option I), a short reversed subchron, and an even shorter normal subchron (the “Vrica subchron”), with respective durations of 115, 30 and 15 ka. For comparison, on the basis of a sedimentation rate of 0.8 cm/ka Ninkovitch et al. [37] deduced durations of 106, 11 and 24 ka for their subchrons in core V20-109, amounting to a total duration of 141 ka.

The following aspect to be discussed is a possible identity for the Vrica subchron and the Gilsa subchron. During Leg 94, an additional normal polarity chron of very short duration (5.5 ka) was found above the Olduvai, corresponding to isotopic stage 54, which was interpreted to represent the Gilsa subchron [41]. The Gilsa subchron was originally found in Eastern Iceland [42,43], and was based on a possibly reversed lava flow between the third and fourth flow of a sequence of normally magnetized lava flows representing the Olduvai subchron. A detailed study of these flows by Watkins et al. [44] suggested that the reversed tendency and the much lower intensities of the single intervening flow was due to “magnetic instability”. Watkins et al. [44] obtained average K/Ar ages of 1.68 ± 0.01 and 1.59 ± 0.01 Ma for the third and fourth flow respectively. The authors rejected the presence of the Gilsa event and the obtained ages have been merged to a single 1.62 ± 0.08 Ma for the younger part of the Olduvai subchron. However, were we to accept the presence of a short reversed interval between the third and fourth flow, a *maximum* duration of 90 ka (1.68–1.59 Ma) would be inferred; the actual duration may be appreciably shorter. A duration of approximately 30 ka can be established for the reversed interval in San Leonardo, whereas the inferred duration of the reversed interval between the upper Olduvai boundary (isotopic stage 64) and the “Gilsa” (stage 54) in Leg 94 is approximately 140 ka, longer than the maximum possible duration inferred from the Icelandic lavas. Hence, it is very unlikely that the Vrica subchron at stage 64 is identical with the “stage 54 subchron” in Leg 94. Moreover, considering the ambiguities concerning the original Gilsa event in the Icelandic lavas, we shall refrain from interpreting the Vrica subchron as the Gilsa subchron.

7. Conclusions

The results from the *Monte Singa area* show that a reliable magnetostratigraphy can be established from below the Gauss/Matuyama boundary (correlated to isotopic stage 104) up to and including the lower Olduvai boundary (isotopic stage 72). Normal polarities just below sapropel B5, at a level corresponding to isotopic stage 81,

most likely represent the Réunion subchron. From the lower Olduvai boundary upward, a reliable magnetostratigraphy could not be established, due to increased weathering of the marls resulting in mainly secondary magnetizations.

The sequences from the *Crotone area* (i.e., the Vrica, San Leonardo and Crotone sections) belong to the reversed Matuyama Chron, and are younger than the Réunion subchron. They include the Olduvai subchron, but the positions found for both the lower and upper boundary of the Olduvai subzone differ markedly from those reported by Tauxe et al. [8]. Besides, the normal polarities reported for the top part of the Vrica section [8] are not confirmed by the results from the fresh outcrops of the parallel Crotone section. Given the very weathered state of the top

part of the Vrica section these normal polarities are almost certainly due to secondary magnetizations related to the weathering and do not represent an extra normal subchron.

Two options exist for the position of the upper boundary of the Olduvai subzone. In option I, the Olduvai subzone is positioned between sapropels C1 and C5/d and has a duration of 115 ka, followed by a short (30 ka) reversed subchron and the short (15 ka) normal *Vrica subchron*. In option II, the Olduvai subzone is positioned between sapropel C1 and a level half-way between C6/e and C7, and has a duration of 160 ka, implying a short reversed interval in its upper part. The latter option is in good agreement with the position and age of the upper Olduvai boundary as reported in the literature.

TABLE 1

Stratigraphic positions (in metres) of magnetostratigraphic and biostratigraphic datum planes in the studied sections. Positions of calcareous nannofossil events derived from the work of Driever ([23] and unpublished data). Also shown are the ages (in Ma) of these datum planes. Ages 1 are based on linear interpolation and extrapolation of conventional radiometric ages for geomagnetic polarity reversals [31]; ages 2 are based on linear interpolation between astronomically dated sapropels [1]

Reversal boundary	Stratigraphic position				Isotopic Stage	Age	
	Singa	Vrica	S. Leonardo	Crotone		1	2
"Upper Olduvai" (option II)	—	144.5-145.5	29.3-30.8	—	64	1.66	1.79
"Upper Olduvai" (option I)	—	127.1-129.8	12.5	—	—	—	1.84
Lower Olduvai	112.6	80.1-83.1	—	—	72	1.88	1.95
n-polarity	—	54.2	—	—	75	—	2.01
Reunion top	85.4	—	—	—	81	—	2.14
Reunion bottom	82.1-83.2	—	—	—	81	—	2.15
Gauss/Matuyama	24	—	—	—	104	2.47	2.60
Biohorizon (foraminiferal)							
FCO <i>sinistral neoglob.</i>	126.6-127.1	139.4-141.2	25.4-25.9	—	64	1.68	1.80
LO <i>S. dehiscentis</i>	105.4-105.9	54.8-58.8	—	—	74	1.93	1.98
re-ap. <i>G. inflata</i>	104.9-105.4	61.8-63.4	—	—	73/74	1.93	1.99
FO <i>G. truncatulinoides</i>	102.9-103.4	50.8-52.7	—	—	75	1.95	2.00
FO <i>G. inflata</i>	91.4-91.9	19.2-21.7	—	—	77/78	2.02	2.09
FO <i>S. dehiscentis</i>	76.8-77.0	—	—	—	83	2.12	2.19
LO <i>G. puncticulata</i>	47.3-47.8	—	—	—	95/96	2.31	2.41
LO <i>N. atlantica</i>	47.3-47.8	—	—	—	95/96	2.31	2.41
FO <i>N. atlantica</i>	12.1-12.7	—	—	—	110	2.57	2.72
Biohorizon (nannofossils)							
base small <i>gephyrocapsids</i>	—	—	—	76.3-78.1	?	1.18	?
LAD <i>H. selli</i>	—	—	—	74.7-76.3	?	1.19	?
LAD <i>C. macintyreii</i>	136.4-136.9	—	—	—	?	1.54	?
FAD <i>G. caribbeanica</i>	130.3-132.2	—	—	—	?	1.61	1.74
FAD <i>D. brouwen</i>	111.9-112.4	—	—	—	72	1.88	1.95
LAD <i>D. pentaradiatus</i>	34.3-34.8	—	—	—	100	2.40	2.51
LAD <i>D. surculus</i>	29.3-31.3	—	—	—	101	2.43	2.55
LAD <i>D. tamalis</i>	7.5-9.0	—	—	—	112?	2.61	2.76

Linear interpolation and extrapolation on the basis of the observed polarity transitions and use of the radiometric ages for them of the geomagnetic polarity time scale of Berggren et al. [33] yields the ages for the late Pliocene–early Pleistocene biostratigraphic datum levels shown in Table 1. In addition, an age of 1.69 Ma is found for the Pliocene–Pleistocene boundary if we use option II for the upper boundary of the Olduvai subzone.

The positions of the polarity transitions determined in the present study form the basis of the new geomagnetic polarity time scale of Hilgen [1]. This time scale has been established by the astronomical calibration of sapropel patterns, using the interference pattern of precession and eccentricity of the Earth's orbit. This astronomical calibration leads to ages for the polarity transitions systematically older than the conventional ages based on radiometric dating. According to this new time scale the Pliocene–Pleistocene boundary has an age of 1.81 Ma. The astronomical ages of the biostratigraphic datum levels are also given in Table 1.

Acknowledgements

Thanks go to P.J. Verplak for his assistance in the field, again to P.J. Verplak and also to H.J. Meijer for measuring the enormous number of samples, to T. van Hinte for the skillful illustrations and to G.J. van 't Veld and G. Ittman for the preparation of the micropaleontological samples. We thank M.B. Cita, C. Kissel and W. Lowrie for reviewing the manuscript. This investigation was partly supported by the Netherlands Foundation for Earth Sciences (AWON) with financial aid from the Netherlands Organization for Scientific Research (NWO). A travel grant from *Shell Internationale Petroleum Maatschappij B.V.* (The Hague) is gratefully acknowledged.

References

- 1 F.J. Hilgen, Astronomical calibration of Gauss to Matuyama sapropels in the Mediterranean and implication for the Geomagnetic Polarity Time Scale, *Earth Planet. Sci. Lett.* 104, 226–244, 1991.

- 2 J.D.A. Zijdeveld, W.J. Zachariasse, P.J.J.M. Verhallen and F.J. Hilgen, The age of the Miocene–Pliocene boundary, *Newslett. Stratigr.* 16, 169–181, 1986.
- 3 F.J. Hilgen and C.G. Langereis, The age of the Miocene–Pliocene boundary in the Capo Rossello area (Sicily), *Earth Planet. Sci. Lett.* 91, 214–222, 1988.
- 4 J.E.T. Channell, D. Rio and R.C. Thunell, Miocene/Pliocene boundary magnetostratigraphy at Capo Spartivento, Calabria, Italy, *Geology* 16, 1096–1099, 1988.
- 5 C.G. Langereis and F.J. Hilgen, The Rossello composite: A Mediterranean and global standard reference section for the Early to early Late Pliocene, *Earth Planet. Sci. Lett.* 104, 211–225, 1991.
- 6 W.J. Zachariasse, J.D.A. Zijdeveld, C.G. Langereis, F.J. Hilgen and P.J.J.M. Verhallen, Early Late Pliocene biochronology and surface water temperature variations in the Mediterranean, *Mar. Micropaleontol.* 14, 339–355, 1989.
- 7 W.J. Zachariasse, L. Gudjonsson, F.J. Hilgen, C.G. Langereis, L.J. Lourens, P.J.J.M. Verhallen and J.D.A. Zijdeveld, Late Gauss to early Matuyama invasions of *Neoglobobulimina atlantica* in the Mediterranean and associated record of climatic change, *Paleoceanography* 5, 239–252, 1990.
- 8 L. Tauxe, N.D. Opdyke, G. Pasini and C. Elmi, Age of the Plio-Pleistocene boundary in the Vrica section, southern Italy, *Nature* 304, 125–129, 1983.
- 9 F.J. Hilgen, Closing the gap in the Plio-Pleistocene boundary stratotype sequence of Crotona (southern Italy), *Newslett. Stratigr.* 22, 43–51, 1990.
- 10 F.J. Hilgen, Sedimentary rhythms and high-resolution chronostratigraphic correlations in the Mediterranean Pliocene, *Newslett. Stratigr.* 17, 109–127, 1987.
- 11 F.J. Hilgen and C.G. Langereis, Periodicities of CaCO₃ cycles in the Mediterranean Pliocene: Discrepancies with the quasi-periods of the Earth's orbital cycles?, *Terra Nova* 1, 409–415, 1989.
- 12 F.J. Hilgen, Extension of the astronomically calibrated (polarity) time scale to the Miocene/Pliocene boundary, *Earth. Planet. Sci. Lett.* 107, 349–368, 1991.
- 13 R.B. Kidd, M.B. Cita and W.B.F. Ryan, Stratigraphy of eastern Mediterranean sapropel sequences recovered during DSDP Leg 42A and their paleoenvironmental significance, *Init. Rep. DSDP 42A*, 421–443, 1978.
- 14 E. Olausson, Description of sediment from the Mediterranean and Red Sea, *Rep. Swed. Deep-Sea Exped., 1947–1948* 8, 337–391, 1961.
- 15 P.J.J.M. Verhallen, Early development of *Bulimina marginata* in relation to paleo-environmental changes in the Mediterranean, *K. N. Akad. Wet., Verh. B* 90, 161–180, 1987.
- 16 E. Aguirre and G. Pasini, The Pliocene–Pleistocene boundary, *Episodes* 8, 116–120, 1985.
- 17 G. Pasini, R. Selli, R. Tampieri, M.L. Colalongo, S. d'Onofrio, A.M. Borsetti and F. Cati, The Vrica section, in: *The Neogene–Quaternary boundary, II Symp. Bologna–Crotona, Excursion Guide-book*, R. Selli, ed., pp. 62–72, 1975.
- 18 R. Selli, C.A. Accorsi, M. Bandini Mazzanti, D. Bertolani Marchetti, G. Bigazzi, F.P. Bonadonna, A.M. Borsetti, F.

- Cati, M.-L. Colalongo, S. d'Onofrio, W. Landini, E. Menesini, R. Mezzeti, G. Pasini, G. Savelli and R. Tampieri, The Vrica section (Calabria). A potential Neogene-Quaternary boundary stratotype, *G. Geol.* 41, 181-204, 1977.
- 19 J.D. Obradovitch, C.W. Naeser, G.A. Izett, G. Pasini and G. Bigazzi, Age constraints on the proposed Plio-Pleistocene boundary stratotype at Vrica, Italy, *Nature* 298, 55-59, 1982.
- 20 J. Backman, N.J. Shackleton and L. Tauxe, Quantitative nannofossil correlation to open ocean deep-sea sections from Plio-Pleistocene boundary at Vrica, Italy, *Nature* 304, 156-158, 1983.
- 21 P. Spaak, Accuracy in correlation and ecological aspects of the planktonic foraminiferal zonation of the Mediterranean Pliocene, *Utrecht Micropaleontol. Bull.* 28, 1-160, 1983.
- 22 M.B. Cita, The Miocene/Pliocene boundary. History and definition, in: *Late Neogene Epoch Boundaries*, T. Saito and L.H. Burckle, *Micropaleontol. Press Spec. Publ.* 1, 1-30, 1975.
- 23 B.W.M. Driever, Calcareous nannofossil biostratigraphy and paleoenvironmental interpretation of the Mediterranean Pliocene, *Utrecht Micropaleontol. Bull.* 36, 245, 1988.
- 24 L.J. Lourens, F.J. Hilgen and W.J. Zachariasse, Late Pliocene-early Pleistocene astronomically forced surface water temperatures and productivity variations in the Mediterranean, *Mar. Micropaleontol.*, in press, 1991.
- 25 M.E. Raymo, W.F. Ruddiman, J. Backman, B.M. Clement and D.G. Martinson, Late Pliocene variation in northern hemisphere ice sheets and North Atlantic deep water circulation, *Paleoceanography* 4, 413-446, 1989.
- 26 D. Rio, R. Sprovieri and J.E.T. Channell, Pliocene-early Pleistocene chronostratigraphy and the Tyrrhenian deep-sea record from Site 653, *Proc. ODP, Sci. Results* 107, 705-715, 1990.
- 27 D. Rio, R. Sprovieri and I. Raffi, Calcareous plankton biostratigraphy and biochronology of the Pliocene-lower Pleistocene succession of the Capo Rossello area, Sicily, *Mar. Micropaleontol.* 9, 135-180, 1984.
- 28 J.H. Linssen, Preliminary results of a study of four successive sedimentary geomagnetic reversal records from the Mediterranean (upper Thvera, lower and upper Sidufjall, lower Nunivak), *Phys. Earth Planet. Inter.* 52, 207-231, 1988.
- 29 F. Heider and D.J. Dunlop, Two types of chemical remanent magnetization during the oxidation of magnetite, *Phys. Earth Planet. Inter.* 46, 24-45, 1987.
- 30 I. McDougall, The present status of the geomagnetic polarity time scale. in: *The Earth, its Origin, Structure and Evolution*, M.W. McElhinny, ed., pp. 543-565. Academic Press, New York, 1979.
- 31 W.A. Berggren, D.V. Kent, J.J. Flynn and J.A. Van Couvering, Cenozoic geochronology, *Geol. Soc. Am. Bull.* 96, 1407-1418, 1985.
- 32 N.J. Shackleton, A. Berger and W.R. Peltier, An alternative astronomical calibration of the lower Pleistocene timescale based on ODP Site 677, *Trans. R. Soc. Edinb., Earth Sci.* 81, 251-261, 1990.
- 33 N.D. Opdyke, Paleomagnetism of deep-sea cores, *Rev. Geophys. Space Phys.* 10, 213-249, 1972.
- 34 K.D. Klitgord, S.P. Huestis, J.D. Mudie and R.L. Parker, An analysis of near-bottom magnetic anomalies: Sea-floor spreading and the magnetized layer, *Geophys. J. R. Astron. Soc.* 43, 387-424, 1975.
- 35 J.L. LaBrecque, D.V. Kent and S.C. Cande, Revised magnetic polarity time scale for Late Cretaceous and Cenozoic time, *Geology* 5, 330-335, 1977.
- 36 E.A. Mankinen and G.B. Dalrymple, Revised geomagnetic polarity time scale for the interval 0-5 m.y. B.P., *J. Geophys. Res.* 84, 615-626, 1979.
- 37 D. Ninkovitch, N.D. Opdyke, B.C. Heezen and J.H. Foster, Paleomagnetic stratigraphy, rates of deposition and tephrochronology in North Pacific deep sea sediments, *Earth Planet. Sci. Lett.* 1, 476-492, 1966.
- 38 N.D. Watkins, Short period geomagnetic polarity events in deep sea sedimentary cores, *Earth Planet. Sci. Lett.* 4, 341-349, 1968.
- 39 N.D. Opdyke and B.P. Glass, The paleomagnetism of sediment cores from the Indian Ocean, *Deep-Sea Res.* 16, 249-261, 1969.
- 40 F. Heller, X.M. Liu, T.S. Liu and T.C. Xu, Magnetic susceptibility of loess in China, *Earth Planet. Sci. Lett.* 103, 301-310, 1991.
- 41 B.M. Clement and D.V. Kent, Short polarity intervals within the Matuyama: transitional field records from hydraulic piston cored sediments from the North Atlantic, *Earth Planet. Sci. Lett.* 81, 253-264, 1986/1987.
- 42 H. Wensink, Secular variation of earth magnetism in Plio-Pleistocene basalts of eastern Iceland, *Geol. Mijnbouw* 43, 403-413, 1964.
- 43 H. Wensink, Paleomagnetic stratigraphy of younger basalts and interval Plio-Pleistocene tillites in Iceland, *Geol. Rundsch.* 54, 364-384, 1964.
- 44 N.D. Watkins, L. Kristjansson and I. McDougall, A detailed paleomagnetic survey of the type location for the Gilsa geomagnetic polarity event, *Earth Planet. Sci. Lett.* 27, 436-444, 1975.

Chapter 7

Periodicities of CaCO₃ cycles in the Pliocene of Sicily: discrepancies with the quasi-periods of the Earth's orbital cycles?

F.J. Hilgen¹ & C.G. Langereis²

¹Department of Geology, Institute of Earth Sciences, Budapestlaan 4, 3584 CD Utrecht, The Netherlands

²Paleomagnetic Laboratory, Hoofddijk, Budapestlaan 17, 3584 CD Utrecht, The Netherlands

ABSTRACT

A high-resolution CaCO₃ record in combination with a detailed magnetostratigraphy is presented for the rhythmically bedded marly sequence of the Pliocene Trubi Formation on Sicily (Italy). Magnetostratigraphic age calibration and subsequent spectral analysis of the variations in CaCO₃ content yield a remarkably consistent discrepancy between the resulting periodicities and the corresponding quasi-periods of the Earth's orbital cycles. This discrepancy can only be explained by assuming that ages assigned to polarity reversal boundaries in the geomagnetic polarity time-scale lack sufficient precision.

A new polarity time-scale is presented for the major part of the Gilbert and Gauss Chron using the radiometrically dated Gilbert–Gauss Chron boundary at 3.40 Ma as an age reference point and extrapolating an average quasi-period of 21.7 kyr of the precession cycle as the periodicity of small-scale colour annex CaCO₃ cycles.

INTRODUCTION

Recent geomagnetic polarity time-scales are primarily and essentially based on marine magnetic anomaly patterns and radiometrically determined age calibration points. Ages of individual polarity reversals are then obtained by interpolation between these calibration points which are linked to the marine magnetic anomaly sequence by direct magnetostratigraphic control (Lowrie and Alvarez, 1981; Berggren *et al.*, 1985). The most recent and generally applied calibration point – apart from the present – is the Gilbert–Gauss polarity reversal boundary which has a radiometric age of 3.40 Ma (Mankinen and Dalrymple, 1979). A reliable polarity time-scale solely based on direct K/Ar dating and polarity observations (of lava flows) can be constructed only for the last 4–5 Myr. In older rocks the error in K/Ar dating approaches the average time-span of polarity subchrons.

Although radiometric dating is at

present the most commonly used geochronological method, Gilbert (1895) already contended that time-scales are, in principle, to be constructed independently by employing sedimentary cycles that are controlled by variations in the Earth's orbit (see also Fischer, 1980). More recently, very refined time-scales have been established for the last 0.3–0.7 Myr by tuning cyclic variations in detailed oxygen isotope records to the astronomical solutions (Morley and Hays, 1981; Imbrie *et al.*, 1984; Martinson *et al.*, 1987). The application of these tuning procedures to immediately older sequences seems to yield slightly, but persistently older ages for the Brunhes–Matuyama and Upper and Lower Jaramillo boundaries than those obtained by radiometric dating (Johnson, 1982; Shackleton, 1989).

Rhythmically bedded marls of the Trubi Formation on Sicily provide an excellent opportunity to explore the geochronological application of Milankovitch-type sedimentary cycles

in the Pliocene, especially since these Trubi marls provide a very good quality magnetostratigraphy (Zijderveld *et al.*, 1986; Hilgen and Langereis, 1988; Channell *et al.*, 1988; Zachariasse *et al.*, 1989). The rhythmic bedding in the Trubi has previously been linked with cyclic variations in the Earth's orbit (Zijderveld *et al.*, 1986; Hilgen, 1987; Gudjonsson, 1987; Zachariasse *et al.*, 1989), but conclusive evidence regarding exact periodicities has not been furnished yet. Therefore, a detailed carbonate and magnetostratigraphic record has been established in order to determine accurately the periodicities of cyclic variations in CaCO₃ content in the Trubi. This is done by direct magnetostratigraphic correlation to the geomagnetic polarity time-scale and subsequent spectral analysis of the resulting age-calibrated record. The resultant periodicities are then compared with the quasi-periods of the orbital cycles of the Earth.

SECTIONS AND LITHOLOGY

The lithostratigraphic term Trubi, although never formally defined as a formation, is commonly used for the whitish coloured Pliocene marls on Sicily (Cita and Gartner, 1973). Very similar marls, however, are also found in nearby southern Calabria (Hilgen, 1987). A dominant feature of the Trubi marls both on Sicily and in Calabria is the distinct rhythmic bedding. On Sicily, these rhythms consist of quadripartite depositional sequences displaying distinct small-scale, grey–white–beige–white, colour cycles with the grey and beige marls being less indurated (de Visser *et al.*, 1989). In southern Calabria, corresponding rhythms are usually bipartite since they lack the beige-coloured marls (Hilgen, 1987) and hence these rhythms consist

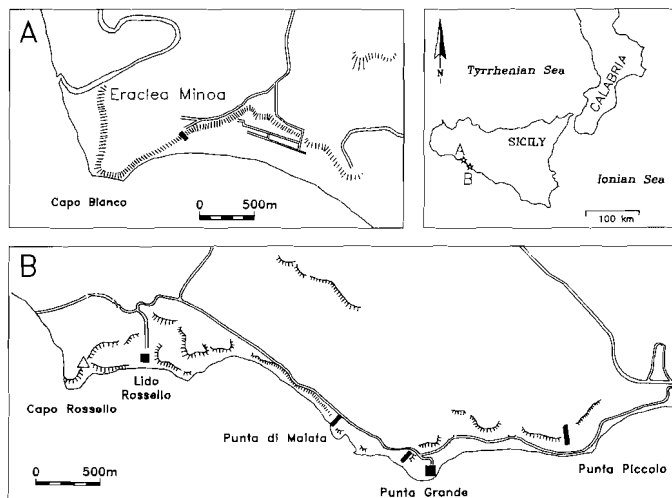


Fig. 1. Location of the subsections of the Rossello composite section. (a) Eraclea Minoa. (b) Capo Rossello area.

of grey–white colour cycles. In addition to these small-scale colour cycles, two larger-scale rhythms are easily distinguished by the regular occurrence of relatively thick and/or indurated marl intervals. On average, these large-scale rhythms contain 5 and 20 small-scale cycles, respectively (Hilgen, 1987).

The Trubi on Sicily is excellently exposed in a series of coastal cliffs in the southern part of the island where it also reaches its maximum thickness. For our study the sections of Eraclea Minoa, Punta di Maiata, Punta Grande and Punta Piccola were selected (Fig. 1) and together they form the Rossello composite section of Hilgen (1987). Despite the good quality of the exposures, there is some uncertainty regarding the actual number of small-scale colour cycles. The disproportionately thick cycles 6, 21, 22 and 59 (see Figs 2 and 3) probably each contain an additional cycle which lacks sedimentary expression; the existence of such an additional cycle could be proved, for instance, for cycle 21 in the Trubi of adjacent southern Calabria (authors' field observations, 1989). In addition, the composition of the small-scale cycles 69 and 96 in terms of colour layering remains problematical. Although this is not directly evident from their thickness, these cycles may

contain an additional cycle as well. Consequently, the actual number of small-scale colour cycles may include six extra cycles.

The detailed magnetostratigraphy – with a resolution generally better than 5 kyr – clearly shows that the Rossello composite section comprises most of the Gilbert and Gauss Chrons (Hilgen and Langereis, 1988; Zachariasse *et al.*, 1989; and unpublished data). The straightforward calibration to the polarity time-scale (using that of Berggren *et al.*, 1985) results in average periodicities of 19.0 kyr for the small-scale colour cycles (or 18.0 kyr if the estimated maximum number of cycles is used) and of 334 kyr for the largest-scale marl rhythm (termed carbonate units in Hilgen, 1987).

CARBONATE ANALYSIS

Samples for CaCO_3 analysis were taken from each individual marl bed; the bulk CaCO_3 content was measured gas-volumetrically. Duplicate analysis on 85 out of 407 samples showed one calculated standard deviation around the mean of 1.05%.

The total CaCO_3 record of the Rossello composite section is shown in Fig. 2(a). In addition, the records for

only the beige marls (the beige record; Fig. 2c) and only the grey marls (the grey record; Fig. 2e) are presented, as well as the records from which are excluded the grey marls (the beige–white–white record; Fig. 2b) and the beige marls (the grey–white–white record; Fig. 2d), respectively. The total CaCO_3 record is dominated by high-frequency fluctuations which can be correlated with the small-scale colour cycles, showing that CaCO_3 minima are centred in the grey and especially in the beige marl beds. Low-frequency fluctuations, on the other hand, are observed in the beige record (Fig. 2c) and, most clearly, in the grey record (Fig. 2e). They correlate with the larger-scale marl rhythms.

SPECTRAL ANALYSIS

Of the original carbonate record both trend and average were eliminated by linear (de)regression of CaCO_3 content versus stratigraphic level. Using the magnetostratigraphic calibration points, a new and equally spaced time-series was generated. Subsequently, spectral analysis was applied to calculate the periodicities of CaCO_3 cycles using the Fourier transform of the autocorrelation function (i.e. the normalized autocovariance function; see Davis, 1973). To reduce the effect of noise, a Tukey spectral window was used (see Jenkins and Watts, 1968).

Spectral analysis was first applied to the total CaCO_3 record. Incorporating all CaCO_3 data, however, is inexpedient in view of the two minima (in the grey and beige marls) per colour cycle: these minima reduce the power of the corresponding harmonic in the spectrum and produce a peak at two times its frequency. In order to eliminate this artificial peak and to enhance the contribution of the colour cycles to the spectrum, spectral analysis was also applied to the grey–white–white record and to the beige–white–white record. Further, spectral analysis was carried out on the grey record and on the beige record to eliminate this contribution of the small-scale colour cycles and thus to obtain better insight into the periodicities of the larger-scale CaCO_3 cycles.

Similar procedures of spectral analysis were also used on the data obtained only from the composite 'Punta'

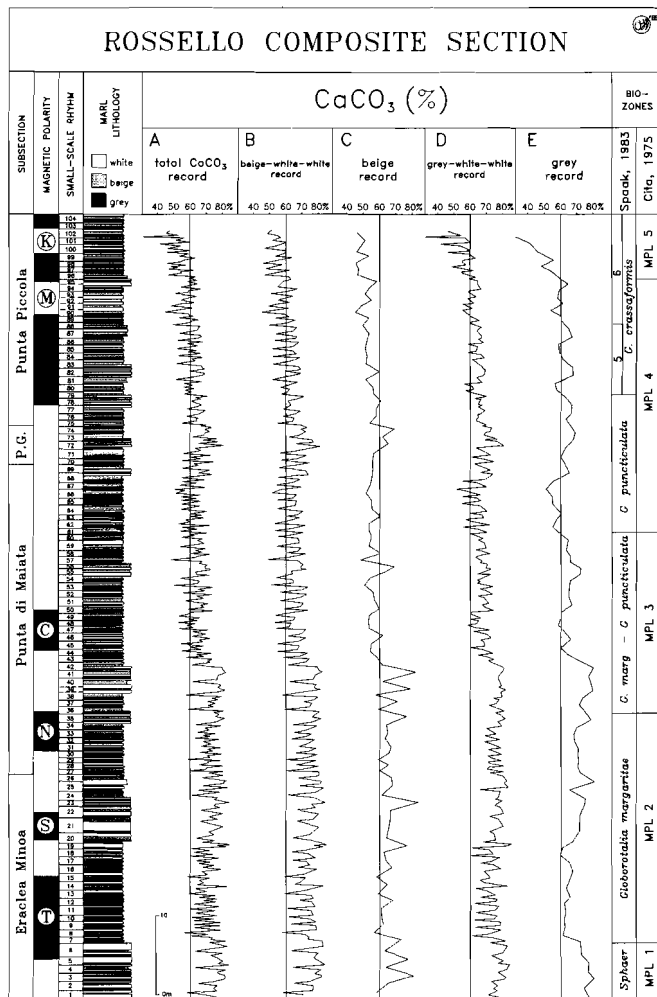


Fig. 2. CaCO_3 records of the Rossello composite section. (a) Total CaCO_3 record. (b) Total record without the data from the grey marls (beige-white-white record). (c) Record for the beige marls (beige record). (d) Total record without the data from the beige marls (grey-white-white record). (e) Record for the grey marls (grey record). Small-scale colour cycles are numbered from the base of the Trubi upward. Magnetostratigraphy and biostratigraphy are based on Hilgen (1987), Hilgen and Langereis (1988), Zachariasse et al. (1989) and unpublished data.

section: i.e. the combined Punta di Maiata, Punta Grande and Punta Piccola sections with the exclusion of the distantly located section of Eraclea Minoa. These analyses were both done

with the maximum number of magnetostratigraphic calibration points as well as with a strongly reduced number. The latter procedure minimizes possible effects of errors in the ages of reversal

boundaries in the geomagnetic polarity time-scale. The results of all spectral analyses are presented in Figs 4 and 5.

In the high-frequency domain, strongly significant peaks corresponding to periodicities between 15 and 20 kyr are found in all spectra except in those of the grey and beige records (see Figs 4a,b,c and 5a,b,e,f). These periodicities correspond to the calculated average periodicity of 19.0 – or 18.0 kyr if we incorporate the possible six extra cycles – of the small-scale colour cycles. A strongly significant double peak is shown in the spectra from the composite Punta section using the minimum number of calibration points (Fig. 5e,f); corresponding periodicities are approximately 15.5 and 18.5 kyr (Fig. 5f). This double peak is in agreement with the distinct bimodality in cycle-thickness distribution of the colour cycles (Fig. 3).

In the low-frequency domain, a pronounced peak corresponding to a

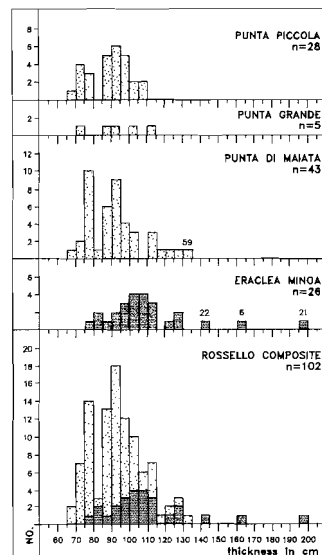


Fig. 3. Thickness distributions for the small-scale colour cycles in the subsections of the Rossello composite section. Thickness of cycles is calculated as the combined bed thickness of successive white-beige-white coloured marls and the sum of half of the bed thickness of both the underlying and overlying grey marls.

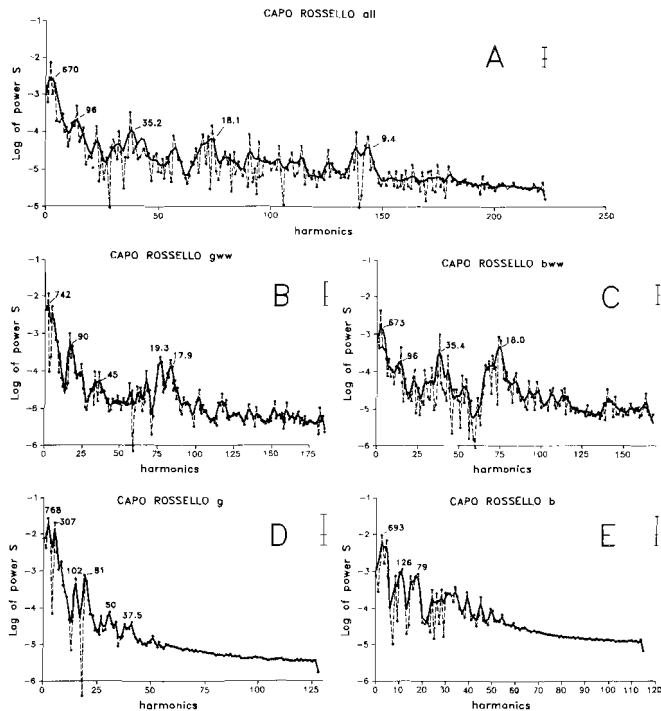


Fig. 4. Power spectra of CaCO_3 records from the Rossello composite section, *i.e.* the Punta sections and the distantly located Eraclea Minoa section. (a) Total CaCO_3 record. (b) Grey-white-white record. (c) Beige-white-white record. (d) Grey record. (e) Beige record. The maximum number (13) of magnetostratigraphic age-calibration points is employed. Unsmoothed spectra are shown by dashed lines, smoothed spectra (using a Tukey spectral window) by heavy lines. Periodicities corresponding to significant peaks are indicated. The 80% confidence interval is shown as a small vertical bar on the right side of each spectrum.

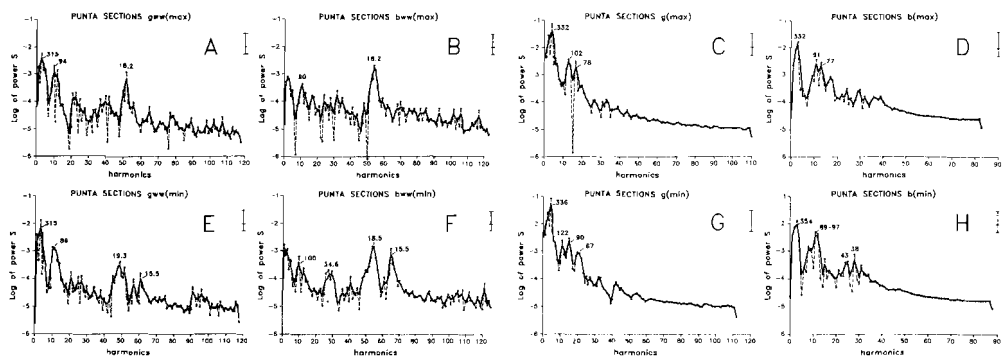


Fig. 5. Power spectra of CaCO_3 records from the Punta sections only. (a) Grey-white-white record. (b) Beige-white-white record. (c) Grey record. (d) Beige record. The maximum number of magnetostratigraphic calibration points is employed. (e)–(h) The same records, but now the minimum number (2) of calibration points is used. See also caption to Fig. 4.

periodicity between 290 and 360 kyr is found in a number of spectra (Fig. 5a,c,d,e,g,h). By slightly changing the number of lags in the autocorrelation function this peak could be very narrowly defined at 332–336 ka in the grey record (Fig. 5c,g). This periodicity perfectly matches the calculated average periodicity of 334 kyr for the largest-scale marl rhythms which were termed carbonate units in Hilgen (1987).

In the intermediate frequency domain, CaCO_3 cycles do show up in the spectra and have peaks corresponding to periodicities between 67 and 126 kyr with a concentration in the 77 to 102 kyr interval (Figs. 4 and 5). Individual peaks, however, are difficult to locate precisely because they do not appear with great consistency in the various spectra. Obviously, this complex and composite CaCO_3 cycle matches the larger-scale marl rhythms which, on average, comprise 5 small-scale colour cycles.

Finally, several peaks fall in the range between the high frequencies – those occupied by the small-scale colour cycles – and intermediate frequencies (Figs. 4 and 5). These peaks are considered to be mainly higher harmonics of the cycles of intermediate wavelength, but this is certainly not true for the pronounced 35 ka peak (Fig. 4a,c; 5f). Most probably, this peak reflects the alternately high and low percentages of CaCO_3 content of the beige marls in some of the relatively thick and indurated marl intervals (see *e.g.* cycles 1 to 6 and 34 to 42 in Fig. 2c).

Table 1. Comparison between significant periodicities of the CaCO₃ cycles as well as the average periodicities of the colour cycles (both for the maximum and minimum number of these cycles) and marl rhythms and the corresponding quasi-periods of the astronomical cycles (in ka). Quasi-periods of astronomical cycles are based on Berger (1978; 1984). The periodicities of the CaCO₃ cycles, colour cycles and marl rhythms are also shown as the percentage of the corresponding quasi-period (in italics and between brackets). Note that the 100 ka eccentricity cycle is clearly reflected in the spectra as a composite cycle, but that the individual peaks and corresponding periodicities could not be determined with great accuracy.

ORBITAL CYCLES SEDIMENTARY CYCLES	PRECESSION			OBLIQUITY	ECCENTRICITY		
	QUASI-PERIODS 19	23	AVERAGE 21.7	QUASI-PERIOD 41	QUASI-PERIODS 95 123 413		
CaCO ₃ CYCLES	15.5 (81.6%)	18.5 (80.4%)	—	± 35.0 (85.3%)	—	—	335 (81.2%)
MARL RHYTHMS (colour cycles)	—	—	18.0 / 19.0 (82.8% / 87.6%)	—	—	—	334 (80.9%)

DISCUSSION AND CONCLUSIONS

The significant periodicities of CaCO₃ cycles as well as the calculated average periodicities of the colour cycles and marl rhythms in the Trubi Formation are summarized in Table 1. Comparison with the main quasi-periods of the Earth's orbital cycles show that significant but very consistent age discrepancies are found between these

periodicities and the supposedly corresponding quasi-periods. This consistency suggests that the CaCO₃ cycles in the Trubi are indeed related to the astronomical cycles which is furthermore confirmed by the distinct bimodality in the cycle-thickness distribution of the small-scale quadripartite marl rhythms in the Trubi (Fig. 3): this bimodality is consistent with the ratio of the 19 and

23 ka frequency components of the precession cycle (Berger, 1984).

We may safely conclude, therefore, that the CaCO₃ cycles of the Trubi are linked to these cyclic variations in the Earth's orbit, most clearly to those of the precession and eccentricity cycle. The presence of CaCO₃ cycles related to the obliquity cycle is less distinct, but this is to be expected because of the relatively low latitudinal position of the Mediterranean area: at these latitudes the influence of the obliquity cycle on seasonal variations in insolation is strongly reduced (van Woerkom, 1953; Berger, 1978).

The very consistent age discrepancies between the periodicities of CaCO₃ cycles and those of the orbital cycles cannot be explained by the presence of faults or hiatuses in the succession. Faults certainly would have been recognized in the distinctly bedded marls, and hiatuses are highly unlikely considering the good correlation between the pattern of polarity zones in the sections and the pattern of (sub)chrons from the geomagnetic polarity time-scale of Berggren *et al.*, (1985) and also because no such features as hardgrounds or slump scars were observed. Moreover, average periodicities of the small-scale colour cycles per polarity interval show that the age discrepancies cannot be pinpointed to a specific stratigraphic horizon, but appear to occur more or less evenly distributed over the whole sequence (Fig. 6).

The consistent age discrepancies, therefore, can be explained either by assuming that ages assigned to the reversal boundaries in the geomagnetic

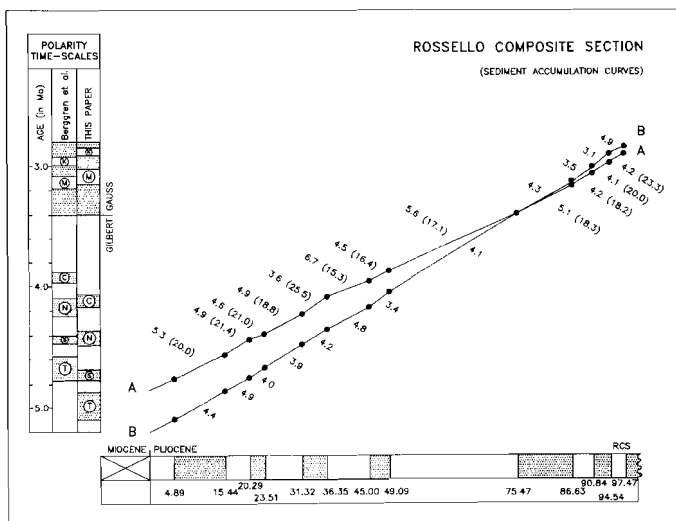


Fig. 6. Sediment accumulation curves for the Rossello composite section. (a) According to the polarity time-scale of Berggren *et al.*, (1985), and (b) According to the new one presented in Fig. 7 (this study). Sedimentation rates are shown per polarity interval in cm/ka. Between brackets the average periodicities of the small-scale colour cycles are presented per polarity interval for option A.

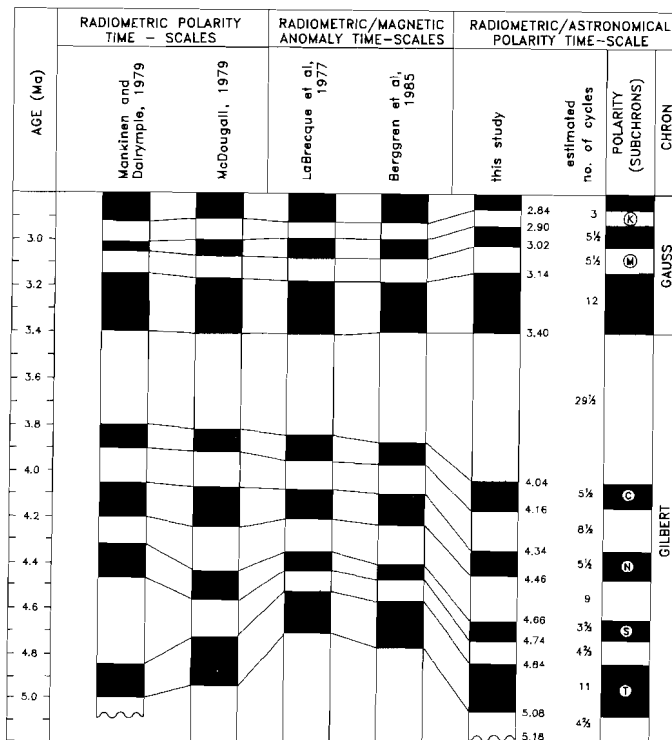


Fig. 7. A new polarity time-scale is presented for the major part of the Gilbert and Gauss Chrons using the radiometrically dated Gilbert–Gauss Chron boundary at 3.40 Ma as an age reference point and extrapolating the average quasi-period of 21.7 ka of the precession cycle as the periodicity of small-scale colour annex CaCO_3 cycles. The estimated maximum number of cycles is used. The resulting time-scale is compared with other polarity time-scales.

polarity time-scale are not sufficiently accurate or that the frequencies of at least the precession and eccentricity cycles have changed considerably over the past 5.0 Myr. At present, astronomical solutions are considered to be highly accurate for the last 5–10 Myr (Berger *et al.*, 1987; 1989) and they show no evidence of such shifts in frequency over this period of time.

It is therefore concluded that the age discrepancies between the periodicities of the CaCO_3 and colour cycles and the quasi-periods of the orbital cycles have to be attributed to poor age-constraints for the geomagnetic reversals in the global polarity time-scale. As a consequence, an alternatively age-calibrated polarity time scale can be

constructed for the major part of the Gilbert and Gauss Chrons for which the radiometrically dated Gilbert–Gauss Chron boundary at 3.40 Ma (Mankinen and Dalrymple, 1979) is used as a reference point. Starting from this reference point, ages were assigned to younger and older polarity reversals by upward and downward extrapolation of the small-scale colour cycles, using an average quasi-period of 21.7 ka of the precession cycle (Berger, 1984). We have employed the maximum number of colour cycles because this figure agrees better with the consistent age discrepancies between the periodicities of the CaCO_3 cycles and those of the orbital cycles (see Table 1). The resultant polarity time-scale is pre-

sented in Fig. 7 and compared with published ones.

Ages have recently been obtained for the Brunhes–Matuyama as well as for the Upper and Lower Jaramillo reversal boundaries by tuning cyclic variations in oxygen isotope records to the astronomical solutions (Johnson, 1982; Shackleton, 1989). They show a slight but persistent deviation from the radiometric ages. Our results so far provide a first accurate age estimate for the duration of polarity intervals in the Gilbert and Gauss Chrons based on employing sedimentary cycles that are connected with the quasi-periodic variations in the Earth's orbit. Current research focuses on tuning the cyclic sedimentation patterns in the Trubi to the astronomical solutions to establish also the ages of the reversal boundaries. The resulting astronomically age-calibrated polarity time-scale may in principle be far more accurate than the traditional ones.

ACKNOWLEDGEMENTS

We would like to thank W.J. Zachariasse and P.L. de Boer who critically read an earlier version of the manuscript, E. Wijffelman who developed an initial version of the spectral analysis computer program and Ton van Hinte, who skilfully produced the drawings. This research was partly funded by the Netherlands Organization of Scientific research (NWO).

REFERENCES

- Berger A.L. (1978) Long-term variations of caloric insolation resulting from the earth's orbital elements, *Quat. Res.*, **9**, 139–167.
- Berger A.L. (1984) Accuracy and frequency stability of the earth's orbital elements during the Quaternary. In: *Milankovitch and Climate* (ed. by Berger A.L., Imbrie J., Hays J., Kukla G. and Saltzman B.), Riedel, Dordrecht, NATO ASI Ser. C, 126, 3–39.
- Berger A.L., Loutre M.F. and Dehant V. (1987). Influence of the variation of the lunar orbit on the astronomical frequencies of the pre-Quaternary paleo-insolation, *Scientific Report 1987/15*, Inst. d'Astronomie et de Geophysique G. Lemaître, Univ. Cath. de Louvain, Louvain-la-Neuve.

- Berger A.L., Loutre M.F. and Dehant V. (1989) The orbital frequencies in pre-Quaternary times, *Terra Abstr.*, **1**, 241.
- Berggren W.A., Kent D.V., Flynn J.J. and Van Couvering J.A. (1985) Cenozoic geochronology, *Bull. Geol. Soc. Am.*, **96**, 1407–1418.
- Channell J.E.T., Rio D. and Thunell R.C. (1988) Miocene/Pliocene boundary magnetostratigraphy at Capo Spartivento, Calabria, Italy, *Geology*, **16**, 1096–1099.
- Cita M.B. (1975) Planktonic foraminiferal biozonation of the Mediterranean Pliocene deep sea record. A revision, *Riv. It. Paleontol. Stratigr.*, **81**, 527–544.
- Cita M.B. and Gartner S. (1973) Studi sul Pliocene e sugli strati del passaggio dal Miocene al Pliocene, IV. The stratotype Zanclean. Foraminiferal and nannofossil biostratigraphy, *Riv. It. Paleontol. Stratigr.*, **79**, 503–558.
- Davis J.C. (1973) *Statistics and data analysis in geology*. Wiley, New York, 550 pp.
- de Visser J.P., Ebbing J.H.J., Gudjonsson L., Hilgen F.J., Jorissen F.J., Verhallen P.J.J.M. and Zevenboom D. (1989) The origin of the rhythmic bedding in the Pliocene Trubi formation of Sicily, southern Italy, *Palaeo-geogr., Palaoclim., Palaecoecol.*, **69**, 45–66.
- Fischer A.G. (1980) Gilbert-bedding rhythms and geochronology. In: *The scientific ideas of G.K. Gilbert* (ed. by Yochelson E.L.), *Spec. Pap. geol. Soc. Am.*, **183**, 93–104.
- Gilbert G.K. (1895) Sedimentary measurement of geologic time, *J. Geol.*, **3**, 121–127.
- Gudjonsson L. (1987) Local and global effects on the Early Pliocene Mediterranean stable isotope records, *Mar. Micropaleontol.*, **12**, 241–253.
- Hilgen F.J. (1987) Sedimentary rhythms and high-resolution chronostratigraphic correlations in the Mediterranean Pliocene, *Newsl. Stratigr.*, **17**, 109–127.
- Hilgen F.J. and Langereis C.G. (1988) The age of the Miocene-Pliocene boundary in the Capo Rossello area (Sicily), *Earth Planet. Sci. Lett.*, **91**, 214–222.
- Imbrie J., Hays J.D., Martinson D.G., McIntyre A., Mix A., Morley J.J., Pisias N.G., Prell W.L. and Shackleton N.J. (1984) The orbital theory of Pleistocene climate: support from a revised chronology of the marine $\delta^{18}O$ record. In: *Milankovitch and Climate* (ed. by Berger A.L. et al.), pp. 269–305. NATO ASI, C, 126.
- Jenkins G.M. and Watts D.G. (1968) *Spectral analysis and its applications*. Holden-Day, San Francisco, 525 pp.
- Johnson R.G. (1982) Brunhes-Matuyama reversal dated at 790,000 yr BP by marine astronomical correlations, *Quat. Res.*, **17**, 135–147.
- LaBrecque J.L., Kent D.V. and Cande S.C. (1977) Revised magnetic polarity time scale for the late Cretaceous and Cenozoic time, *Geology*, **5**, 330–335.
- Lowrie W. and Alvarez W. (1981) One hundred million years of geomagnetic polarity history, *Geology*, **9**, 392–397.
- McDougall I. (1979) The present status of the Geomagnetic Polarity Time Scale. In: *The Earth. Its origin, structure and evolution*. (ed. by McElhinney M.W.), pp. 543–565. Academic Press, London.
- Mankinen E.A. and Dalrymple G.B. (1979) Revised geomagnetic polarity time scale for the interval 0–5 m.y. B.P., *J. geophys. Res.*, **84**, 615–626.
- Martinson D.G., Pisias N.G., Hays J.D., Imbrie J., Moore T.C. and Shackleton N.J. (1987) Age dating and the orbital theory of the Ice Ages: Development of a high-resolution 0 to 300,000-year chronostratigraphy, *Quat. Res.*, **27**, 1–29.
- Morley J.J. and Hays J.D. (1981) Towards a high-resolution, global, deep-sea chronology for the last 750,000 years, *Earth Planet. Sci. Lett.*, **53**, 279–295.
- Shackleton N.J. (1989) A case for revising the astronomical calibration for the Brunhes-Matuyama and Jaramillo boundaries, *Terra abstr.*, **1**, 185.
- Spaak P. (1983) Accuracy in correlation and ecological aspects of the planktonic foraminiferal zonation of the Mediterranean Pliocene. *Utrecht Micropal. Bull.*, **28**, 160 pp.
- van Woerkom A.J.J. (1953) The astronomical theory of climatic changes. In: *Climatic change* (ed. by Shapley H.), pp. 147–157.
- Zachariasse W.J., Zijdeveld J.D.A., Langereis C.G., Hilgen F.J. and Verhallen P.J.J.M. (1989) Early Late Pliocene biochronology and surface water temperature variations in the Mediterranean, *Mar. Micropaleont.*, **14**, 339–355.
- Zijdeveld J.D.A., Zachariasse W.J., Verhallen P.J.J.M. and Hilgen F.J. (1986) The age of the Miocene-Pliocene boundary, *Newsl. Stratigr.*, **16**, 169–181.

Chapter 8

Astronomical calibration of Gauss to Matuyama sapropels in the Mediterranean and implication for the Geomagnetic Polarity Time Scale

F.J. Hilgen

Department of Geology, Institute of Earth Sciences, Budapestlaan 4, 3584 CD Utrecht, The Netherlands

ABSTRACT

The late Pliocene–early Pleistocene sapropel-bearing sequences exposed in the Vrica, Semaforo, Singa and Punta Piccola sections of southern Italy and the Francocastello section on Crete have been calibrated to the new astronomical solutions for the precession of the equinox and the eccentricity of the Earth's orbit using inferred phase relationships between these orbital cycles and the sapropel cycles. A new Mediterranean Precession-Related Sapropel (MPRS) coding is introduced according to which sapropels are coded after the correlative peak of the precession index as numbered from the Recent. These sapropels can now be dated with an accuracy of 1 ka by taking a time lag of 4 ka between orbital forcing, and maximum climate response and sapropel formation into account.

This tuning further results in ages for the Pliocene–Pleistocene boundary (1.81 Ma), the top of the Olduvai (1.79 or 1.84), the bottom of the Olduvai (1.95 ± 0.01), the Reunion (2.14–2.15), the Gauss/Matuyama (2.59/2.62) and the top of the Kaena (3.02 ± 0.01). These ages are remarkably similar to the astronomically calibrated ages obtained independently by Shackleton et al. based on ODP Site 677 ([1], *Trans. R. Soc. Edinb.*, 81, 1990), but deviate considerably from those provided by Ruddiman et al. ([2], *Paleoceanography*, Vol. 4) and Raymo et al. based on DSDP Site 607 ([3], *Paleoceanography*, Vol. 4). The constant discrepancy of 130 ka with the time scale of Ruddiman et al. and Raymo et al. is explained by the new age of 0.78 instead of 0.73 Ma for the Brunhes/Matuyama, as recently proposed by Shackleton et al., and the fact that Ruddiman et al. missed two obliquity related cycles in the Brunhes/Matuyama to top Olduvai interval. Our astronomically calibrated ages do not confirm the conventional radiometric ages of the reversal boundaries, but, on the contrary, imply that K/Ar radiometric dating yields ages that are consistently too young by 5–7%.

1. Introduction

The Olduvai Subchron was originally defined as the event of normal polarity within the reversed Matuyama Chron, which was recorded in basalts and tuffs intercalated in the basal part of the sedimentary succession in the Olduvai Gorge in Tanzania [4,5]. Based on numerous radiometric (K/Ar) datings from different localities, it is presently assumed that the Olduvai Subchron lasted from 1.87 to 1.67 Ma [6]. By approximation, these ages also appear in widely used polarity time scales which are essentially based on linear interpolation between radiometrically dated age calibration points in marine magnetic anomaly sequences [7,8].

At present, an alternative method is being developed which can be used to assign absolute ages to geomagnetic polarity reversals, i.e. the tuning of proxy records climatic to the astronomical solutions for the variations in the Earth's orbit. The primary goal of these tuning procedures was to evaluate the orbital theory of the Pleistocene ice ages and to develop a high-resolution time scale for the last 780,000 years [9]. At the same time, this tuning procedure may provide very accurate, absolute ages for polarity reversals if a detailed magnetostratigraphy of these proxy records can be determined. This tuning is already well established for records spanning the last 700,000 years [9–12], and application of this procedure to immediately older sequences yielded ages for the reversal

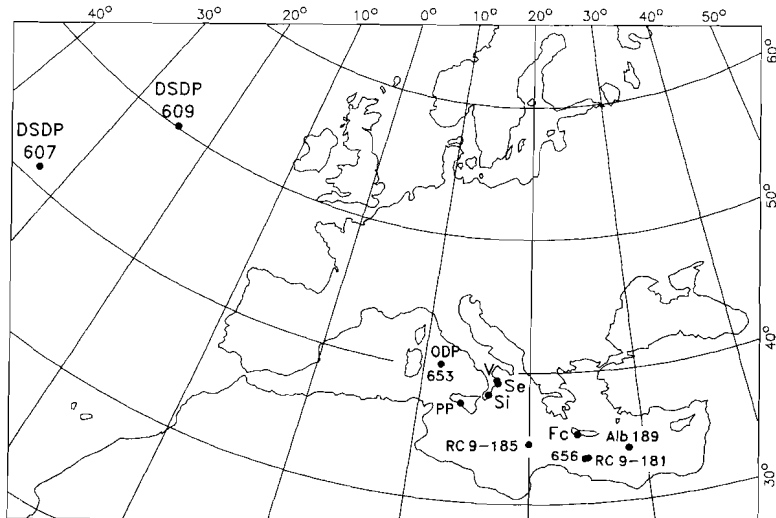


Fig. 1. Location of land sections and deep-sea cores used in this study. *PP* = Punta Piccola; *Se* = Semaforo; *Si* = Singa; *V* = Vrica; *Fc* = Francocastello.

boundaries which, except for the bottom of the Olduvai, fall within the uncertainty range of the radiometric dating [2,3,13]. Johnson [14] and Shackleton [15], on the other hand, reported ages for the Brunhes/Matuyama and Jaramillo boundaries older than those obtained by radiometric dating. Concurrent with, but independent of, the present study Shackleton et al. [1] constructed an astronomically calibrated time scale with significantly older ages for all the major reversal boundaries down to the Gauss/Matuyama boundary.

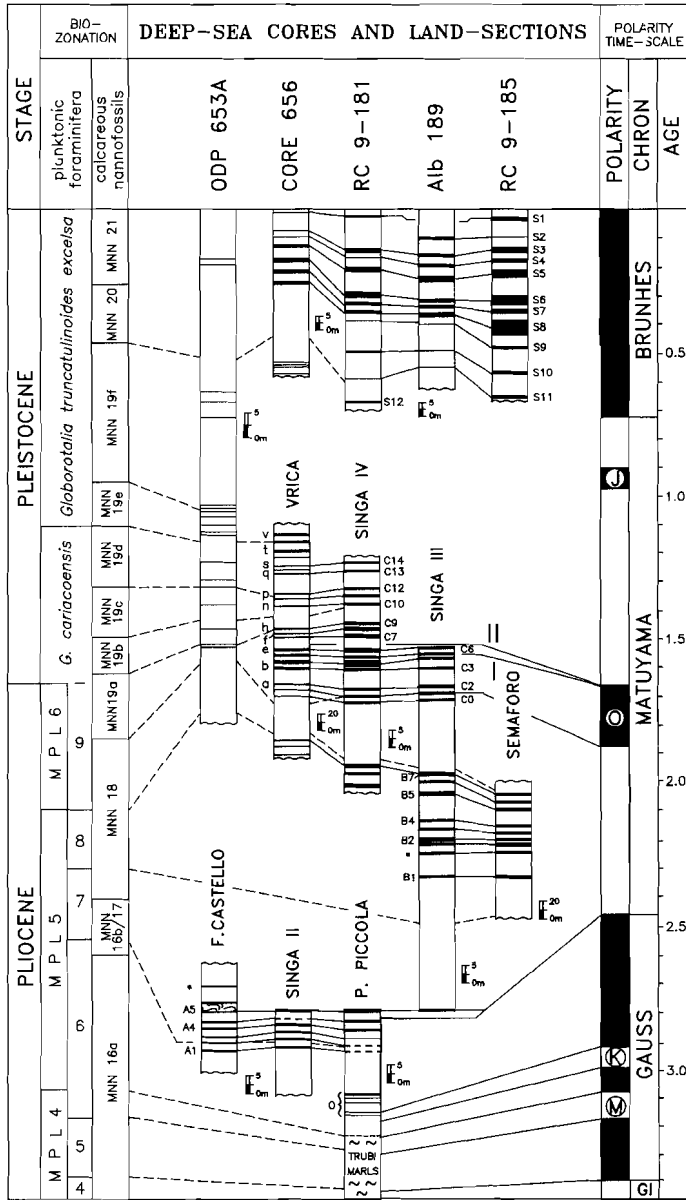
In this paper, we first establish the astronomically calibrated age of the Olduvai Subchron as recorded in the Pliocene–Pleistocene boundary stratotype section of Vrica. This is done by correlating cyclic sapropel (brownish, often laminated interbeds) patterns in the Vrica section and in the sections Semaforo, Singa, Punta Piccola and Francocastello to the astronomical solutions, using inferred phase relationships between the sapropel and orbital cycles. The resultant ages for the Olduvai, as well as for older reversal boundaries, are then compared with both conventional as well as other orbitally tuned ages for these polarity transitions.

2. The position of the Olduvai in the Pliocene–Pleistocene boundary stratotype section of Vrica

The Vrica section, in northern Calabria (Fig. 1), was formally designated as the Pliocene–Pleistocene boundary stratotype [16] after it had been intensely studied for a decade [e.g. 17–23]. The boundary was defined at the base of the homogeneous claystones which conformably overlie the sapropelic layer coded *e* in this section [16] (sapropel coding after [18], see also Fig. 2).

Initial paleomagnetic measurements on the Vrica section were carried out by Nakagawa et al. [19] who used the for this type of sediment less suitable alternating field demagnetization method [22]. Tauxe et al. [22] demonstrated that an interval of normal polarity is present in the Vrica section, which in combination with biostratigraphic evidence [23] was shown to represent the Olduvai. In addition, normal polarities were observed in the top part of the section.

Recent paleomagnetic investigations [24], however, showed that the top of the Vrica section contains reversed polarities only. The normal polarities reported earlier [22] are caused by a secondary overprint due to weathering. In ad-



dition, the stratigraphic position of the rather inaccurately defined lower boundary of the Olduvai is now more precisely located. The position of the top of the Olduvai, however, remains ambiguous. The new and very detailed paleomagnetic data show that reversed polarities are present in the top part of the normal polarity zone, resulting in two options for the exact position of the upper Olduvai [24]. In option I, the boundary coincides with sapropel *d* [18], implying a short normal polarity subchron slightly above the Olduvai. In option II, the boundary is located substantially higher in the succession, i.e. between sapropels *e* and *f*, and implies that an interval of reversed polarity is present in the upper part of the Olduvai. As a consequence, the Pliocene–Pleistocene boundary defined on top of the sapropelic marker bed *e* is positioned either within or slightly above the Olduvai [24].

3. Tuning the sapropels to the astronomical solutions

In the Vrica section, a total of 21 sapropelic layers have been distinguished (Fig. 2). In addition, sapropels are not only found in the Vrica section, but they occur frequently and are widespread in marine depositional sequences of the Mediterranean Neogene and Quaternary [e.g. 25,26]. Generally, they are not distributed evenly throughout the stratigraphic record but occur in distinct clusters on various scales: large-scale clusters usually comprise a number (2 to 3) of small-scale clusters which in turn contain 2 to 4 individual sapropels. The resulting patterns are complex and have been interpreted as superimposed sedimentary cycles connected with the Earth's orbital cycles, more precisely with those of precession

(individual sapropels) and eccentricity (sapropel clusters) [26]. The reflection of the obliquity cycle is seemingly absent in the sedimentary record, which has been related to the relatively low (paleo-)latitudinal position of the Mediterranean [26].

In order to tune the sapropel sequence of the Vrica section to the astronomical solutions, it is necessary to determine the phase relationships between the sedimentary and orbital cycles. These phase relationships can be established by correlating the most recently deposited sapropels of late Pleistocene age in the Mediterranean to the astronomical solutions, using oxygen isotope stage boundaries for age calibration (Fig. 3). This correlation shows that individual sapropels correlate to minimum peak values of the precession index and that small- and large-scale sapropel clusters correlate to eccentricity maxima connected with the 100 and 400 ka eccentricity cycles respectively.

On the basis of these phase relationships, progressively older sapropel-bearing sequences can then be calibrated to the astronomical records by extending the tuning until the Vrica sequence is reached. However, at present this procedure is not possible due to the lack of a coherent and continuous record of middle Pleistocene sapropels, both from land sections and from deep-sea cores (Fig. 2). Although this missing interval has recently been recovered at ODP Site 653, it did not yield a sufficiently detailed sapropel record (see Fig. 2). Considering the location of this site (Tyrrhenian Sea), this is not surprising because sapropels are more frequent and widespread in the eastern Mediterranean [e.g. 27]. Unfortunately, results of deep-sea drilling in the eastern basin have also been unsuccessful because of serious coring disturbance and the sometimes poor core recovery [27,28].

Fig. 2. Review of the most relevant sapropel-bearing sequences of late Pliocene–Pleistocene age in land-based sections and deep-sea cores of the Mediterranean. Lithostratigraphy of deep-sea cores is based on Cita et al. [48], Murat and Got [49] and the Shipboard Scientific Party of ODP Leg 107 [50]. Lithostratigraphy of the land sections from Hilgen [26,31], Verhallen [29], Zachariasse et al. [33,51] and Zijderveld et al. [24]. Sapropel coding after Ryan [25] for the late Pleistocene and Selli et al. [18], Verhallen [29] and Zijderveld et al. [24] for the late Pliocene–early Pleistocene. Biozonations used are those of Cita [52] and Spaak [53] for the planktonic foraminifera and Raffi and Rio [54] for the calcareous nannofossils. Biostratigraphic data are taken from Backman et al. [23], Zijderveld et al. [24], Driever [30], Zachariasse et al. [33,51] and Glaçon et al. [55]. Also shown is the calibration to the Geomagnetic Polarity Time Scale (the conventional scale of Berggren et al. [8]) based on first-order magnetostratigraphic records (Punta Piccola section—Zachariasse et al. [33,51]; Semaforo section—Tauxe et al. [22]; Singa and Vrica sections—Zijderveld et al. [24]). Solid lines mark lithostratigraphic and magnetostratigraphic correlations, dashed lines biostratigraphic correlations.

Below this hiatus in the sapropel record, a coherent and distinctly cyclic sapropel pattern emerges again in late Pliocene–early Pleistocene sequences exposed onland. In these land sections, four successive large-scale clusters of sapropels are distinguished, separated by relatively thick intervals of homogeneous sediments. In stratigraphic order, these clusters have been coded informally as *O*, *A*, *B* and *C* ([29,30]; see Fig. 2). The Vrica section contains the uppermost sapropels of the *B*-cluster and the *C*-cluster [31]. Both in the Vrica and the Singa sections (located in nearby southern Calabria, see Fig. 1), the *C*-cluster contains a very conspicuous small-scale cluster. This key-cluster

contains four sapropels which are extraordinarily thick.

From the established phase relationships between the late Pleistocene sapropels and the orbital cycles (Fig. 3), it can be inferred that this prominent key-cluster corresponds not only to a 100 ka eccentricity maximum, but also to a maximum of the 400 ka eccentricity cycle, because it contains more and thicker sapropels than the adjacent small-scale clusters. In the time interval considered, 400 ka eccentricity maxima occur at 1.4 and 1.8 Ma in the astronomical solutions [32]. However, these ages do not correspond to the conventional (radiometric) age of 1.67 Ma for the top of

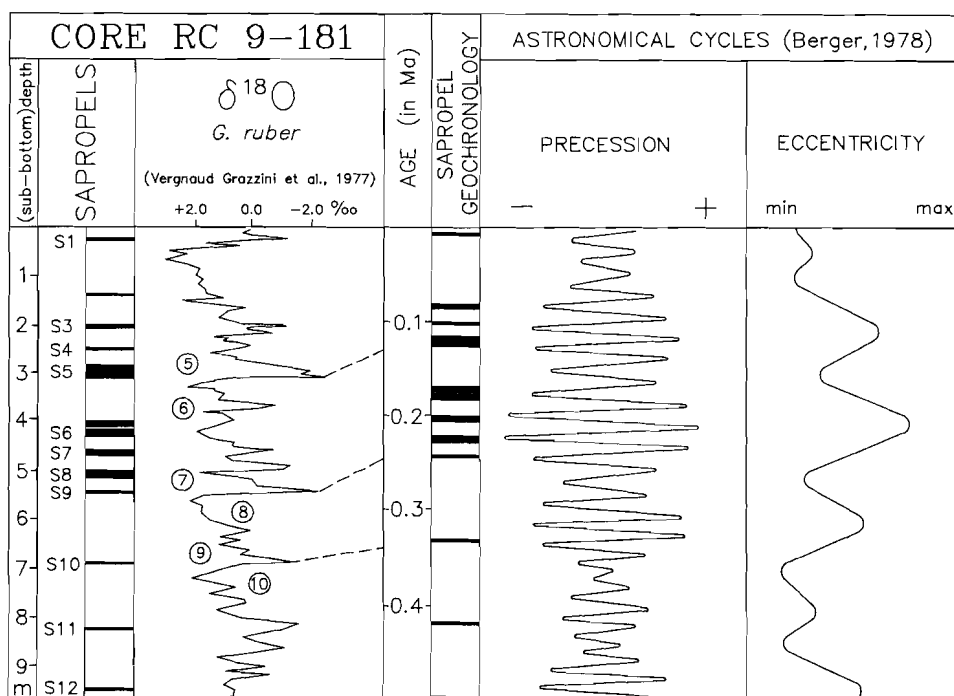


Fig. 3. Determination of phase relationships between sapropel cycles and the orbital cycles of precession and eccentricity based on the correlation of the upper Pleistocene sapropel sequence of standard core RC 9-181 in the eastern Mediterranean to the astronomical solutions. Sapropel chronology has been established according to a procedure outlined by Rossignol-Strick [46] using oxygen isotope stage boundaries 6.0, 8.0 and 10.0 dated at 128, 245 and 339 ka [9] for age calibration. The oxygen isotope record is based on Vergnaud-Grazzini et al. [47]. The astronomical records are based on the old solution of Berger [34] which is considered more accurate than the new solution for the last 1 Ma (Berger, pers. commun.)

the Olduvai [6], located either within (option I) or nearly on top (option II) of this key-cluster. The correlations of the sapropels in the lower parts of the Vrica and Singa IV sections according to both eccentricity maxima are presented in Fig. 4. Starting from the 1.4 Ma maximum, the tuning results in an age of 1.41 (option II) or 1.46 Ma (option I) for the top of the Olduvai and of 1.57 Ma for the bottom of the Olduvai. If we start from the 1.8 Ma maximum, the age for the top of the Olduvai arrives at 1.79 (option II) or 1.84 Ma (option I) and the age for the bottom of the Olduvai at 1.95 Ma (Fig. 4B). This correlation is preferred because the small-scale sapropel cluster which underlies

the prominent key-cluster is more clearly reflected in the astronomical record if we use the 1.8 Ma maximum.

To determine more conclusively which of both correlations is correct, we must consider the older part of the late Pliocene–early Pleistocene sapropel record as well. The most remarkable feature in this older part of the record is the deviating pattern of sapropels found in the large-scale *A*-cluster (Fig. 2). This *A*-cluster contains a single small-scale sapropel cluster which in turn comprises no less than six successive individual sapropels. Note that the youngest but one sapropel of this cluster is missing in the Singa section. However, the pres-

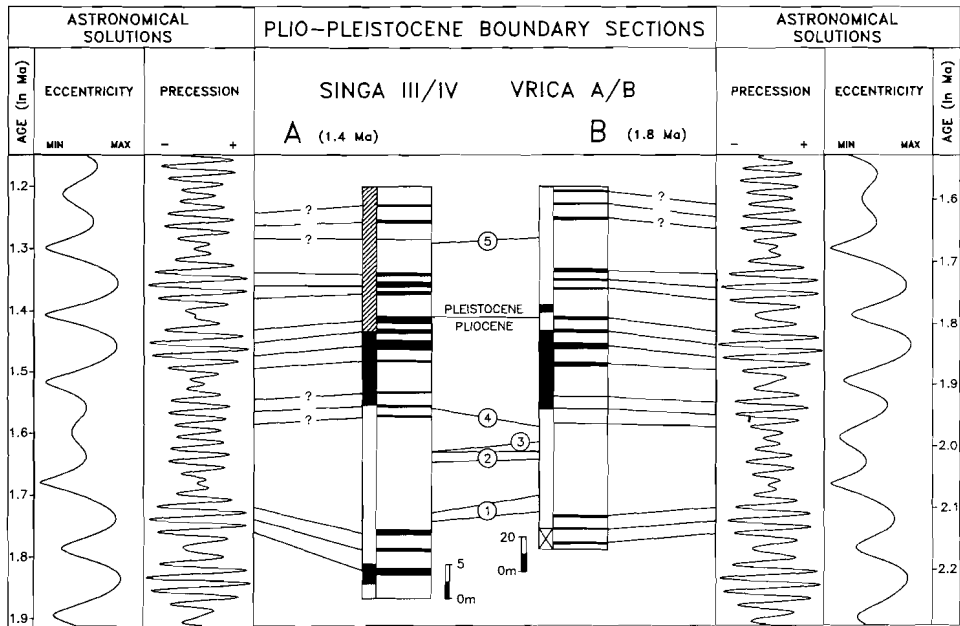


Fig. 4. The two possible alternatives for correlating the pattern of sapropels in the lower parts of the Plio-Pleistocene boundary sections of Vrica and Singa IV to the new astronomical solutions for precession and eccentricity [35] based on the established phase relationships between sapropel and orbital cycles. (A) The distinct small-scale key-cluster of four sapropels (*b–e* according to the coding of [18]; C3–C6 after [29]; see also Fig. 2) correlates with the maximum in eccentricity of the 400 ka eccentricity cycle dated around 1.4 Ma. (B) This key-cluster correlates with the successive older maximum of the 400 ka cycle of eccentricity dated around 1.8 Ma. Lithostratigraphy, biostratigraphy and magnetostratigraphy after [24,29,30]. Biostratigraphic correlations shown: 1 = *G. inflata* influx; 2 = *G. truncatulinoides* FOD and influx; 3 = *G. inflata* reappearance; 4 = *D. brouweri* LOD; 5 = *C. macintyreii* FOD. Hatching in magnetostratigraphic records denotes inconclusive paleomagnetic results or lack of data [see 24]. Astronomical records are based on the new solutions of Berger and Loutre [32; version BER–90]. The original data by Berger and Loutre [32] cannot be reproduced without their permission.

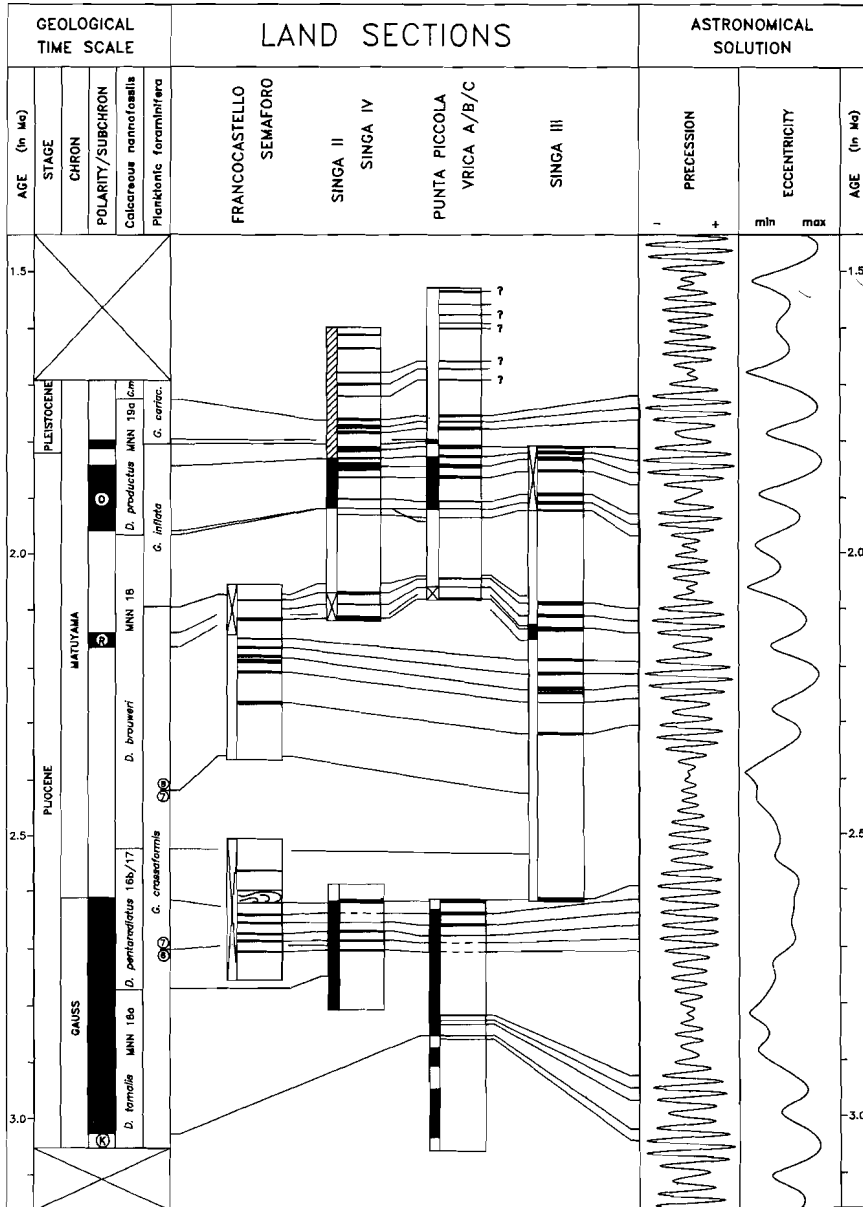


Fig. 5. Correlation of upper Pliocene-lower Pleistocene sapropel sequences to the new astronomical solutions for precession and eccentricity [32] using corresponding aberrations in the pattern of sapropels (the A-cluster) and the precession record for calibration. The original data by Berger and Loure [32] cannot be reproduced without their permission. See further explanation in Fig. 2.

ence of pyritic lumps and framboids at a time-equivalent level indicates that lowered bottom-water oxygen conditions, which are responsible for the deposition of sapropels, also persisted at Monte Singa at that time [33]. At Punta Piccola, the two lowermost beds of this cluster do not contain true sapropelic sediments but merely consist of dark-coloured marly clays. The Francocastello section on Crete, on the other hand, reveals an additional (seventh) sapropel. Close inspection of the astronomical solutions reveals a remarkably similar deviation in the record of the precession index connected with the 400 ka eccentricity maximum at 2.60 Ma. In this interval, the amplitude variations of the precession index lack the usual pronounced modulation by the 100 ka eccentricity cycle, resulting in 6–7 successive, high-amplitude excursions of the precession index to negative values. The six sapropels of the *A*-cluster can now be calibrated to the astronomical record in such a way that the most prominently developed sapropels in the Singa section (A2 and A5; see also [33]) correlate with the most negative excursions of the precession index (Fig. 5). It is emphasized that the use of the new astronomical solutions of Berger and Loutre [32] is of decisive importance here. The new calculations start to deviate significantly

from the old, less accurate solutions of Berger [34] at 1.5 Ma. The aberrant pattern in the precession record at 2.6 Ma is crucial to the astronomical calibration of our sapropels and it is not found in the old solution. Instead, an essentially similar deviation was observed before at 1.85 Ma.

Based on the calibration to the new solution, the remaining part of the sapropel record can be correlated straightforwardly to the astronomical record (Fig. 5). This correlation results in ages of 1.95 (± 0.01) Ma for the bottom of the Olduvai, 1.84 (option I) or 1.79 Ma (option II) for the top of the Olduvai and 1.81 Ma for the Pliocene–Pleistocene boundary. It confirms that the small-scale key-cluster in the large-scale *C*-cluster indeed correlates with the 400 ka eccentricity maximum at 1.8 Ma. In addition, ages are obtained for the Reunion (2.14–2.15), the Gauss/Matuyama (2.59/2.62) and the top of the Kaena (3.02 \pm 0.01), because detailed magnetostratigraphic records are presently available for the majority of these land sections (Fig. 5).

Nevertheless, some discrepancies remain, the most important of which is the correlation of the sapropels in the upper part of the Vrica section to the astronomical record. This correlation is severely hampered for several reasons. Firstly, pre-

TABLE 1

Old coding and new precession-related MPRS coding for sapropels in the Mediterranean. *l* = after Ryan [25]; *2* = after Selli et al. [18]; *3* = after Verhallen [29]. MPRS coding and lagged age using the correlative peak of the precession index as numbered from the Recent. Asterisk denotes unnamed or unnumbered sapropel

1	2	MPRS-Coding	age	lagged age	2	3	MPRS-Coding	age	lagged age	3	MPRS-Coding	age	lagged age
S1	-	2	0.012	0.008	r	-	?	-	-	B5	208	2.141	2.137
S2	-	6	0.060	0.056	q	C13	?	-	-	B4	212	2.191	2.187
S3	-	8	0.083	0.079	p	C12	?	-	-	B3	214	2.213	2.209
S4	-	10	0.106	0.102	o	C11	?	-	-	B2	216	2.235	2.231
S5	-	12	0.127	0.123	n	C10	?	-	-	*	218	2.257	2.253
S6	-	16	0.176	0.172	h	C9	168	1.719	1.715	B1	222	2.306	2.302
S7	-	18	0.198	0.194	f	C8	170	1.741	1.737	A5	250	2.593	2.589
S8	-	20	0.220	0.216	*	C7	172	1.762	1.758	*	252	2.616	2.612
S9	-	22	0.242	0.238	e	C6	176	1.812	1.808	A4	254	2.639	2.635
S10	-	30?	0.335	0.331	d	C5	178	1.834	1.830	A3'	256	2.663	2.659
S11	-	38?	0.409	0.405	c	C4	180	1.855	1.851	A2	258	2.686	2.682
S12	-	46?	0.485	0.481	b	C3	182	1.877	1.873	A1	260	2.708	2.704
-	v	?	-	-	a	C2	186	1.928	1.924	O*	280	2.928	2.924
-	u	?	-	-	-	C1	188	1.949	1.945	O*	282	2.950	2.946
-	t	?	-	-	-	C0	190	1.969	1.965	O*	284	2.972	2.968
-	*	?	-	-	-	B7	204	2.098	2.094	O*	288	3.021	3.017
-	s	?	-	-	-	B6	206	2.120	2.116	O*	290	3.042	3.038

liminary attempts to correlate the frequency distribution of sinistrally coiled neogloboquadrinids to the northern Atlantic DSDP Site 607 suggest that an hiatus is present in the top part of the Vrica section. Secondly, the characteristic cyclicality in the sapropel pattern—related to precession and eccentricity—is probably distorted in this particular interval by the following factors:

(1) The additional influence of obliquity on the distribution of the sapropels.

(2) the steady increase in the number of sapropels per large-scale cluster. This trend, which may be related to a gradual lowering of some threshold value for sapropel formation, eventually results in the disappearance of the distinct, eccentricity-related pattern in the distribution of the sapropels.

(3) Changes in sediment accumulation rate.

Current research is focussed on the solution of these problems by combining the complex sapropel pattern with a very detailed record of the frequency distribution of sinistral neogloboquadrinids. This record contains additional information on the influence of the obliquity cycle and will be reported on in a forthcoming paper. These forthcoming results will most probably not affect the calibration of the older sapropels to the astronomical record.

It is important to note that our present solution differs markedly from an earlier attempt to correlate the sapropels in the Vrica and Semaforo sections to summer insolation curves for this latitude [35]. This attempt was severely hindered by the assumption that a stratigraphic gap is present between both sections, whereas they actually proved to contain a considerable overlap [31]. Moreover, the insolation curve used by Combourieu-Nebout [35] was based on astronomical solutions which presently are considered to be less accurate for this interval of time [32].

4. A new integrated Mediterranean sapropel codation

In Table 1, we formalize our sapropel correlation to the astronomical record by introducing new coding for sapropels in the Mediterranean Pliocene–Pleistocene. In existing coding, sapropels are continuously numbered [18,25,29]. Our new Mediterranean Precession Related Sapropel (MPRS) coding is based on coding sapropels after

the correlative peak of the precession index as numbered from the Recent. This MPRS coding has the distinct advantage that newly found sapropels can always be incorporated. More importantly, all coded sapropels can be dated with an accuracy of 1 ka by reference to the corresponding peak in the precession record (Table 1). For a truly accurate dating of the sapropels, a time lag of 4 ka between orbital forcing and maximum climate response and sapropel deposition must be taken into account. This time lag is based on the age of 9–6 ka for the youngest sapropel in the eastern Mediterranean (S1; [36,37]) as compared with the age of 11.5 ka for the correlative negative peak of the precession index. A time lag of 4 ka agrees well with other time lags inferred for the climate response to orbital forcing by precession [38–40].

5. Discussion

The correlation of sapropels to the astronomical solutions results in ages for the top of the Olduvai (1.79 or 1.84 Ma), the bottom of the Olduvai (1.95 ± 0.01), the Reunion (2.14–2.15), the Gauss/Matuyama (2.59/2.62) and the top of the Kaena (3.02 ± 0.01). These ages deviate considerably from conventional ages which are either based on K/Ar radiometric dating only [6] or on linear interpolation between radiometrically dated calibration points in marine anomaly sequences [e.g. 8]. In addition, they also differ from ages which have been established previously by orbital tuning procedures and which have essentially confirmed the radiometric datings [2,3,13] (see Table 2). It is easily shown that no apparent relationships exist between our sapropel pattern and the precession record if we use either the conventional polarity time scale of Berggren et al. [8] or the orbitally tuned polarity time scale of Ruddiman and Raymo [2,3] (Fig. 6).

On the other hand, the ages reported here are almost identical to those obtained recently by Shackleton et al. ([1]; table 2). Both time scales have been established using totally independent data-sets and basically the same orbital tuning method. The time scale of Shackleton et al. [1] was constructed on the basis of the high-resolution oxygen isotope record from ODP Site 677, located in the low-latitude eastern Pacific, whereas we

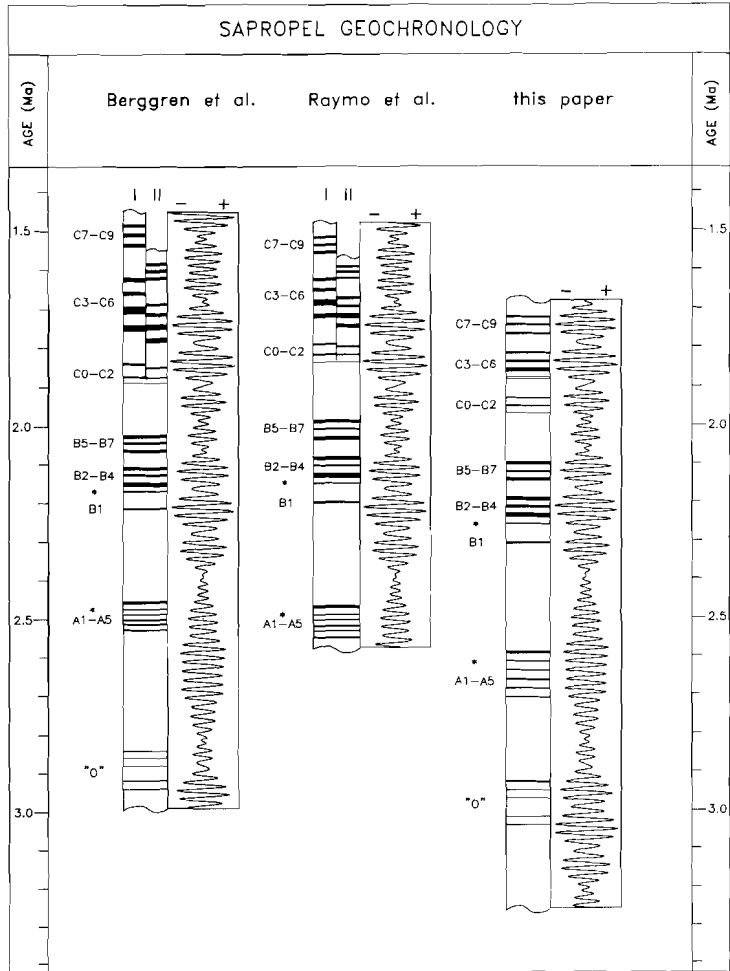


Fig. 6. Sapropel chronologies for the late Pliocene-early Pleistocene according to the different time scales. Our chronology is based on the correlation of sapropels to the astronomical solutions shown in Fig. 5. In the case of the polarity time scales of Berggren et al. [8] and Raymo et al. [3], the sapropel chronology is based on linear inter- or extrapolation of sediment accumulation rates using magnetostratigraphic datum planes for age calibration. The Singa section was employed for the interval between the base of the A-cluster to the base of the C-cluster. From the base of the C-cluster onward, we used the Vrica section instead; note that for the time scales of Berggren et al. [8] and Raymo et al. [3] two alternative sapropel chronologies are shown for this interval based on the two different options (I and II) for the position of the top of the Olduvai. The Punta Piccola section was used for the lowermost sapropels (O-cluster). The original data by Berger and Loure [32] cannot be reproduced without their permission.

used the sapropel record in the Mediterranean. However, our tuning procedure strongly resembles the procedure followed by Shackleton et al. [1] in

employing the precession rather than the obliquity component in climatic proxy records. The latter has been used in other attempts to establish an

TABLE 2

Ages for polarity reversals according to the different time scales. *M&D* = Mankinen and Dalrymple [6]; *R&R* = Ruddiman et al. [2] and Raymo et al. [3]

reversal boundary	M&D, 1979	Berggren et al., 1985	R&R, 1989	Shackleton et al., in press	this paper
Brunhes/Matuyama	0.73	0.73	0.73	0.78	-
Olduvai top	1.67	1.66	1.65	1.77	1.79 (II) 1.84 (I)
Olduvai bottom	1.87	1.88	1.82/1.83	1.95	1.95
Reunion 1 top	2.01	-	1.98/2.00	-	2.14
Reunion 1 bottom	2.04	-	2.02	-	2.15
Reunion 2 top	2.12	-	-	-	-
Reunion 2 bottom	2.14	-	-	-	-
Gauss/Matuyama	2.48	2.47	2.48/2.49	2.60	2.59/2.62
top Kaena	2.92	2.92	-	-	3.02

astronomically calibrated time scale for the late Pliocene to early Pleistocene [2,3,13], but is considered less suitable because of the regular character of the obliquity cycle. The precession signal, on the other hand, displays a far more distinctive pattern due to its modulation by eccentricity. A difference in the procedures followed is that Shackleton et al. [1] employed the Recent as a fixed calibration point, while we established our time scale independently of the Recent by correlating similar deviating patterns in the geological and astronomical records.

5.1. Discrepancies with other astronomically calibrated time scales

A comparison of the astronomically calibrated polarity time scale of Ruddiman et al. [2] and Raymo et al. [3] and ours shows that the age discrepancy for the reversal boundaries is remarkably constant, i.e. 130 ka. An exception is the older age for the top of the Olduvai in our time scale (option I in Table 2) in which case the discrepancy is even larger. This constant discrepancy, and the resulting younger ages of the sapropels according to their time scale (Fig. 6), cannot be explained by a lag effect of approximately 100 ka connected with the 400 ka eccentricity cycle because the expression of eccentricity in our sapropel record merely reflects the modulation of precession by eccentricity (see also the remarks on p. 432 in [3]). Also, the correlation of late Pleistocene sapropels to the astronomical record (Fig. 3) does not reveal any indication of the existence of such a time lag. It is therefore anticipated that the origin of this dis-

crepancy must be found in the interval younger than the Olduvai. According to our time scale, the age of the top of the Olduvai is either 1.84 (option I) or 1.79 Ma (option II), which in both cases departs markedly from the age of 1.65 Ma obtained by Ruddiman et al. [2]. As a consequence, the duration of the interval between the Brunhes/Matuyama and the top of the Olduvai differs from 0.92 Ma [2] to 1.06 or even 1.11 Ma (our options II and I) if we also use an age of 0.73 Ma for the Brunhes/Matuyama boundary. In order to explain this discrepancy, we have re-examined the records of Site 607 on which Ruddiman et al. [2] and Raymo et al. [3] based their time scale.

Ruddiman et al. [2] proceeded from an age of 0.73 Ma for the Brunhes/Matuyama boundary to establish an orbitally tuned (polarity) time scale for the older part of the Pleistocene by extrapolating the 41 ka quasi-period of obliquity as the periodicity of distinct cyclic changes in their $\delta^{18}\text{O}$ and CaCO_3 records. This approach, however, depends critically on neither skipping cycles nor adding extra ones [2, p. 359]. It is not surprising that, if their obliquity-tuned time scale is used for calibration (according to this tuning procedure, the cycles in the original records are either slightly stretched or compressed to fit the 41 ka period), spectral analysis applied on the records from Site 607 yields a single dominant peak corresponding exactly to a periodicity of 41 ka (fig. 13 in [2]). If, on the other hand, the conventional magnetic polarity time scale is used, the resulting spectrum shows that this peak has shifted to slightly higher frequencies (fig. 4 in [41]). We also applied spec-

tral analysis to the $\delta^{18}\text{O}$ and CaCO_3 records of Site 607, using the conventional ages of 0.73 and 1.66 Ma for the Brunhes/Matuyama and the top of

the Olduvai [8]. For our purpose, we used a spectral analysis program in which the Fourier transform is applied to the autocorrelation function

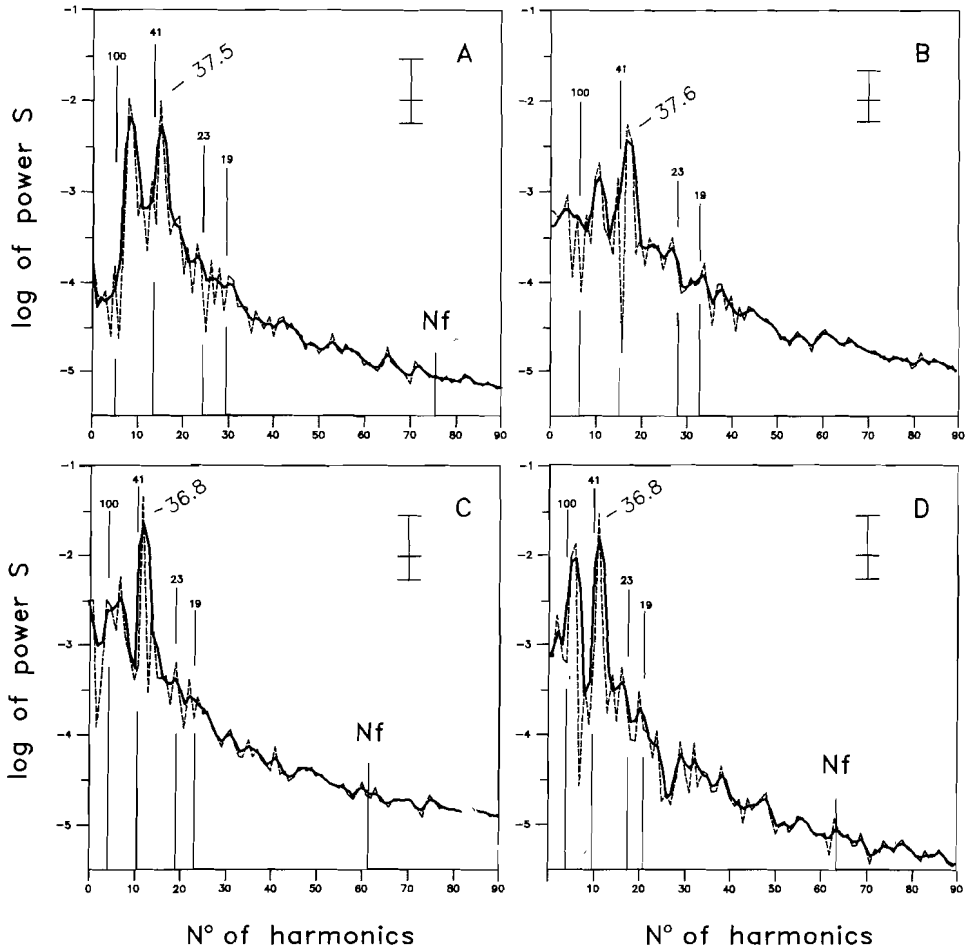


Fig. 7. Representative spectra based on the $\delta^{18}\text{O}$ (A and C) and CaCO_3 (B and D) records from DSDP Site 607 as published in Ruddiman et al. [2] and Raymo et al. [3]. (A) and (B) based on the interval between the Brunhes/Matuyama and the top of the Olduvai using the conventional ages of 0.73 and 1.66 Ma of the respective reversal boundaries [8] for age calibration. (C) and (D) based on the interval between the Gauss/Matuyama and the bottom of the Olduvai using the respective conventional ages of 2.47 and 1.88 Ma for calibration. The periodicity of the dominant peak in the obliquity frequency domain is shown in ka. Also indicated are the positions of frequencies corresponding to the main quasi-periods of the orbital cycles. Nf = Nyquist frequency of original time series using twice the average time spacing. The 80% confidence interval is shown as a small vertical bar on the right-hand side of each spectrum.

[42] of an equally spaced time series of the original record. By slightly changing the number of lags of that part of the autocorrelation function on which the Fourier transform is employed, the exact position of the spectral peaks can be accurately determined. Figure 7A shows that the most prominent peak of the $\delta^{18}\text{O}$ spectrum has indeed shifted to a higher frequency and matches a periodicity of 37.4 ± 0.1 ka. The CaCO_3 spectrum is more complex and yields two separate peaks with periodicities of 34.9 ± 0.1 and 37.9 ± 0.1 ka. In addition, a less prominent and significant peak is found at a frequency corresponding to a periodicity of 43.6 ka. Nevertheless, the CaCO_3 spectrum too shows a strong tendency to shift to higher frequencies (Fig. 7B).

This shift in the dominant spectral peak(s) in the obliquity frequency band to a higher frequency than that of the dominant quasi-period of obliquity can be explained by assuming that the interval between the Brunhes/Matuyama and the top of the Olduvai lasted longer than suggested by the conventional ages of 0.73 and 1.66 Ma for these reversal boundaries. If we correct for this frequency shift so that the corresponding periodicity matches the main 41 ka quasi-period, the estimate of the amount of time in this interval increases from 0.93 to 1.02 Ma, an increase of 90 ka. A repetition of this procedure, using the ages of 0.73 and 1.65 Ma of Ruddiman et al. [2], results in a corresponding increase from 0.92 to 1.02 Ma. At the same time, these results imply that Ruddiman et al. [2] failed to notice at least two obliquity-related cycles in this particular interval. Close inspection of the $\delta^{18}\text{O}$ and CaCO_3 records from Site 607 indeed reveals that the stratigraphic distance between their glacial stages 20 and 22 and between 34 and 36 is almost twice the distance

normally observed in this interval, indicating that two extra cycles are present but not distinctly manifested. The reflection of these extra cycles, however, is clearly detectable in the records of Site 609 (fig. 2 in [41]; fig. 11 in [2]). To provide further support for this alternative interpretation, we applied a Tukey band-pass filter centred at a frequency of 0.0267 cycles per year (i.e. corresponding to a periodicity of 37.4 ka as indicated by the results of our spectral analysis) to the conventional time-series of the records from Site 607. The filtered components clearly reveal the two extra obliquity-related cycles missed by Ruddiman et al. (Fig. 8A). Moreover, comparison with the actual, but lagged record of obliquity confirms that these components contain two extra cycles in this interval (Fig. 8B). Essentially the same results are obtained if we apply a band-pass filter centred at the main orbital frequency of obliquity of 0.0244 cycles per year (a periodicity of 41 ka). Consequently, the estimate of 0.92 Ma of Ruddiman et al. [2] for the duration of this interval would increase by 82 ka to 1.0 Ma. Shackleton et al. [1] independently arrived at more or less the same conclusion although they interpreted Stage 21 to contain three precession peaks rather than two obliquity peaks.

Although this re-examination of Site 607 reveals that as much as 1.02 Ma may be present between the Brunhes/Matuyama and the top of the Olduvai, this still does not agree with our estimates of 1.06 (option II) or 1.11 Ma (option I). It must be remembered, however, that our estimates depended on an age of 0.73 Ma for the Brunhes/Matuyama boundary. Following the earlier ideas of Johnson [14], Shackleton et al. [1] convincingly demonstrated that the (orbitally tuned) age of 0.73 Ma is too young and that the

Fig. 8. Time-series of the variations in $\delta^{18}\text{O}$ and CaCO_3 and their filtered obliquity components for the interval between the Brunhes/Matuyama and the top of the Olduvai at DSDP Site 607 using either the conventional ages of 0.73 and 1.66 Ma [8] (A) or the new astronomically calibrated ages of 0.78 [1] and 1.79 Ma (C) of these reversal boundaries. The Tukey band-pass filters were centred at frequencies of 0.0267 (dotted line in (A); bandwidth = 0.104) and 0.0244 (dashed lines in (A) and (C); bandwidth = 0.095) cycles per year. The former corresponds to a periodicity of 37.4 ka, as indicated by the results of spectral analysis (see Fig. 7), the latter to the main 41 ka quasi-period of obliquity. Arrows mark the obliquity-related cycles missed by Ruddiman et al. [2]. Note that the $\delta^{18}\text{O}$ and CaCO_3 records have been detrended and averaged around zero. Variations in obliquity and the corresponding frequency components of $\delta^{18}\text{O}$ and CaCO_3 at DSDP Site 607 for the Brunhes/Matuyama to top Olduvai interval are also shown. Frequency components taken from Fig. 8A are shown in (B) and those from Fig. 8C are shown in (D). Solid line shows 8 ka lagged versions of actual obliquity after the new astronomical solutions [32]. The original data by Berger and Loutre [32] cannot be reproduced without their permission. Note that the filtered components have been normalized to obliquity.

ASTRONOMICAL CALIBRATION OF GAUSS TO MATUYAMA SAPPPELS

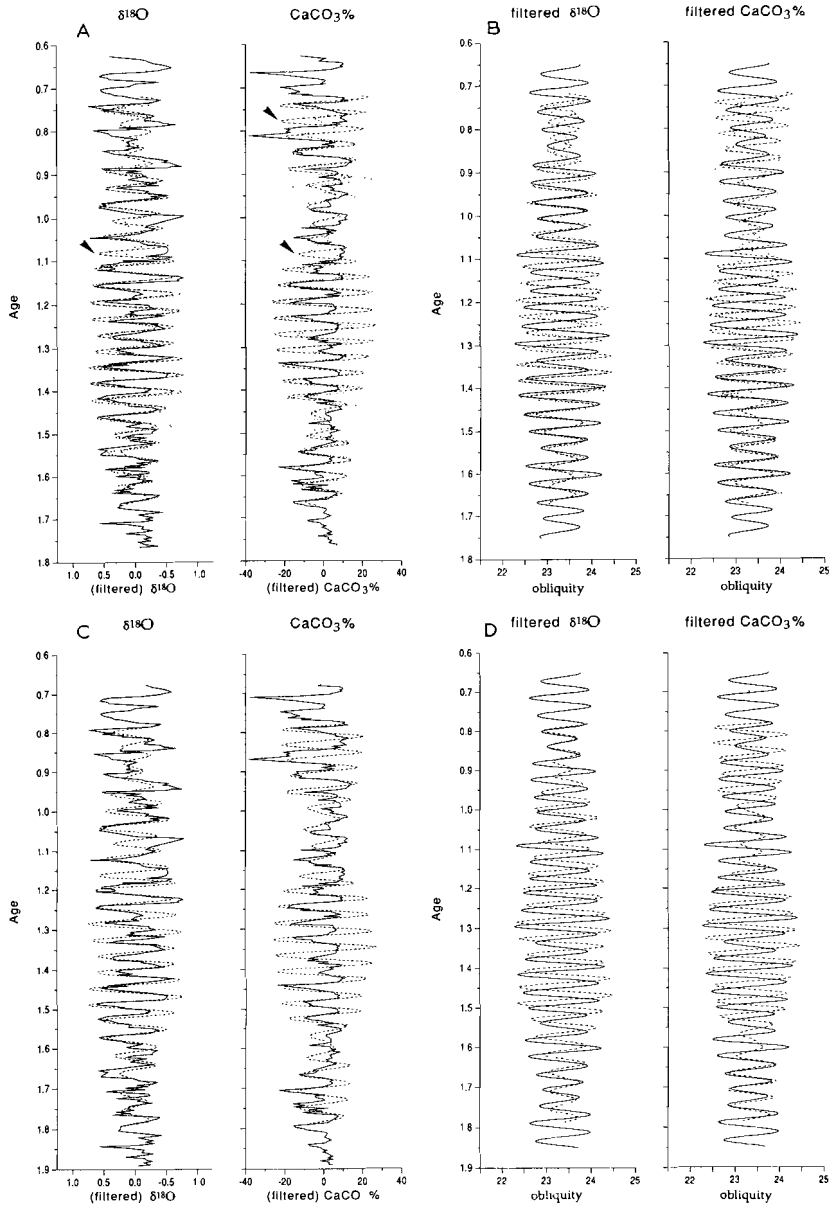


TABLE 3

Age differences between our polarity time scale and those of Ruddiman et al. (1989) [2] and Raymo et al. (1989) [3], and Mankinen and Dalrymple (1979) [6]. These differences are also given as the percentage of their ages for the reversals. The age of 0.78 Ma* for the Brunhes/Matuyama boundary is taken from Shackleton et al. [1]

reversal boundary	our age	Ruddiman & Raymo, 1989			Mankinen & Dalrymple, 1979		
		age	Δ	%	age	Δ	%
Brunhes/Matuyama	(0.78)*	0.73	0.05*	6.85*	0.73	0.05*	6.85*
Olduvai top	1.79	1.65	0.14	8.48	1.67	0.12 (II)	7.19
	1.84	-	0.19	11.52	-	0.17 (I)	10.18
Olduvai bottom	1.95	1.82	0.13	7.14	1.87	0.08	4.28
Reunion top	2.14	1.99	0.15	7.54	-	-	-
Reunion bottom	2.15	2.02	0.13	6.44	-	-	-
Gauss/Matuyama	2.59/2.62	2.48	0.11/0.14	5.04	2.48	0.11/0.14	5.04
Kaena top	3.02	-	-	-	2.92	0.10	3.43

actual age for the Brunhes/Matuyama is 0.78 Ma. As a consequence of this new age, the duration of the Brunhes/Matuyama to Olduvai period is reduced by 50 ka to either 1.06 (option I) or 1.01 Ma (option II). In conclusion, our estimate is now consistent with the record of Site 607 if we use the younger age of the top of the Olduvai (option II in Table 2). In option I, the Olduvai would only span 110 ka, which is definitely too short (Table 2), while according to the preferred second option, the Olduvai lasts 160 ka [24]. This agrees well with the estimate of 170 ka of Raymo et al. [3] and the 180 ka of Shackleton et al. [1]. Moreover, the resulting astronomically calibrated age of 1.79 Ma for the top of the Olduvai is close to the age estimate of 1.77 Ma of Shackleton et al. [1] for this boundary.

As a final test of our age model, a band-pass filter centred at the dominant frequency of obliquity was again applied to the records from Site 607, but this time we employed the new astronomically calibrated ages of the Brunhes/Matuyama (0.78 Ma) and the top of the Olduvai (1.79 Ma) to generate the time series. The filtered components are almost exactly in phase with actual obliquity at the age calibration points, but they are slightly out of phase in between (Fig. 8D). Very importantly, however, they do contain the same number of cycles, suggesting that slight changes in sedimentation rate are responsible for the observed out of phase relationship in between the calibration points. The near in-phase relationship observed at the top of the Olduvai further indicates that 1.79 Ma (or 1.78) is a more accurate age

for this reversal boundary than the 1.77 Ma suggested by Shackleton et al. [1]. This discrepancy might be explained by the slight uncertainty concerning the exact position of this boundary with respect to the isotopic stages (see [2]). Shackleton et al. [1] listed the base of Stage 63 as the position of this reversal boundary, whereas at Site 607 it actually occurs in the top part of Stage 64 [3]. The latter position determines the near in-phase relationship between the filtered components and lagged obliquity at the top of the Olduvai in Fig. 8D.

In order to have an additional check on our ages for reversal boundaries older than the Olduvai, we have applied spectral analysis to the interval between the Gauss/Matuyama and the bottom of the Olduvai at Site 607, followed by the adjustment of consistent shifts of the dominant peak in the obliquity frequency domain with respect to the main frequency of obliquity. The resultant spectra for both the variations in $\delta^{18}\text{O}$ and $\text{CaCO}_3\%$ revealed a single peak in this frequency domain corresponding to a periodicity of 36.8 ± 0.1 ka, if the conventional ages of 1.88 and 2.47 Ma for the bottom of the Olduvai and the Gauss/Matuyama [8] are used (Figs. 7C and D). The correction necessary to adjust for this consistent frequency shift results in an increase of the duration of this particular interval from 0.59 to 0.66 Ma. This perfectly matches both the estimate of Raymo et al. [3], indicating that no obliquity-related cycles have been missed in this interval, as well as our estimate and that of Shackleton et al. [1] (see Table 2). It deviates,

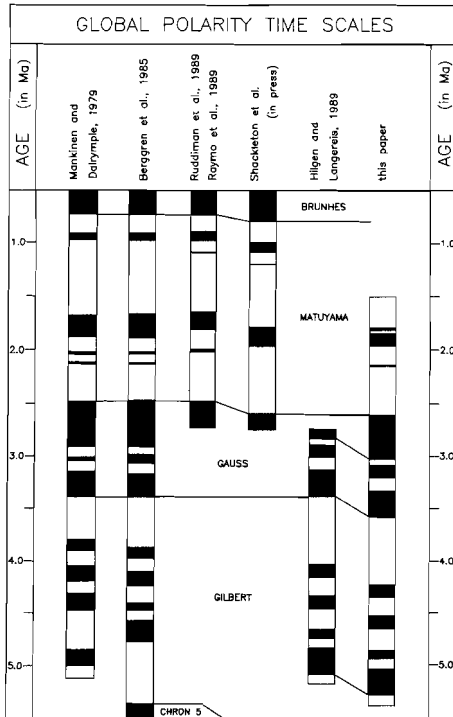


Fig. 9. Comparison of the extended astronomical time scale with other polarity time scales.

however, considerably from the duration of this interval according to the more conventional time scales [6,8].

5.2. Discrepancies between radiometric ages for polarity reversals

The discrepancies between our astronomically calibrated polarity time scale and the conventional time scales (Tables 2 and 3, Fig. 9), which for this period of time rely heavily on K/Ar radiometric dating, are more difficult to explain. Although we cannot provide a solution to this problem, a comparison between these methodologically totally different time scales shows that the discrepancy is, proportionally, fairly constant if only the radiometrically more accurately dated Brunhes/Matuyama and Gauss/Matuyama Chron boundaries are considered (5–7%; see Table 3). Possible errors

in the radiometric dating method include the inaccuracy of the decay constants (note that these constants were readjusted in 1979 which resulted in an increase in the K/Ar ages by 2.66% for the period of time under consideration [43]), the imperceptible loss of radiogenic argon and the (possible) lack of sensitivity in accurately measuring low concentrations of radioactive decay gas at such young levels. It is expected that new radiometric methods, such as single crystal laser dating, will give more insight into the accuracy of the K/Ar ages and thereby in the origin of the discrepancy between the radiometric and astronomically calibrated ages for reversal boundaries.

5.3. Extension of the astronomically calibrated time scale to the Miocene/Pliocene boundary

The procedure of tuning climatic proxy records to the new astronomical solutions is a very promising tool for constructing a truly high-resolution time scale for at least the last 5–10 Ma, i.e. the period of time for which the astronomical solutions are now considered to be reliable [32]. At present, this time scale can be extended back to the Miocene/Pliocene boundary if we also take the detailed record of small-scale, precession-related CaCO_3 cycles in the Trubi Formation on Sicily [44] into account. For these Trubi marls, we also found a remarkably consistent shift in spectral peaks to frequencies higher than the orbital frequencies. This shift has been explained by assuming that the conventional ages assigned to reversal boundaries were not sufficiently accurate. In addition, an alternative time scale was provided for the major part of the Gilbert and Gauss Chrons by extrapolating an average quasi-period of 21.7 ka of the precession cycle [45] as the periodicity of these small-scale cycles, using the Gilbert/Gauss Chron boundary dated radiometrically at 3.40 Ma as a fixed age reference point. The thus obtained age of 2.84 Ma for the top of the Kaena, however, is significantly younger than our present age of 3.02 Ma for this boundary. By adding this difference of 180 ka to the ages assigned to reversal boundaries by Hilgen and Langereis [44], our orbitally tuned polarity time scale is extended back to the Miocene/Pliocene boundary (Fig. 8). This results in an age of 3.58 Ma for the Gilbert/Gauss boundary, which is 5.3% older than the conventional radiometric age of 3.40 Ma. This

confirms the proportional constancy of the age discrepancy between our time scale and the radiometric scale. The extension of the astronomically calibrated time scale to the Miocene/Pliocene boundary will be presented in more detail in a separate paper.

6. Conclusions

The calibration of cyclic sapropel patterns of late Pliocene to early Pleistocene age to the new astronomical solutions for precession and eccentricity [32] results in ages for the top of the Olduvai (1.79 Ma), the bottom of the Olduvai (1.95 ± 0.01), the Reunion (2.14–2.15), the Gauss/Matuyama (2.59–2.62) and the top of the Kaena (3.02 ± 0.01). The age for the Pliocene/Pleistocene boundary arrives at 1.81 Ma.

This tuning furthermore provides an excellent opportunity for introducing a Mediterranean Precession-Related Sapropel (MPRS) coding according to which sapropels in the Mediterranean Pliocene–Pleistocene are coded using the correlative peak of the precession index as numbered from the Recent. These sapropels can be dated with an accuracy of 1 ka if we consider a time lag of 4 ka between orbital forcing and maximum climate response and sapropel formation, as observed for the youngest, Holocene sapropel.

Our ages are remarkably identical to the independently established, astronomically calibrated ages of Shackleton et al. [1]. The age discrepancy of 130 ka between our new polarity time scale and that of Ruddiman et al. [2] and Raymo et al. [3] is explained by the age of 0.78 instead of 0.73 Ma for the Brunhes/Matuyama (50 ka), in combination with the finding that Ruddiman et al. [2] most probably missed two obliquity-related cycles (80 ka) in the interval between the Brunhes/Matuyama and the top of the Olduvai in the records from DSDP Site 607.

A proportionally constant age discrepancy is found between our polarity time scale and the conventional polarity time scales which depend primarily on K/Ar radiometric dating. This discrepancy of 5–7% cannot easily be explained at present and must await further research.

In order to confirm our age model, it is necessary to complete the sapropel record of the Mediterranean Pliocene–Pleistocene by the recovery of

continuous and relatively undisturbed marine sequences from the eastern Mediterranean, preferably by hydraulic piston coring of multiple holes. Continued work in the Mediterranean is especially relevant because the Mediterranean is a marginal sea, which is particularly sensitive to the climatic effect of precession due to its low latitudinal position, its basin configuration and the related hydrological conditions. Due to the modulation by eccentricity, the precession signal is far more distinctive than that of the more regular obliquity cycle. We therefore consider the precession-dominated sedimentary record of the Mediterranean more suitable for the construction of an astronomically calibrated time scale than the isotope records from DSDP Site 607 or even ODP Site 677, which primarily reflect the dominant control of the obliquity cycle on global ice volume.

Finally, our astronomically calibrated time scale can be extended back to the Miocene/Pliocene boundary by incorporating the time scale of Hilgen and Langereis [44] for the major part of the Gilbert and Gauss Chrons and adding the difference of 180 ka for the age of the top of the Kaena to the ages assigned to the older reversal boundaries in Hilgen and Langereis' time scale.

Acknowledgements

T. van Hinte skillfully made the drawings. A. Berger and M.F. Loutre kindly provided their new astronomical records. The stimulating discussions with A. Berger, W.A. Berggren, P. de Boer, C.G. Langereis, L. Lourens, M.F. Loutre, N.J. Shackleton and W.J. Zachariasse are gratefully acknowledged and they led to considerable improvement of the manuscript. J. Imbrie and an anonymous reviewer are thanked for their reviews. This study was partly funded by the Netherlands Organization for Scientific Research (NWO).

References

- 1 N.J. Shackleton, A. Berger and W.R. Peltier, An alternative astronomical calibration of the Lower Pleistocene time scale based on ODP Site 677, *Trans. R. Soc. Edinb.*, 81, 251–261, 1990.
- 2 W.F. Ruddiman, M.E. Raymo, D.G. Martinson, B.M. Clement and J. Backman, Pleistocene evolution: Northern hemisphere ice sheets and North Atlantic Ocean, *Paleoceanography* 4, 353–412, 1989.

- 3 M.E. Raymo, W.F. Ruddiman, J. Backman, B.M. Clement and D.G. Martinson, Late Pliocene variation in northern Hemisphere ice sheets and North Atlantic deep water circulation, *Paleoceanography* 4, 413–446, 1989.
- 4 C.S. Gromme and R.L. Hay, Magnetization of basalt bed I, Olduvai Gorge, Tanganyika, *Nature* 200, 560–561, 1963.
- 5 C.S. Gromme and R.L. Hay, Geomagnetic polarity epochs: Age and duration of the Olduvai normal polarity event, *Earth Planet. Sci. Lett.* 10, 179–185, 1971.
- 6 E.A. Mankinen and G.B. Dalrymple, Revised geomagnetic polarity time scale for the interval 0–5 m.y. B.P., *J. Geophys. Res.* 84, 615–626, 1979.
- 7 W.B. Hartland, A.V. Cox, P.G. Llewellyn, A.G. Smith and R. Walters, *A geological time scale*, Cambridge University Press, Cambridge, 127 pp, 1982.
- 8 W.A. Berggren, D.V. Kent, J.J. Flynn and J.A. Van Couvering, *Cenozoic geochronology*, *Geol. Soc. Am. Bull.*, 96, 1407–1418, 1985.
- 9 J. Imbrie, J.D. Hays, D.G. Martinson, A. McIntyre, A.C. Mix, J.J. Morley, N.G. Pisias, W.L. Prell and N.J. Shackleton, The orbital theory of Pleistocene climate: Support from a revised chronology of the marine $\delta^{18}\text{O}$ record, in: *Milankovitch and Climate*, NATO ASI Ser. C, 126, A.L. Berger et al., eds., Reidel, Dordrecht, pp. 269–305, 1984.
- 10 J.D. Hays, J. Imbrie and N.J. Shackleton, Variations in the earth's orbit: Pacemaker of the ice ages, *Science* 194, 1121–1132, 1976.
- 11 J.J. Morley and J.D. Hays, Towards a high-resolution, global, deep-sea chronology for the last 750,000 years, *Earth Planet. Sci. Lett.* 53, 279–295.
- 12 D.G. Martinson, N.G. Pisias, J.D. Hays, J. Imbrie, T.C. Moore and N.J. Shackleton, Age dating and the orbital theory of the ice ages: Development of a high-resolution 0 to 300,000-year chronostratigraphy, *Quat. Res.* 27, 1–29, 1987.
- 13 N.G. Pisias and T.C. Moore, The evolution of Pleistocene climate: A time series approach, *Earth Planet. Sci. Lett.* 52, 450–458, 1981.
- 14 R.G. Johnson, Brunhes–Matuyama dated at 790,000 yr B.P. by marine astronomical correlations, *Quat. Res.* 17, 135–147, 1982.
- 15 N.J. Shackleton, A case for revising the astronomical calibration for the Brunhes–Matuyama and Jaramillo boundaries, *Terra Abstr.* 1, 185, 1989.
- 16 E. Aquirre and G. Pasini, The Pliocene–Pleistocene boundary, *Episodes* 8, 116–120, 1985.
- 17 G. Pasini, R. Selli, R. Tampieri, M.L. Colalunga, S. d'Onofrio, A.M. Borsetti and F. Cati, The Vrica section, in: *The Neogene–Quaternary Boundary, II Symp. Bologna–Crotone*, Excursion Guide-book, R. Selli, ed., pp. 62–72, 1975.
- 18 R. Selli, C.A. Accorsi, M. Bandini Mazzanti, D. Bertolani Marchetti, G. Bigazzi, F.P. Bonnadonna, A.M. Borsetti, F. Cati, M.-L. Colalunga, S. d'Onofrio, W. Landini, E. Menesini, R. Mezzeti, G. Pasini, G. Savelli and R. Tampieri, The Vrica section (Calabria). A potential Neogene–Quaternary boundary stratotype, *G. Geol.* 41, 181–204, 1977.
- 19 H. Nakagawa, N. Niitsuma, T. Takayama, S. Tokunaga, H. Kitazato and I. Koizumi, Preliminary results of magneto- and biostratigraphy of the Vrica section (Calabria, southern Italy), *Proc. 2nd Symp. Neogene/Quaternary Boundary (U.S.S.R., 1977)*, pp. 145–156, 1980.
- 20 H. Nakagawa, Neogene/Quaternary boundary and correlation of Vrica section, *Proc. Neogene/Quaternary Boundary Field Conference (India, 1979)*, pp. 107–111, 1981.
- 21 J.D. Obradovitch, C.W. Naeser, G.A. Izett, G. Pasini and G. Bigazzi, Age constraints on the proposed Plio-Pleistocene boundary stratotype at Vrica, Italy, *Nature* 298, 55–59, 1982.
- 22 L. Tauxe, N.D. Opdyke, G. Pasini and C. Elmi, Age of the Plio-Pleistocene boundary in the Vrica section, southern Italy, *Nature* 304, 125–129, 1983.
- 23 J. Backman, N.J. Shackleton and L. Tauxe, Quantitative nanofossil correlation to open ocean deep-sea sections from Plio-Pleistocene boundary at Vrica, Italy, *Nature* 304, 156–158, 1983.
- 24 J.D.A. Zijderfeld, F.J. Hilgen, C.G. Langereis, P.J.J.M. Verhallen and W.J. Zachariasse, Integrated magnetostratigraphy and biostratigraphy of the Upper Pliocene–Lower Pleistocene from the Monte Singa and Crotone areas in Calabria (Italy), *Earth Planet. Sci. Lett.*, submitted, 1991.
- 25 W.B.F. Ryan, Stratigraphy of Late Quaternary sediments in the eastern Mediterranean, in: *The Mediterranean Sea: A Natural Sedimentation Laboratory*, D.J. Stanley, ed., Dowden, Hutchinson and Ross, Stroudsburg, Pa., pp. 146–169, 1972.
- 26 F.J. Hilgen, Sedimentary rhythms and high-resolution chronostratigraphic correlations in the Mediterranean Pliocene, *Newslett. Stratigr.* 17, 109–127, 1987.
- 27 R.B. Kidd, M.B. Cita and W.B.F. Ryan, The stratigraphy of eastern Mediterranean sapropel sequences as recovered by DSDP leg 42A and their paleoenvironmental significance, *Init. Rep. DSDP 42A*, 421–443, 1978.
- 28 R.C. Thunell, D.F. Williams and P.R. Belyea, Anoxic events in the Mediterranean Sea in relation to the evolution of Late Neogene climates, *Mar. Geol.* 59, 105–134, 1984.
- 29 P.J.J.M. Verhallen, Early development of *Bulimina marginata* in relation to paleoenvironmental changes in the Mediterranean, *Proc. K. Ned. Akad. Wetensch.*, B 90, 161–180, 1987.
- 30 B.W.M. Driever, Calcareous nanofossil biostratigraphy and paleoenvironmental interpretation of the Mediterranean Pliocene, *Utrecht Micropaleontol. Bull.* 36, pp. 245, 1988.
- 31 F.J. Hilgen, Closing the gap in the Plio-Pleistocene boundary stratotype sequence of Crotone (southern Italy), *Newslett. Stratigr.* 22, 43–51, 1990.
- 32 A. Berger and M.F. Loutre, New insolation values for the climate of the last 10 Myr, *Inst. Astron. Geophys. G. Lemaitre, Univ. Cathol. Louvain. Intern. Rep.*, 1988.
- 33 W.J. Zachariasse, L. Gudjonsson, F.J. Hilgen, C.G. Langereis, L.J. Lourens, P.J.J.M. Verhallen and J.D.A. Zijderfeld, Late Gauss to early Matuyama invasions of *Neogloboquadrina atlantica* in the Mediterranean and associated record of climatic change, *Paleoceanography* 5, 239–252, 1990.
- 34 A. Berger, Long term variations of daily insolation and Quaternary climatic changes, *J. Atmos. Sci.* 35, 2362–2367, 1978.

- 35 N. Combourieu-Nebout, Les premiers cycles glaciaire-interglaciaire en region mediterraneenne d'après l'analyse palynologique de la série Crotoné (Italie meridionale), Thesis, Univ. Sci. Tech. Languedoc, Montpellier, 1987.
- 36 C. Vergnaud-Grazzini, M. Devaux and J. Znaidi, Stable isotope "anomalies" in Mediterranean Pleistocene records, *Mar. Micropaleontol.* 10, 35–69, 1986.
- 37 F.J. Jorissen, K. van der Borg, A.M. Borsetti, L. Gudjonsson, F.J. Hilgen, S. Iaccarino, A.F.M. de Jong, E.J. Rohling, J.P. de Visser and W.J. Zachariasse, Late Quaternary high-resolution biochronology for the central Mediterranean, *Mar. Micropaleontol.* in press, 1991.
- 38 W.L. Prell, Monsoonal climate of the Arabian Sea during the late Quaternary; A response to changing solar radiation, in: Milankovitch and Climate, NATO ASI Ser. C, 126, A.L. Berger et al., eds., Reidel, Dordrecht, pp. 349–366, 1984.
- 39 D.A. Short and J.G. Mengel, Tropical climatic lags and Earth's precession cycle, *Nature* 323, 48–50, 1986.
- 40 A. McIntyre, W.F. Ruddiman, K. Karlin and A.C. Mix, Surface water response of the equatorial Atlantic Ocean to orbital forcing, *Paleoceanography* 4, 19–55, 1989.
- 41 W.F. Ruddiman, A. McIntyre and M. Raymo, Matuyama 41,000-year cycles: North Atlantic Ocean and northern hemisphere ice sheets, *Earth Planet. Sci. Lett.* 80, 117–129, 1986.
- 42 J.C. Davis, *Statistics and data analysis in geology*, Wiley, New York, 1973.
- 43 R.H. Steiger and E. Jager, Subcommission on geochronology: Convention on the use of decay constants in geo- and cosmochronology, *Earth Planet. Sci. Lett.* 36, 359–362, 1977.
- 44 F.J. Hilgen and C.G. Langereis, Periodicities of CaCO_3 cycles in the Mediterranean Pliocene: Discrepancies with the quasi-periods of the Earth's orbital cycles?, *Terra Nova* 1, 409–415, 1989.
- 45 A.L. Berger, Accuracy and frequency stability of the Earth's orbital elements during the Quaternary, in: Milankovitch and Climate, NATO ASI Ser. C, 126, A.L. Berger et al., eds., Reidel, Dordrecht, pp. 3–39, 1984.
- 46 M. Rossignol-Strick, African monsoons, an immediate climatic response to orbital insolation, *Nature* 303, 46–49, 1983.
- 47 C. Vergnaud-Grazzini, W.B.F. Ryan and M.B. Cita, Stable isotope fractionation, climatic change and episodic stagnation in the eastern Mediterranean during the Late Quaternary, *Mar. Micropaleontol.* 2, 353–370, 1977.
- 48 M.B. Cita, C. Vergnaud-Grazzini, C. Robert, H. Chamley, N. Ciaranfi and S. d'Onofrio, Paleoclimatic record of a long deep-sea record from the eastern Mediterranean, *Quat. Res.* 8, 205–235, 1978.
- 49 A. Murat and H. Got, Middle and Late Quaternary depositional sequences and cycles in the eastern Mediterranean, *Sedimentology* 34, 885–899, 1987.
- 50 Shipboard Scientific Party, Site 653, *Proc. Init. Rep. (Pt. A) ODP 107*, 599–745, 1987.
- 51 W.J. Zachariasse, J.D.A. Zijderveld, C.G. Langereis, F.J. Hilgen and P.J.J.M. Verhallen, Early Late Pliocene biochronology and surface water temperature variations in the Mediterranean, *Mar. Micropaleontol.* 14, 339–355, 1989.
- 52 M.B. Cita, Planktonic foraminiferal biozonation of the Mediterranean Pliocene deep sea record. A revision, *Riv. Ital. Paleontol. Stratigr.* 81, 527–544, 1975.
- 53 P. Spaak, Accuracy in correlation and ecological aspects of the planktonic foraminiferal zonation of the Mediterranean Pliocene, *Utrecht Micropaleontol. Bull.* 28, 1–160, 1983.
- 54 I. Raffi and D. Rio, Calcareous nannofossil biostratigraphy of DSDP Site 132-Leg 13 (western Mediterranean), *Riv. Ital. Paleontol. Stratigr.* 85, 127–172, 1979.
- 55 G. Glaçon, D. Rio and R. Sprovieri, Calcareous plankton Pliocene–Pleistocene biostratigraphy in the Tyrrhenian Sea (western Mediterranean, Leg 107), *Proc. ODP, Sci. Results* 107, 683–693, 1990.

Chapter 9

Extension of the astronomically calibrated (polarity) time scale to the Miocene/Pliocene boundary

F.J. Hilgen

Department of Geology, Institute of Earth Sciences, Budapestlaan 4, 3584 CD Utrecht, The Netherlands

ABSTRACT

The early Pleistocene to late Pliocene astronomically calibrated time scale of Shackleton et al. [1] and Hilgen [2] is extended to the Miocene/Pliocene boundary. This is done by correlating the detailed record of CaCO_3 cycles in the Trubi and the lower part of the overlying Narbone Formation (Rossello composite section; Sicily) to the astronomical record, using (1) inferred phase relations between these CaCO_3 cycles and the corresponding orbital cycles of precession and eccentricity, and (2) calibration points provided by the previously established astronomical calibration of sapropelitic layers which occur in the topmost part of the CaCO_3 record [2].

This correlation allows all small-scale CaCO_3 cycles in the Rossello composite section to be coded after the correlative precession peak and to be dated astronomically with an accuracy of 1 ky. In combination with the available high-resolution magnetostratigraphy, it further allows the construction of an astronomically calibrated Geomagnetic Polarity Time Scale for the major part of the Gilbert and Gauss Chrons. This new time scale gives ages for the reversal boundaries of the Kaena (3.04–3.11 Ma) and Mammoth (3.22–3.33 Ma), the Gilbert/Gauss Chron boundary (3.58 Ma), and the reversal boundaries of the Cochiti (4.18–4.29 Ma), Nunivak (4.48–4.62 Ma), Sidufjall (4.80–4.89 Ma) and Thvera (4.98–5.23 Ma). These ages are significantly older than the ages given by conventional time scales. Age discrepancies gradually increase with increasing age: the age of 5.32 Ma for the Miocene/Pliocene boundary, as defined by the base of the Trubi on Sicily, is almost 0.5 m.y. (9.5%) older than the presently accepted age of 4.86 Ma [3].

These considerable discrepancies with the conventional time scale can either be explained by an (consistent) error in the decay constants used in K/Ar radiometric dating or, more likely, by diffusional loss of radiogenic argon.

1. Introduction

Astronomical calibration of climatic proxy records provides an alternative method to construct (polarity) time scales which, in principle, have a higher resolution and are more accurate than conventional time scales based on linear interpolation between radiometrically dated calibration points in marine anomaly sequences (e.g. [4]). This astronomical calibration is now firmly established for the last 700,000 years [5–7]. Initial attempts to extend this time scale to the early Pleistocene – late Pliocene yielded ages for geomagnetic reversal boundaries that were essentially consistent with the radiometric datings [8–10]. However, results of recent studies indicate that these radiometric ages are consistently too young by 5–7% [1,2]. At present, this alternatively astronomically calibrated (polarity) time scale extends back to 3.0 Ma (late Gauss).

To accomplish this new time scale, Hilgen [2] correlated the characteristic cyclic pattern of Pliocene–Pleistocene sapropels in marine sequences from southern Italy to the astronomical record using inferred phase relations between these sedimentary (= sapropel) cycles and the orbital cycles of precession and eccentricity. (Sapropel is used here to designate brownish coloured, often well-laminated, discrete layers relatively enriched in organic carbon. We refrained from using the redefinition proposed by Kidd et al. [11] because their (lower) limit of > 2% organic carbon is rather arbitrarily chosen and disregards the basic and, from a paleoenvironmental point of view, more important similarities between these layers. Our use is similar to the original meaning of this term introduced by Olausson [12]). It was further anticipated that this time scale could be extended back to the Miocene/Pliocene boundary using the CaCO_3 cycles of the Trubi Formation on Sicily.

Like the sapropels, these CaCO_3 cycles are connected with the Earth's orbital cycles [13,14]. Moreover, they are supposedly underlain by similar climatic oscillations held responsible for sapropel formation [13,15], i.e., dominantly precession forced variations in the intensity of the monsoonal system and circum-Mediterranean climate [16–18].

Magnetostratigraphic calibration and subsequent spectral analysis of a high-resolution CaCO_3 record of the Trubi yielded significant peaks in the orbital frequency bands of the spectrum [14]. Nevertheless, these peaks showed a remarkably consistent shift to slightly higher frequencies than those of the supposedly corresponding orbital cycles. This shift could only be explained by assuming that ages assigned to polarity reversals in the conventional Geomagnetic Polarity Time Scales lack sufficient precision. Consequently, Hilgen and Langereis [14] presented an alternative Geomagnetic Polarity Time Scale for the major part of the Gilbert and Gauss Chrons by extrapolating an average quasi-period of 21.7 ky of the precession cycle [19] being the periodicity of small-scale CaCO_3 cycles in the Trubi. The radiometric age of 3.40 Ma for the Gilbert/Gauss Chron boundary [20] was employed as fixed reference point. The astronomically calibrated time scale of Hilgen [2] was provisionally extended to the Miocene–Pliocene boundary by adjusting the time scale of Hilgen and Langereis [14] for the observed age discrepancy of 180 ky for the mutually dated reversal boundary, the upper Kaena [2].

However, this procedure can only be considered preliminary for several reasons. In the first place, the inferred average periodicity of 21.7 ky for the precession cycle may not be representative for the time interval under consideration. Secondly, the exact number of small-scale CaCO_3 cycles in the Trubi is still uncertain due to the sometimes problematic identification of individual small-scale cycles in CaCO_3 maxima of larger-scale, eccentricity related cycles (see [14]). Therefore, the ages provided by Hilgen [2] represent only a fair approximation of the true astronomical age of these small-scale cycles and, hence, of the geomagnetic reversal boundaries.

In the present paper, the exact calibration of the sedimentary cycles in the Trubi to the astronomical record is discussed in detail to determine

the age of the individual sedimentary cycles as well as of the reversal boundaries as accurately as possible. For this purpose, we used the new astronomical solution which is considered accurate in the time domain over the last 5.0 Ma [21].

2. Sections and lithology

The lithostratigraphic term Trubi is commonly used to denote the characteristic, whitish coloured marls of the lower Pliocene on Sicily. A striking feature of these Trubi marls is the pronounced cyclic bedding on a different scale. Small-scale CaCO_3 cycles are quadripartite and display grey-white(I)-beige-white(II) colour alternations. The grey and, especially, beige layers represent the less indurated, CaCO_3 -poor marls [13–15]. These small-scale cycles have been individually numbered from the base of the Trubi upward [14]. This numbering could be continued in the (lower part of the) overlying Narbone Formation in which sapropelitic layers first appear. These sapropels are intercalated in the grey marl beds of the small-scale CaCO_3 cycles. The average thickness of the small-scale CaCO_3 cycles is approximately one meter. A small number of cycles, however, is significantly thicker. These cycles are considered to contain an extra cycle, which lacks sedimentary expression [14]. The exceptional thickness of these cycles remains confined to one of the white marl beds in these cycles.

Larger-scale CaCO_3 cycles can be distinguished on the basis of the cyclic recurrence of relatively thick, indurated and CaCO_3 -rich intervals. The expression of the small-scale, quadripartite cycles in these intervals is less obvious and the identification of individual small-scale cycles is more difficult. Both the small-scale as well as the larger-scale CaCO_3 cycles are linked to variations in the Earth's orbit [13,14]: small-scale CaCO_3 cycles are related to precession and the larger-scale cycles to variations in eccentricity. In addition, some indication was found for obliquity related variations in $\text{CaCO}_3\%$, but these variations are not directly relevant to the present study.

In this paper, the Rossello composite section of Hilgen [13] is used. This composite section is composed of the Eraclea Minoa, Punta di Maiata, Punta Grande and Punta Piccola subsections (Figs. 1 and 2) and has been constructed using high-reso-

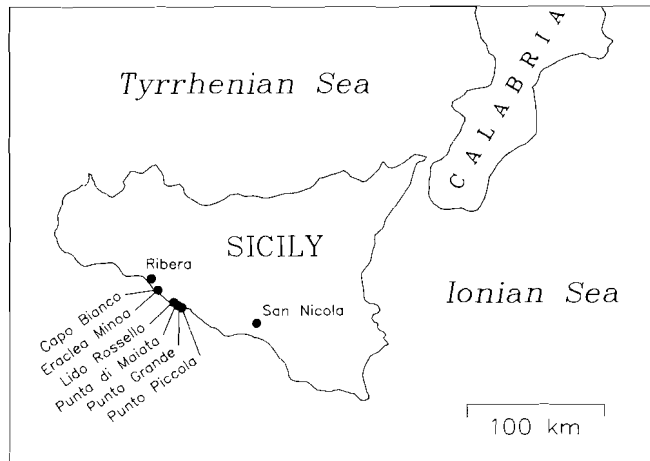


Fig. 1. Locations of sections.

lution cyclostratigraphic ('bed-to-bed') correlations between subsections. The Eraclea Minoa and Punta di Maiata subsections were correlated using the pronounced beige layer of cycle 24 in combination with the white marlbed, which contains white 11 of cycle 25 and grey and white I of cycle 26. The former occurs on top of the prominent interval which contains the extra-ordinary thick cycles 21 and 22, and cycle 23 of normal thickness. The correlation between the Punta di Maiata and Punta Grande subsections is based on the whitish marl bed which contains white II of cycle 68 and grey and white I of cycle 69. Finally, the Punta Grande and Punta Piccola subsections were correlated on the basis of the white marl bed which comprises white II of cycle 77 and grey and white I of cycle 78. The characteristic thickness and colour patterns of the cyclic bedding were verified in a number of parallel sections (Fig. 2) with the purpose of excluding stratigraphic complications present in time equivalent sections of the Rossello composite [22–24]. These parallel sections confirm that the Rossello composite section contains an uninterrupted, relatively undisturbed sequence of the Trubi and the lower part of the Narbone Formation. To fully appreciate the quality, and thus the significance, of this composite section, it should be realized that (1) all sections

are excellently exposed; (2) the marls are tectonically only slightly disturbed (with the exception of Monte San Nicola), whereas the cyclic bedding is extremely helpful in tracing faults which otherwise might upset the stratigraphic continuity, and (3) the between-section cyclostratigraphic correlations are unambiguous and are confirmed by both magnetostratigraphic and biostratigraphic correlations (Fig. 2).

For this Rossello composite section, both a high-quality magnetostratigraphy and planktonic foraminiferal biostratigraphy (with a sample resolution of ± 10 ky) as well as a detailed CaCO_3 record (sample resolution ± 5 ky) have been established [3,14,25–27]. The polarity sequence revealed that the composite ranges from the lower reversed subchron(ozone) of the Gilbert into the lower reversed subchron(ozone) of the Matuyama Chron [27].

3. Astronomical calibration of the Trubi

Two conditions must be met before the Trubi sequence can be calibrated accurately to the astronomical record. Firstly, the phase relations between the CaCO_3 cycles and the corresponding astronomical cycles of precession and eccentricity must be known. Secondly, the astronomical

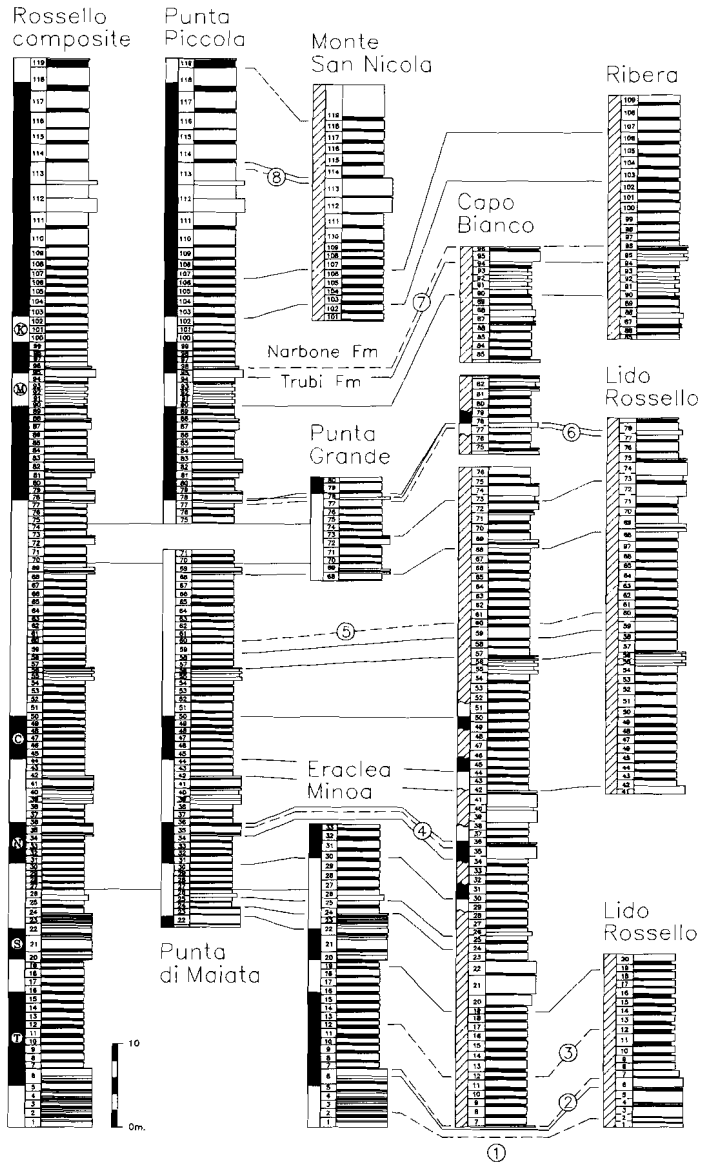


Fig. 2. Review of sections in the Trubi and lower part of the Narbone Formation on southern Sicily. Solid lines mark magnetostratigraphic and the most obvious cyclostratigraphic correlations. Dashed lines mark biostratigraphic correlations: 1 = bottom of the *Sphaeroidinellops* acme; 2 = top of the *Sphaeroidinellops* acme; 3 = first common occurrence of *G. margaritae*; 4 = first occurrence of *G. puncticulata*; 5 = last common occurrence of *G. margaritae*; 6 = first occurrence of *G. crassaformis*; 7 = last occurrence of *Sphaeroidinellops seminulina*, and 8 = first occurrence of *N. atlantica*. Biostratigraphic and magnetostratigraphic data based on Hilgen and Langereis [3], Zachariasse et al. [25,26] and Langereis and Hilgen [27] and partly on unpublished data.

calibration of the Trubi would be strongly facilitated by a calibration point which is already tied to the astronomical record.

With respect to the first condition, phase relations between sedimentary and astronomical cycles have already been established for sapropels. These phase relations were determined by correlating late Quaternary sapropels in the Mediterranean to the new astronomical solution [2]. This correlation reveals that individual sapropels correspond to minimum peak values of the precession index, while small- and large-scale sapropel clusters correspond to eccentricity maxima connected with the 100 and 400 ky eccentricity cycles, respectively. In addition, the sequential relationships between these sapropel cycles and the CaCO_3 cycles could be established in the Punta Piccola subsection of the Rossello composite in which both types of sedimentary cycles co-occur. Field observations revealed that individual sapropels correspond to the grey marl beds in the small-scale CaCO_3 cycles and that sapropel clusters correspond to CaCO_3 minima in the larger-scale cycles. Consequently, the following phase relations between the CaCO_3 cycles and the astronomical cycles can be inferred:

Grey marl beds in the small-scale, precession related CaCO_3 cycles correspond to minimum peak values of the precession index; and CaCO_3 minima of the larger-scale, eccentricity related cycles correspond to eccentricity maxima, or more correctly to maximum amplitude variations of the precession index related to the eccentricity modulation of precession.

The second condition, i.e., the necessary fixed calibration point with respect to the astronomical record, is more easily fulfilled because the lowermost sapropels in the Narbone part of the Rossello composite have already been astronomically calibrated [2]. These sapropels coincide with the topmost part of our CaCO_3 record.

3.1. Calibration of the larger-scale CaCO_3 cycles to eccentricity

A first-order astronomical calibration of the Trubi is established by correlating the largest-scale CaCO_3 maxima connected with the 400 ky eccentricity cycle to the astronomical record. These 400 ky CaCO_3 maxima can easily be recognized in

the field by the regular recurrence of extraordinary thick and indurated marly intervals which encompass the small-scale cycles 1-6, 20-23, 38-42, 55-56, 73-75 and 95-96 of the Trubi. A next maximum is distinguishable in the upper (Narbone) part of the Rossello composite and includes the cycles 112 and 113 (Fig. 3). The thus defined largest-scale CaCO_3 cycles contain 17, 19, 14, 19, 21 and 17 small-scale cycles, if we consider the top of the indurated intervals to delimit these cycles. The average number of 18 is consistent with our assumption that these cycles mirror the 400 ky (or more precisely 413 ky) eccentricity cycle. This astronomical cycle should correspond to 19 precession cycles, if 21.7 ky [19] is taken as an average periodicity for precession. Extraordinary thick small-scale cycles are supposed to contain an extra cycle, and may well account for the observed discrepancy—18 versus 19—in the number of precession (related) cycles.

To further illustrate these 400 ky CaCO_3 cycles, we applied a moving average on the total CaCO_3 record of the Trubi. A 20-point moving average was used to smooth variations in $\text{CaCO}_3\%$ connected with both the small-scale, precession related cycles as well as the larger-scale CaCO_3 cycles linked to the 100 ky eccentricity cycle. The filtered record clearly reveals the successive 400 ky CaCO_3 cycles (Fig. 3). Only the pattern between the fifth and sixth CaCO_3 maximum, as counted from the base of the Trubi, is slightly complicated. This is probably caused by a strong overprint of 100 ky variations in $\text{CaCO}_3\%$. The reflection of this 100 ky cycle is clearly revealed if we use a 8-point instead of a 20-point moving average (Fig. 3). This moving average only eliminates the expression of the small-scale, precession related cycles.

Using the inferred phase relations between the CaCO_3 and astronomical cycles in combination with the fixed astronomical calibration provided by the sapropelitic layers, the largest-scale CaCO_3 maxima can be correlated to successive 400 ky eccentricity minima in the astronomical record (Fig. 3). This correlation yields ages of 2.81, 3.21, 3.67, 4.07 (or 3.99), 4.38, 4.82 and 5.25 Ma for these CaCO_3 maxima and can further be employed to correlate the distinct 100 ky CaCO_3 maxima to 100 ky eccentricity minima (Fig. 3). The latter correlation in addition provides an ex-

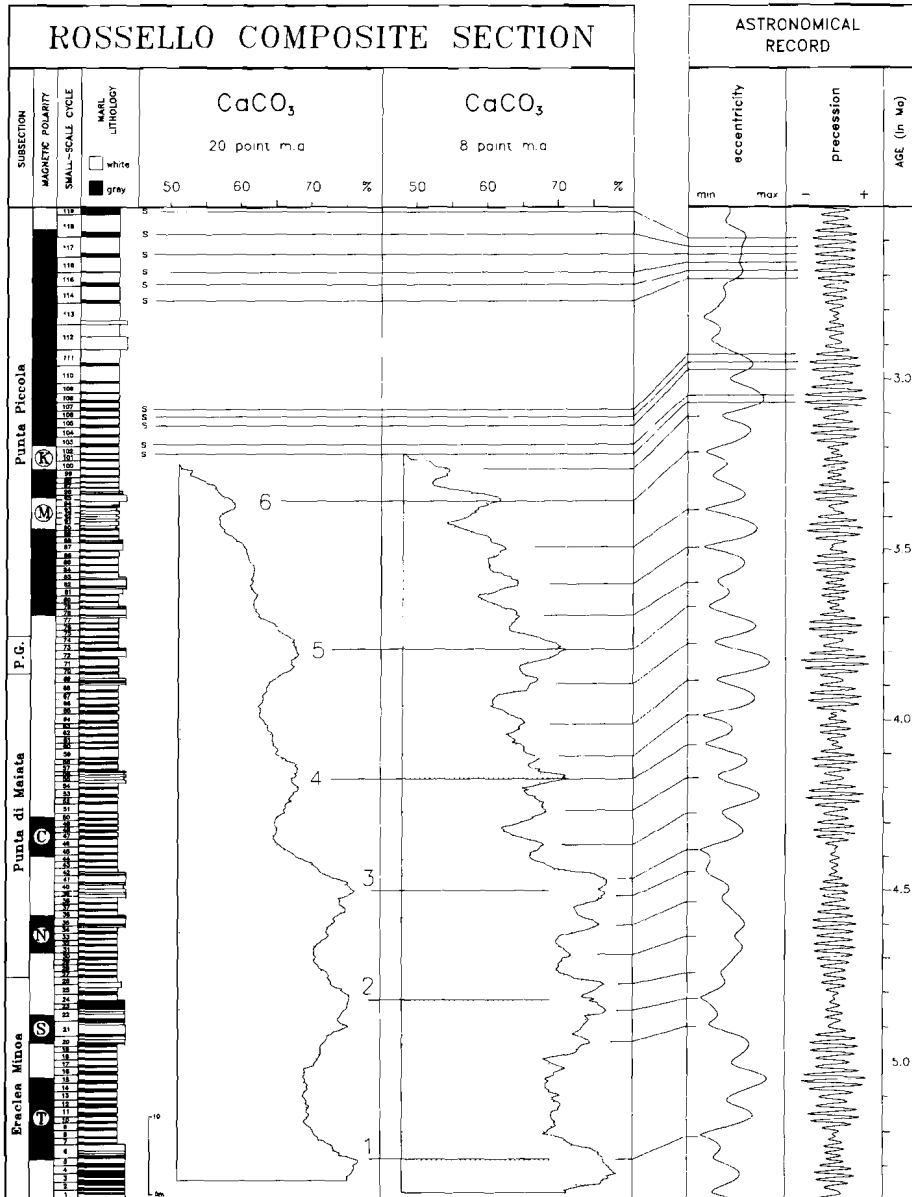


Fig. 3. Correlation of CaCO₃ maxima in the larger-scale cycles of the Trubi in the Rosello composite section to eccentricity minima in the astronomical record. Successive largest-scale maxima are numbered 1 to 6 from the base of the section upward. Sapropels in the uppermost, Narbone part of the section are marked with an *s* and provide fixed calibration points with the astronomical record [2]. Magnetostratigraphy based on Hilgen and Langereis [3], Zachariasse et al. [25,26] and Langereis and Hilgen [27]. The astronomical record is based on the new solution of Berger and Loutre [21].

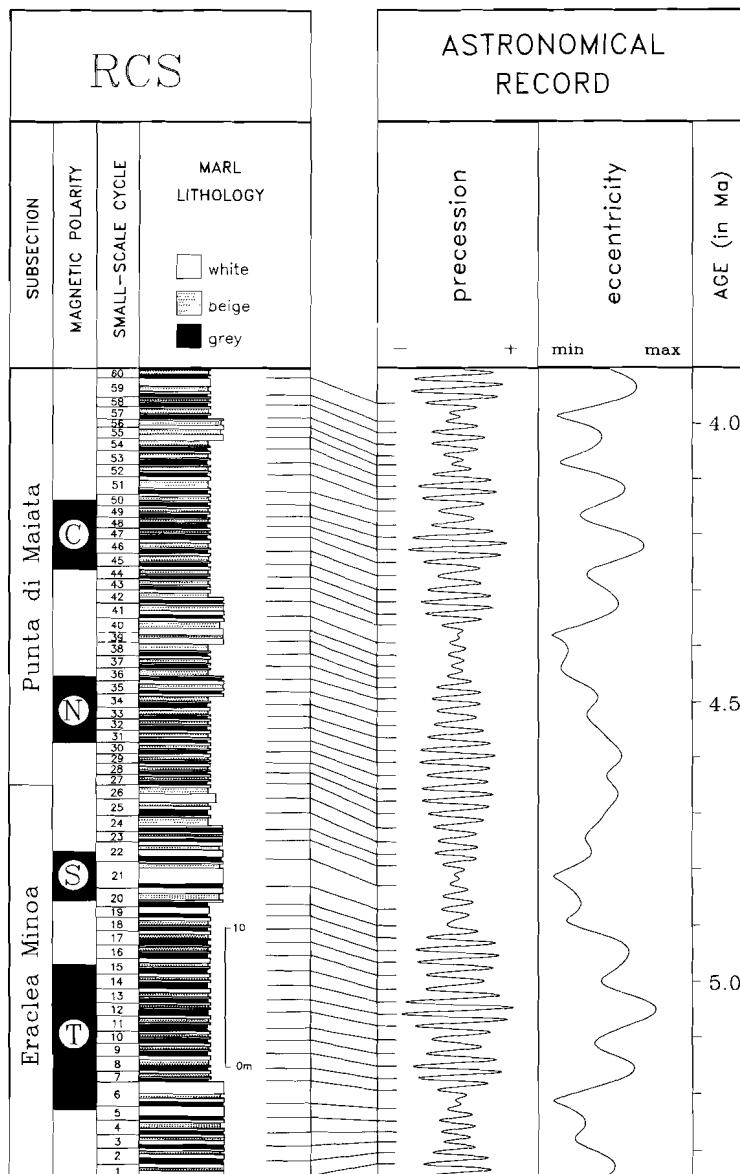


Fig. 4. Correlation of the small-scale cycles 1–60 of the Trubi in the Rossello composite section to the astronomical record based on the astronomical calibration of the larger-scale cycles (Fig. 3) and the inferred phase relation with precession. See caption to Fig. 3.

planation for the observed strong overprint of the 100 ky variations in CaCO_3 between 3.2 and 3.7 Ma. This overprint is in perfect agreement with the eccentricity pattern, which displays the most pronounced 100 ky minima in this particular interval. Now that these larger-scale, eccentricity-related CaCO_3 cycles have been astronomically calibrated, the next step is the correlation of the small-scale cycles to the precession record.

3.2. Calibration of small-scale CaCO_3 cycles to precession

3.2.1. Cycles 1–60

Using the astronomical calibration of the larger-scale, eccentricity-related CaCO_3 cycles as a starting point, the small-scale cycles 1–60 can be correlated straightforwardly to precession (Fig. 4). This correlation implies that the extra-ordinary thick cycles 6, 21, 22 and 59 each correlate with

two (low amplitude) precession cycles. Consequently, these small-scale cycles indeed represent composite cycles, i.e., cycles which contain an extra cycle that lacks sedimentary expression (note that the composite character of cycle 21 is actually perceptible at Capo Spartivento in adjacent southern Calabria, because it contains an additional grey marl bed; author's field observations). In addition, cycle 41 should comprise an extra cycle. This composite cycle had not been expected on the basis of its thickness. Its presence, however, is not in contradiction with the actual lithologic observations. Cycle 41 constitutes (the major) part of the upper protruding marl bed in a succession of two such beds which combined encompass the small-scale cycles 38–42 and compose the largest-scale 400 ky CaCO_3 maximum dated at 4.38 Ma (Figs. 3 and 4). The subdivision of such thick beds into individual marl beds of the small-scale cycles is usually complicated by their massive appearance and any attempt in this direction may

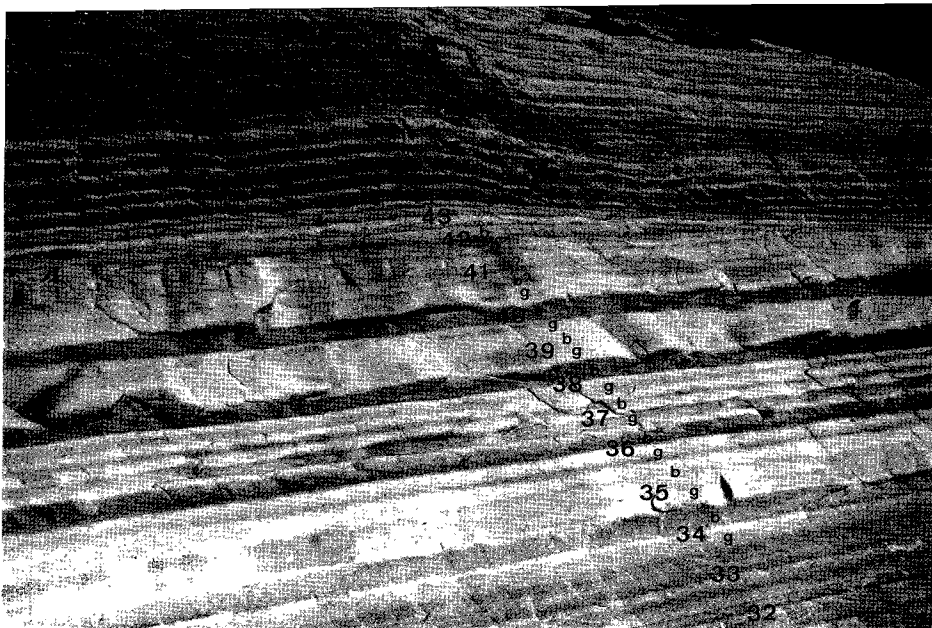


Fig. 5. Punta di Maiata. The CaCO_3 maximum of the largest-scale, 400 ky cycle which encompasses the small-scale cycles 34–42. *G* denotes grey marl layers and *b* beige marl layers.

therefore be subject to error. In this respect, the interpretation of cycle 41 being a single small-scale cycle of average thickness may not be correct. Close reexamination of the weathering profile of the massive bed containing cycle 41, provides some evidence for the presence of an extra cycle (Fig. 5). Our probably incorrect first interpretation seems to have originated partly from the fact that the two correlative precession cycles lasted less than two times the average periodicity of a precession cycle (i.e. 38 ky). Consequently, the presence of this extra cycle is less evident from the increase in bed-thickness itself.

Such periodicities, which markedly differ from the average duration of a precession cycle, can be held responsible for other (consistent) irregularities in the thickness pattern of the small-scale cycles as well. From the other small-scale cycles containing an additional cycle, only cycle 21 is almost twice as thick as a single regular cycle, whereas cycles 6, 22 and 59 are considerably less thick. Accordingly, the two precession cycles which correlate with cycles 6, 22 and 59 lasted 34, 35 and 32 ky, respectively, whereas those corresponding to cycle 21 show a combined duration of 43 ky. Evidently, only the latter is two times the average periodicity of precession.

The thicker-than-average cycle 20, on the other hand, clearly represents a single and not a composite small-scale cycle: this cycle does not contain an extra cycle because its increased thickness is not confined to one of the white marls, as in composite cycles, but is distributed (more) evenly over the individual lithologies. The correlative, single precession cycle shows a corresponding longer-than-average periodicity of 28 ky.

An important observation is that the presence of these small-scale cycles with deviant thicknesses remains confined to 400 ky CaCO_3 maxima, i.e., they occur at times of 400 ky eccentricity minima. This observation is consistent with the astronomical theory because, during periods of 400 ky eccentricity minima, the contribution of the dominant 23 ky quasi-period to precession is significantly reduced and less dominant quasi-periods may start to interfere (see also fig. 3 in Imbrie et al. [6]).

3.2.2. Cycles 59–110

The astronomical calibration of the small-scale cycles 59–110 is less straightforward and some

minor discrepancies are present. The most likely correlation is presented in Fig. 6. This correlation starts from the assumption that cycle 59 represents a composite cycle. This is based on the fact that the exceptional thickness of this cycle remains totally confined to the upper white marl bed in this cycle. This implies, however, that the precession cycle with the "prolonged" periodicity of 29 ky at 3.88 Ma does not correspond to the significantly thicker than average cycle 64, but to cycle 63. Also the relative position of cycles 69 and 99 is not in complete accordance with the precession record (Fig. 6). The grey marl beds in these cycles clearly mark 100 ky CaCO_3 maxima. According to the established phase relations, these cycles should correlate to minimum amplitude peaks of the precession index to negative values, which result from the eccentricity modulation of precession. The corresponding peaks in the precession record, however, are positioned either one precession cycle too low (in case of cycle 69) or one cycle too high (in case of cycle 99). The latter also accounts for cycle 104. In contrast to the preceding cycle 103, this cycle contains a very faint, non-laminated sapropelitic layer. From the established phase relations, it can be inferred that the grey bed of cycle 103 and not the vague sapropelitic layer of cycle 104 should correlate with the minimum amplitude peak in the precession record (Fig. 6). Finally, our correlation implies that cycle 96 represents a composite cycle although this is not directly evident from the thickness of this cycle (Fig. 6). A second lithologic log obtained during the paleomagnetic sampling campaign revealed that this cycle is thicker than our measurements suggest [25]. We refrained from modifying our correlation scheme to correct for these small discrepancies because even a slight modification would immediately result in similar discrepancies elsewhere.

A partial explanation for these discrepancies may be found in the problematic logging of the stratigraphic interval which ranges from cycle 70 to cycle 76. To cover this particular interval, we had to incorporate the somewhat less clearly exposed and therefore less suitable Punta Grande subsection in our Rossello composite. At Lido Rossello, this interval is complicated by tectonic deformation in the uppermost part of the section. Also at Capo Bianco it proved impossible to log this interval in a single, continuously exposed and

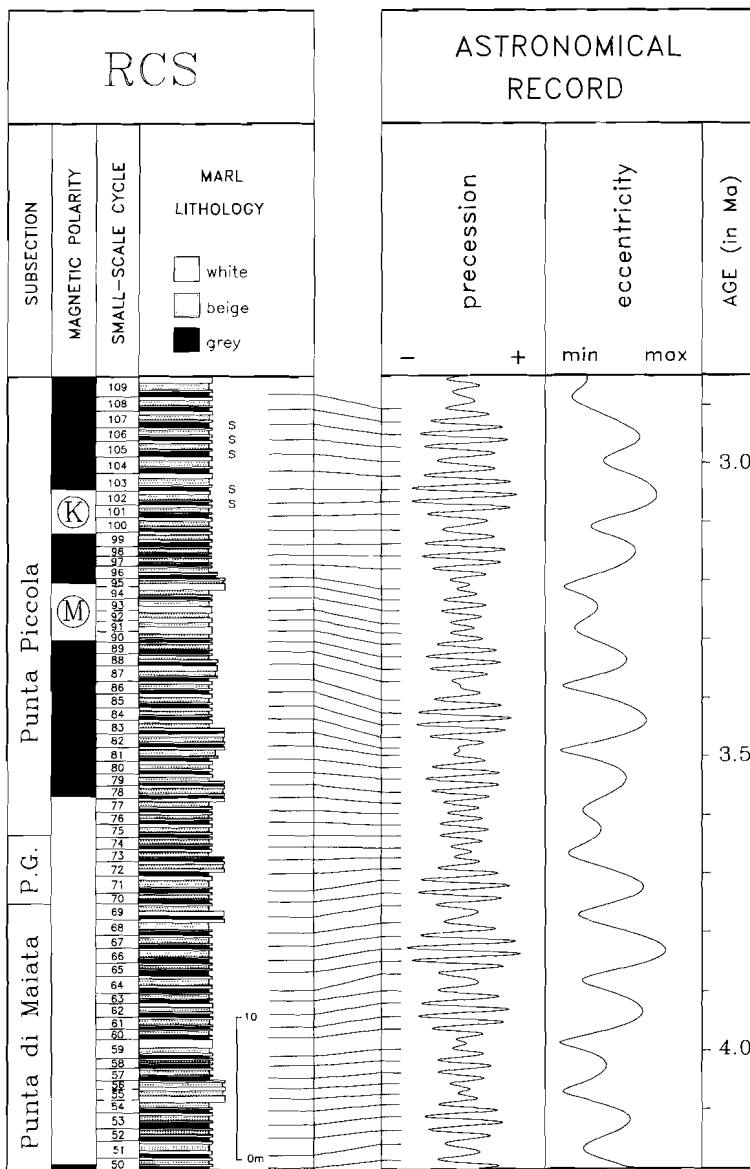


Fig. 6. Correlation of the small-scale cycles 50-109 in the Rossello composite section to the astronomical record based on the astronomical calibration of the larger-scale cycles (Fig. 3) and the inferred phase relation with precession. See caption to Fig. 3.

undisturbed succession (see also Fig. 2). Despite these stratigraphic problems, an error in the logging, which exceeds one small-scale cycle, can be excluded with certainty.

The astronomical solution offers an alternative explanation for the observed (minor) discrepancies. Although the astronomical record is considered reliable in the time domain over the last 5.0 Ma [21], slight modifications of specific details can not be ruled out completely. Finally, the applied phase relations may represent a simplification of the actual relationship between the sedimentary and astronomical cycles. For the moment, however, these phase relations do represent a fair and useful approximation.

Summarizing, there is in general a good coherence between the detailed record of CaCO_3 cycles and the astronomical record for this interval. This coherence applies in particular to the relative position of CaCO_3 maxima of the larger-scale, eccentricity-related cycles with respect to the corresponding eccentricity minima in the astronomical record (Fig. 3). As far as the precise calibration of the small-scale cycles 59–110 to precession is concerned, some minor discrepancies remain, but these discrepancies never exceed one cycle.

3.2.3. Cycles 110–120

A more serious problem was initially encountered in correlating the uppermost cycles 110–120 to the astronomical record. A considerable discrepancy with the astronomical record for this interval would cast serious doubt on the correctness of the astronomical calibration of cycles 1–110 as presented in the previous sections.

In the uppermost part of the Rossello composite section, a succession of six sapropelitic layers can be distinguished comprising the small-scale cycles 114–119 (Fig. 3). At Punta Piccola, these layers actually consist of dark grey coloured marly clays of which only the uppermost three or four can be termed sapropels. This succession composes a very characteristic pattern, which can easily be recognized elsewhere in the Mediterranean and which has been correlated to the precession record [2]. Consequently, these sapropels provide fixed calibration points with the astronomical record.

The five lowermost sapropels in the Rossello

composite occur in cycles 102, 103 and 105–107 (Fig. 3) and have been correlated to the astronomical record as well [2]. This correlation actually differs one precession cycle from the presently advocated astronomical calibration (Fig. 6). Initial attempts to extend this new calibration to the calibrated succession of 6 sapropelitic layers failed due to a substantial lack of small-scale cycles in the interjacent interval (Fig. 3). This discrepancy is only partially reduced if cycles 112 and 113 are considered composite cycles. This assumption is based on the exceptional thickness of these cycles and the fact that they contain a relatively thick and indurated white marl bed (Fig. 3). Unfortunately, a thorough analysis of this interval is strongly hampered by a conspicuous increase in sedimentation rate by a factor of 2–2.5 deduced from the overall increase in the thickness of the sedimentary cycles (Fig. 3). From this increase in cycle thickness, it can be inferred that the sedimentation rate started to increase between cycles 108 and 110; cycle 109 represents a cycle of intermediate thickness.

An alternative interpretation of this interval is possible, however, and more plausible from our point of view. This alternative implies that the increase in sedimentation rate occurred higher in the succession and that, in addition to cycles 112 and 113, cycles 110 and 111 contain an extra cycle as well. The intermediate thickness of cycle 109 is then explained by the longer-than-average periodicity, i.e. 28 ky, of the correlative precession cycle (Fig. 7). According to this interpretation, there is no discrepancy between the number of (small-scale) sedimentary cycles and the number of precession cycles (Fig. 7).

To find supporting evidence for this interpretation, we logged the time-equivalent part of the (Monte) San Nicola section on Sicily (Figs. 1 and 2), because it is less affected by an increase in sedimentation rate (Fig. 7). The succession of sedimentary cycles observed in the Punta Piccola subsection of the Rossello composite can easily be recognized at Monte San Nicola and essentially confirms our interpretation (Fig. 7). Cycles 112 and 113 are twice as thick as the overlying regular small-scale cycles 114–119 and cycle 110 and, although to a lesser extent, also cycle 111 are considerably thicker than the preceding small-scale cycles. According to the preferred astronomi-

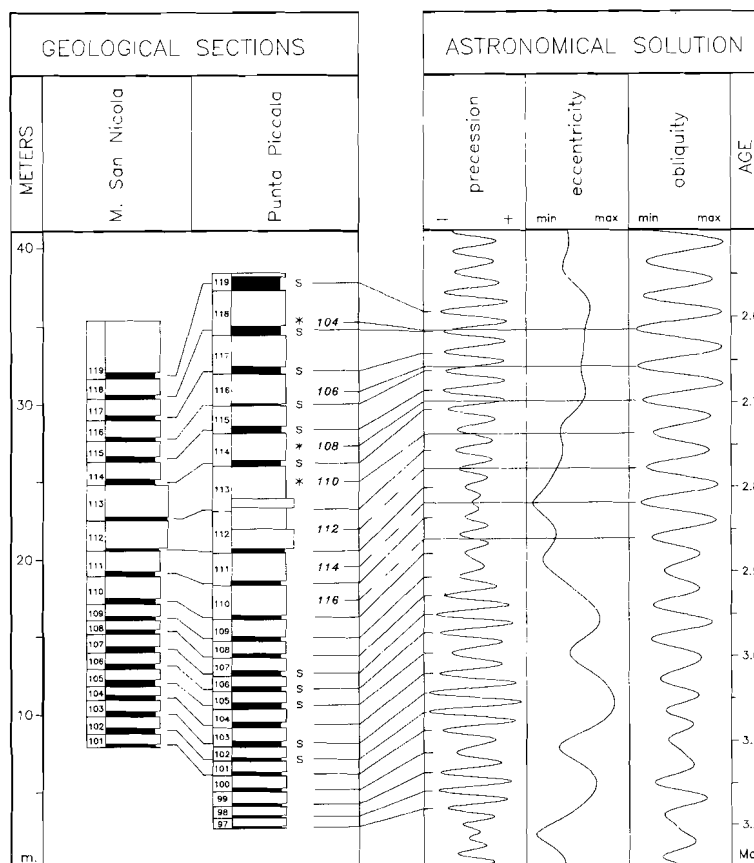


Fig. 7. Correlation of the small-scale cycles 97–119 in the Narbone part of the Rossello composite section to precession. Small-scale cycles 110–113 represent composite cycles and correspond to two precession cycles. Positions of glacial isotope stages 104 to 110 (based on [26,28]) as well as the inferred positions of glacial stages 112 to 116 and their correlation to obliquity minima are also shown (isotope stages in italics). Associated influxes of *N. atlantica* are marked with an asterisk. See caption to Fig. 3.

cal calibration to precession, the composite cycle 111 has a duration of 35 ky only, whereas the composite cycles 110, 112 and 113 lasted 42, 44 and 46 ky, respectively.

The most strongly marked increase in sedimentation rate according to this option occurred around the lowermost sapropel of the distinct cluster of six sapropelitic layers in the uppermost part of the Rossello composite section (Fig. 8). This increase coincides with the first influx of

Neogloboquadrina atlantica in the Mediterranean which has been correlated with glacial oxygen isotope stage 110 of Raymo et al. [10] (see [28]). Stage 110 represents the oldest glacial in the Pliocene for which extensive ice rafting in the northern Atlantic can be demonstrated on the basis of the colour variation in the DSDP sites from Leg 94 [29]. This coincidence suggests that glacio-eustatic sealevel fall and associated lowering of the base level of erosion invoked the observed in-

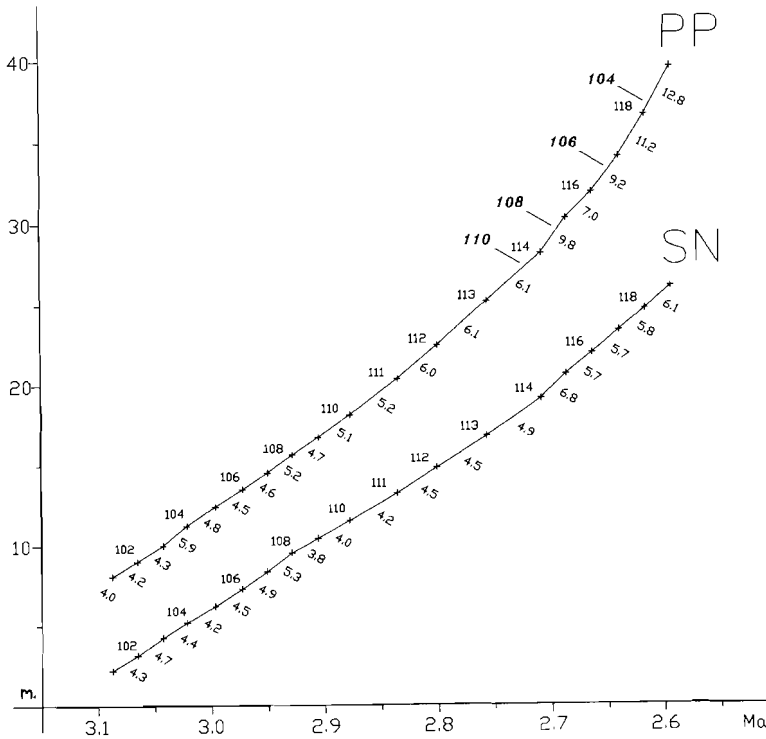


Fig. 8. Sediment accumulation diagrams of the Monte San Nicola section and the Punta Piccola subsection of the Rossello composite section, using the astronomical ages of the small-scale cycles. Number of the small-scale cycles in the Rossello composite and the sedimentation rate per small-scale cycle are indicated. Also shown is the position of the glacial isotope stages 104 to 110 [26,28].

crease in sedimentation rate. An earliest increase in sedimentation rate is already perceptible in cycles 111–113 at Punta Piccola (Fig. 8). This increase may be related to glacio-eustatic sealevel changes as well. Indications for older (less severe) glacials are found in the isotope and CaCO_3 records from DSDP Site 607 ([10]; i.e., stages 112, 114 and 116).

Finally, the stratigraphic position of glacial stages 104 to 110, as well as the inferred position of stages 112 to 116, and their correlation to obliquity minima suggest that the composite character of our sedimentary cycles 110–113 is related to the interference of precession and obliquity. The position of glacial stages 110 to 116 matches the position of the extra small-scale cycles which

lack sedimentary expression in the composite cycles. Apparently, obliquity forced glacial periods—corresponding to relative dry climatic condition in the Mediterranean Pliocene (Combourieu-Nebout, pers. commun)—counterbalanced the opposite effect exerted by precession minima on Mediterranean climate—corresponding to wet climatic conditions [16–18]—during this time interval. However, this almost perfect interference with precession is not the only factor which contributed to the reflection of obliquity in the sedimentary record. At the same time, the influence of precession itself on climate was strongly reduced due to the low amplitude variations of the precession index connected with the 400 ky eccentricity minimum at 2.8 Ma.

4. Results

4.1. Ages of CaCO_3 cycles

With the accurate calibration of the CaCO_3 cycles to the astronomical record, ages can be assigned to the individual grey beds of the small-scale cycles. Strictly speaking, a time lag between astronomical forcing, and climate response and deposition of small-scale sedimentary cycles must be taken into account. For the base of the youngest, Holocene sapropel, a time lag of 2–3 ky can be inferred from the accurate AMS ^{14}C -dating of this lithohorizon at 9 ka [30,31] and the age of 11.5 ka for the correlative precession peak. At Punta Piccola and Monte San Nicola, sapropels are intercalated in the basal part of the grey beds. The base of these sapropels, however, is not coincident with the bottom of the grey beds but is usually found somewhat higher—5–10 cm—in the succession. Consequently, an approximate time lag of 1 ky can be inferred for the base of the grey beds while a time lag of 4 ky can be inferred for the mid-points of these beds, at least if we assume that the sedimentation rate remains constant in the small-scale cycles. The (lagged) ages of the small-scale cycles in the Rossello composite section are presented in Table 1. These ages depend critically on (1) the correctness of the proposed astronomical calibration, and (2) the accuracy of the astronomical solutions. As far as the first point is concerned, this calibration can only be 400 ky or multiples of 400 ky in error, because the largest-scale 400 ky cycle was used for a preliminary first-order calibration of the CaCO_3 record to the astronomical (eccentricity) record, preceding the high-resolution correlation of the small-scale CaCO_3 cycles to precession. The new astronomical solution seems to be valid over the last 5 Ma in the time domain and over at least the last 10 Ma in the frequency domain [21].

Recently, Hilgen [2] introduced a MPRS (Mediterranean Precession Related Sapropel) coding according to which Pliocene–Pleistocene sapropels are coded after the correlative peak of the precession index numbered from the Recent. In order to incorporate also the small-scale CaCO_3 cycles in this coding scheme, we substitute MPRS for MPRC which stands for Mediterranean Precession Related Cycle. The MPRC coding for all

small-scale CaCO_3 cycles in the Rossello composite has been included in Table 1 as well. It actually refers to the grey beds in the small-scale cycles only. In principle, the beige layers can be included in this coding scheme as well. These layers should correlate with positive peaks of the precession index because they represent the opposite lithology in the small-scale cycles with respect to the grey layers.

4.2. Ages of bioevents

The astronomical dating of the CaCO_3 cycles further provides new ages for the planktonic foraminiferal and nannofossil bioevents recorded in the Rossello composite section. These ages have been summarized and compared with the conventional ages in Table 2. The stratigraphic positions of planktonic foraminiferal events are based on Hilgen and Langereis [3], Zachariasse et al. [25,26] and Langereis and Hilgen [27]. For the nannofossil events, we used the work of Driever [32].

4.3. Ages of reversal boundaries

The astronomical calibration of the CaCO_3 cycles, in addition, provides very accurate ages for the geomagnetic polarity reversals recorded in the Rossello composite section. The stratigraphic positions of these reversals are based on a high-resolution magnetostratigraphy, which showed that almost the complete Gilbert and Gauss Chrons are represented in the Rossello composite [27]. The astronomically calibrated ages of the reversal boundaries as well as their stratigraphic position with respect to the MPRC-coded CaCO_3 cycles are given in Table 3. In this table, the resulting ages are further compared with the ages for these boundaries according to more conventional time scales. These conventional time scales are either based on K/Ar radiometric dating of volcanic rocks of known polarity [20,33] or on linear interpolation between radiometrically dated magnetostratigraphic calibration points in marine magnetic anomaly sequences (e.g. [4,34]). With the present study, the astronomically calibrated (polarity) time scale of Shackleton et al. [1] and Hilgen [2] for the late Pliocene–Pleistocene has been extended to the Miocene/Pliocene boundary. Consequently, this astronomically calibrated time

scale covers now the complete Pliocene and Pleistocene.

The astronomical calibrated age of 3.58 Ma for the Gilbert/Gauss Chron boundary confirms

earlier conclusions that K/Ar dating yields ages that are consistently too young (5–7%; [1,2]) This is particularly true for the radiometrically more accurately dated Gilbert/Gauss, Gauss/Matuya-

TABLE 1

Cycle number, MPRC-code, age and lagged age of small-scale sedimentary cycles in the Rossello composite section. Cycle number in the Rossello composite as numbered from the base of the Trubi upwards. MPRC (Mediterranean Precession Related Cycle) coding and (lagged) age after the correlative peak of precession as numbered from the Recent. Age refers to the age of the precession peak, lagged age to the age of the mid-point of the correlative grey bed in the small-scale cycle

Rcs cycle no.	MPRC- code	age	lagged age	Rcs cycle no.	MPRC- code	age	lagged age	Rcs cycle no.	MPRC- code	age	lagged age
119	250	2.593	2.589	79	342	3.559	3.555	39	426	4.434	4.430
118	252	2.616	2.612	78	344	3.579	3.575	38	428	4.452	4.448
117	254	2.639	2.635	77	346	3.597	3.593	37	430	4.472	4.468
116	256	2.663	2.659	76	348	3.615	3.611	36	432	4.493	4.489
115	258	2.686	2.682	75	350	3.635	3.631	35	434	4.515	4.511
114	260	2.708	2.704	74	352	3.654	3.650	34	436	4.540	4.536
113	264	2.756	2.751	73	354	3.672	3.668	33	438	4.563	4.559
112	268	2.800	2.796	72	356	3.690	3.686	32	440	4.586	4.582
111	272	2.835	2.831	71	358	3.711	3.707	31	442	4.608	4.604
110	276	2.877	2.873	70	360	3.731	3.727	30	444	4.631	4.627
109	278	2.905	2.901	69	362	3.753	3.749	29	446	4.655	4.651
108	280	2.928	2.924	68	364	3.782	3.778	28	448	4.677	4.673
107	282	2.950	2.946	67	366	3.804	3.800	27	450	4.700	4.696
106	284	2.972	2.968	66	368	3.826	3.822	26	452	4.723	4.719
105	286	2.996	2.992	65	370	3.847	3.843	25	454	4.748	4.744
104	288	3.021	3.017	64	372	3.869	3.865	24	456	4.770	4.766
103	290	3.042	3.038	63	374	3.897	3.893	23	458	4.792	4.788
102	292	3.065	3.061	62	376	3.920	3.916	22	462	4.826	4.822
101	294	3.087	3.083	61	378	3.941	3.937	21	466	4.870	4.866
100	296	3.113	3.109	60	380	3.962	3.958	20	468	4.897	4.893
99	298	3.137	3.133	59	384	3.996	3.992	19	470	4.920	4.916
98	300	3.158	3.154	58	386	4.015	4.011	18	472	4.942	4.938
97	302	3.179	3.175	57	388	4.036	4.032	17	474	4.964	4.960
96	306	3.215	3.211	56	390	4.057	4.053	16	476	4.987	4.983
95	308	3.233	3.229	55	392	4.073	4.069	15	478	5.012	5.008
94	310	3.253	3.249	54	394	4.091	4.087	14	480	5.035	5.031
93	312	3.272	3.268	53	396	4.112	4.108	13	482	5.057	5.053
92	314	3.290	3.286	52	398	4.133	4.129	12	484	5.079	5.075
91	316	3.309	3.305	51	400	4.156	4.152	11	486	5.102	5.098
90	318	3.330	3.326	50	402	4.183	4.179	10	488	5.128	5.124
89	320	3.351	3.347	49	404	4.206	4.202	9	490	5.150	5.146
88	322	3.371	3.367	48	406	4.227	4.223	8	492	5.171	5.167
87	326	3.402	3.398	47	408	4.249	4.245	7	494	5.192	5.188
86	328	3.423	3.419	46	410	4.274	4.270	6	498	5.226	5.222
85	330	3.445	3.441	45	412	4.298	4.294	5	500	5.246	5.242
84	332	3.466	3.462	44	414	4.320	4.316	4	502	5.266	5.262
83	334	3.486	3.482	43	416	4.341	4.337	3	504	5.283	5.279
82	336	3.497	3.493	42	418	4.362	4.358	2	506	5.302	5.298
81	338	3.518	3.514	41	422	4.394	4.390	1	508	5.322	5.318
80	340	3.538	3.534	40	424	4.414	4.410				

TABLE 2

Conventional and new astronomically calibrated age of the main calcareous plankton datum planes (in the Rossello composite section). Also indicated in the position of these datum planes with respect to the MPRC-coded small-scale cycles. Uneven (MPRC) numbers refer to beige layers in the small-scale cycles after the correlative peak of the precession index to positive values. Position and conventional age of planktonic foraminiferal datum planes based on Langereis and Hilgen [27], and of nannofossil datum planes on Driever [32]

Biostratigraphic datum planes	Old age	New age	Cycle
Planktonic foraminifera			
<i>N. atlantica</i> FO	2.55*	2.72	262
<i>G*. altispira</i> LO	3.04–3.05	3.17	302
<i>S*. seminulina</i> LO	3.07	3.21	304
<i>G. puncticulata</i> reappearance	3.15–3.18	3.31	317
<i>G. crassaformis</i> reappearance	3.20±0.01	3.35	321
<i>G. puncticulata</i> disappearance	3.38±0.01	3.55	342
<i>G. crassaformis</i> FO	3.40±0.01	3.58	345
<i>G. margaritae</i> LO	3.56–3.59	3.79	365
<i>G. margaritae</i> LCO	3.71±0.01	3.96	380
<i>G. puncticulata</i> FO	4.12–4.13	4.50	433
<i>G. margaritae</i> FCO	4.64±0.01	5.07	483
<i>Sphaeroidinellopsis</i> top acme	4.74±0.01	5.20	495
<i>Sphaeroidinellopsis</i> bottom acme	4.83±0.01	5.29	505
Calcareous nannoplankton			
<i>D. tamalis</i> subtop	2.87	2.99	286
<i>D. pentaradiatus</i> top paracme	3.51	3.59	346
<i>Sphenolithus spp.</i> subtop	3.50	3.69	356
<i>R. pseudoumbilica</i> subtop	3.63	3.86	372
<i>D. pentaradiatus</i> bottom			
paracme	3.66	3.92	376
<i>D. tamalis</i> subbottom	3.69	3.96	380
<i>D. asymmetricus</i> subbottom	3.83	4.10	394/6

N. = *Neogloquadrina*; *G**. = *Globoquadrina*; *S**. = *Sphaeroidinellopsis*; *G.* = *Globorotalia*; *D.* = *Discoaster*; *R.* = *Reticulofenestra*.

ma and Brunhes/Matuyama Chron boundaries [20]. For polarity reversals older than the Gilbert/Gauss boundary, both the absolute and relative difference with the most commonly used conventional time scale [4] increases with (increasing) age. For the oldest astronomically dated reversal boundary, the lower Thvera, this discrepancy even amounts to 460 ky or 9.5%. The K/Ar age of 5.07 Ma for the Thvera from its type locality on Iceland [33], however, is in good agreement with the age constraints set by the astronomical calibration of the reversal boundaries. This finding is in contradiction with our previous conclusion that K/Ar dating results in systematically younger ages. On

Iceland, such younger ages, however, are found for polarity zones other than the Thvera. These younger ages may result from the diffusional loss of radiogenic argon; this process is supposed to underlie the occurrence of anomalously young K/Ar ages of lavas in otherwise "continuous" sequences on Iceland [33,35] and it can not be excluded that most if not all samples may have lost variable amounts of radiogenic argon [35]. For instance six out of 23 datings in the study of McDougall et al. [33] are demonstrably too young with respect to their stratigraphic position. Nevertheless, only the most obvious one out of four was excluded from the 17-point age data set they employed to construct their polarity time scale on the basis of a linear regression analysis.

This implies that the oldest K/Ar age for a certain polarity event may approach its true age better than the average K/Ar age. Supportive evidence for this conclusion is provided by the radiometric ages which are presently available for the Reunion. The oldest K/Ar age (2.14 ka; [36]) is remarkably consistent with the astronomically calibrated age of 2.14–2.15 Ma for this event [2], whereas the younger ages, even if obtained from (apparently) the same event on Reunion island, are evidently not. This spread in ages has even led to the supposition of the existence of a second Reunion event [37]. Similarly, the oldest ages for the Jaramillo and Cobb Mountain normal polarity events may be in line with the astronomically calibrated ages but, in these cases, it is uncertain whether the samples actually belong to these events because they were not obtained from a well established polarity sequence [20,36,38–40]. Moreover, serious doubt on the correctness of the conventional age of 0.73 Ma for the Brunhes/Matuyama boundary has recently been expressed on the basis of new radiometric datings [41,42]. Except for the Brunhes/Matuyama, this still does not provide a satisfactory explanation for the observed discrepancy between the radiometric and astronomically calibrated ages of the major (chron) boundaries and the fact that this discrepancy is proportionately constant. This proportional constancy initially provided the reasonable argument to suggest that the discrepancy might be explained by a systematic error in the K/Ar radiometric dating method, more specifically in the accuracy of the decay constants [1,2]. This, however, is

TABLE 3

Comparison of conventional and astronomically calibrated ages of Pliocene–Pleistocene geomagnetic polarity reversals. Also indicated is the position of the reversals with respect to the MPRC-coding of the small-scale cycles. Uneven numbers refer to beige layers in the small-scale cycles after the correlative peak of the precession index to positive values. Between brackets in the last column is the cycle number in the Rossello composite/the sapropel coding after Verhallen [47]. M&D = [20]; McD = [48]; Ber. = [4]; Har. = [34]; Sha. = [1]; Hil. = [2]

Reversal boundary	K/Ar dated		Seafloor anomaly		Astronomically calibrated			MPRC position
	M&D, 1979	McD, 1982	Ber., 1985	Har., 1989	Sha., 1990	Hil., 1991	This paper	
Brunhes/Matuyama	0.73	0.72	0.73	0.72	0.78			
Jaramillo top	0.90	0.89	0.92	0.91	0.99			
Jaramillo bottom	0.97	0.94	0.98	0.97	1.07			
Cobb Mountain	–	–	1.10	–	1.19			
Olduvai top	1.67	1.76	1.66	1.65	1.77	1.79		174
Olduvai bottom	1.87	1.91	1.88	1.88	1.95	1.95		188 (C1)
Reunion 1 top	2.01	2.07	–	2.06	–	2.14		208 (B5)
Reunion 1 bottom	2.04	2.07	–	2.09	–	2.15		208 (B5)
Reunion 2 top	2.12	–	–	–	–	–		
Reunion 2 bottom	2.14	–	–	–	–	–		
Gauss/Matuyama	2.48	2.47	2.47	2.45	2.60	2.59/2.62		250/252 (A5)
Kaena top	2.92	2.91	2.92	2.91		3.02	3.04	290 (103)
Kaena bottom	3.01	3.00	2.99	2.98		[3.08]	3.11	296 (100)
Mammoth top	3.05	3.07	3.08	3.07		[3.20]	3.22	308 (95)
Mammoth bottom	3.15	3.17	3.18	3.17		[3.32]	3.33	318 (90)
Gilbert/Gauss	3.40	3.41	3.40	3.40		[3.58]	3.58	344 (78)
Cochiti top	3.80	3.82	3.88	3.87		[4.22]	4.18	402 (50)
Cochiti bottom	3.90	3.92	3.97	3.99		[4.34]	4.29	412 (45)
Nunivak top	4.05	4.07	4.10	4.12		[4.52]	4.48	434 (35)
Nunivak bottom	4.20	4.25	4.24	4.26		[4.64]	4.62	444 (30)
Sidufjall top	4.32	4.44	4.40	4.41		[4.84]	4.80	462 (22)
Sidufjall bottom	4.47	4.57	4.47	4.48		[4.92]	4.89	468 (20)
Thvera top	4.85	4.72	4.57	4.79		[5.02]	4.98	476 (16)
Thvera bottom	5.00	4.94	4.77	5.08		[5.26]	5.23	500 (5)

difficult to reconcile with the K/Ar datings, discussed above, which are in complete agreement with the astronomically calibrated ages. Such a large error in the decay constants is also difficult to reconcile with the supposed accuracy of these constants on the order of 0.5% [43].

4.4. Age of the Miocene / Pliocene boundary

Finally, the astronomical calibration of the Trubi marls provides a new age for the Miocene/Pliocene boundary. These marls were deposited in an open, deep marine environment after the Messinian salinity crisis had suddenly come to an end. The base of the Trubi marls at Capo Rossello, therefore, has been taken to define the Miocene/Pliocene boundary [44].

Only recently, magnetostratigraphic age calibration (using the conventional time scale of Berggren et al. [4]) allowed the assessment of the age of the Miocene/Pliocene boundary by linear extrapolation of sediment accumulation rate or (small-scale) cycle duration [3,45,46]. Ages for the Miocene/Pliocene boundary, based on the latter procedure, range from 4.86 [3] to 4.93 Ma [46]. These ages are considerably younger than the traditional age of 5.3 Ma [4]. The latter age was based on long-distance biostratigraphic correlations to magnetostratigraphically dated extra-Mediterranean sequences. The new astronomically calibrated age of 5.32 Ma paradoxically implies a rehabilitation of the traditional age which at that time was based on correlation to a somewhat older stratigraphic level.

5. Conclusions

CaCO₃ cycles in the Rossello composite section can be calibrated accurately to the astronomical record using inferred phase relations between these CaCO₃ cycles and astronomical precession and eccentricity in combination with fixed astronomical calibration points provided by the sapropelitic layers in the upper part of the section. A Mediterranean Precession Related Cycle code is assigned to the grey beds in the small-scale CaCO₃ cycles after the correlative peak of the precession index numbered from the Recent. This correlation allows all cycles to be dated with an accuracy of approximately 1 ky.

The high-resolution magnetostratigraphy for the Rossello composite section further allows the construction of an astronomically calibrated Geomagnetic Polarity Time Scale with ages for the reversal boundaries of the Kaena (3.04–3.11 Ma) and Mammoth (3.22–3.33 Ma), the Gilbert/Gauss Chron boundary (3.58 Ma), and the reversal boundaries of the Cochiti (4.18–4.29 Ma), Nuni-vak (4.48–4.62 Ma), Sidufjall (4.80–4.89 Ma) and Thvera (4.98–5.23 Ma). The age of the Miocene/Pliocene boundary, as currently defined at the base of the Trubi, is 5.32 Ma. New ages have also been assigned for early to early late Pliocene planktonic foraminiferal and nannofossil datum planes in the Mediterranean.

This discrepancy between astronomically calibrated and radiometric age assignments is proportionately constant for the radiometrically most accurately dated geomagnetic polarity reversals, i.e., the Gilbert/Gauss, Gauss/Matuyama and Brunhes/Matuyama Chron boundaries [20]. This suggests that a systematic error in the decay constants used in K/Ar dating is responsible for the observed discrepancies. This conclusion, however, is not confirmed by K/Ar ages for a number of polarity events which are consistent with the astronomically calibrated ages. In these cases, the oldest K/Ar ages provide the most accurate age estimate suggesting that the diffusional loss of radiogenic argon has a more pronounced and "widespread" influence on the accuracy of K/Ar datings than previously assumed. Also in view of the assumed accuracy of 0.5% of the decay constants [43], argon loss provides a far more plausible explanation to account for the observed age

discrepancies between the astronomically calibrated and conventional time scales.

Acknowledgements

C.G. Langereis and W.J. Zachariasse critically read earlier versions of the manuscript. The reviews of W.F. Ruddiman, C. Laj and an anonymous reviewer are gratefully acknowledged. This study was funded by the Netherlands Organization for Scientific Research.

References

- 1 N.J. Shackleton, A. Berger and W.R. Peltier, An alternative astronomical calibration of the Lower Pleistocene time scale based on ODP Site 677, *Trans. R. Soc. Edinburgh* 81, 251–261, 1990.
- 2 F.J. Hilgen, Astronomical calibration of Gauss to Matuyama sapropels in the Mediterranean and implication for the Geomagnetic Polarity Time Scale, *Earth Planet. Sci. Lett.* 104, 226–244, 1991.
- 3 F.J. Hilgen and C.G. Langereis, The age of the Miocene–Pliocene boundary in the Capo Rossello area, *Earth Planet. Sci. Lett.* 91, 214–222, 1988.
- 4 W.A. Berggren, D.V. Kent, J.J. Flynn and J.A. Van Couvering, Cenozoic geochronology, *Geol. Soc. Am. Bull.* 96, 1407–1418, 1985.
- 5 J.D. Hays, J. Imbrie and N.J. Shackleton, Variations in the earth's orbit: Pacemaker of the ice ages, *Science* 194, 1121–1132, 1976.
- 6 J. Imbrie, J.D. Hays, D.G. Martinson, A. McIntyre, A.C. Mix, J.J. Morley, N.G. Pisias, W.L. Prell and N.J. Shackleton, The orbital theory of Pleistocene climate: Support from a revised chronology of the marine $\delta^{18}\text{O}$ record, in: *Milankovitch and Climate*, A.L. Berger et al., eds., NATO ASI Ser. C, 126, pp. 269–305, Reidel, Dordrecht, 1984.
- 7 D.G. Martinson, N.G. Pisias, J.D. Hays, J. Imbrie, T.C. Moore and N.J. Shackleton, Age dating and the orbital theory of the ice ages: Development of a high-resolution 0 to 300,000-year chronostratigraphy, *Quat. Res.* 27, 1–29, 1987.
- 8 N.G. Pisias and T.C. Moore, The evolution of Pleistocene climate: A time series approach, *Earth Planet. Sci. Lett.* 52, 450–458, 1981.
- 9 W.F. Ruddiman, M.E. Raymo, D.G. Martinson, B.M. Clement and J. Backman, Pleistocene evolution: northern Hemisphere ice sheets and north Atlantic Ocean, *Paleoceanography* 4, 353–412, 1989.
- 10 M.E. Raymo, W.F. Ruddiman, J. Backman, B.M. Clement and D.G. Martinson, Late Pliocene variation in northern Hemisphere ice sheets and North Atlantic deep water circulation, *Paleoceanography* 4, 413–446, 1989.
- 11 R.B. Kidd, M.B. Cita and W.B.F. Ryan, Stratigraphy of eastern Mediterranean sapropel sequences recovered during DSDP Leg 42A and their paleoenvironmental significance, *Init. Repts. D.S.D.P. 42A*, 421–443, U.S. Gov. Print Off., Washington, D.C., 1978.

- 12 E. Olausson, Description of sediment from the Mediterranean and Red Sea, Rep. Swed. Deep-Sea Exped. 1947-1948 8, 337-391, 1961.
- 13 F.J. Hilgen, Sedimentary rhythms and high-resolution chronostratigraphic correlations in the Mediterranean Pliocene, *Newsl. Stratigr.* 17, 109-127, 1987.
- 14 F.J. Hilgen and C.G. Langereis, Periodicities of CaCO₃ cycles in the Mediterranean Pliocene: Discrepancies with the quasi-periods of the Earth's orbital cycles?, *Terra Nova* 1, 409-415, 1989.
- 15 J.P. de Visser, J.H.J. Ebbing, L. Gudjonsson, F.J. Hilgen, F.J. Jorissen, P.J.J.M. Verhallen and D. Zevenboom, The origin of the rhythmic bedding in the Pliocene Trubi of Sicily, southern Italy, *Palaeogeogr., Palaeoclimat., Palaeoecol.* 69, 45-66, 1989.
- 16 M. Rossignol-Strick, African monsoons, an immediate climatic response to orbital insolation, *Nature* 303, 46-49, 1983.
- 17 M. Rossignol-Strick, Rainy periods and bottom water stagnation initiating brine accumulation and metal concentrations: 1. The Late Quaternary, *Paleoceanography* 2, 333-360, 1987.
- 18 E. Rohling and F.J. Hilgen, The eastern Mediterranean climate at times of sapropel formation: a review, *Geol. Mijnbouw*, 70, 253-264, 1991.
- 19 A.L. Berger, Accuracy and frequency stability of the Earth's orbital elements during the Quaternary, in: *Milankovitch and Climate*, A.L. Berger et al., eds., NATO ASI Ser. C 126, pp. 3-39, Reidel, Dordrecht, 1984.
- 20 E.A. Mankin and G.B. Dalrymple, Revised geomagnetic polarity time scale for the interval 0-5 m.y. B.P., *J. Geophys. Res.* 84, 615-626, 1979.
- 21 A. Berger and M.F. Loutre, Insolation values for the climate of the last 10 m.y., *Quat. Sci. Rev.* in press, 1991.
- 22 M.B. Cita and S. Gartner, Studi sul Pliocene e sugli strati del passaggio dal Miocene al Pliocene. IV. The stratotype Zanclean. Foraminiferal and nannofossil biostratigraphy, *Riv. Ital. Paleontol. Stratigr.* 79, 503-558, 1973.
- 23 P. Spaak, Accuracy in correlation and ecological aspects of the planktonic foraminiferal zonation of the Mediterranean Pliocene, *Utrecht Micropaleontol. Bull.* 28, 1-160, 1983.
- 24 D. Rio, R. Sprovieri and I. Raffi, Calcareous plankton biostratigraphy and biochronology of the Pliocene-Lower Pleistocene succession of the Capo Rossello area, Sicily, *Mar. Micropaleontol.* 9, 135-180, 1984.
- 25 W.J. Zachariasse, W.J., J.D.A. Zijderveld, C.G. Langereis, F.J. Hilgen and P.J.J.M. Verhallen, Early Late Pliocene biochronology and surface water temperature variations in the Mediterranean, *Mar. Micropaleontol.* 14, 339-355, 1989.
- 26 W.J. Zachariasse, L. Gudjonsson, F.J. Hilgen, C.G. Langereis, L.J. Lourens, P.J.J.M. Verhallen and J.D.A. Zijderveld, Late Gauss to early Matuyama invasions of *Neoglobobuadrina atlantica* in the Mediterranean and associated record of climatic change, *Paleoceanography* 5, 239-252, 1990.
- 27 C.G. Langereis and F.J. Hilgen, The Rossello composite: A Mediterranean and global reference section for the Early to early Late Pliocene, *Earth Planet. Sci. Lett.* 104, 211-225, 1991.
- 28 L.J. Lourens, F.J. Hilgen and W.J. Zachariasse, Late Pliocene-Early Pleistocene astronomically forced sea surface temperature and productivity variations in the Mediterranean, *Mar. Micropaleontol.* in press.
- 29 W.F. Ruddiman, R.B. Kidd, E. Thomas, et al., *Init. Repts. D.S.D.P.*, 94, U.S. Gov. Print. Off. Washington, D.C., 1987.
- 30 F.J. Jorissen, K. van der Borg, A.M. Borsetti, L. Gudjonsson, F.J. Hilgen, S. Iaccarino, A.F.M. de Jong, E.J. Rohling, J.P. de Visser and W.J. Zachariasse, Late Quaternary high-resolution biochronology for the central Mediterranean, *Mar. Micropaleontol.* in press.
- 31 S.R. Troelstra, G.M. Ganssen and G.T. Klaver, High-resolution analysis of eastern Mediterranean sapropel S1: Chronostratigraphy, oxygen isotopes and geochemistry, IX RCMNS Congress, Barcelona, Abstr., 349, 1990.
- 32 B.W.M. Driever, Calcareous nannofossil biostratigraphy and paleoenvironmental interpretation of the Mediterranean Pliocene, *Utrecht Micropaleontol. Bull.* 36, 245, 1988.
- 33 I. McDougall, K. Saemundsson, H. Johannesson, N.D. Watkins and L. Kristjansson, Extension of the geomagnetic polarity time scale to 6.5 m.y.: K-Ar dating, geological and paleomagnetic study of a 3,550-m lava succession in western Iceland, *Geol. Soc. Am. Bull.* 88 1-15, 1977.
- 34 W.B. Harland, R.L. Armstrong, A.V. Cox, L.E. Craig, A.G. Smith and D.G. Smith, *A Geologic Time Scale 1989*, Cambridge Univ. Press, Cambridge, 1989.
- 35 N.D. Watkins, L. Kristjansson and I. McDougall, A detailed paleomagnetic survey of the type location for the Gilsa geomagnetic polarity event, *Earth Planet. Sci. Lett.* 27, 436-444, 1975.
- 36 I. McDougall and F.H. Chamalaun, Geomagnetic polarity scale of time, *Nature*, 212, 1415-1418, 1966.
- 37 C.S. Gromme and R.L. Hay, Geomagnetic polarity epochs: Age and duration of the Olduvai normal polarity event, *Earth Planet. Sci. Lett.* 10, 179-185, 1971.
- 38 A. Abdel-Monem, N.D. Watkins and P.W. Gast, Potassium-argon ages, volcanic stratigraphy, and geomagnetic polarity history of the Canary Islands: Tenerife, La Palma, and Hierro, *Am. J. Sci.* 272, 805-825, 1972.
- 39 R.J. Fleck, J.H. Mercer, A.E.M. Nairn and D.N. Peterson, Chronology of late Pliocene and early Pleistocene glacial and magnetic events in southern Argentina, *Earth Plan. Sci. Lett.* 16, 15-22, 1972.
- 40 N.D. Watkins and A. Abdel-Monem, Detection of the Gilsa geomagnetic polarity event on the Island of Madeira, *Geol. Soc. Am. Bull.* 82, 191-198, 1971.
- 41 G.A. Izett, J.D. Obradovitch and H.H. Mehnert, The Bishop ash bed (Middle Pleistocene) and some older (Pliocene and Pleistocene) chemically and mineralogically ash beds in California, Nevada and Utah, *U. S. Geol. Surv. Bull.* 1675, 37 pp., 1988.
- 42 A.K. Baksi and E. Farrar, A preliminary attempt at ⁴⁰Ar/³⁹Ar dating of lavas spanning the Brunhes-Matuyama geomagnetic polarity transition, *EOS* 71, 1296, 1990.
- 43 N.H. Gale, The physical decay constants, in: *Numerical dating in stratigraphy*, G.S. Odin, ed., Wiley-Interscience, Chichester, 107-122, 1982.
- 44 M.B. Cita, The Miocene/Pliocene boundary: history and definition, in: *Late Neogene Epoch Boundaries*, T. Saito

- and L.H. Burckle, eds., Micropaleontology, Spec. Publ. 1, 1-30, 1975.
- 45 J.D.A. Zijderveld, W.J. Zachariasse, P.J.J.M. Verhallen and F.J. Hilgen, The age of the Miocene-Pliocene boundary, *Newsl. Stratigr.* 16, 169-181, 1986.
- 46 J.E.T. Channell, D. Rio and R.C. Thunell, Miocene/Pliocene boundary magnetostratigraphy at Capo Spartivento, Calabria, Italy, *Geology* 16, 1096-1099, 1988.
- 47 P.J.J.M. Verhallen, Early development of *Bulimina marginata* in relation to paleoenvironmental changes in the Mediterranean, *Proc. Ned. Akad. Wet., Ser. B* 90, 161-180, 1987.
- 48 I. McDougall, The present status of the Geomagnetic Polarity Time Scale, in: *The Earth, Its origin, structure and evolution*, M.W. McElhinney, ed., pp. 543-565, Academic Press, London, 1979.

Chapter 10

THE NEW ASTRONOMICALLY CALIBRATED TIME SCALE FOR THE LATE PLIOCENE CONFIRMED

F.J. Hilgen¹, L.J. Lourens¹, A. Berger² & M.F. Loutre²

¹ *Dept. of Geology, Inst. of Earth Sciences, Budapestlaan 4, 3584 CD Utrecht, The Netherlands*

² *Inst. d'Astronomie et de Geophysique G. Lemaître, Univ. Cath. de Louvain, Louvain-la-Neuve, Belgium*

A new astronomically calibrated time scale has recently been established for the Pliocene - earliest Pleistocene¹, based on the correlation of dominantly precession controlled sedimentary cycles to the astronomical solution Ber_90². This time scale differs substantially from conventional time scales^{3,4,5}. In order to test the new time scale, both precession and obliquity related frequency components were extracted from late Pliocene - early Pleistocene climatic proxy records in the Mediterranean (Lourens et al., manuscript subm.) and compared with the respective orbital time series. The new time scale is confirmed by the good to excellent coherence between the geological filtered 21 ky components and precession and the consistent relationship between the geological 41 ky components and obliquity. Only a slight discrepancy of 2 ky is found if we compare late Pleistocene phase relations between orbital forcing and climate response with those obtained for the late Pliocene. This discrepancy can be explained by a change in these phase relations, by a very small error in the astronomical solution or by a combination of these factors.

Climatic proxy records have been calibrated astronomically to evaluate the orbital theory of the ice ages and to develop a high-resolution time scale for the late Pleistocene^{6,7,8}. This astronomically calibrated time scale has recently been extended into the Pliocene^{1,9} and even down to the Miocene-Pliocene boundary¹⁰. It differs markedly from more conventional (polarity) time scales^{3,4,5} which, for this interval of time, rely on K/Ar dating. The age discrepancy ranges from 3 to 10 % and has been related to the loss of radiogenic argon which results in K/Ar ages that are too young¹⁰.

To construct the new time scale, Hilgen¹ correlated characteristic patterns of brownish coloured beds (sapropels) in upper Pliocene to lower Pleistocene marine sequences of the Mediterranean to the astronomical solution Ber_90², using relationships between sapropel cycles of late Pleistocene age and orbital precession and eccentricity (fig. 1; Ber_90 is assumed to be accurate in the time domain over the last 5.0 Ma²). The almost complete lack of the expression of obliquity in the sapropel pattern is explained by the fact that these sapropels reflect changes in wetness of regional, (circum)Mediterranean and monsoonal climate and the relatively low latitudinal position of the Mediterranean^{11,12,13,14}. The influence of both precession and obliquity, however, is distinctly recorded in the oxygen isotope ($\delta^{18}\text{O}$) and planktonic foraminiferal sea surface temperature (SST) and productivity (SSP) proxy records (Lourens et al., manuscript subm.). In addition to precession induced, regional climatic oscillations, these records clearly register glacial-interglacial alternations which at that time were dominantly obliquity controlled^{15,16}. To test the validity of the new time scale, we extracted 21 and 41 ky components from these climatic proxy records and compared them with precession and obliquity.

For a thorough evaluation, however, time lags between orbital forcing and climate response must be determined as accurately as possible. For this purpose, we used the late Pleistocene core RC 9-181 from the eastern Mediterranean^{12,17}. We assigned ages of the correlative precession peak to sapropel mid-points¹ and extracted the 41 ky component from the resulting $\delta^{18}\text{O}$ time series, using a Tukey bandpass filter (fig. 2). Subsequent cross-correlation yielded the strongest correlation with actual obliquity if the latter was shifted 7 ky towards younger levels. Since we had introduced non-lagged, precessional ages for the sapropels, this period of 7 ky equals the obliquity lag effect minus that of precession. The latter can be determined accurately for the youngest, Holocene sapropel. Comparison of A(cellarator) M(ass) S(pectrometry) ¹⁴C dates - 7.9 to 8.7 ka (Troelstra et al., manuscript in prep.) - for this sapropel and the age of 11.5 ka of the correlative precession peak reveals that the sapropel mid-point lags precession by 3.2 ky. The time lag between obliquity and induced ice volume changes, as recorded by $\delta^{18}\text{O}$ in the Mediterranean, consequently arrives at ~10 ky (namely 10-3=7), which agrees with the 8 - 10 ky range of published estimates^{6,7,18,19}.

Next, we applied the same procedure to the sapropel, $\delta^{18}\text{O}$ and planktonic foraminiferal records from the late Pliocene - earliest Pleistocene in the Mediterranean. Again, we used precession ages of the astronomically dated sapropels¹ to generate our time series. From the $\delta^{18}\text{O}$ record, both the precession and obliquity related components were extracted. From the SSP record we extracted the 21 ky component and from the SST record the 41 ky component, because these records reveal the dominant reflection of precession and obliquity only (Lourens et al., manuscript subm.). The filtered components were subsequently compared with the respective orbital time series (figs. 3, 4). Due to the distinct reflection of the eccentricity modulation, the 21 ky component reveals a good to excellent coherence with actual precession (fig. 3). This coherence essentially confirms the correctness of the astronomical calibration of

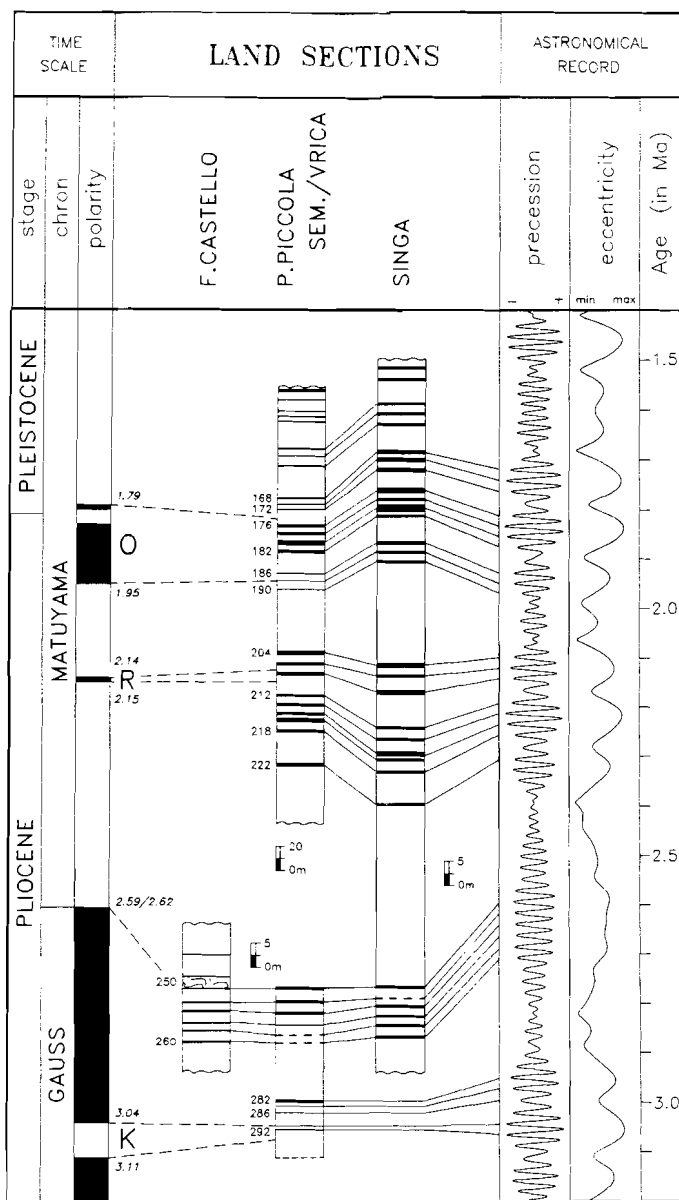


Figure 1. Astronomical calibration of late Pliocene to earliest Pleistocene sapropels in the Mediterranean to the astronomical solution Ber_90. The correlation was established using phase relations between late Pleistocene sapropels and astronomical precession and eccentricity¹. The resulting polarity time scale is shown on the left and based on magnetostratigraphic records of the sections^{24,25,26} (not shown). Ages of polarity transitions (in italics) and number of MPRC (Mediterranean Precession Related Cycle) codification of sapropels are indicated. O = Olduvai; R = Reunion; and K = Kaena.

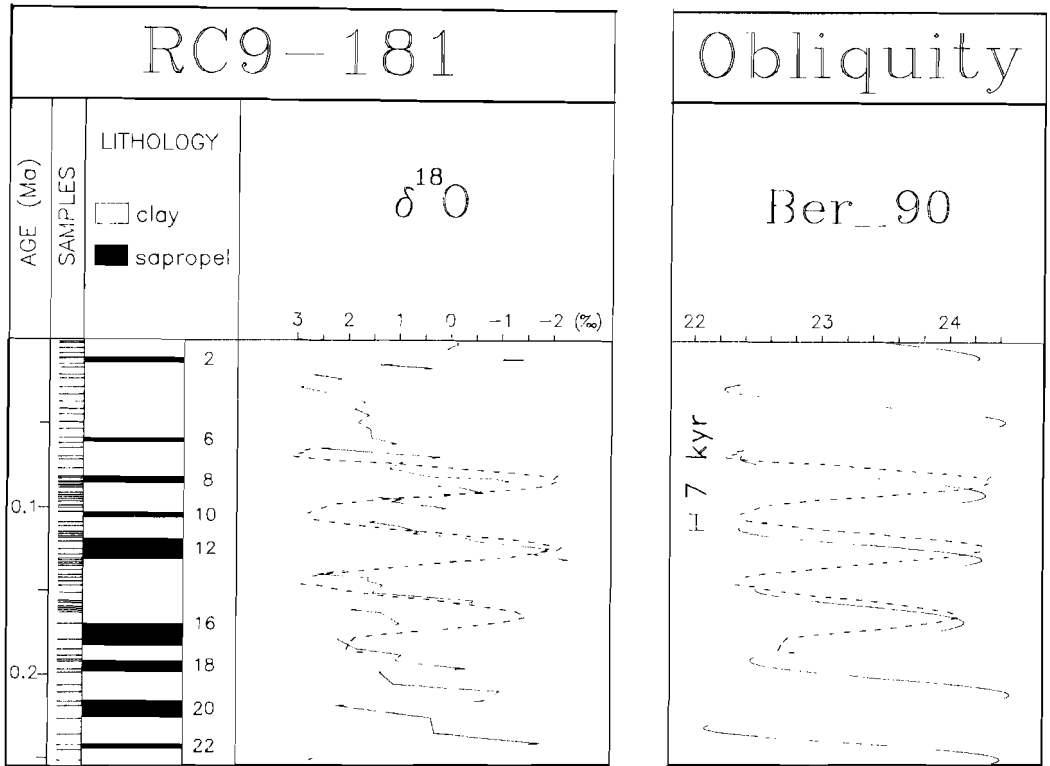


Figure 2. Determination of the time lag between the 41 ky component in $\delta^{18}\text{O}$ and obliquity for the Mediterranean late Pleistocene. Non-lagged, precessional ages of sapropel mid-points¹ were used to generate the time series of the $\delta^{18}\text{O}$ record from core RC 9-181^{12,17} (solid line in first column). The obliquity related component (dashed line) was extracted using a Tukey bandpass filter with a central frequency of 0.0244 cycles per kyr and a bandwidth of 0.055, and compared with obliquity (Ber_90 solution; solid line in second column). Cross-correlation with a resolution of 0.5 kyr yielded the strongest correlation when obliquity is shifted 7 kyr towards younger levels. Sapropel numbers refer to MPRC codification of sedimentary cycles in the Mediterranean Pliocene and Pleistocene^{1,10}.

the sapropels and, thereby, the validity of the new time scale. Further confirmation is given by the very consistent relationship between the 41 ky components in our proxy records and actual obliquity (fig. 4). However, the calculated lag of 9 ky differs slightly but significantly from the 7 ky obtained for the late Pleistocene. This discrepancy of 2 ky can be explained by a small error in the astronomical solution, by a change in one of the two phase relations between orbital forcing and climate response or by a combination of these factors.

Both during the late Pliocene - early Pleistocene and the late Pleistocene, the time lag associated with the 41 ky component in $\delta^{18}\text{O}$ reflects the lag between obliquity and global ice volume changes initiated at high northern latitudes. At present, it is not possible to decide whether this time lag remained constant throughout the late Pliocene - Pleistocene. This is due to the complexity of processes underlying the growth and decay of ice sheets²⁰ and the fact that the late Pliocene cannot be considered a true analogue of the late Pleistocene. There is, for instance, a marked difference in frequency distribution of ice volume variations^{21,22}. The smaller dimensions of late Pliocene ice sheets nevertheless suggests a reduction of this time lag with respect to the late Pleistocene because the response time of ice sheets is likely to be proportional to their size²⁰. An extra complication is that the magnitude of obliquity forced ice volume variations did not necessarily change because, during the late Pleistocene, they occurred superimposed on dominant 100 ky variations. It remains however difficult to explain an increase in time lag from 10 (7+3=10) ky in the late Pleistocene to 12 (9+3=12) ky in the late Pliocene to early Pleistocene.

On the other hand, a reduction of the lag between precessional forcing and sapropel formation from 3 (10-7=3) ky during the late Pleistocene to 1 (10-9=1) ky in the late Pliocene - early Pleistocene would also suffice. This reduction may be related to the almost complete lack of precession induced ice volume changes during the late Pliocene - earliest Pleistocene^{15,16}. This lack in turn may lead to a more direct thermal response of circum-Mediterranean climates to precession induced variations in insolation. However, climate modelling experiments showed that low latitude, tropical/monsoonal climate may lag precession by 3 ky due to direct thermal response²³. This suggests that the 3 ky time lag associated with sapropels of late Pleistocene age is largely independent from ice volume changes and that it remained constant throughout the Pliocene-Pleistocene.

Finally, a small error in the astronomical solution is certainly feasible. It must be understood that a relative error of $6 \cdot 10^{-4}$ in the main period of the obliquity would lead to a discrepancy of 2 ky in the time scale after $3 \cdot 10^6$ years. This means that the corresponding frequency must be known with an accuracy of 0.02"/year, which is very close to what we might expect from our present-day knowledge.

For the time interval considered, the Ber_90 solution would be in agreement with the climatic proxy records if obliquity is shifted 2 ky towards younger levels with respect to precession. This can be realised by increasing all the precession frequencies by 0.033% and all obliquity frequencies by 0.1%. In such a case the application of the strategy described in this

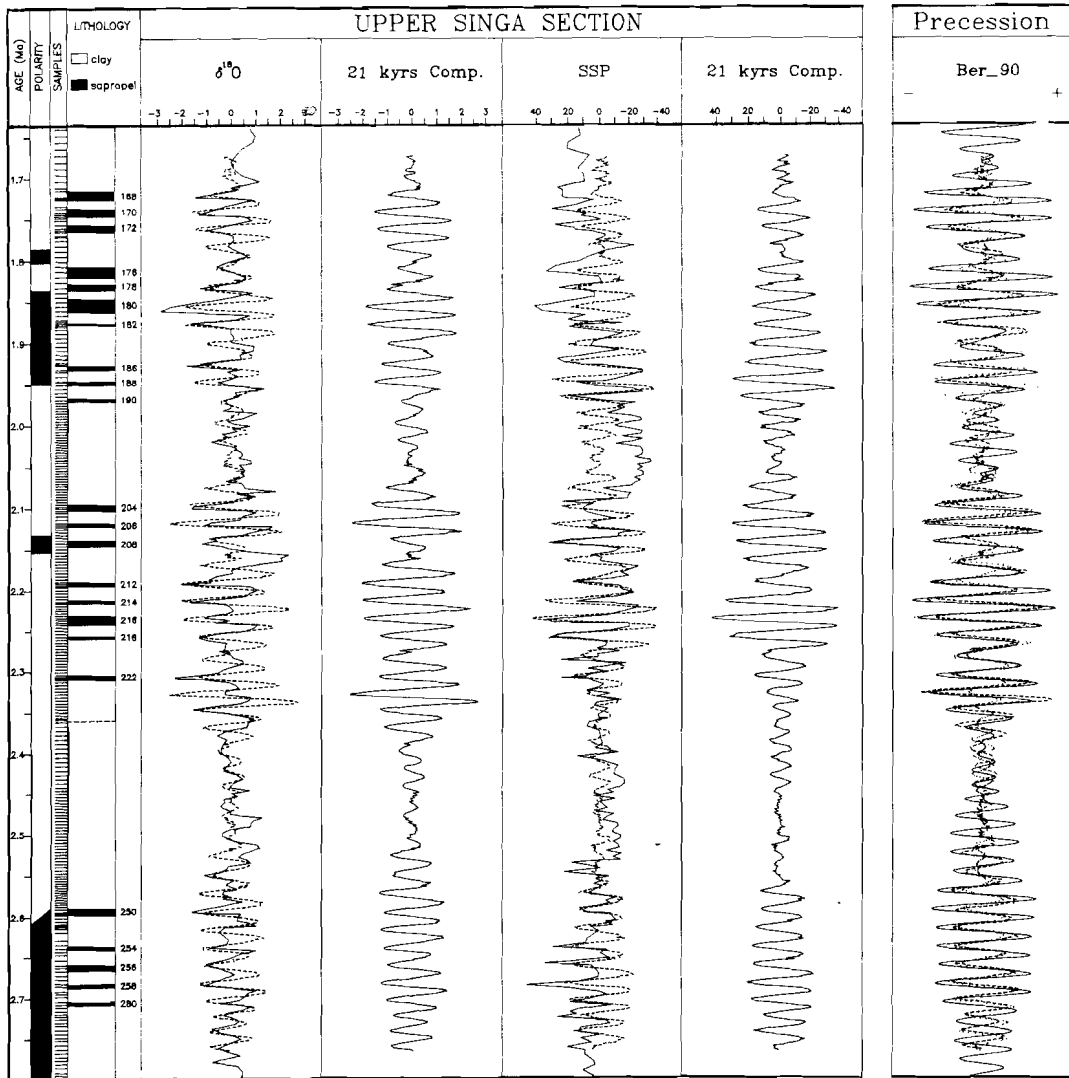


Figure 3. Comparison of the 21 ky components in $\delta^{18}\text{O}$ and SSP from the Monte Singa section and precession after Ber_90². Time series of $\delta^{18}\text{O}$ and SSP (solid lines in the first and third column) were established using non-lagged, precessional ages of sapropel mid-points. Sapropel numbers refer to MPRC codification^{1,10}. We added two more calibration points based on the correlation of quantitative planktonic foraminiferal patterns from Monte Singa to the Francocastello section on Crete where two extra sapropelitic layers are present¹ (partly unpublished data). Furthermore, we made a correction for the stratigraphic distance between the glacial isotopic stages 92 and 96 in the Singa section (Lourens et al., manuscript subm.), which is reduced in thickness with respect to DSDP Site 607¹⁶. The correction consisted of stretching the problematic interval to two times the average distance between the successive glacial stages 78 to 92 in our record. The precession related components were extracted using a Tukey bandpass filter with a central frequency of 0.0476 cycles per ky and a bandwidth of 0.106. A 21 ky period was selected to extract information from the proxy records connected with both the 19 and 23 ky main quasi-periods of precession. Filtered components are shown by dashed lines in the first and third column and by solid lines in the second and fourth column. In the fifth and last column, they have been normalized to precession (solid line) are shown by a dashed ($\delta^{18}\text{O}$) and a dotted (SSP) line.

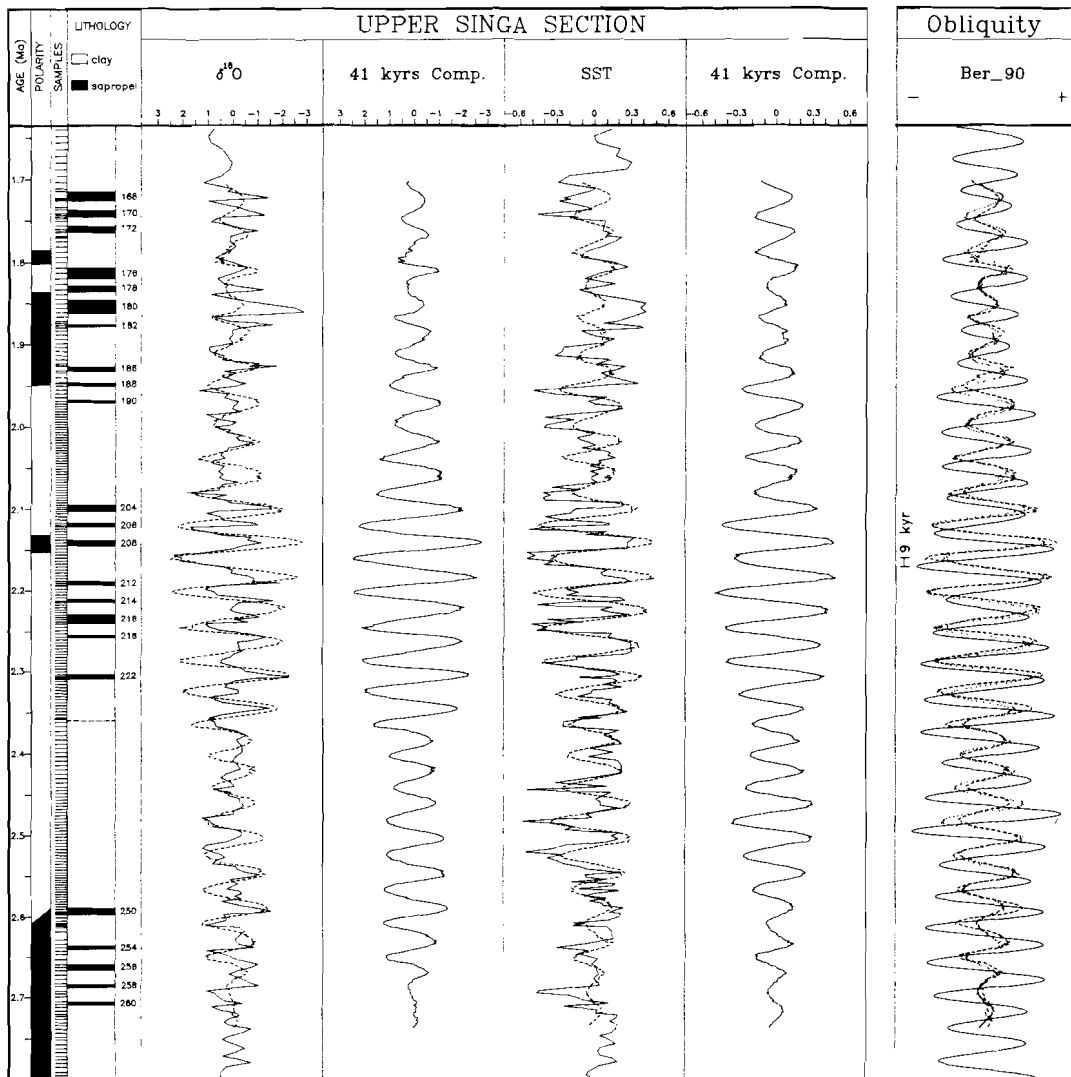


Figure 4. Comparison of the 41 ky components in $\delta^{18}\text{O}$ and SST from the Monte Singa section (southern Calabria, Italy) and obliquity after Ber_90. Time series of $\delta^{18}\text{O}$ and SST (solid lines in the first and third column) were established using non-lagged, precessional ages of sapropels. The obliquity components were extracted using a Tukey bandpass filter with a central frequency of 0.0244 cycles per ky and a bandwidth of 0.055. Filtered components are shown by dashed lines in the first and third column and by solid lines in the second and fourth column. In the fifth and last column, they have been normalized to obliquity (solid line) and are shown as a dashed ($\delta^{18}\text{O}$) and a dotted (SST) line. Cross correlation with a resolution of 0.5 ky yielded the strongest correlation when obliquity is shifted 9 ky towards younger levels for both proxy records.

paper would lead to a phase lag of 3 and 10 ky between proxy data and orbital parameters in the precession and obliquity bands, respectively, throughout the whole Pliocene-Pleistocene. However, at the present time such a change of the frequencies cannot be attributed to any physical process in the astronomical calculations, but can just be seen as a means to build an *astronomical solution* (further refer to as BL91) which *fits* one particular set of geological data.

As a conclusion, the origin of the discrepancy will have to be looked for not only in further refinements of the astronomical solution, but also in additional comparisons between other climatic proxy records and the astronomical solutions, in improving the transfer function of these proxy data and in modelling the response of the climate system to the astronomical forcing over the last 3 Ma with a particular attention paid to the phase relations between insolation, simulated climate and proxy records buried in the sediment.

References

1. Hilgen, F.J. *Earth Planet. Sci. Lett.* **100**, 226-244 (1991).
2. Berger, A. & Loutre, M.F. *Quat. Sci. Reviews* **10** (1991, in press).
3. Mankinen, E.A. & Dalrymple, G.B. *J. geophys. Res.* **84**, 615-626 (1979).
4. Berggren, W.A., Kent, D.V., Flynn, J.J. & Van Couvering, J.A. *Geol. Soc. Am. Bull.* **96**, 1407-1418 (1985).
5. Harland, W.B., Armstrong, R.L., Cox, A.V., Craig, L.E., Smith, A.G. & Smith, D.G. *A geological time scale* (Cambridge Univ. Press, Cambridge, 1989).
6. Hays, J.D., Imbrie, J. & Shackleton, N.J. *Science* **194**, 1121-1132 (1976).
7. Imbrie, J., Hays, J.D., Martinson, D.G., McIntyre, A., Mix, A.C., Morley, J.J., Pisias, N.G., Prell, W.L. & Shackleton, N.J. in *Milankovitch and Climate* (eds. Berger et al.), 269-305 (D. Reidel, Dordrecht, 1984).
8. Martinson, D.G., Pisias, N.G., Hays, J.D., Imbrie, J., Moore, T.C. & Shackleton, N.J. *Quat. Res.* **27**, 1-29 (1987).
9. Shackleton, N.J., Berger, A. & Peltier, W.R. *Trans. Royal Soc. Edinburg* **81**, 251-261 (1990).
10. Hilgen, F.J. *Earth Planet. Sci. Lett.* (in press).
11. Hilgen, F.J. *Newsl. Stratigr.* **17**, 109-127 (1987).
12. Rossignol-Strick, M. *Nature* **303**, 46-49 (1983).
13. Rossignol-Strick, M. *Paleoceanography* **2**, 333-360 (1987).
14. Rohling, E. & Hilgen, F.J. *Geol. & Mijnb.* **70**, 253-264 (1991).
15. Ruddiman, W.F., Raymo, M.E., Martinson, D.G., Clement, B.M. & Backman, J. *Paleoceanography* **4**, 353-412 (1989).
16. Raymo, M.E., Ruddiman, W.F., Backman, J., Clement, B.M. & Martinson, D.G. *Paleoceanography* **4**, 413-446 (1989).
17. Cita, M.B., Vergnaud-Grazzini, C., Robert, C., Chamley, H., Cariani, N. & d'Onofrio, S. *Quat. Res.* **8**, 205-235 (1978).
18. Ruddiman, W.F. & McIntyre, A. in *Milankovitch and Climate* (eds. Berger et al.), 671-686 (D. Reidel, Dordrecht, 1984).
19. Imbrie, J., McIntyre, A. & Mix, A. in *Climate and Geo-Sciences* (eds. Berger et al.), 121-164 (D. Reidel, Dordrecht, 1989).
20. Oerlemans, J. & van der Veen, C.J. *Ice Sheets and Climate*, Kluwer, Dordrecht, 217 pp. (1984).
21. Shackleton, N.J. & Opdyke, N.D. *Mem. Geol. Soc. Am.* **145**, 449-464 (1976).
22. Pisias, N.G. & Moore, T.C. *Earth Planet. Sci. Lett.* **52**, 450-458 (1981).
23. Short, D.A. & Mengel, J.G. *Nature* **323**, 48-50 (1986).
24. Tauxe, L., Opdyke, N.D., Pasini, G. & Elmi, C. *Nature* **304**, 125-129 (1983).
25. Zachariasse, W.J., Gudjonsson, L., Hilgen, F.J., Langereis, C.G., Lourens, L.J., Verhallen, P.J.J.M. & Zijderveld, J.D.A. *Paleoceanography* **5**, 239-252 (1990).
26. Zijderveld, J.D.A., Hilgen, F.J., Langereis, C.G., Verhallen, P.J.J.M. & Zachariasse, W.J. *Earth Planet. Sci. Lett.* (in press).

Curriculum vitae

Toegevoegd op verzoek van het College van Decanen van de Rijksuniversiteit Utrecht.

Frederik Johan Hilgen werd geboren op 27 november 1957 te Almelo. In 1976 behaalde hij het diploma Atheneum B aan het Erasmus Lyceum te Almelo. In het zelfde jaar begon hij met de studie Geologie aan de Rijksuniversiteit te Utrecht. Het kandidaats-examen werd in december 1980 afgelegd. In augustus 1984 werd het doctoraal-examen Stratigrafie/Paleontologie afgelegd met bijvakken Sedimentologie en Economische Geologie. Van 1 juni tot 1 augustus 1985 en 1986 was hij door de Faculteit Aardwetenschappen aangesteld als toegevoegd docent bij het doctoraal veldwerk stratigrafie. Vanaf juli 1986 tot 1 januari 1989 was hij als toegevoegd onderzoeker werkzaam bij de Afdeling Stratigrafie/Paleontologie van de Vakgroep Geologie te Utrecht in dienst van de Nederlandse Organisatie voor Wetenschappelijk Onderzoek (NWO) en vanaf 1 november 1989 tot 1 juli 1990 bij het Paleomagnetisch Laboratorium "Fort Hoofddijk" te Utrecht. Vanaf 1 mei 1992 heeft hij een tijdelijke aanstelling als post-doc bij de Afdeling Stratigrafie/Paleontologie van de Vakgroep Geologie te Utrecht via een stimulerings-subsidie van NWO voor de onderzoeksschool Sedimentaire Geologie i.o.